[redacted]

CENTRAL RESEARCH LIBRARY
DOCUMENT COLLECTION

MARTIN MARIETTA ENERGY SYSTEMS LIBRARIES
3 4456 0349805 2

ORNL-1813
Progress
74

Inv
56

AEC RESEARCH AND DEVELOPMENT REPORT

HOMOGENEOUS REACTOR PROJECT

QUARTERLY PROGRESS REPORT

FOR PERIOD ENDING OCTOBER 31, 1954

DECLASSIFIED
CLASSIFICATION CHANGED TO:
BY AUTHORITY OF: AEC-4-10-58
BY: P.C. Hansen 6-23-58

OAK RIDGE NATIONAL LABORATORY
CENTRAL RESEARCH LIBRARY
CIRCULATION SECTION
4500N ROOM 175
LIBRARY LOAN COPY
DO NOT TRANSFER TO ANOTHER PERSON
If you wish someone else to see this report, send in name with report and the library will arrange a loan.
UCN 7969 (3 9-77)

OAK RIDGE NATIONAL LABORATORY
OPERATED BY
CARBIDE AND CARBON CHEMICALS COMPANY
A DIVISION OF UNION CARBIDE AND CARBON CORPORATION
UCC
POST OFFICE BOX P
OAK RIDGE, TENNESSEE

[redacted]

[redacted]

[redacted]

ORNL-1813

This document consists of 202 pages.
Copy 7 of 225 copies. Series A.

Contract No. W-7405-eng-26

HOMOGENEOUS REACTOR PROJECT

QUARTERLY PROGRESS REPORT

For Period Ending October 31, 1954

Project Director – J. A. Swartout
Associate Director – C. E. Winters

Experimental Reactors – S. E. Beall
Thorium Breeder Reactor – W. C. Moore
Corrosion – E. G. Bohlmann
Engineering Development – J. A. Lane
Chemical Engineering Development – F. R. Bruce
Supporting Chemical Research – E. H. Taylor

Compiled by

H. F. McDuffie
D. C. Kelly

DATE RECEIVED BY INFORMATION AND REPORTS DIVISION
(NOVEMBER 10, 1954)

DATE ISSUED

DEC 10 1954

OAK RIDGE NATIONAL LABORATORY
Operated by
CARBIDE AND CARBON CHEMICALS COMPANY
A Division of Union Carbide and Carbon Corporation
Post Office Box P
Oak Ridge, Tennessee

[redacted]

MARTIN MARIETTA ENERGY SYSTEMS LIBRARIES

3 4456 0349805 2

[redacted]

196. USAF Headquarters
197. USAF Project Rand
198. U. S. Naval Radiological Defense Laboratory
199-200. University of California Radiation Laboratory, Berkeley
201-202. University of California Radiation Laboratory, Livermore
203. Vitro Engineering Division
204. Walter Kidde Nuclear Laboratories, Inc.
205-210. Westinghouse Electric Corporation
211-225. Technical Information Service, Oak Ridge

[redacted]

[redacted]

Reports previously issued in this series are as follows:

ORNL-527	Date issued, December 28, 1949
ORNL-630	Period Ending February 28, 1950
ORNL-730	Feasibility Report – Date Issued, July 6, 1950
ORNL-826	Period Ending August 31, 1950
ORNL-925	Period Ending November 30, 1950
ORNL-990	Period Ending February 28, 1951
ORNL-1057	Period Ending May 15, 1951
ORNL-1121	Period Ending August 15, 1951
ORNL-1221	Period Ending November 15, 1951
ORNL-1280	Period Ending March 15, 1952
ORNL-1318	Period Ending July 1, 1952
ORNL-1424	Period Ending October 1, 1952
ORNL-1478	Period Ending January 1, 1953
ORNL-1554	Period Ending March 31, 1953
ORNL-1605	Period Ending July 31, 1953
ORNL-1658	Period Ending October 31, 1953
ORNL-1678	Period Ending January 31, 1954
ORNL-1753	Period Ending April 30, 1954
ORNL-1772	Period Ending July 31, 1954

[redacted]

[redacted]

SUMMARY

PART I. EXPERIMENTAL REACTORS

1. Homogeneous Reactor Test

1.1 Project Status. Approximately 80% of the projected expenditures for hardware has been obligated in purchase or construction contracts. An estimate of the cost of the completed HRT indicates that the final cost will be $1,840,000. A breakdown of this estimate is presented.

1.2 Design. The design has been completed for all the major high-pressure and low-pressure components except the reactor pressure vessel. Contained in this report are the most recent revisions of the low-pressure-system flow sheet, a description of important details of the reactor cell, and the final design of the main heat exchangers, the inner dump tanks and separator, the recombiner and recombiner-condenser, and the outer dump tanks and reflux condenser.

1.3 Nuclear Calculations. The HRT has been analyzed for situations which could cause physical damage to the reactor. After minor design changes were made, no conditions appear to exist which could damage the HRT. The pressure vessel would probably rupture at a differential of 8000 psi and the core at a differential of about 1000 psi between the core and reflector. Conservative safety limits of 200-psi differential between the core and reflector and 4000 psi between the reflector and the atmosphere were chosen for the safety analysis of the HRT. The corresponding maximum allowable rates of reactivity increase are 0.5 and 2% per second, respectively.

Some miscellaneous radiation hazards have been considered. The concentration of radioactive argon resulting from the release of the activated air from valve operators in the process cell into the control room of the HRT operating at 10-Mw power is less than one-third of tolerance. The shielding over the steam drums is adequate to keep radiation levels below 12 r/hr above the steam drum and the valve pit in the event of rupture of a heat-exchanger tube. The streaming of fast neutrons through cracks between the top shield plugs could give a directed dose rate of 30 mrem per hour of fast neutrons.

1.4 Component Development. Tests of a full-scale mockup of the HRT core, which contains nine screens or perforated plates mounted in a double-cone inlet diffuser, have permitted final design specifications to be made. In the program for development of the HRT core tank and pressure vessel by the Newport News Shipbuilding & Dry Dock Co., welding techniques using local inert-gas shielding have given test welds of satisfactory strength, and pressure tests of an aluminum full-scale mockup of the HRT core tank have given results in good agreement with design calculations. Materials for the Zircaloy-2 core tank are on hand for fabrication.

Two 400A pumps have been received from Westinghouse. One pump will be tested at HRT fuel-pump conditions; the other is for long-range pump development. The loops in which these pumps will be tested are nearing completion.

A contract has been placed with Westinghouse to supply two 400-gpm pumps and two 230-gpm pumps for the HRT. One of each of these pumps will be all-stainless-steel; the others will have titanium replacements for those parts which are subject to high velocity and/or turbulence at temperatures above 212°F.

The HRT injection pump, which was developed to serve as both a fuel and a blanket feed pump for the HRT, is an HRE-type diaphragm pumping head driven by a Scott and Williams Hydropulse pump. Operation and testing of this pump are described.

Tests were conducted on a simulated HRT pressurizer in order to study the rates of liquid mixing and the pickup of gas from the main circulating stream. The solution to these problems is reported.

Comprehensive tests to determine the feasibility of the HRT dump-tank evaporator have been completed. A full-scale steel mockup of one of the two dump tanks was operated. The data indicate that 75-psig steam will evaporate 1 gpm per tank and that 33-psig steam is required for 0.5 gpm.

A mockup of critical HRT components will test the engineering operation of the high-pressure loop and the let-down system. Essentially all parts are now on hand, and assembly has started. The 80-kw test-model steam-condensing heat exchanger reported previously has been completed and shipped. A report covering fabrication, inspection, and testing techniques will be issued.

1.5 Controls and Instruments. The instrument engineering flow sheets have been completed, together with layout and design of the control and auxiliary rooms.

[redacted]

The HRT control-circuit proposal has been issued, and the design criteria for the instruments inside the main shield have been established.

Testing verified the acceptability of the thermocouple-material selection and indicated that a satisfactory electropneumatic transducer has been developed.

The valve designs for the low-pressure and high-pressure valves are shown, and data collected from bellows tests are given.

Instrument purchase is approximately 60% complete, and the cost of the installed instruments is estimated at about $300,000.

PART II. THORIUM BREEDER REACTOR

2. Conceptual Design

2.1. Design Program Objective. An analysis of the relative effects of major process variables on the economics and characteristics of two-region thorium breeder reactors is nearing completion, and the results to date are presented in this report. From these results most of the major reactor characteristics have been determined; they are reported with certain other engineering studies pertinent to the early phases of the program.

2.2 Reactor Analysis. The results of calculations for over 100 reactors show that the net unit cost of electrical power is only slightly affected by rather large changes in process variables. For reasonable ranges of the major variables, the unit cost varies only about 0.4 mill/kwhr for an average reactor temperature around 280°C.

At the apparent economic optimum conditions, the core power densities rise to nearly 400 kw/liter. Therefore it is probable that operation at the economic optimum will be limited by engineering or chemical considerations. However, this is not serious in view of the insensitivity of the unit cost to changes in the process variables. Power density could be lowered to 150 kw/liter with only a negligible effect on costs. Increasing the average reactor temperature from 280 to 320°C reduces the cost by only 0.1 mill/kwhr. Increasing the thorium blanket concentration from 1000 to 1500 g/liter reduces the cost by only a negligible amount (0.02 mill/kwhr), and the difference between 500 and 1500 g/liter is only 0.15 mill/kwhr. Even for 500 g/liter, the breeding ratio is greater than unity. The costs for power are relative only and should not be interpreted as predicting presently attainable costs.

2.3 Engineering Studies. In order that cost estimates for the TBR may be placed on a firmer basis and all engineering problems defined, a preliminary design of a 300-Mw (electrical) power station, utilizing three reactors and containing its own fuel and blanket reprocessing facility, has been undertaken. As a first step, the selection of the design characteristics of a particular reactor was based on proved performance of components and systems wherever possible and on the cost optimization calculations performed on the ORACLE. The reactor consists of a 5-ft-dia core containing uranyl sulfate in heavy water and a $2\frac{1}{4}$-ft blanket of thorium oxide slurry in heavy water. The slurry contains 1000 g of thorium per liter and 3 g of U^{233} per kilogram of thorium. Core and blanket heat generation are 313 and 72 Mw, respectively, to yield 100 Mw (electrical) on an assumed net station efficiency of 26%. Core and blanket processing cycles of 200 and 150 days, respectively, have been chosen.

Since the fissionable material produced by breeding in the TBR appears in the blanket and contributes to power generation immediately, an economic comparison was made between starting up a reactor at reduced power with no fissionable material initially in the blanket and starting up at full power with the blanket fissionable-material inventory initially supplied. Because the time required to establish the blanket fissionable-material concentrations by breeding alone exceeds the blanket doubling time under steady-state conditions, there is a net gain in U^{233} production which makes startup at full power appear to be more economical.

Studies of xenon removal by entrainment with dissociated D_2 and O_2 leaving the core system were completed for the case of recombining the D_2 and O_2 at low pressure and pumping the condensate back into the circulating system and the case where the D_2 and O_2 are recombined at high pressure. In the low-pressure system there is virtually complete removal of the xenon, whereas there is only partial removal in the high-pressure system. However, the choice of high- or low-pressure recombination will depend on the relative investments and operating costs, since the xenon poisoning can be evaluated in terms of slightly increased cost of power.

To facilitate optimization of equipment design, layout, and piping studies, engineering and cost

[redacted]

data pertinent to TBR design are being compiled in consistent units for scaling. To date, cost and thermodynamic data for heavy water and solutions of uranyl sulfate in heavy water have been correlated with concentration and temperature, assuming $40 per pound for heavy water and $20 per gram for highly enriched uranium. Cost curves in relation to size and strength (or capacity) for pressure vessels, heat exchangers, and stainless steel welding, piping, and fittings have also been prepared.

A preliminary examination has been made of the thermal stresses which could occur in the reactor pressure vessel because of radiation absorption, and the stresses have been determined in relation to vessel thickness both with and without a steel thermal shield. For a design pressure of about 2500 psia it appears that the combined thermal and pressure stresses can be held to acceptable values by placement of a 4-in.-thick steel thermal shield just inside the vessel but spaced sufficiently to allow circulation of the blanket fluid between the shield and vessel wall for cooling.

PART III. CORROSION

3. Pump-Loop Corrosion Tests

3.1 Pump-Loop Operation and Maintenance. One loop was removed from service and cross sectioned for inspection of the internal surfaces. This loop was of type 347 stainless steel pipe and had a cumulative operating time of more than 12,000 hr with uranyl sulfate solutions varying in concentration from 0.004 to 1.34 *m*. No excessive or localized corrosion attack was noted except in one highly turbulent area immediately downstream from the in-line corrosion sample holder.

Two new 100A pump loops have been designed to circulate thorium oxide slurries. These loops will be used to evaluate corrosion and/or erosion of these slurries with corrosion specimens similar to those now in use in the uranyl sulfate studies.

Several unsuccessful attempts were made to pump thorium oxide slurry in an in-pile type of loop designed for solutions. These tests have been terminated pending further studies of thorium oxide slurries and the design requirements for maintaining circulation.

3.2 Results of Loop Tests. The corrosion resistance of types 347 and 304L stainless steel to 0.06 *m* uranyl sulfate containing 0.006 *m* sulfuric acid has been determined at 200 and 225°C. The observed corrosion rates were intermediate between those for 0.02 and 0.17 *m* uranyl sulfate at the same temperature; and, as at the other concentrations, type 347 stainless steel was superior to type 304L in that the critical velocity was higher. The oxide scale formed on the stainless steel specimens under the above conditions contained at least some hydrated iron oxide, as has been the case at all other uranyl sulfate concentrations investigated.

The beneficial action of chromate ions in uranyl sulfate–stainless steel systems has again been demonstrated. In 0.02 *m* uranyl sulfate at 250°C and high flow rates, stainless steel corroded at a low rate if chromate ions were present but at a relatively high rate if they were absent. Also, in one run at the 0.11 *m* level, the corrosion rates were very low as a result of the very high concentration of hexavalent chromium in solution. Other runs under identical conditions with lower chromate-ion concentrations gave considerably higher corrosion damage.

4. Radiation Corrosion

4.1 Static-Bomb Studies. Studies of the effect of reactor radiation on the corrosion of Zircaloy-2 by uranyl sulfate solutions were initiated. In two of the four in-pile experiments that have been made, the solutions were approximately 0.16 *m* in UO_2SO_4 and 0.02 *m* in $CuSO_4$. The fission power density was about 5 w/ml when the LITR was operating at 3 Mw. The results of oxygen-consumption measurements in these experiments indicate corrosion rates of approximately 9 mpy during irradiation at the maximum reactor power. For each experiment, the total oxygen which had been lost at any time was roughly proportional to the total fission energy which had been dissipated within the bomb. Pin corrosion specimens from the bombs indicate a total corrosive penetration in fair agreement with that calculated from oxygen data.

The third in-pile experiment was with a solution of roughly twice the above concentration of UO_2SO_4 and $CuSO_4$. The estimated fission power density was 8 w/ml when the LITR was at 2.5 Mw. The oxygen-consumption data indicate little difference in corrosion rate between this and the system of lower uranium concentration.

The fourth experiment, now in operation, is a duplicate of the first two except that H_2SO_4 was added to the solution. A corrosion rate of about

[redacted]

6 mpy is indicated by the results to date.

Comparable out-of-pile experiments with Zircaloy-2 gave corrosion rates of 0.5 mpy or less.

The number of radiation facilities for this work in the LITR is being increased. Conceptual-design studies of an MTR experiment have begun.

4.2 In-Pile Loop. In-pile loop CC was dismantled in the remote-handling facility to check procedures and equipment; this loop had not been irradiated but was otherwise an exact duplicate of the in-pile loops for which the facility was designed. The corrosion specimens and loop parts were examined for corrosion damage. Some pitting type of corrosion was found on the specimens (type 347 stainless steel) exposed to the highest velocity of approximately 45 fps. Excessive corrosion attack was also found around the impeller discharge holes.

The successful completion of the in-pile loop development program and the initiation of the in-pile loop radiation-corrosion program came during the quarter with the first in-pile experiment in the LITR. Loop DD, after out-of-pile testing in the mockup, was installed in beam hole HB-4 of the LITR, and a radiation-corrosion experiment of 465.5 hr was carried out. During most of the run the LITR was operating at full power. Operation of the loop was very smooth, and the loop package was withdrawn at the conclusion of the run as scheduled. The stainless steel and zirconium specimens are being removed for metallurgical examination.

Two additional in-pile loops (EE and FF) have been built. One of them, loop FF, in which Zircaloy-2 corrosion specimens have been used instead of type 347 stainless steel, is now under test in the mockup. Loop FF will be installed in hole HB-4 at the LITR for the second in-pile test, replacing loop DD.

Bearings in the in-pile circulating pumps are now hardened type 17-4 PH stainless steel and Graphitar. The 17-4 PH stainless steel was substituted for the Stellite 98M2 to eliminate introduction of cobalt in the circulating solution. A continued effort is being made to improve the over-all reliability of the pumps.

5. Laboratory Corrosion Studies

No acceleration of corrosion attack by electrochemical couples between various Stellites and type 347 stainless steel was found at 100°C in oxygen-pressurized 0.17 *m* uranyl sulfate solutions, some of which contained 0.01 *m* cupric sulfate. Stellite 98M2 showed a diminishing rate of attack of 1 to 2 mpy, while Stellites 6 and 12 did not show significant attack. Stellite 12, and particularly Stellite in the form of torch-applied hard-facing on type 347 stainless steel, exhibited extremely severe pitting attack in a number of cases, while no attack occurred on similar specimens from other sources. Heliarc-applied hard-facing of Stellites 6 and 12 on type 347 stainless steel showed no significant attack. In general, the attack appeared to be only slightly greater in solutions containing copper.

Thermocouple materials attached to type 347 stainless steel were exposed for 100 hr in aerated Oak Ridge tap water at room temperature, simulating conditions expected in the HRT tank when it is flooded during shutdown for maintenance. Corrosion data, quantitative and visual, showed the iron-constantan couple to be unsatisfactory, while Chromel-Alumel and copper-constantan couples exhibited satisfactory performance.

Aluminum oxide, proposed as a bearing material for small canned-rotor pumps, exhibited good corrosion resistance to 0.17 *m* uranyl sulfate solutions over the temperature range 150 to 250°C.

Tap-water corrosion of carbon-steel nuts on stressed stainless steel bolts gave voluminous amounts of rust but did not result in galling and is not regarded as serious for the HRT.

Some early analyses indicated the presence of relatively large amounts of chlorine (0.1 to 0.4%) in Graphitar No. 14 bearings. More recent analyses have shown the chlorine content to be of the order of 100 to 200 ppm (0.01 to 0.02%), corresponding to about 20 to 40 mg of chlorine in the bearings of the size used in canned-rotor pumps. There is no evidence that gamma irradiation at room temperature removed appreciable quantities of the chlorine from the Graphitar.

Thoria slurries prepared from Ames 100-mesh thorium oxide have been circulated in small toroids of type 347 stainless steel. Suitable oscillation of the toroids causes circulating-slurry slugs to impinge on pin specimens inserted across the flow. Tests at 250°C and 26 fps with slurry concentrations of 90 to 1000 g of thorium per kilogram of water showed little effect on titanium 75A and Zircaloy-2, small weight gains generally being observed. The corrosion rate of type 347 stainless

steel under these conditions was twice as great under a helium atmosphere as that observed when 40 ppm of oxygen was present. The rate decreases further with increasing oxygen concentration up to 600 ppm. The toroids showed significantly different corrosion rates for slurries of thorium oxide prepared by Lindsay and by Ames.

PART IV. ENGINEERING DEVELOPMENT

6. Development of Fuel-System Components

The electrical control and power circuits of the high-pressure recombiner loop were completed during the past quarter. The high-pressure hydrogen-oxygen electrolytic cells, which have been operated at atmospheric pressure and have given no trouble, will next be tested at high pressure prior to initiation of the actual experimental program.

A loop for testing the performance and useful life of dump valves and trims is being designed.

Negotiations are continuing with the Allis-Chalmers Mfg. Co. for the construction of the 500-gpm canned-rotor pump and the 20-cfm canned-rotor gas circulator. The contract has been delayed because of a decision to use solid-wire conductors with an auxiliary cooling system, since hollow conductors will not be desirable in future large pumps.

The ORNL gas circulator has been calibrated for operation at electrical frequencies of 60 to 120 cps. A series of 30 starts and stops has also been performed. It has been found that the circulator will not operate satisfactorily for extended periods of time when it is circulating completely noncondensable gas because the bearings will begin to run dry.

The ORNL 5-gpm pump, which has operated in an endurance test to determine the life expectancy of the various parts, has run for a total of about 4500 hr while circulating water at a temperature of 250°C.

Development is nearing completion for tube-joint welding (in which manual techniques are used) for the 50-Mw main fuel heat exchanger. A series of corrosion studies has been performed on weldments fabricated by Foster Wheeler Corp. containing various percentages of ferrite. Investigation of high-frequency, ultrasonic, and x-ray tube-testing methods is continuing. Cost information on tube sheet machining, tube-joint preparation and welding, stainless steel tubes, steam-drum fabrication, and other exchanger construction and testing costs relating to a 300-Mw heat exchanger have been supplied to the ORNL Engineering Design Section by Foster Wheeler Corp.

A single U-tube heat exchanger is being built to obtain heat-transfer data. A velocity of 20 fps and a concentration of 6 g of uranium per kilogram of solvent have been tentatively selected as operating conditions.

The past quarter has been devoted to debugging the components of the 4000-gpm loop and to adjusting instrument settings for smoother operation. The loop operates at 1000 psi and heats to 250°C in about 2 hr. The system has been operated intermittently to test the effect of thermal cycles on the tightness of the flanges.

The feed-pump loop, which had been operated with Ames ThO_2 slurry, was charged with Lindsay thoria; subsequently, valve erosion rates increased greatly. Tests with thoria from a third source (ORNL) are now being performed.

7. Development of Blanket-System Components

7.1 Slurry-Component Development. A specially designed Allis-Chalmers 5-gpm slurry pump with fluid-piston bearings failed because of accumulation of solids in stagnant regions of the pump.

The type and degree of circulation and solids accumulation expected in proposed HRT pressurizers are being studied in room-temperature glass systems.

Studies of slurry flow through a mockup of the HRT pressure vessel have led to methods for preventing stagnant regions and for reslurrying solids which settle out during a shutdown.

7.2 HRT Blanket Mockup. Essentially all the preliminary drawings for the HRT mockup have been completed, and requisitions for a major part of the materials have been placed.

7.3 Slurry-Circulation Studies. In addition to confirming the beneficial effects of oxygen on stainless steel in a slurry-circulating system, slurries containing several milligrams of $Th(SO_4)_2$ per gram of thorium were found to attack stainless steel apparently less than those with lower sulfate content. However, there was also evidence that higher sulfate content may cause formation of a soft cake in relatively stagnant regions.

7.4 Mechanical Properties of Slurries. When being pumped at high temperatures, many of the thorium oxide slurries change from low-viscosity Newtonian fluids to Bingham plastics or pseudo-

plastics with very high, effective, viscosities at low rates of shear, when cooled to room temperature. A number of additives have been found which appear to reconvert the slurries to low-viscosity Newtonian fluids. Among these are oxalic acid and sodium silicate. There appears to be a correlation between the sulfate content of the slurry and the amount of silicate required to reduce the effective viscosity at room temperature to a reasonable value.

7.5 Boiling Studies. A new method of correlating data on vapor-rise rate in a vapor-liquid mixture indicates that the diameter of the vessel is not so important as was thought previously. Steam-water data up to 40 atm and air-water data at atmospheric pressure can be correlated, but the influence of physical properties is still not clear.

ThO_2 slurries have been boiled in a volume-heated, natural-circulation loop, with little difference from ordinary boiling liquids being noted except for settling in low-velocity regions.

Corrugated-plate-type vapor separators permitted a large entrainment of vapor in the exit liquid phase in work performed under subcontract by The Babcock & Wilcox Co.

Work has been completed under subcontract at the University of California on density transients during a power pulse in a volume-heated boiling system, and a final report has been prepared.

8. Experimental Valve Program

Two makes of bellows for sealing 2000-psi valves have been received. One type of bellows, made and tested by Breeze Corporations, Inc., has withstood 3600 psi of external pressurization without being distorted; it is being incorporated into three ½-in. experimental valves. Two similar 1-in. bellows-sealed valves will be delivered later for possible use as HRT blanket dump valves. Four sets of experimental valve trim and a valve body have been completed in the ORNL shops. A second type of bellows has proved unsatisfactory and is being redesigned by the manufacturer.

9. Metallurgy

Several weld-design combinations have been proposed for the final girth-closure weld on the carbon-steel pressure vessel (clad with type 347 stainless steel) for the HRT; this closure is complicated by the requirement that the weld be made entirely from the outside. Tests of six proposed weld designs have been made on available clad material. The completed welds have been radiographed and are being examined metallurgically and tested mechanically.

Metallurgical examination has been made of dynamic-corrosion-loop test weld pads to observe the effect of ferrite content on the corrosion resistance. The results demonstrate that ferrite content is not the sole controlling factor under the conditions of these tests, but they have not conclusively eliminated ferrite content as a contributory variable.

Stress-corrosion tests, in boiling concentrated magnesium chloride solutions, have been made on simulated tube-to-tube-sheet assemblies, in which the degree of expansion by rolling was the variable. These tests indicated that lighter expansions lessen susceptibility to stress-corrosion failure.

The program to evaluate, by means of impact testing, the possibility of hydrogen contamination and consequent embrittlement of titanium exposed to various simulated homogeneous reactor conditions has continued. Previous tests on samples exposed for varying periods of time to several concentrations of uranyl sulfate in corrosion test loops have given no indication of any increased impact brittleness beyond that already present in the unexposed material. Recently, however, an increased impact-brittleness susceptibility has been observed for the first time in an unalloyed-titanium specimen holder, exposed over a period of almost 2000 hr at 250°C to several concentrations of uranyl sulfate and a variety of additives, in addition to frequent cathodic defilming. Although the brittle transition temperature of the material was increased after the prolonged exposure, chemical and vacuum analysis did not reveal any increase in the hydrogen content. A metallurgical investigation is now being made into the possible causes and prevention of this embrittling behavior.

PART V. CHEMICAL ENGINEERING DEVELOPMENT

10. Slurry Fuel and Blanket Studies

The development of an aqueous thorium oxide slurry for use in the blanket of a thermal power breeder has continued. Emphasis is now being placed on a study of the properties of slurries under irradiation, radiolytic gas production, gas recombination, and radiation damage.

Thorium dioxide of sufficient purity to meet tentative specifications for use in a homogeneous reactor blanket has been made in 5-kg lots. The process consists in precipitating thorium oxalate from thorium nitrate and calcining the oxalate first at 370°C and then at 650°C.

A thorium oxide slurry containing 8% U^{235} as the oxide was irradiated for six days in the Graphite Reactor at a fission density of about 1 kw/liter. Slurry and gas-phase temperatures were 290 to 300°C and 200 to 250°C, respectively. Radiolytic gas pressures varied between 1000 and 2000 psi and varied inversely with the gas-phase temperature.

The addition of either uranium oxide or copper oxide to the thorium oxide slurries enhanced catalytic activity for the recombination of hydrogen and oxygen over that of thorium oxide alone. A mixed thorium oxide–copper oxide slurry containing 530 g of thorium per kilogram of water and 0.1 *m* CuO recombined hydrogen with oxygen at a rate which should be sufficient to maintain at 2000-psi total pressure a slurry blanket dissipating 6 kw of fission heat per liter at 300°C.

A concentrated thorium oxide slurry (prepared from thorium formate), which had become plastic upon being pumped at 250°C and cooled to room temperature, became fluid upon the addition of 0.01 *m* $Na_2O(SiO_2)_2$. Sodium carbonate, sodium pyrophosphate, and sodium hexametaphosphate were also found to be good dispersing agents for thorium oxide slurries. Particle-size analyses and x-ray diffraction studies of the pumped material and the effectiveness of deflocculents in restoring fluidity to the pumped slurry suggest that the increase in viscosity during pumping results primarily from a degradation of the slurry particles and subsequent flocculation of the fragments.

Electron-diffraction studies of hydroxide precipitated from thorium formate showed it to be crystalline as precipitated, or after drying, or when autoclaved in water at 250°C, although x-ray diffraction patterns of similar materials had indicated them to be amorphous.

11. Plutonium-Producer Blanket Processing

Addition of 0.4 *m* sulfuric acid increases Pu(IV) solubility in 1.3 *m* uranyl sulfate at 250°C to about 100 mg per kilogram of water.

In a series of experiments designed to study the adsorption of plutonium on materials of construction, two type 347 stainless steel containers adsorbed plutonium to the extent of 0.06 and 0.11 mg/cm^2 and two titanium vessels adsorbed 0.18 and 0.21 mg/cm^2 with no indication that equilibrium had been reached. Plutonium adsorption on a zirconium container appeared to have reached equilibrium at about 0.03 mg/cm^2.

Plutonium(IV) oxide calcined at 825°C can be dissolved in concentrated nitric acid containing ammonium hexanitratocerate. At least tracer amounts of neptunium were adsorbed from 0.1 *m* uranyl sulfate on manganese dioxide.

12. Fuel and Thermal-Breeder Blanket Processing

The study of the behavior of rare-earth sulfates has been extended from small-scale laboratory equipment (10 ml to 1 liter) to a larger scale test in a circulating loop (10 liters). As in the small-scale experiments, the equilibrium solubility of cerous sulfate in simulated homogeneous reactor fuel solution was less than 0.01 g per kilogram of H_2O.

Rare-earth sulfates, traced with Nd^{147}, which had been coprecipitated with iron and chromium hydrous oxides at 280°C, did not redissolve immediately when the simulated homogeneous reactor fuel was cooled rapidly to room temperature. Removal of the rare-earth sulfates from a simulated homogeneous reactor fuel solution by centrifugation at room temperature therefore may be possible.

Iodine was removed from a simulated uranyl sulfate fuel solution by heating the solution to the neighborhood of 300°C and contacting the gas phase, which contained air, above the solution with a metallic silver wire or silver-impregnated Alundum chips. Iodine removals as high as 80% were obtained, and the amount removed was independent of the initial oxidation state of the iodine.

In further liquid-solid separation studies with 0.25-in.-dia hydroclones, about 90% of water-suspended ThO_2 particles 0.7 to 8 μ in diameter were recovered in the underflow at feed rates of 0.8 to 1.0 gpm. With a 0.25-in.-dia hydroclone at a feed rate of 0.2 gpm and similar conditions otherwise, an efficiency of 95% was obtained. Comparison of these data with those obtained from a 0.5-in.-dia hydroclone indicates that the 0.25-in.-dia hydroclone is superior to the larger unit. The rate of 0.2 gpm with the 0.25-in.-dia hydroclone is near the proposed rate for the HRT chemical processing

plant and for the final stage of a full-scale TBR processing hydroclone cascade.

Test loop A has been put into operation to study sampling devices and to determine the physical properties of the rare-earth sulfates and other solids expected in the homogeneous reactor uranyl sulfate fuel. Test loop B, for testing the hydroclones at high temperature and pressure, has been designed and is being constructed.

13. Decontamination of the HRE

The principal radioactivity on metal specimens that had been in the HRE circulating-fuel system and then decontaminated with nitric acid and alkaline-tartrate-peroxide solution was due to niobium and zirconium. This remaining activity could be removed only by removing the corrosion film from the metals.

14. Work of Vitro Laboratory

Pilot-plant equipment has been set up to study the precipitation of fission and corrosion products from aqueous solutions at elevated temperatures.

In studies on simulated uranyl sulfate fuel solution containing iodate, a high percentage of the iodine was removed from either the solution or vapor phase by contact with silver at about 300°C.

PART VI. SUPPORTING CHEMICAL RESEARCH

15. Radiation Chemistry Studies

Yields for chromate reduction in fissioning and nonfissioning solutions exposed to mixed reactor radiation at temperatures around 100°C and in the absence of dissolved oxygen have been measured.

Yields of hydrogen and nitrogen from reactor-irradiated high-concentration solutions of thorium nitrate have been revised upward from previously reported values to 0.2 and 0.02 molecules, respectively, produced per 100 ev of energy absorbed. The nitrogen appears not to be produced via the nitrite ion but probably comes from direct dissociation of the nitrate ion.

16. Effective Capture Cross Section of Np^{239}

The effective capture cross section of Np^{239} for thermal reactor neutrons, previously reported as being less than 100 barns, is presently reported as 80 ± 20 barns. That for Pu^{239} is presently reported as 380 ± 40 barns.

17. The System UO_3-SO_3-H_2O

Continued work on the pressure-volume-temperature-composition relationships in the two-liquid-phase region of the system UO_3-SO_3-H_2O has produced data for the volumes of each of the three phases as a function of temperature and fractional filling for two stoichiometric system compositions. Several more compositions must be determined and pressure data must be obtained before a thermodynamic interpretation can be made.

18. The System NiO-UO_3-SO_3-H_2O

Solubility studies in the four-component system NiO-UO_3-SO_3-H_2O have shown that the surface representing saturation in the NiO-UO_3-rich portion of the composition space isotherm is essentially a plane surface at 25, 100, 175, and 250°C, respectively. The compositions of two new complex solid phases formed at 250°C have been partially fixed as $NiO{\cdot}UO_3{\cdot}SO_3{\cdot}xH_2O$ and $NiO{\cdot}2.3\text{–}2.5UO_3{\cdot}SO_3{\cdot}6H_2O$.

19. The Systems CuO-SO_3-H_2O and CuO-UO_3-SO_3-H_2O

Solubility studies in the CuO-rich portion of the system CuO-SO_3-H_2O at 25°C have failed to yield uniquely interpretable data. Work on this system and on the system CuO-UO_3-SO_3-H_2O will therefore be confined to temperatures above 100°C, where equilibrium is more readily obtainable.

20. The System UO_3-CrO_3-H_2O

A series of static-corrosion tests with a uranyl chromate solution at 265°C has indicated that corrosion of carbon steel is less than that with uranyl sulfate solution by a factor of 25 to 70. On type 304 stainless steel the chromate was less corrosive than the sulfate by a factor of 30 when no oxygen was added to the system. In the presence of oxygen the two solutions did not show a measurable difference, both giving extremely low corrosion rates.

21. Concentration of N^{15}

Distillation of liquid nitrogen or of liquid ammonia does not appear to offer a competitive method for the separation of nitrogen isotopes because of the low separation factors involved and the expense of low-temperature operations.

[redacted]

Column studies of the proposed closed-cycle ammonia–ammonium carbonate system have established the separation factor for the system under the conditions specified to be approximately 1.015. This separation factor is quite good for operation at atmospheric pressure and, along with the high concentration of total ammonia in the aqueous phase and the possibility of a closed-cycle reflux, supports an optimistic view of this system for the low-cost production of concentrated N^{15}.

[redacted]

[redacted]

[redacted]

[redacted]

CONTENTS

SUMMARY vii

PART I. EXPERIMENTAL REACTORS

1. HOMOGENEOUS REACTOR TEST 3
   1.1 Project Status 3
      1.1.1 Installation 3
      1.1.2 Cost estimate 3
   1.2 Design 6
      1.2.1 General design considerations for the HRT 6
      1.2.2 Flow sheets and design data 6
      1.2.3 Reactor cells 9
      1.2.4 Reactor equipment 9
   1.3 Nuclear Calculations 18
      1.3.1 Safety considerations 18
      1.3.2 Optimum temperature for the experimental determination of the breeding ratio in the HRT 23
      1.3.3 Argon activation in operator air of HRT valves 23
      1.3.4 Shielding over steam drums 24
      1.3.5 Neutron streaming through cracks between the top shield plugs 24
   1.4 Component Development 24
      1.4.1 Core hydraulic studies 24
      1.4.2 Core-vessel development 24
      1.4.3 Pump development 27
      1.4.4 Fuel and blanket pumps 27
      1.4.5 Injection pump 27
      1.4.6 Fluid flow in HRT pressurizer 30
      1.4.7 Test of HRT dump-tank evaporator and entrainment separator 32
      1.4.8 Mockup loop 33
   1.5 Controls and Instruments 33
      1.5.1 General design 33
      1.5.2 Component development and testing 33
      1.5.3 Valves 37
      1.5.4 Instrumentation costs 38

PART II. THORIUM BREEDER REACTOR

2. CONCEPTUAL DESIGN 43
   2.1 Design Program Objective 43
   2.2 Reactor Analysis 43
      2.2.1 Method and conditions of calculation 43
      2.2.2 Results 44
      2.2.3 Effect of substantial errors in some of the two-group constants upon the TBR calculations 47
      2.2.4 Comparison of multigroup and two-group breeder reactor calculations 48
   2.3 Engineering Studies 48
      2.3.1 Selection of reactor characteristics for preliminary design 48
      2.3.2 Comparison of two methods for starting up the TBR 50
      2.3.3 Xenon-removal problem 53

[redacted]

[redacted]

2.3.4 Correlations of engineering data 54
2.3.5 Preliminary study of pressure-vessel design 56

PART III. CORROSION

3. PUMP-LOOP CORROSION TESTS 63
3.1 Pump-Loop Operation and Maintenance 63
3.1.1 Loop status 63
3.1.2 Westinghouse 100A pumps 65
3.2 Results of Loop Tests 67
3.2.1 Introduction 67
3.2.2 Results 67
3.2.3 Discussion 78
3.2.4 IBM corrosion file 80

4. RADIATION CORROSION 81
4.1 Static-Bomb Studies 81
4.1.1 Zircaloy-2 81
4.1.2 LITR experimental facilities 86
4.1.3 MTR in-pile experiment 86
4.2 In-Pile Loop 87
4.2.1 LITR operations 87
4.2.2 HB-4 mockup 87
4.2.3 Loop package testing 88
4.2.4 In-pile pumps 91
4.2.5 Radioactive specimen evaluation 92

5. LABORATORY CORROSION STUDIES 93
5.1 Corrosion of Thermocouple Wires by Filtered Water at Room Temperature 93
5.2 Tap-Water Corrosion of Carbon-Steel Nuts 93
5.3 Corrosion of Aluminum Oxide Bearing Material by Uranyl Sulfate Solution 95
5.4 Corrosion of Stellite–Type 347 Stainless Steel Coupons 95
5.5 Chlorine in Graphitar 97
5.6 Small-Scale Dynamic-Corrosion Program 100
5.6.1 General studies 100
5.6.2 Comparison of thoria slurries 102

PART IV. ENGINEERING DEVELOPMENT

6. DEVELOPMENT OF FUEL-SYSTEM COMPONENTS 109
6.1 Recombiner Development 109
6.2 Dump-Valve Test Loop 109
6.3 Small Reactor Components 110
6.3.1 Allis-Chalmers 500-gpm pump and 20-cfm gas circulator 110
6.3.2 ORNL gas circulator 110
6.3.3 ORNL 5-gpm pump 111
6.4 Large Reactor Components 111
6.4.1 50-Mw main fuel heat exchanger 111
6.4.2 Large heat exchanger 112
6.5 4000-gpm Loop 112
6.6 Slurry-Injection Pump Loop 114

[redacted]

[redacted]

7. DEVELOPMENT OF BLANKET-SYSTEM COMPONENTS 116

7.1 Slurry-Component Development 116
7.1.1 5-gpm pumps 116
7.1.2 Westinghouse 200A slurry pump 116
7.1.3 Pressurizer studies 116
7.1.4 Pressure-vessel studies 116
7.2 HRT Blanket Mockup 117
7.3 Slurry-Circulation Studies 117
7.4 Mechanical Properties of Slurries 123
7.4.1 Viscous properties of pumped thoria 123
7.4.2 Mechanism of viscosity increase upon pumping 124
7.4.3 Addition of dispersing agents 125
7.4.4 Effect of calcining temperature 126
7.5 Boiling Studies 126
7.5.1 Vapor transport in the mixture 126
7.5.2 Vapor separation 128
7.5.3 Density transients due to a power pulse 128

8. EXPERIMENTAL VALVE PROGRAM 130

9. METALLURGY 133

9.1 Welding Development 133
9.1.1 Welding development on 1-in. carbon-steel plates clad with type 347 stainless steel 133
9.2 Metallurgy of Corrosion 133
9.2.1 Dynamic corrosion of austenitic-stainless-steel weld specimens 133
9.2.2 Stress-corrosion cracking of austenitic stainless steels 134
9.3 Properties of Titanium and Zirconium Alloys 135
9.3.1 Commercial titanium 135
9.3.2 Bureau of mines titanium 138
9.3.3 Zirconium alloys 139

PART V. CHEMICAL ENGINEERING DEVELOPMENT

10. SLURRY FUEL AND BLANKET STUDIES 143

10.1 Preparation of Thorium Dioxide 143
10.2 Gas-Recombination Studies 143
10.3 Slurry-Irradiation Studies 144
10.4 Deflocculation of Thorium Oxide Slurries 145
10.5 Thorium Hydroxide Studies 146

11. PLUTONIUM-PRODUCER BLANKET PROCESSING 147

11.1 Solubility of Pu(IV) in Uranyl Sulfate Solutions 147
11.2 Dissolution of PuO_2 147
11.3 Adsorption of Plutonium on Stainless Steel, Titanium, and Zirconium 147
11.4 Particle Size of PuO_2 148
11.5 Neptunium Chemistry 149
11.6 Determination of Reactor Neutron Capture Cross Section of Np^{239} 149

12. FUEL AND THERMAL-BREEDER BLANKET PROCESSING 150

12.1 Fission-Product and Corrosion-Product Chemistry 150

[redacted]

[redacted]

12.1.1 Rare-earth solubility 150
12.1.2 Coprecipitation of rare earths with other elements 151
12.1.3 Iodine removal 151
12.2 Engineering Studies 151
12.2.1 Hydroclone liquid-solid cyclone separators 151
12.2.2 High-pressure test loops 153

13. DECONTAMINATION OF THE HRE 156

14. WORK OF VITRO LABORATORY 157

14.1 Pilot-Plant Modifications 157
14.2 Iodine Removal 157

PART VI. SUPPORTING CHEMICAL RESEARCH

15. RADIATION CHEMISTRY STUDIES 161

15.1 Reactor Irradiations of Chromate Solutions 161
15.2 Radiation Studies on Thorium Nitrate Solutions 161

16. EFFECTIVE CAPTURE CROSS SECTION OF Np^{239} 163

17. THE SYSTEM UO_3-SO_3-H_2O 164

18. THE SYSTEM NiO-UO_3-SO_3-H_2O 166

19. THE SYSTEMS CuO-SO_3-H_2O AND CuO-UO_3-SO_3-H_2O 168

20. THE SYSTEM UO_3-CrO_3-H_2O 171

21. CONCENTRATION OF N^{15} 177

21.1 Separation of Nitrogen Isotopes by Distillation 177
21.2 Exchange in the Ammonia–Ammonium Carbonate System 177

[redacted]

Part I

EXPERIMENTAL REACTORS

S. E. Beall

HRP QUARTERLY PROGRESS REPORT

1. HOMOGENEOUS REACTOR TEST

1.1 PROJECT STATUS

S. E. Beall
J. J. Hairston S. I. Kaplan

1.1.1 Installation

Delayed deliveries of material and revisions in component designs have necessitated moving the HRT construction schedule forward approximately two months. However, completion is still planned for late in the summer of 1955.

Bid awards totaling approximately $121,000 have been made on reactor construction materials, such as pipe fittings, flanges, etc. Awards for fabricated components to outside vendors, including pumps, pressure vessel, heat exchangers, condensers, etc., currently total about $265,000. The total amount of money currently obligated, including instrument commitments, is over $800,000, or roughly 80% of the projected expenditures for hardware.

Work orders have been initiated on all other major components, which are to be fabricated locally, so that labor time can be estimated and shop schedules can be established. Actual construction of these components will be possible as soon as stocks of large-diameter piping, currently being fabricated by Stainless Welded Products, Inc., New Jersey, are received. At the present time, two feed-pump reagent heads and two gas separators are being fabricated in the ORNL shops.

Installation of the reactor shield pit and control-room area is 40% complete. Approximately 500 yd^3 of concrete has been poured in the shield-tank foundation and control-area walls. Three months of working time will be required to install the steel walls and structural-steel framing. Figures 1.1 and 1.2 are photographs which show the progress of construction to October 29. The open area opposite the control area walls is the excavation for the chemical processing cells.

Figure 1.3 is an artist's concept of the completed HRT installation as viewed from the southeast corner of the building with the chemical processing cells in the center foreground. Underneath the high-bay area of the building is the reactor vessel, with the core process equipment on the left and the blanket equipment on the right. Covering the steel reactor cell are the concrete shielding plugs, in two layers with a gastight steel barrier in between. The HRE turbine-generator remains in the northwest corner.

The instrument and control area occupies four elevations, starting at the floor (28 ft below grade) of the reactor tank. The operating console is at ground level.

1.1.2 Cost Estimate

The estimated cost of the completed HRT is shown in Table 1.1. A finished-reactor cost of $1,840,000 is indicated. Except for the installation cost, which was estimated on the basis of

TABLE 1.1. ESTIMATED COST OF COMPLETED HRT

Process Components	
For core and blanket systems	$ 468,000
Pipe, fittings, and flanges to interconnect components	70,000
	538,000
Shield and Reactor Pit	
Steel cell, installed (contract)	223,000
Top shield plugs	75,000
Miscellaneous concrete work	28,000
	326,000
Instrumentation, Reactor	
Sensing elements and receivers	90,000
Valves and operators	60,000
	150,000
Heat Removal System	
Components	60,000
Valves, fittings, piping	25,000
Instrumentation	14,000
	99,000
Building Modifications	
Control-room area	52,000
Installation of Above Equipment	
Miscellaneous hardware	175,000
Labor plus overhead, 70 men for 10 months	500,000
	675,000
Total	$1,840,000

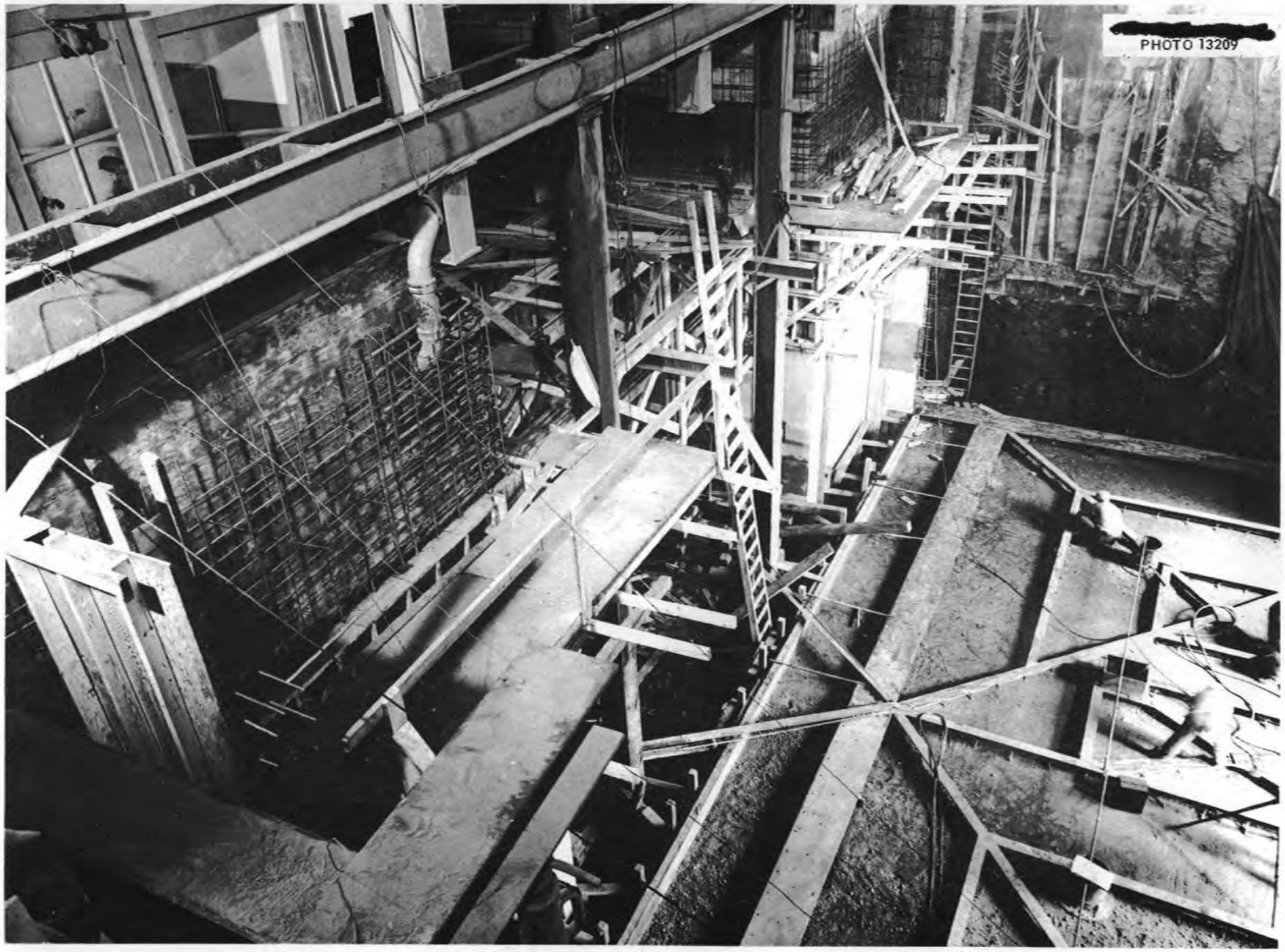

Fig. 1.1. Progress of Construction of HRT.

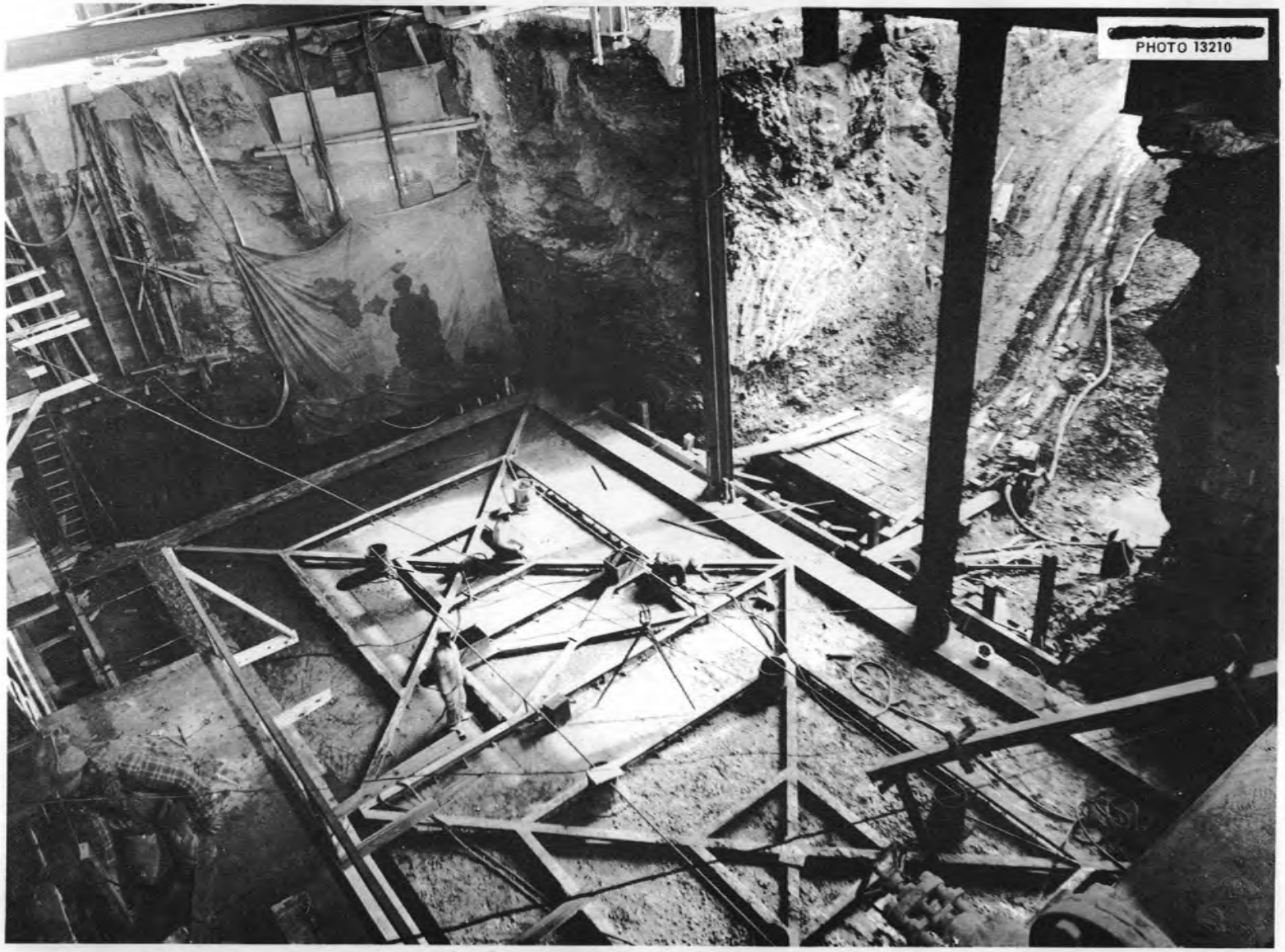

Fig. 1.2. Progress of Construction of HRT.

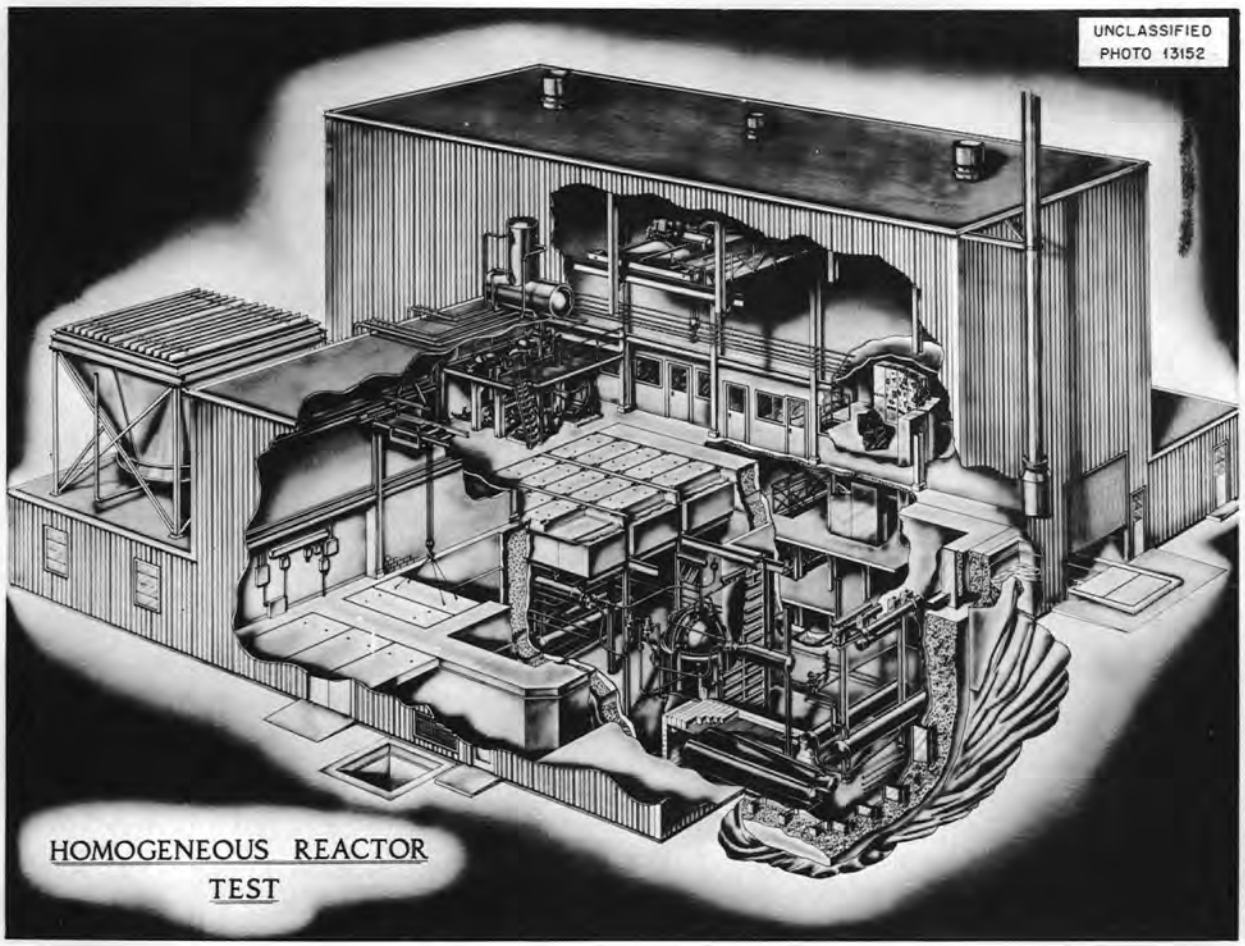

Fig. 1.3. Artist's Concept of the Completed HRT Installation.

HRE experience and other similar work currently in progress, all figures are firm, being based on actual quotations.

1.2 DESIGN

R. B. Briggs

R. E. Aven	R. G. Pitkin[1]
R. H. Chapman	J. N. Robinson
R. D. Cheverton	W. Robinson
W. R. Gall	C. L. Segaser
J. W. Hill, Jr.	W. Terry
T. H. Mauney	R. VanWinkle
J. R. McWherter	F. C. Zapp

1.2.1 General Design Considerations for the HRT

Design data, flow sheets, a plot plan for the area, drawings showing the general concept of the reactor building, the cell, and the general proposal for arrangement of equipment in the cell, and some equipment details were presented in the last progress report.[2] During this quarter the design of the reactor cell was completed. Detailing of all the major equipment in the reactor cell is nearing completion, and detailing of the piping and of mounting of equipment has begun.

1.2.2 Flow Sheets and Design Data

A continuing study of the HRT flow sheets and of information obtained in the design and development of the reactor equipment has resulted in some changes in the low-pressure core and blanket systems. The most recent flow sheet for the low-pressure systems is shown in Fig. 1.4. A major

[1]On loan from the Vitro Corp.

[2]R. B. Briggs *et al.*, *HRP Quar. Prog. Rep. July 31, 1954*, ORNL-1772, p 14 ff.

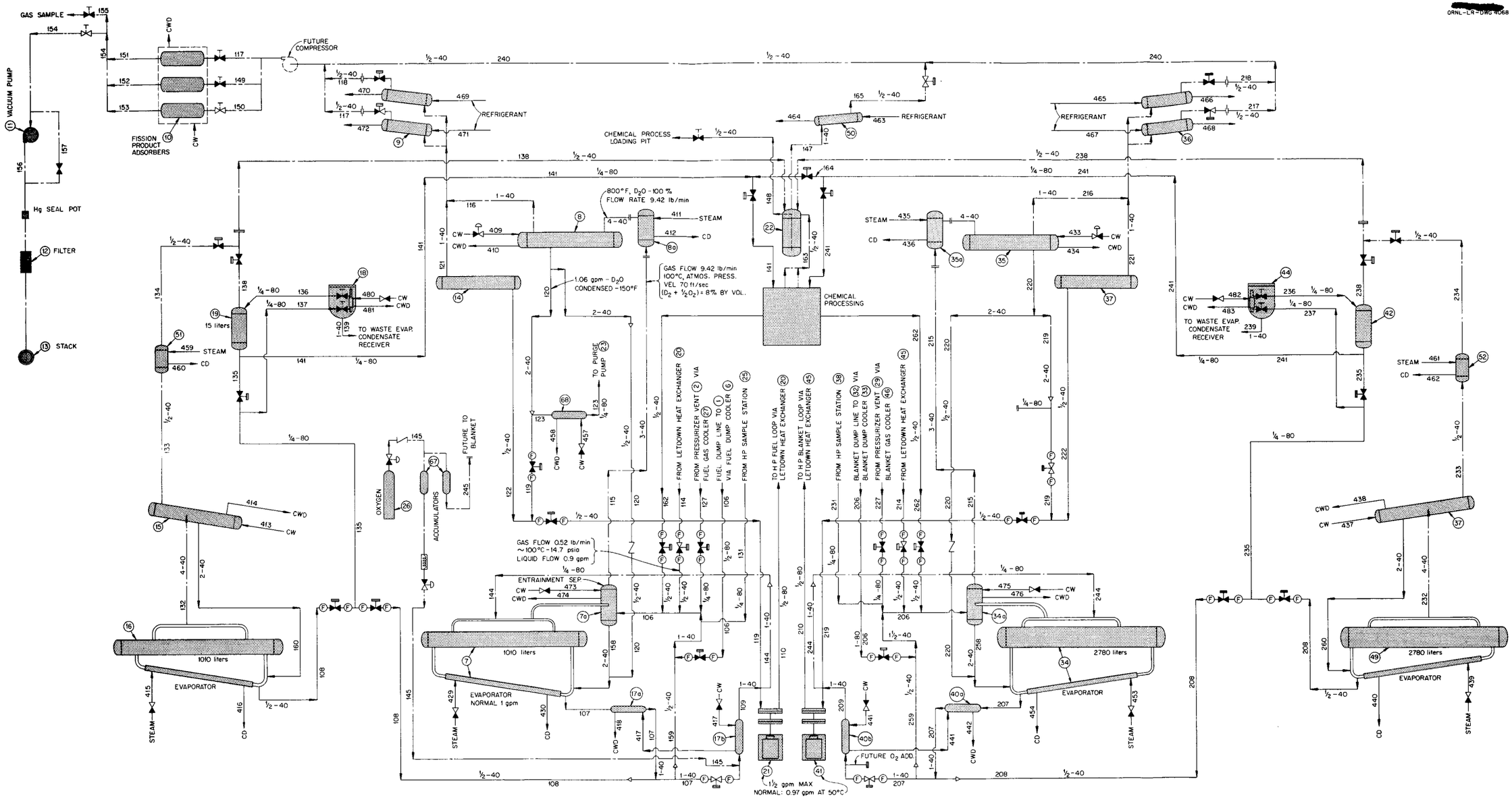

Fig. 1.4. HRT Low-Pressure Systems, Fuel and Blanket.

change is the addition of oxygen to the suction stream of the fuel feed pump. Formerly, oxygen was added to the reactor in the discharge from the fuel feed pump at a pressure of 2000 psi. Recent tests have demonstrated that as much as 300 to 400 cc of gas per minute can be added to the 1.5-gpm, low-pressure suction stream without seriously affecting the operation of the pump (cf. Sec. 1.4). There is evidence that the 80 to 100 ppm of oxygen that can be added is sufficient for chemical stability of the uranyl ion.

Minor changes have been made in the flow sheet to show in greater detail the waste lines, sampler lines, and connections to the chemical processing area.

1.2.3 Reactor Cells

The design of the tank which contains the reactor and associated equipment has been completed by the K-25 Plant Engineering Department, and the shop drawings are being prepared by the Chicago Bridge & Iron Co. A general description of the tank has been reported;[2] details of the construction are presented here.

The HRT reactor cell (Fig. 1.5) consists of a steel tank, designed and fabricated by the Chicago Bridge & Iron Co., with a roof of removable concrete blocks, designed by the K-25 Plant Engineering Department. The entire tank is erected on a structural concrete slab, which stiffens the bottom plates. The walls are of steel plate stiffened on the outside by structural shapes. Eight columns support the roof structure, and struts on the column lines just under the roof support the upper edge of the cell wall against pressure and vacuum loading.

The roof structure consists of two rows of girders, running east and west, which are connected to the columns and cell walls with shear pins. These girders, in turn, support the 5-ft-thick top shield, which runs north and south in two layers of slabs anchored by continuous shear keys to the upper edge of the girders. Details of these connections are indicated in Fig. 1.6.

The cell and roof structures have been designed to resist the normal operating pressure of –7.5 psig as well as a 30-psig positive pressure.

In order to prevent the release of radioactive materials in the instance of a reactor-vessel failure and a sudden positive pressure, a metal seal sheet is located between the two layers of roof plugs and will be seal welded in place to make the cell gastight.

A watertight partition divides the cell in half and permits flooding (shielding) of one side at a time. The center panel of this partition is a removable door, which will be stored outside the cell during normal operation; thus, if a reactor-pressure-vessel fracture should occur, the entire cell would absorb the released pressure.

1.2.4 Reactor Equipment

(a) Reactor Vessel and Core Tank. Although it was expected that the reactor design would be approved by November 1, some of the tests of gasketed joints, nozzle welds, girth welds, and collapsing pressures for the core tank remain to be completed before the design can be finished. The status of this development work is reported elsewhere (cf. Sec. 1.4).

(b) Main Heat Exchanger. Design of the HRT fuel and blanket heat exchangers, which are duplicate units, has been completed by Foster Wheeler Corp. and approved by ORNL. The only major change from the design reported previously[3] is the addition of a perforated baffle plate across the entire water surface to permit satisfactory operation at heat loads up to approximately 10 Mw (see Fig. 1.7). The final design data are shown in Table 1.2.

At present there is some uncertainty about the head-to-tube plate seal weld (see Fig. 1.8). A simplified stress analysis made at ORNL indicates that the joint lacks sufficient flexibility to withstand the calculated differential movement under operating conditions. A similar analysis by Foster Wheeler indicates that it will be satisfactory; consequently, Foster Wheeler is proceeding with further study of the problem in greater detail. In any event, the design selected for the joint will be satisfactorily proved before the heat exchanger is accepted.

Materials on a long-delivery schedule, such as the clad head and tube sheet forgings, tubes, and steel to be used for containment of high pressure, have been ordered. A considerable amount of extra inspection is being planned for the tubing for the dual purpose of improving tubing quality before exchanger fabrication and of proving inspection techniques. These inspection techniques are

[3] W. L. Ross, L. F. Goode, and R. E. Wascher, *HRP Quar. Prog. Rep. July 31, 1954*, ORNL-1772, p 35.

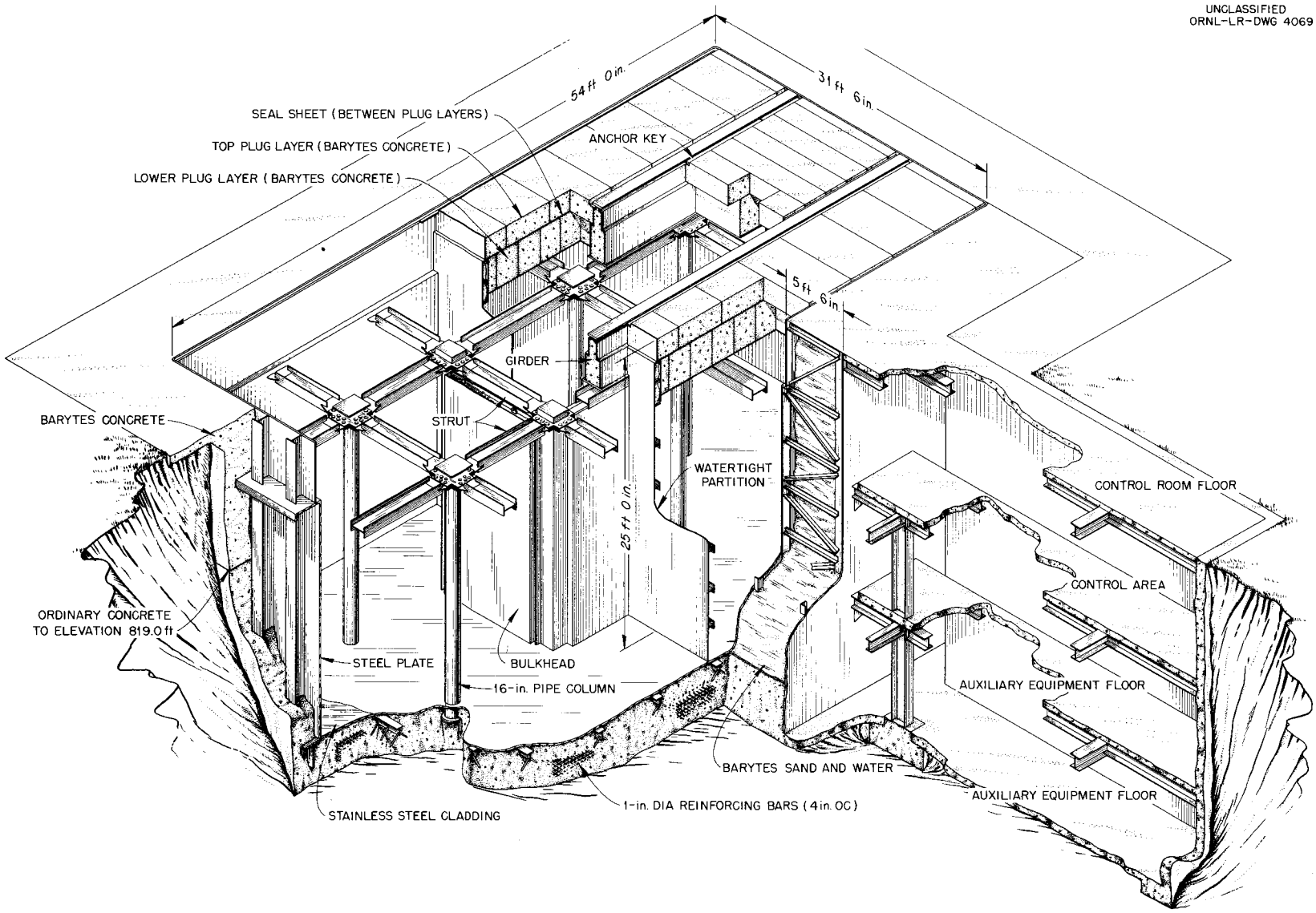

Fig. 1.5. Plan of Reactor Cell; North-South Section of Reactor Cell; East-West Section of Reactor Cell.

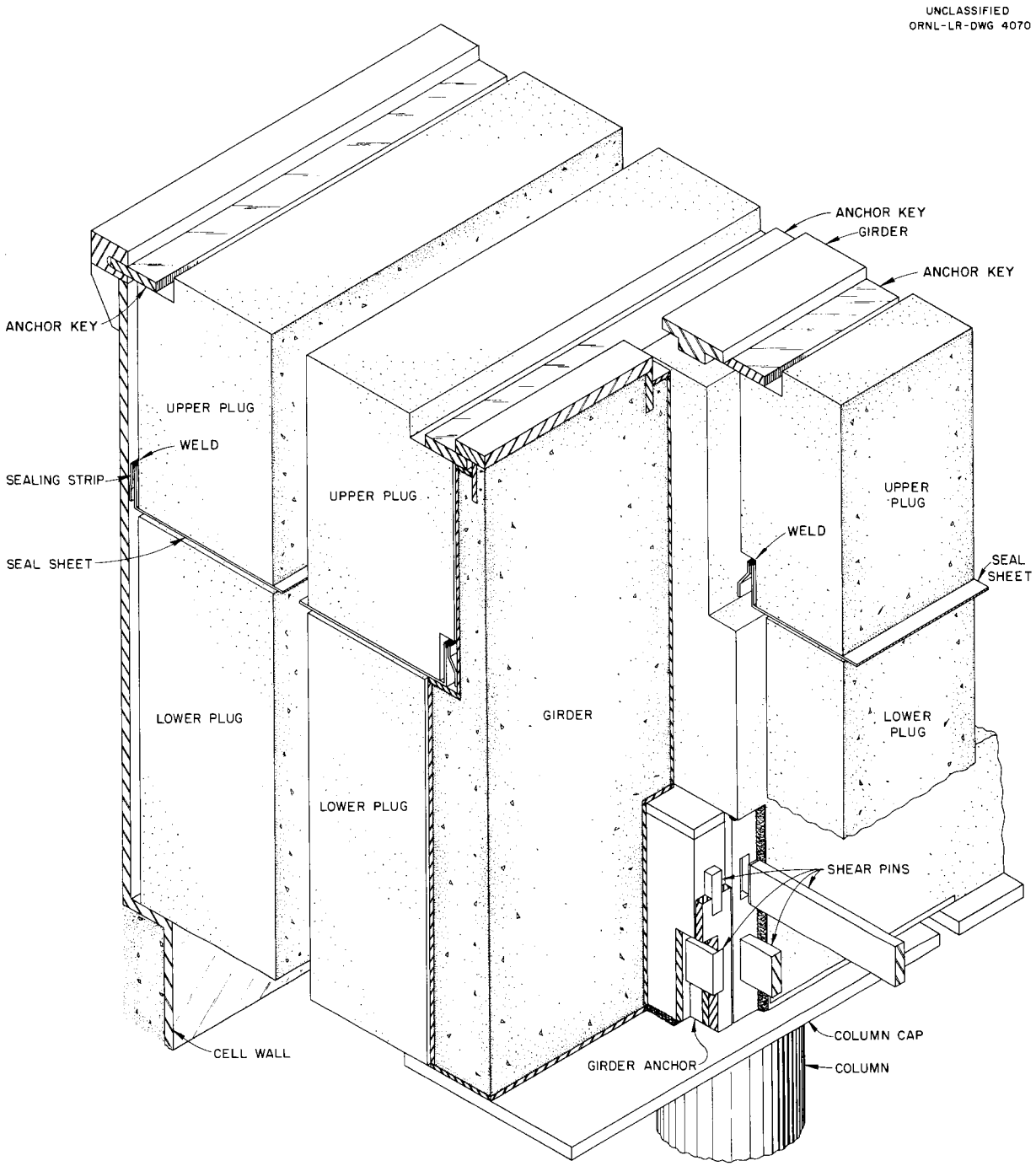

Fig. 1.6. Details of Cell Roof Structure.

TABLE 1.2. DESIGN DATA FOR THE HRT MAIN HEAT EXCHANGER

	Location			
	Shell Side			Tube Side
Temperature in, °F	180			572
Temperature out, °F	471			494.5
Operating pressure, psia	520			2000
Design pressure, psi	1250			2000
Test pressure, psi	2500			4000
Design temperature, °F	600			600
Velocity, fps	67 (in outlet pipe)			11
Pressure drop, psi				18.5
Holdup volume, total	~45 ft^3 (normal level)			14.8 gal
Fluid circulated	Distilled water and steam			10 g of UO_2SO_4 per kg of D_2O
Circulation rate, lb/hr	1.62×10^4			1.79×10^5
Fluid properties	H_2O at 471°F	H_2O at 180°F	Saturated Steam at 520 psia	Fuel at $T_{av} = 533°F$
Density, lb/ft^3	50.2	60.7	1.12	53.4
Viscosity, lb/hr·ft	0.28	0.85		0.266
Specific heat, Btu/lb·°F	1.11	1.00		1.23
Thermal conductivity, Btu/hr·ft^2 (°F/ft)	0.360	0.390		0.339
Heat exchanged, kw	5000 (1.71×10^7 Btu/hr)			
Apparent U_F, Btu/hr·ft^2·°F	670 (based on $U_F = \frac{3}{4}U_C$)			
Log mean temperature difference, °F	53.2			
Heat-transfer area (fouled)	251 U-tubes, $\frac{3}{8}$-in. OD, 0.065-in. wall, ~21 ft long, 480 ft^2 of outside tube surface (based on $A_C = \frac{3}{4}A_F$)			
Steam quality	Not less than 99%			

discussed in Sec. 6.4. March 11, 1955 is the anticipated delivery date for the heat exchanger.

(c) Inner Dump Tanks and Separator. Tests run on the mockup of the inner dump tanks (cf. Sec. 1.4.7) have indicated the need for some modifications in the design. To reduce surging of the liquid in the tanks, it has been necessary to add four 6-in.-wide transverse baffles to each tank. To reduce entrainment of liquid in the vapor line, a second vapor outlet has been connected from the mid-point of the tanks to the original outlet which leads into the separator. Figure 1.9 shows the final design of these tanks. The core and blanket tank systems are similar except for the tank diameter.

A study of the problem of taking inventory[4] of uranium and heavy water has resulted in an arrangement of the dump-tank piping which minimizes the vertical thermal-expansion forces on the tanks.

[4]R. G. Pitkin, *Inner Dump Tanks, Their Piping and Supports*, ORNL CF-54-8-167 (Aug. 17, 1954).

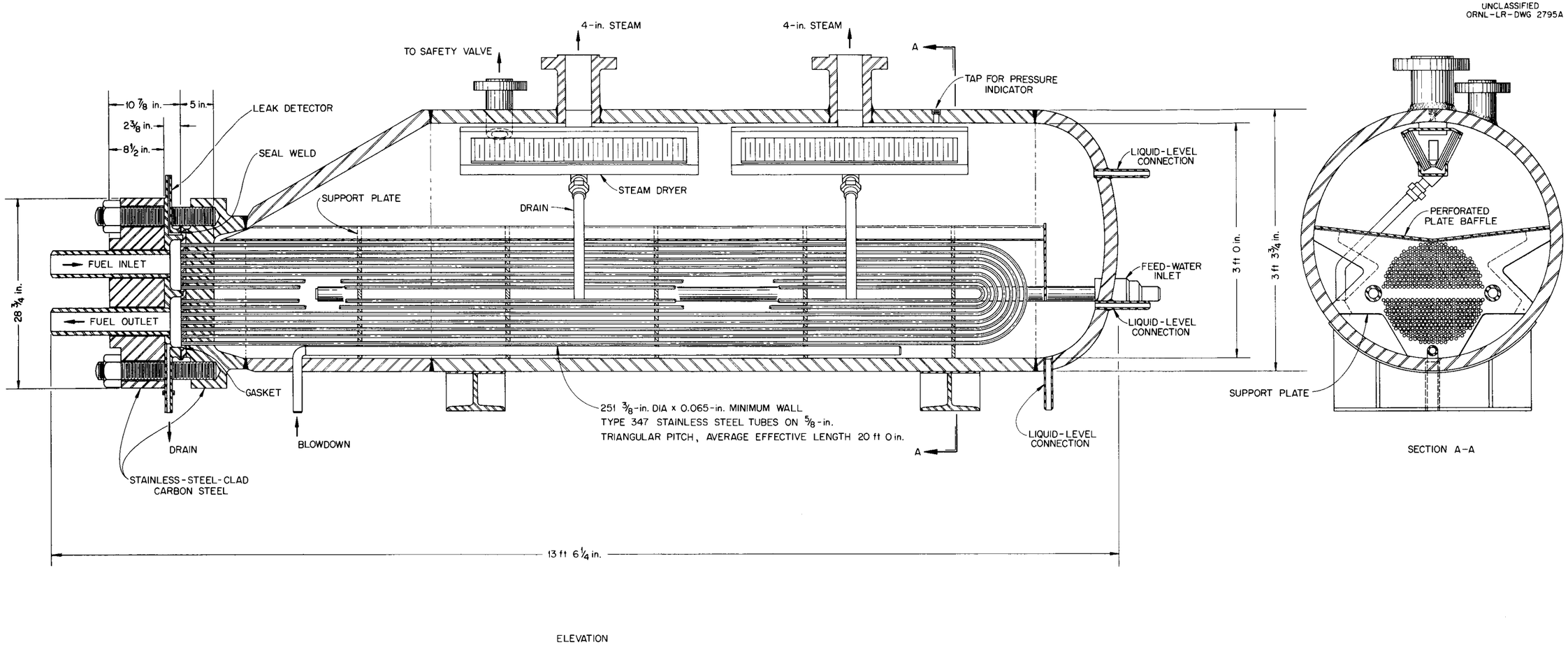

Fig. 1.7. Main Heat Exchanger.

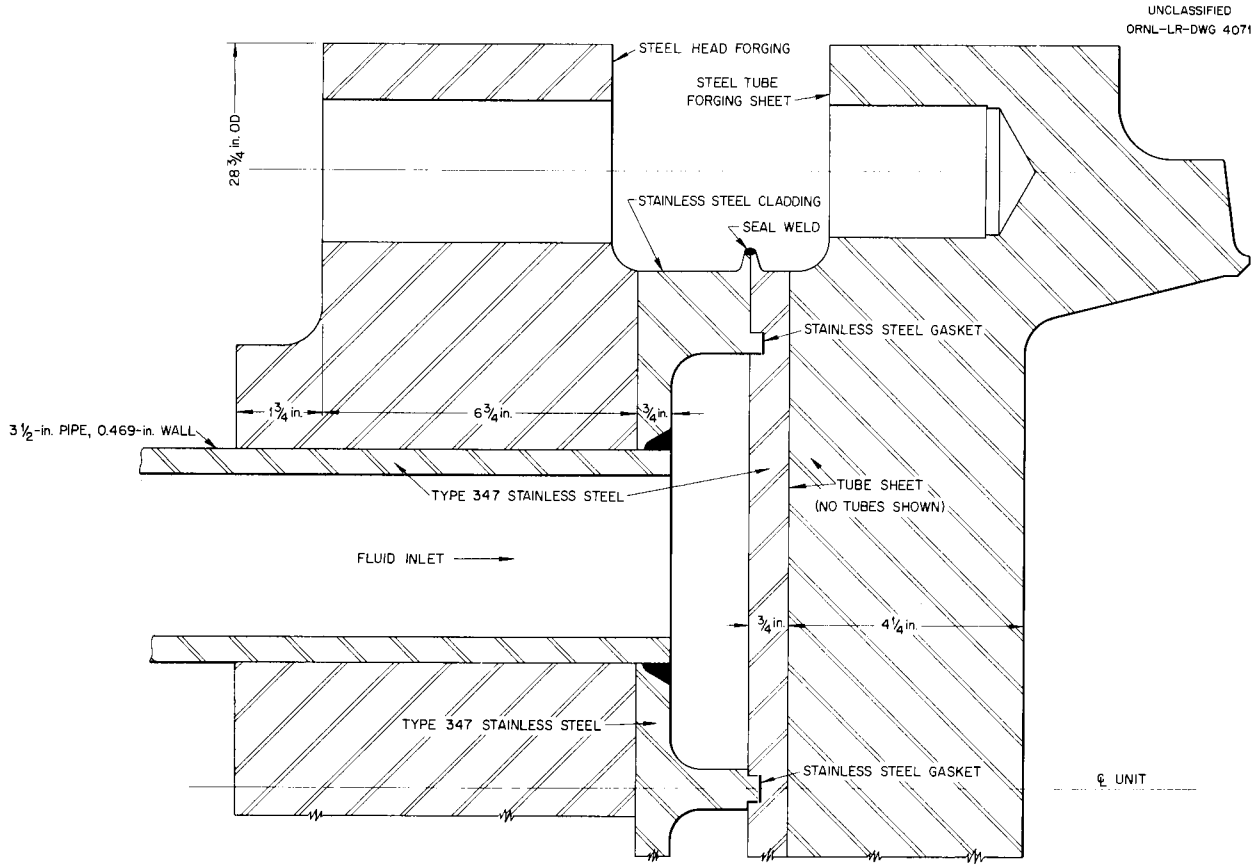

Fig. 1.8. Heat-Exchanger Head Joint.

It is estimated[5] that under inventory conditions the maximum vertical thermal force on the tanks will be approximately 5 lb, which is well within the tolerance limits established for inventory. A design is in progress for suspending the dump tanks on weigh beams that are attached to pneumatic weigh cells located in the upper part of the reactor cell so that the tanks may be removed for maintenance.

The final design of the dump-tank entrainment separator is shown in Fig. 1.9. Two modifications have been made in its design: the liquid drain pipe has been increased in size from ½ to 2 in. to permit better drainage; and the supports for the wire-mesh de-misters were strengthened, and a coarse-mesh hold-down screen was placed on top of the filters to prevent their upward displacement during a dump.

The dump and let-down inlets to the inner dump tanks have been combined to reduce the number of pipes connecting to the tanks. The combined line connects to the entrainment separator and is positioned concentrically inside one of the tangential vapor inlets. This arrangement gives rotation to the entering liquid-gas mixture and thereby improves separation at the point where much of the liquid is flashed.

(d) Outer Dump Tanks. The outer dump tanks have also been modified by addition of a second vapor outlet which connects through a tee to the reflux condenser. These tanks are also provided with four transverse baffles to control surging.

(e) Recombiner and Recombiner-Condenser. As shown in Fig. 1.10, the final design of the recombiner-condenser differs from that previously reported[6] in that it consists of two separate units

[5] R. G. Pitkin, *Inner Dump Tank Piping and Weighing System*, ORNL CF-54-10-63 (Oct. 13, 1954).

[6] R. B. Briggs *et al.*, *HRP Quar. Prog. Rep. April 30, 1954*, ORNL-1753, p 33.

UNCLASSIFIED
E-18182B

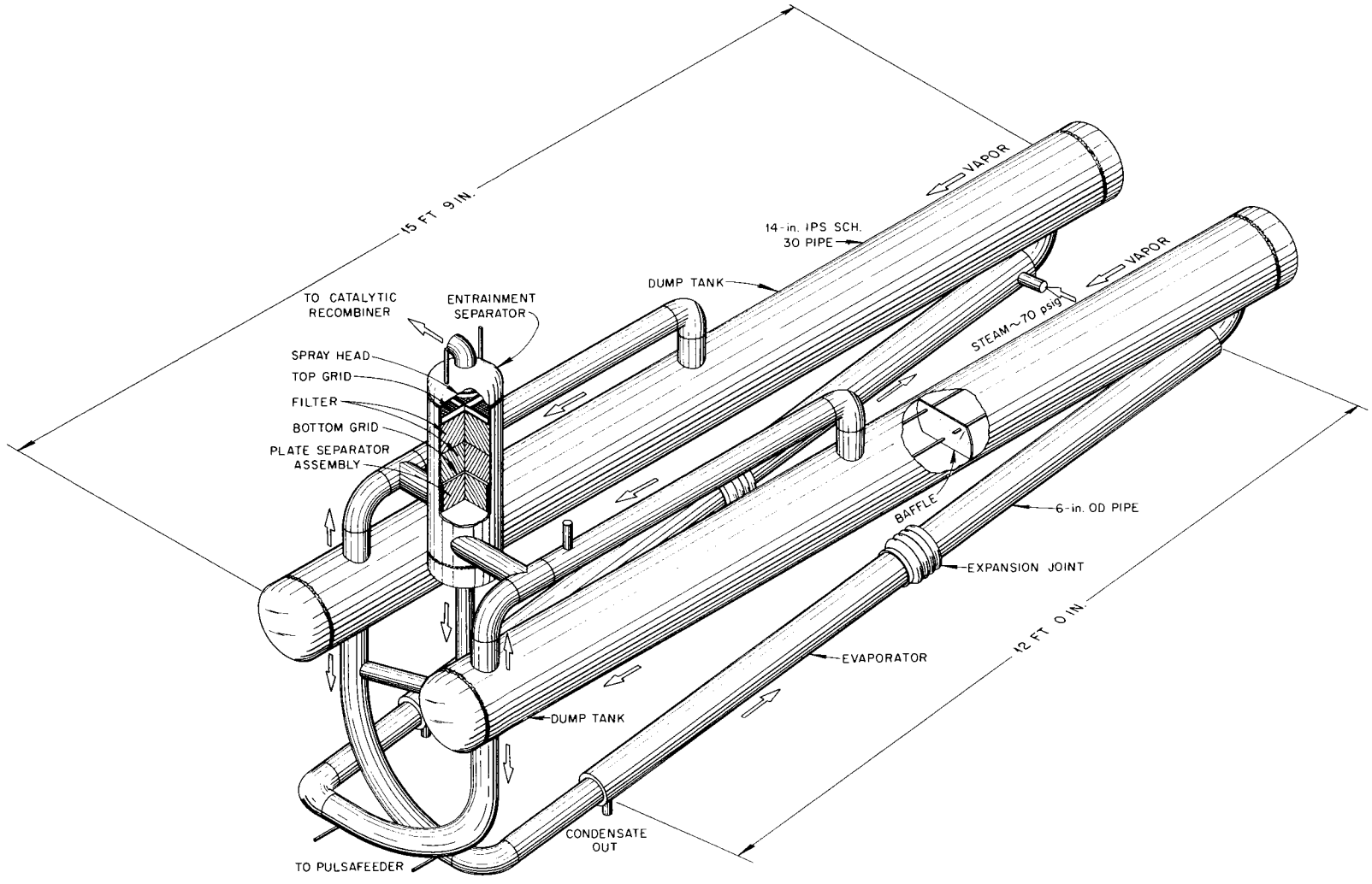

Fig. 1.9. HRT Dump-Tank Evaporator and Entrainment Separator.

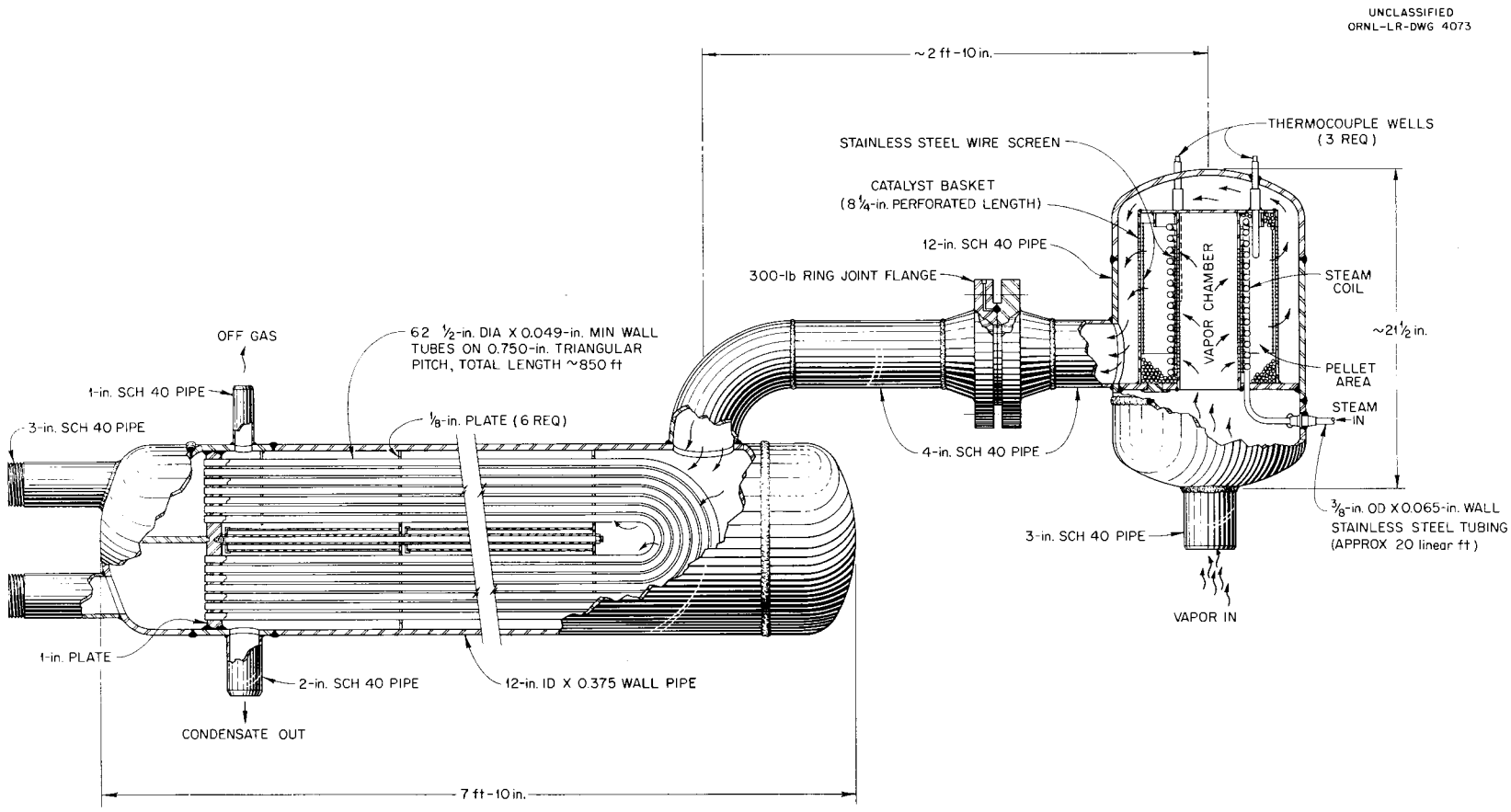

Fig. 1.10. Assembly of HRT Recombiner and Condenser.

connected by a 4-in. flanged pipe. Gas passes through the annular catalyst bed from inside to outside; gas cooling, condensing, and subcooling take place on the shell side of the condenser section, which utilizes a water-cooled U-type tube bundle.

The use of only one tube sheet in the new design eliminates a previous thermal-stress problem. It also prevents flooding of a catalyst bed and provides for better venting during dumping conditions. The shell side has a series of baffle plates which channel the gas in a horizontal plane and provide for better heat-transfer coefficients along the tube bundle. Gas binding and venting during a dump are minimized by baffle design and placement. Based on a 1-gpm evaporation rate (previously ½ gpm), the normal heat exchanged is 740,000 Btu/hr and the maximum heat exchanged is 3,000,000 Btu/hr. The heat-transfer area based on the outside diameter of the tubes is 112 ft^2.

A recombiner-condenser specification has been written (ORNL-HRT-1008 dated Sept. 13, 1954). The catalytic-recombiner assembly and details are shown on ORNL drawing E-18228, and the recombiner-condenser is shown on ORNL drawing E-18226.

(f) Reflux Condenser. The design calculations and specifications for the outer-dump-tank condenser have been described previously.[7] The final design has been completed, and Fig. 1.11 shows a drawing of the unit that will be built for use in the HRT. The condenser consists of four bayonet-type tubes (1½-in. schedule-10 pipe, 14 ft long) welded into a tube sheet. Condensation occurs on the outside of the tubes, and cooling water flows in the inside (entering through a 1-in. reentrant tube and leaving through the annulus formed between the 1-in. tube and the 1½-in. pipe). The tube bundle is inserted in a 6-in. schedule-80 pipe jacket. About 21 gpm of cooling water (100°F) is required to dissipate the design load of 170 kw of heat at 212°F.

1.3 NUCLEAR CALCULATIONS

M. C. Edlund, Section Chief

P. R. Kasten P. M. Wood

1.3.1 Safety Considerations

P. R. Kasten

Some situations which could cause physical damage to the reactor system have been considered. The most drastic accident would be the rupture of the outer pressure shell. With no safety factors, the pressure vessel would probably rupture at a maximum internal pressure of 8000 psi. Thus the assumption that the vessel would rupture from a 6000-psi rise in pressure above normal operating conditions is not unreasonable. For purposes of nuclear safety calculations, an upper safety limit for this pressure rise has been set at 2000 psi above normal operating conditions. Although this limit appears to be very conservative from a mechanical viewpoint, the safety factor in terms of reactivity addition is somewhat smaller.

A less drastic, although still undesirable, condition would result from rupture of the zirconium core tank from an internal pressure surge. On the basis of calculations and of mockup tests by Newport News Shipbuilding & Dry Dock Co., the core tank would probably rupture at a maximum pressure differential of 1000 psi between the core and blanket regions. For purposes of nuclear safety calculations, an upper safety limit of 200 psi has been set on this differential pressure.

The pressure rise depends on the reactivity added to the system, and, as was shown previously,[8,9] the reactivity added is a function of the rate of reactivity addition and the power at which the reactor becomes prompt-critical. The pressure rise resulting from various rates of reactivity addition when the reactor fluid temperature is 280°C and the minimum power is 0.04 w (corresponding to a source of 10^7 neutrons/sec) is given below:

Reactivity Added (%/sec)	Peak Pressure Rise (psi)
0.3	100
0.5	200
1.5	1000
2.0	2000
3.0	6000

At lower reactor temperatures the pressure rise is smaller for a given reactivity change; for example,

[7] R. B. Briggs *et al.*, *HRP Quar. Prog. Rep. April 30, 1954*, ORNL-1753, p 35.

[8] M. C. Edlund *et al.*, *HRP Quar. Prog. Rep. July 31, 1954*, ORNL-1772, p 51-54.

[9] P. R. Kasten, *HRT Safety Considerations*, ORNL CF-54-9-226 (Sept. 30, 1954).

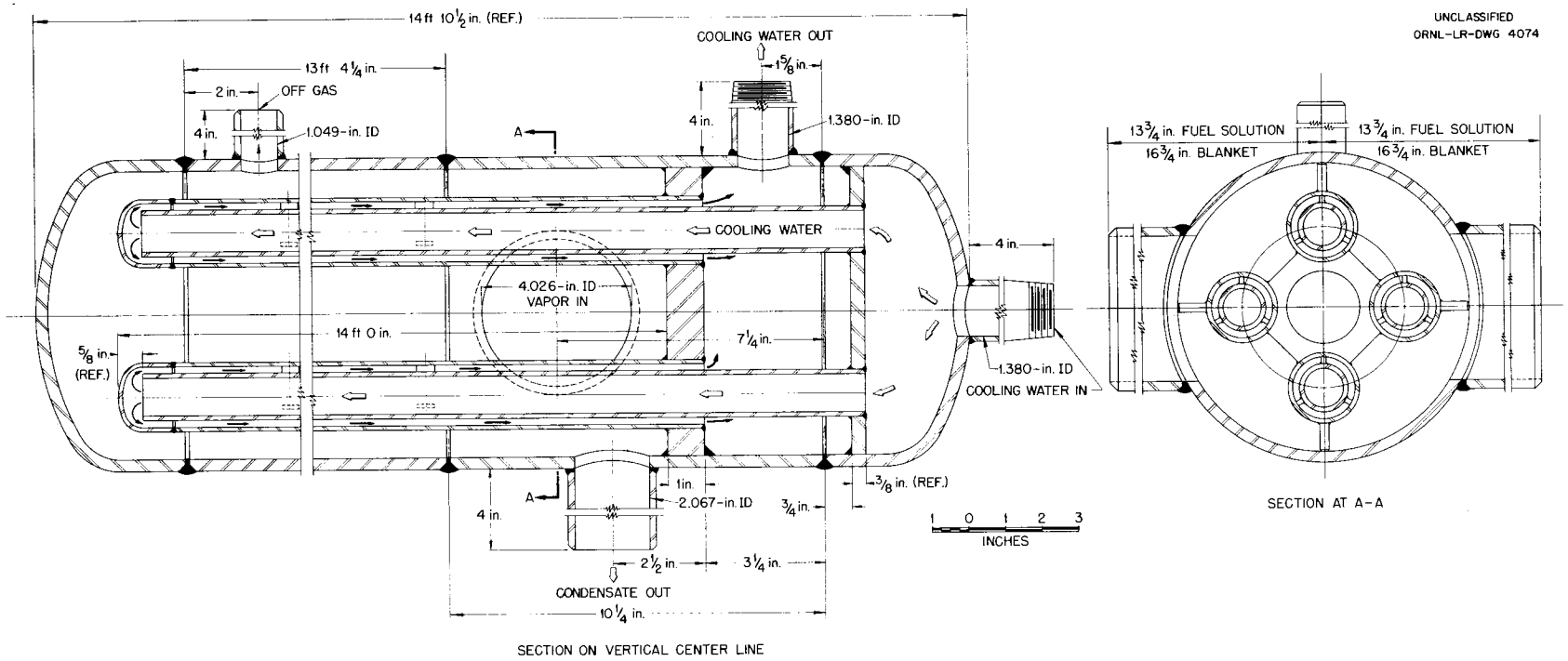

Fig. 1.11. HRT Reflux Condenser.

at 20°C a rate of 0.8% per second (rather than 0.5%) gives a pressure rise of 200 psi.

Several operational conditions which can lead to large reactivity additions are possible, particularly if several operating mistakes coincide with interlock failures. The conditions considered were the following:

1. By means of the high-pressure steam boiler, fresh fuel solution is heated up to about 280°C, while concentrated fuel is added to give a concentration sufficient for criticality at about 250°C. At this time the 400A pump is turned off and the shell side of the heat exchanger is vented to the steam condenser; so the fuel solution in the heat exchanger is cooled. Cooling of the fuel solution to 100°C appears to be possible in about 1 min, during which time natural convection cooling does not cause the reactor to reach a critical condition. Startup of the pump at this time could add reactivity at about 1.5% per second. To reduce the rate of reactivity addition to 0.5% per second, the 400A pump speed should be kept at one-third its rated value until all the fluid in the high-pressure system has passed through the heat exchanger. Experiments are in progress to determine whether the pump can be started so slowly.

2. With fresh fuel solution in the core and the core subcritical, concentrated fuel solution is added to the core system by means of the injection pump. With the D_2O-reflected core critical at 20°C and a total of 5.0 kg of U^{235} available, calculations showed that if the fuel in the dump tanks is concentrated to about 320 g/liter and if the pump injects the concentrated fuel solution into the core at a rate of 6.3 kg/min, reactivity can be added at about 1.7% per second. Protection against such a high ramp rate has been provided by adjusting the fuel intake line so that 25 liters of solution is always present in the dump tanks. With this change, the fuel concentration will

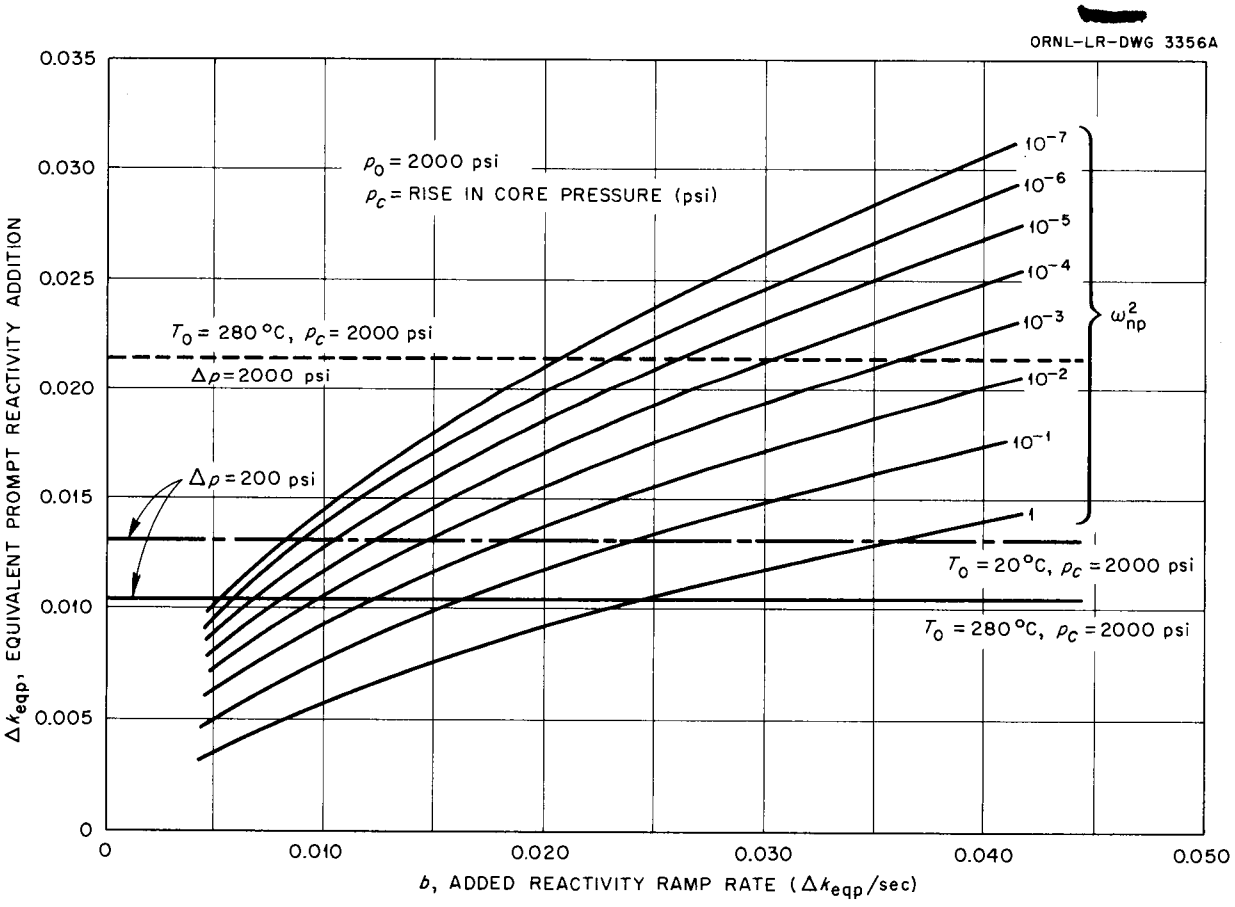

Fig. 1.12. Rate of Reactivity Addition and Equivalent Prompt Reactivity Addition.

always be less than about 160 g/liter, limiting the rate of reactivity addition to about 0.8% per second even when the injection pump operates at maximum speed. With the core fluid at 280°C, the corresponding reactivity rate is less than 0.2% per second.

3. With the 400A pump off, the injection pump adds concentrated fuel solution to the high-pressure system, allowing a buildup of fuel in the system external to the core. Startup of the 400A pump at this time could add reactivity at about 130% per second if fuel solution containing 100 g of uranium per liter were in the external piping. This situation was corrected by locating the fuel inlet into the high-pressure system so that the fuel immediately enters the core and by allowing fuel addition only when the 400A pump is running at full speed. If highly concentrated fuel solution is prevented from accumulating in the high-pressure system external to the core before circulation is begun, no conditions are foreseen which will result in rupture of the outer pressure vessel.

In the situations considered above, only source neutrons were assumed to be present. If the reactor power is in the kilowatt range, less restriction will be imposed upon the reactivity rate. For example, when the reactor power is 400 kw, a reactivity rate of 2% per second is required to increase the core pressure by 200 psi and a rate of about 7% per second is required to increase the core and blanket pressure by 2000 psi.

The relations between initial power level of the reactor, rate of reactivity addition, equivalent prompt reactivity addition, and pressure rise inside the reactor are given in Figs. 1.12–1.14. In Fig. 1.12, ω_{np}^2 is the modified nuclear frequency and is proportional to the power level of the reactor at prompt critical. For the HRT, ω_{np}^2 is about 10^{-7} sec^{-2} if the neutron power level at prompt critical is 0.04 w.

[redacted]

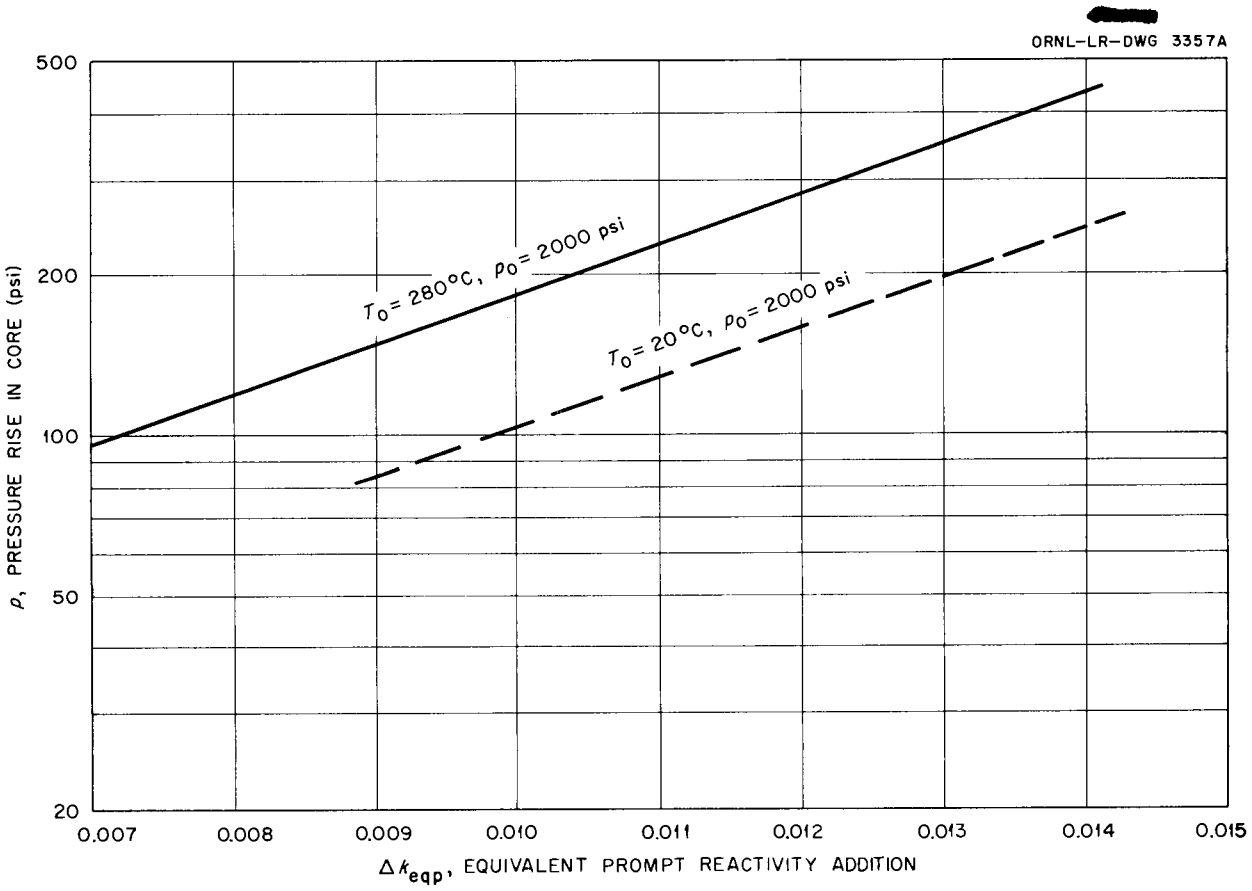

Fig. 1.13. Rise in Core Pressure as a Function of Equivalent Prompt Reactivity Addition.

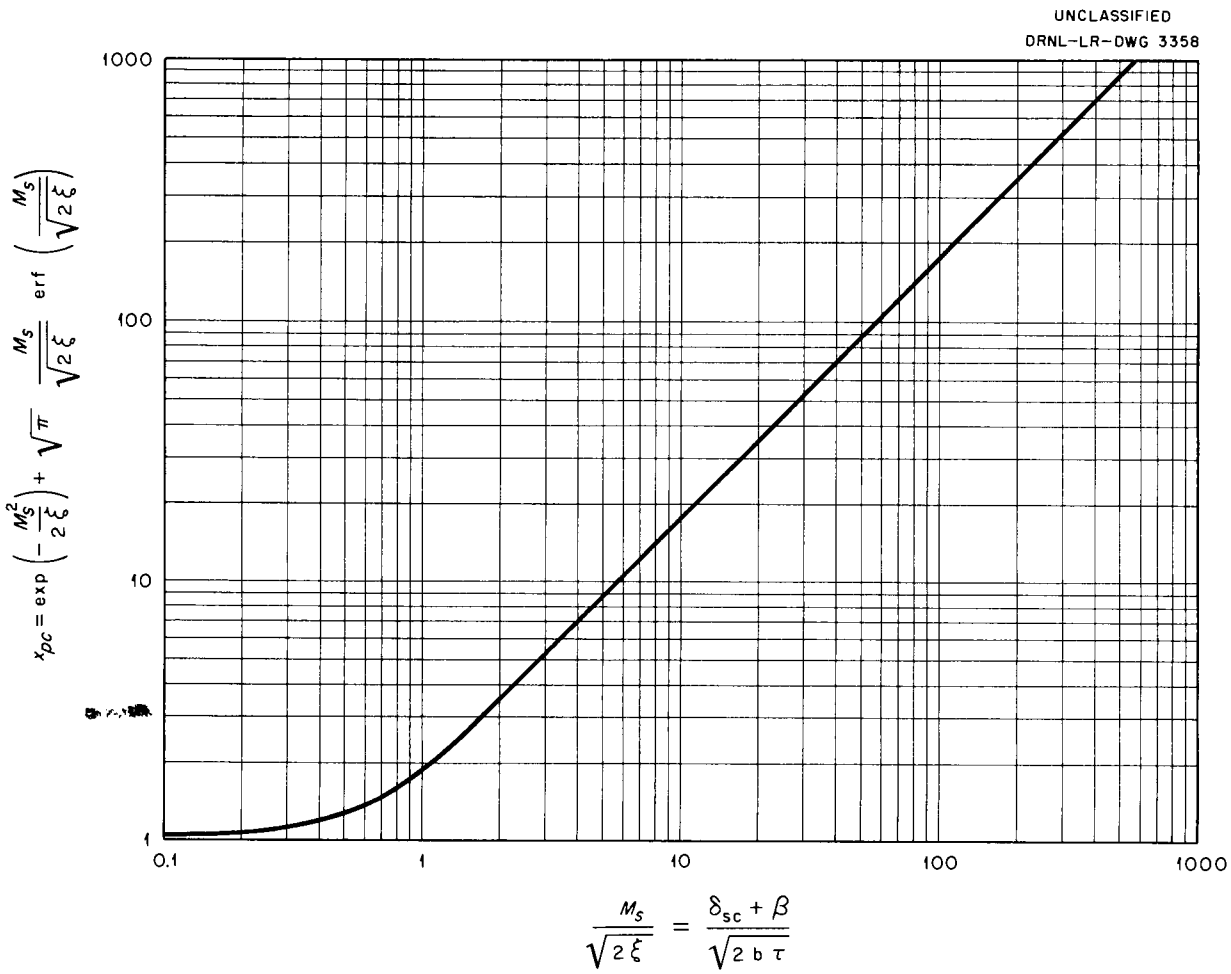

Fig. 1.14. Neutron Power at Prompt-Critical Relative to Initial Power as a Function of $M_s/\sqrt{2\xi} = (\delta_{sc} + \beta)/\sqrt{2b\tau}$.

In Fig. 1.14, x_{pc} is the ratio of the neutron power level to the initial steady-state power when the reactor is prompt critical; δ_{sc} is the amount the reactor is subcritical initially; β is the effective fraction of delayed neutrons; b is the rate at which reactivity is added; τ is the mean lifetime of prompt neutrons; ξ is the rate of reactivity increase divided by τ, sec^{-2}; and $M_s = (\delta_{sc} + \beta)/\tau$. The following case will illustrate how the data in Figs. 1.12–1.14 can be used. It is desired to know the rate of reactivity addition which will cause the core pressure to rise 200 psi above its initial value, if the reactor is initially critical at a power level of 1 kw. On the assumption that the reactor power at prompt critical is 1 kw, $\omega_{np}^2 \approx 2.5 \times 10^{-3}$, Fig. 1.12 gives the relation between the equivalent prompt reactivity addition and the rate of reactivity addition when $\omega_{np}^2 = 2.5 \times 10^{-3}$, while Fig. 1.13 relates core pressure rise to the equivalent prompt reactivity addition. With the average core fluid at 280°C, a Δk_{eqp} of 0.0104 will cause the core pressure to rise 200 psi. Figure 1.12 then gives the rate of reactivity addition as 1.06% per second. The above needs to be modified, since x_{pc} is actually greater than 1. For the HRT with D_2O reflector, $\tau \approx 5.7 \times 10^{-4}$ sec and $\beta = 0.005$. With $\delta_{sc} = 0$ and $b = 0.0106$, Fig. 1.14 gives $x_{pc} = 2.6$; so the value of ω_{np}^2 should be 6.5×10^{-3}. Only one iteration is necessary, which gives the rate of reactivity addition as 1.16% per second.

Figure 1.12 shows that if only source neutrons are present and the core fluid is at 280°C, the

rate of reactivity addition should be limited to about 0.5% per second if the core pressure rise is to be limited to 200 psi.

In the case of pump failure, followed by pump startup, natural convective cooling of the high-pressure loop does not eliminate the possibility of a high rate of reactivity addition to the core if the fluid fuel is unirradiated. In the case of pump failure after reactor operation at power for a long period of time, natural convection, in combination with the reactor decay power, assures reactor safety for reactivity rate additions up to 2% per second if the heat exchanger continues to operate. If the heat exchanger does not remain in operation and the cooling of the core fluid is limited by the heat capacity of the water in the shell side of the heat exchanger, it appears that natural convection cooling will keep the core fluid from boiling for at least 1000 sec after pump failure (initial reactor power, 5 Mw). To improve natural convective cooling, the 400A pump should be well below the fuel-solution line leaving the heat exchanger. In the calculations reported above, the 400A pump was assumed to be 2 ft below this fuel-solution line.

Reactor safety could be enhanced by increasing the present volume of the pressurizer and/or increasing the present cross-sectional area of the piping between the core and the pressurizer. If both were doubled, the maximum core pressure rise would be about halved for a given reactivity addition. However, design complications make it impractical to incorporate these changes.

1.3.2 Optimum Temperature for the Experimental Determination of the Breeding Ratio in the HRT

P. M. Wood

The problem of breeding in the HRT has been discussed in a previous progress report.[10] Additional calculations have been made to determine the effect (on the breeding ratio) of the $CuSO_4$ necessary to recombine the radiolytic gas formed at 5 Mw core power.

The breeding ratio of the HRT with U^{233} fuel and a ThO_2–D_2O slurry blanket containing 1349 g of thorium per kilogram of D_2O (Fig. 1.15) was calculated by using the harmonics method with a four-term expansion. In the calculation, $\eta(U^{233}) = 2.32$ was assumed for both resonance and thermal fissions. The effect, on the breeding ratio, of $CuSO_4$ necessary to recombine 100% of the radiolytic gas formed at 5-Mw core power is shown in Fig. 1.15. The poisoning of the copper is not significant above 230°C but becomes important at 200°C.

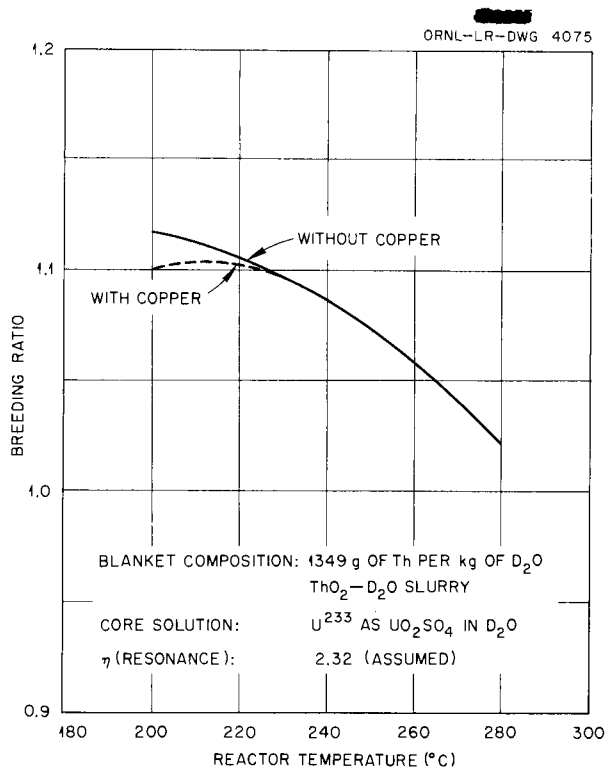

Fig. 1.15. Breeding Ratio in HRT.

1.3.3 Argon Activation in Operator Air of HRT Valves

P. M. Wood

The concentration of radioactive argon in the control-room area that will result from the release of activated air from valve operators in the process cell has been estimated. The maximum activity level that could be expected is approximately one-third of tolerance.

The thermal-neutron flux in the vicinity of the valves will be approximately 10^8 neutrons/cm^2/sec at 10 Mw core power. At saturation, the 46 valves in the cell will contain 1.7×10^{-4} curie of $_{18}A^{41}$. If all this activity is released into the control

[10] M. C. Edlund *et al.*, *HRP Quar. Prog. Rep. July 31, 1954*, ORNL-1772, p 30.

room and dispersed in the 32,500 ft^3 volume, the concentration of radioactive gas will be 1.9×10^{-13} curie/cm^3. Tolerance is 5×10^{-13} curie/cm^3.

1.3.4 Shielding over Steam Drums

P. M. Wood

If a tube in the fuel heat exchanger should rupture, highly radioactive fuel solution will be released into the steam system. The flow of radioactive steam out of the shield will be prevented by a fast-acting valve which will be closed by a signal from a monitron on the steam line.

A calculation has been made of the radiation which might result if the fuel steam drum and piping in the steam valve pit were filled with radioactive steam, and it has been determined that the shielding is adequate to keep radiation levels below a hazardous figure. The shielding over the valve pit is 2 ft of barytes concrete, and over the steam drum is 2 ft of barytes concrete and 9 in. of barytes gravel. The rupture of one heat-exchanger tube at the header would release 3 lb of fuel per second into the heat exchanger. It was assumed that this material all evaporates but is diluted by the generation of 4.6 lb of steam per second. The fuel was assumed to be saturated with fission products at 5 Mw core power; no decay was assumed. If the steam drums and piping are filled with this radioactive steam at 1250 psia pressure, the radiation level above the steam drum will be 8 r/hr and above the valve pit, 12 r/hr. Such dose rates do not constitute a serious hazard.

1.3.5 Neutron Streaming Through Cracks Between the Top Shield Plugs

P. M. Wood

The streaming of fast neutrons through the cracks between the top shield plugs of the HRT cell has been estimated. A 1/8-in. crack in the 40-in.-thick bottom layer of plugs directly over the reactor was assumed. The attenuation of the fast-neutron current by the 4-in. pressure shell, the 2-ft-thick barytes sand and water shield directly around the reactor, and the 20-in.-thick top layer of plugs was taken into account. With the D_2O-reflected reactor operating at 5 Mw core power, the dose rate directly over a crack in the bottom layer of plugs may be 30 mrem/hr of fast neutrons. Because this beam is highly collimated, a fast-neutron detector with a sensitive volume 1 in. in diameter would indicate only 5 mrem/hr.

1.4 COMPONENT DEVELOPMENT

C. B. Graham, Section Chief

J. A. Hafford, J. W. Skillern, P. H. Harley, I. Spiewak, B. A. Hannaford, D. S. Toomb, Jr.[11], W. L. Ross, R. E. Wascher

R. B. Briggs, Section Chief
W. R. Gall, Asst. Section Chief
R. D. Cheverton

E. C. Miller

1.4.1 Core Hydraulic Studies

I. Spiewak, P. H. Harley, D. S. Toomb, Jr.

During the past quarter, tests of the full-scale steel HRT core model have permitted final specifications to be made.[12,13] The core now contains nine screens (or perforated plates) mounted in a double-cone inlet diffuser (Fig. 1.16). If screens are used, the first seven should have 48% solid area, the last two 51%. If plates are used, the first seven should have 40% solid area, the last two 45%.

Slug flow was obtained in the sphere, except for a separated boundary layer 1 in. thick in the southern hemisphere. This boundary layer was removed easily when small density differences were introduced. The temperature distribution in the HRT should consist of essentially horizontal isotherms going gradually from inlet temperature at the bottom to outlet temperature at the top. The pressure drop in the specified geometry is 1.42 inlet velocity heads, or 6.6 ft of fluid at 400 gpm.

Measurements of gas holdup time in the straight-through core indicate that average reactor gas composition will be 25% of that in the outlet pipe. Similar measurements were made on the alternate concentric-core geometry, and the gas composition was equal to that in the outlet pipe.

1.4.2 Core-Vessel Development

R. B. Briggs, E. C. Miller, W. R. Gall, R. D. Cheverton

A program is under way at the Newport News Shipbuilding & Dry Dock Co. to build and test the

[11] Instrumentation and Controls Section.

[12] P. H. Harley, *Straight-Through HRT Core Model Tests*, ORNL CF-54-9-129 (Sept. 22, 1954).

[13] P. H. Harley and I. Spiewak, *Perforated Plates in HRT Core*, ORNL CF-54-9-192 (Sept. 30, 1954).

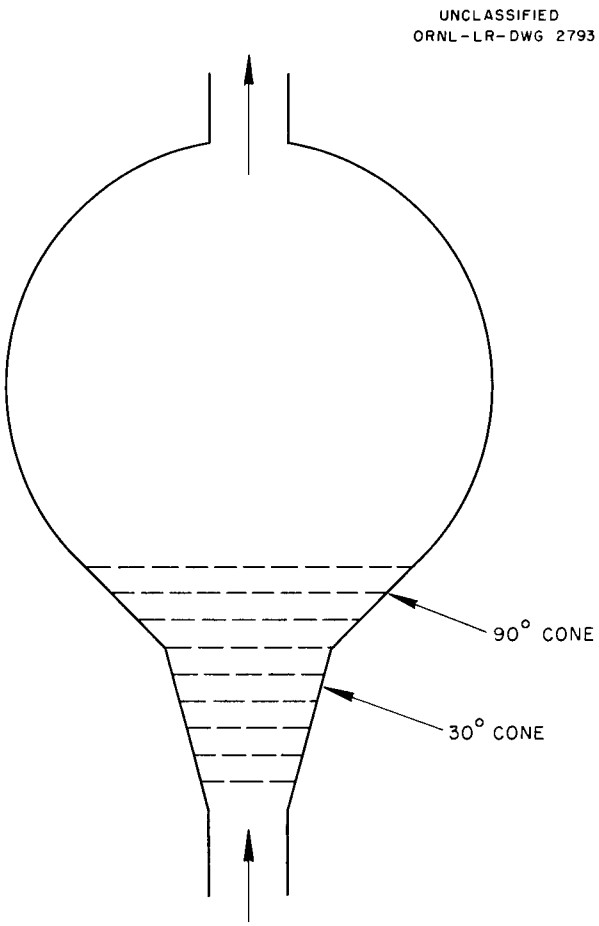

Fig. 1.16. HRT Flow Model with Double-Cone Diffuser.

core and pressure vessels for the HRT. The six specific problems under investigation are as follows:

1. development of techniques for rolling, forming, forging, and welding required in fabrication of the Zircaloy-2 core vessel for the HRT;
2. design and fabrication of the 60-in.-ID pressure vessel;
3. experimental stress analysis of the core vessel by using aluminum mockup vessels subjected to internal and external pressure and axial tension and compression;
4. life testing of several expansion joints in order to select one for use in joining the core vessel to the pressure vessel (see Fig. 1.17);
5. design and testing of a bolted joint to seal Zircaloy-2 to stainless steel;
6. design and testing of a joint for stainless steel connections to the stainless-steel-clad pressure vessel.

Welding techniques using local inert gas shielding have been developed for the last item listed above. Test welds made by this method have shown satisfactory strength but somewhat less ductility than the parent metal. Figure 1.18 shows the type of inert-gas shield employed in the Zircaloy-2 welding. Figure 1.19 illustrates the method of application of this type of shield on curved plate welds. Figure 1.20 shows a Zircaloy-2 plate $\frac{5}{16}$ in. thick formed to the shape for welding into the HRT core vessel.

Table 1.3 gives a comparison of the properties of Zircaloy-2 at the design temperature of 600°F and the properties of 54S aluminum alloy at room temperature. Due to the similarity of properties, it is hoped that data from pressure tests of vessels made of this aluminum alloy will be a good indication of the strength to be expected of the HRT core vessel. Two aluminum-alloy vessels have been tested. In each case the final step of the test was to determine the external pressure required to collapse the vessel. The first vessel, consisting of a $\frac{1}{4}$-in.-thick conical section on a $\frac{1}{4}$-in. spherical section, required 264 psi to collapse it. The second vessel, similar except having a $\frac{3}{8}$-in.-thick conical section like the HRT core, required 435 psi.

Both vessels withstood an external pressure of 150 psi without further collapse or leakage after the initial collapse failure occurred. Figure 1.21 shows one of the vessels being installed in the lower half of the test pressure vessel with strain gages in place and lead wires going out through the bottom of the pressure vessel. Figure 1.22 shows the cover being lowered into place over it, and Fig. 1.23 is the thin-wall vessel after collapse.

All materials for the Zircaloy-2 vessel are on hand at the Newport News Shipbuilding & Dry Dock Co., except for the forgings and the perforated plate for screens. The stainless-steel-clad hemispheres for the pressure vessel are scheduled for delivery in November. Shipment of the completed vessel assembly is scheduled for March 21, 1955.

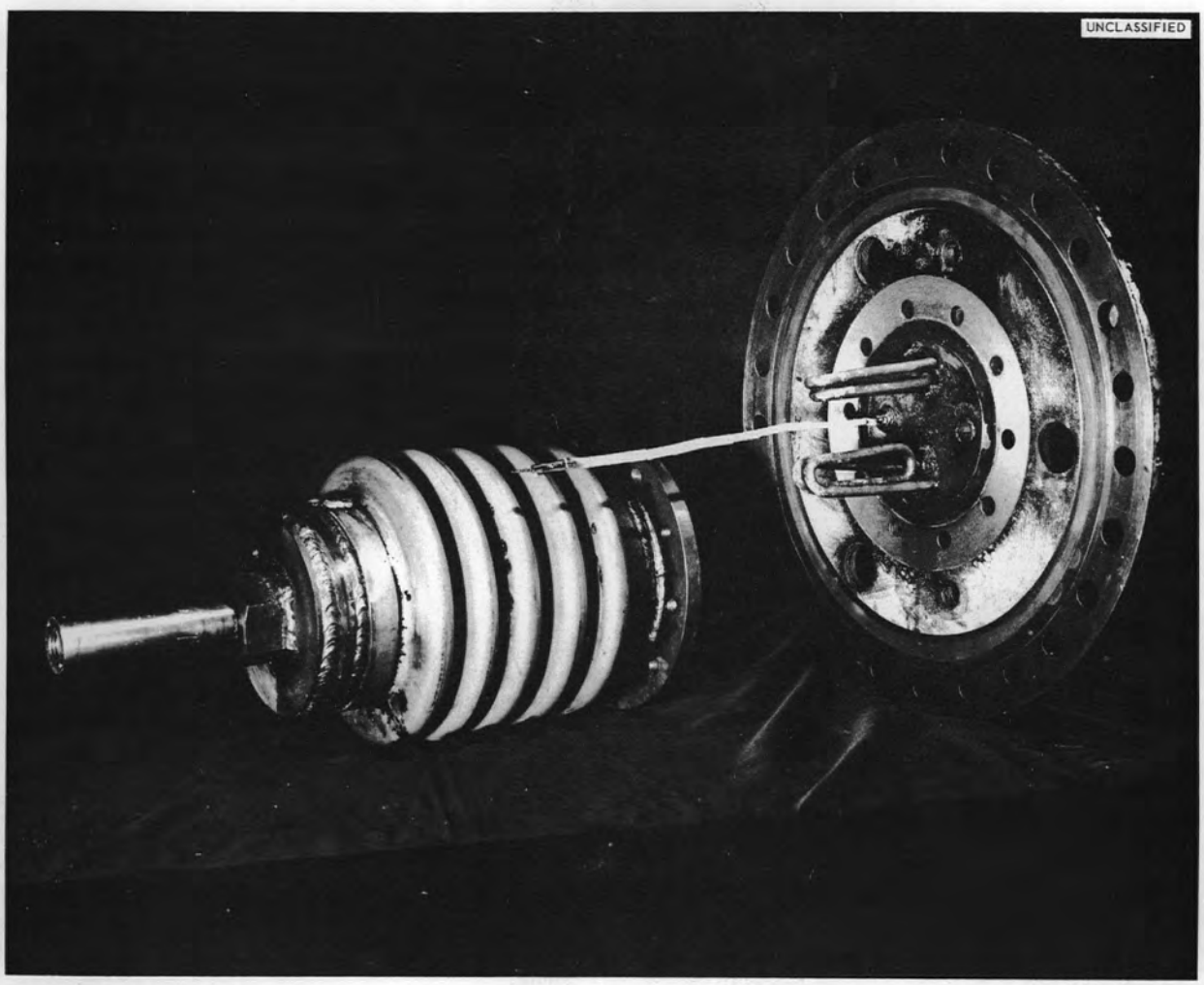

Fig. 1.17. Arrangement for Testing Expansion Joint Under Internal Conditions.

TABLE 1.3. HRT CORE AND MOCKUP MATERIALS

	Zircaloy-2 (at 600°F)		54S Aluminum (at 70°F)
Orientation	Transverse	Longitudinal	Any
Modulus of elasticity (E), psi	9,580,000	9,750,000	11,100,000
Yield point for 0.2% offset, psi	18,200	16,700	19,750
Ultimate strength, psi	26,900	28,400	37,500
Reduction in area, %	72.8	70.8	
Elongation in 2 in., %	46.0	46.5	27

Fig. 1.18. Auxiliary Welding Shield.

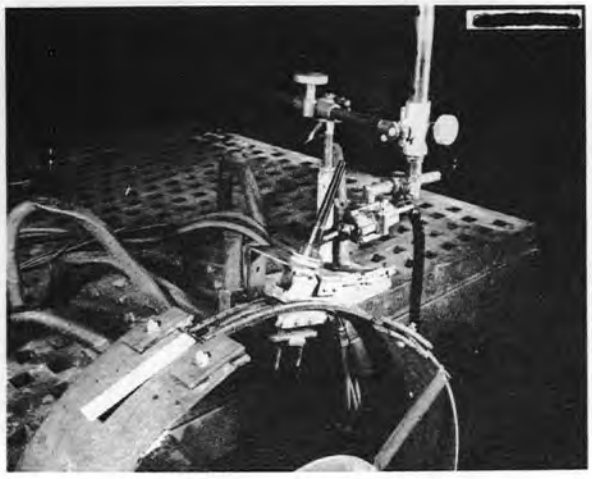

Fig. 1.19. Application of Latest-Design Auxiliary Welding Shield to Curved Surfaces.

1.4.3 Pump Development

W. L. Ross R. E. Wascher

Two model 400A pumps have been received from Westinghouse. Figures 1.24 and 1.25 are assembled and exploded views of the pump. Figure 1.26 shows the measured characteristics of the pump, including flow, developed head, over-all efficiency, and power input.

One pump will be tested at HRT fuel-pump conditions. The other will be used for long-range pump development. The loops[14] in which these pumps will be tested are nearing completion.

Fig. 1.20. Hot-Formed Zircaloy-2 Plate.

The three blanket-development pumps described previously[15] are expected to be delivered in the near future.

1.4.4 Fuel and Blanket Pumps

W. L. Ross R. E. Wascher

A contract has been placed with Westinghouse to supply two pumps of 400-gpm capacity as per ORNL specification HRT 1005 and two pumps of 230-gpm capacity as per ORNL specification HRT 1028. One of each of these pumps will be all stainless steel; the others will have titanium replacements for those parts which are subject to high velocity and/or turbulence at temperatures above 212°F. If the service requirements call for pumping extremely corrosive solutions, the titanium should prevent excess corrosion and damage to pump parts.

1.4.5 Injection Pump

The pump developed to serve as the high-pressure feed pump for the HRT is a combination of an HRE-type diaphragm pumping head driven by a Scott and Williams Hydropulse pump. The rubber pulsators of the Hydropulse pump provide an intermediate isolation system to prevent diffusion of radioactive solution out of the shield in the event of a diaphragm failure.

---

[14] W. L. Ross, L. F. Goode, and R. E. Wascher, *HRP Quar. Prog. Rep. July 31, 1954*, ORNL-1772, p 36.

[15] *Ibid.*, p 37.

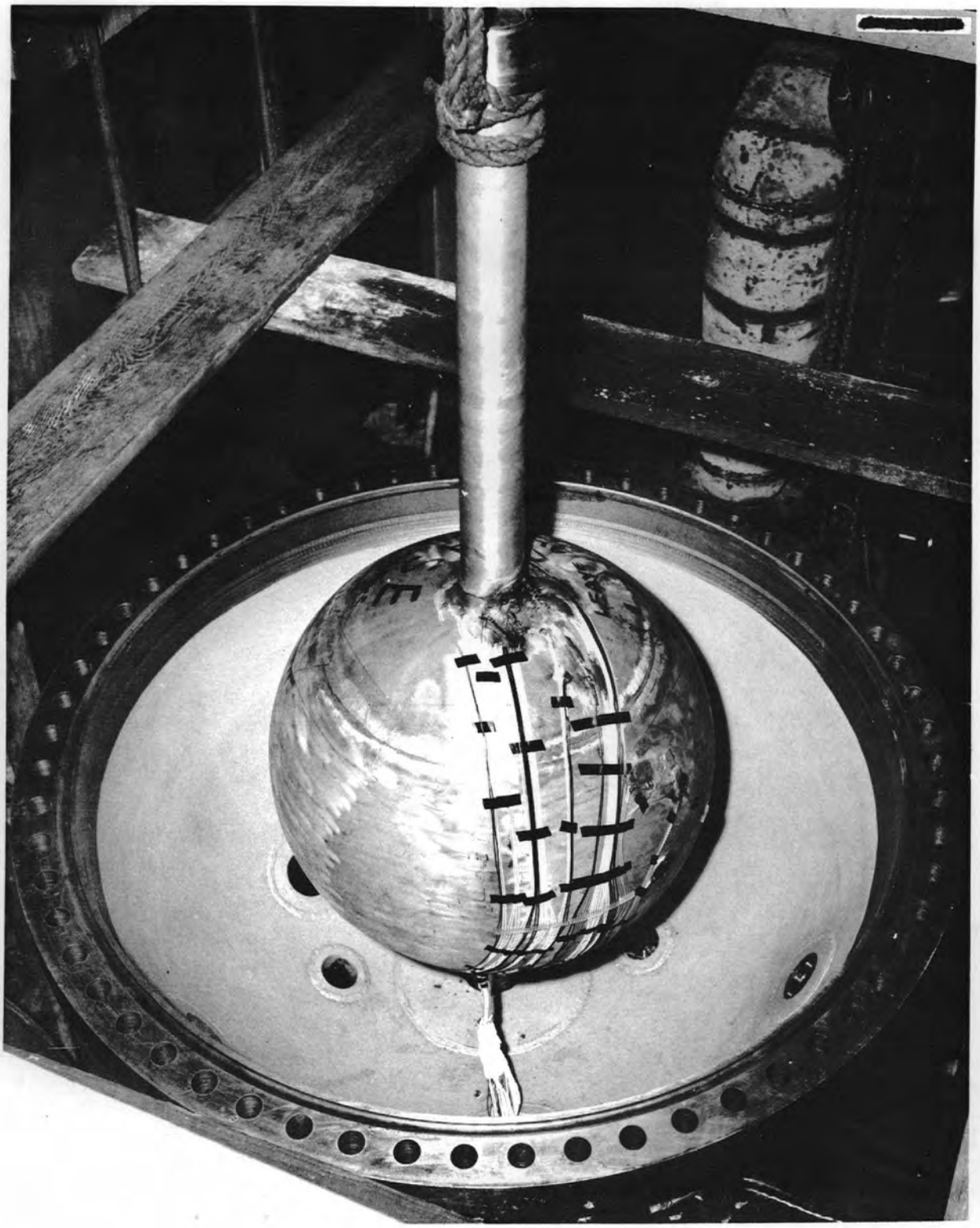

Fig. 1.21. Lowering Core Tank No. 2 into Outer Vessel. Cables lead to outlets and insulated studs.

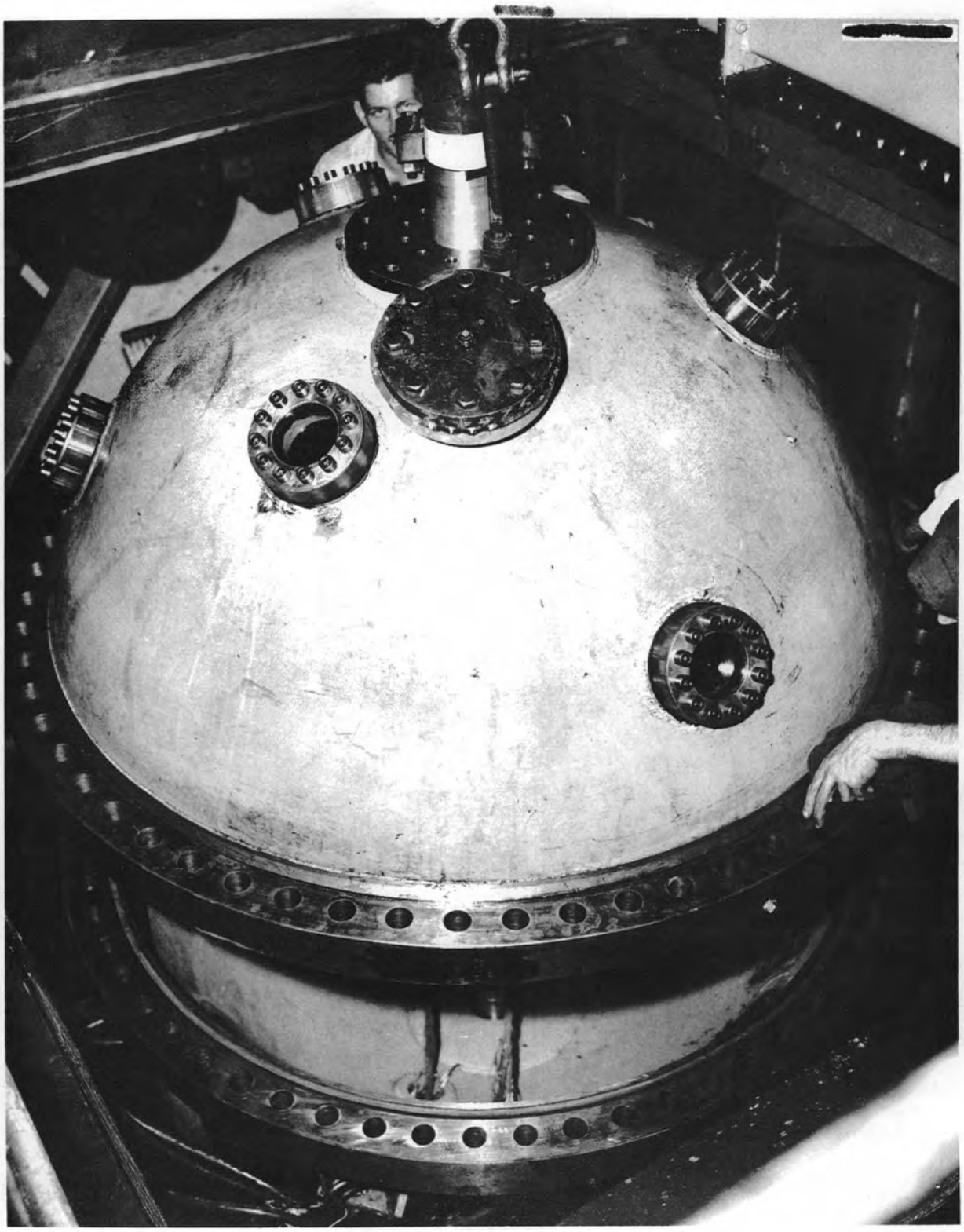

Fig. 1.22. Lowering Upper Half of Pressure Vessel into Place.

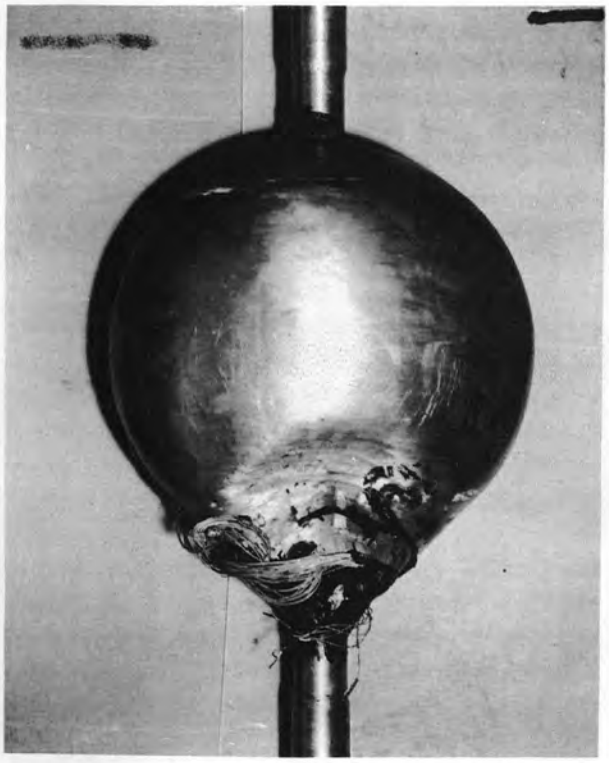

Fig. 1.23. Collapse Failure of Core Tank No. 1.

In performance tests the pump has provided adequate flow with smooth delivery. The pump-suction conditions do not seem to be so critical as on previous pumps, and no check-valve trouble developed at speeds as high as 100 strokes per minute. Output of the pump, which is normally rated at 1.5 gpm at 2000 psi discharge pressure, is shown in Fig. 1.27. The operation and testing of this pump are described elsewhere.[16]

To test the feasibility of adding oxygen to the pump suction, a test was run in which air was added to the suction stream. The operating conditions simulated those expected in the reactor except that the suction stream was saturated; hence all air added was in the form of bubbles. The results are shown in Fig. 1.28.

1.4.6 Fluid Flow in HRT Pressurizer

I. Spiewak B. A. Hannaford

Experiments were conducted on a simulated HRT pressurizer[17] (Fig. 1.29) to study the rates of liquid mixing and the pickup of gas from the main circulating stream.

Vigorous mixing with the main circulating stream

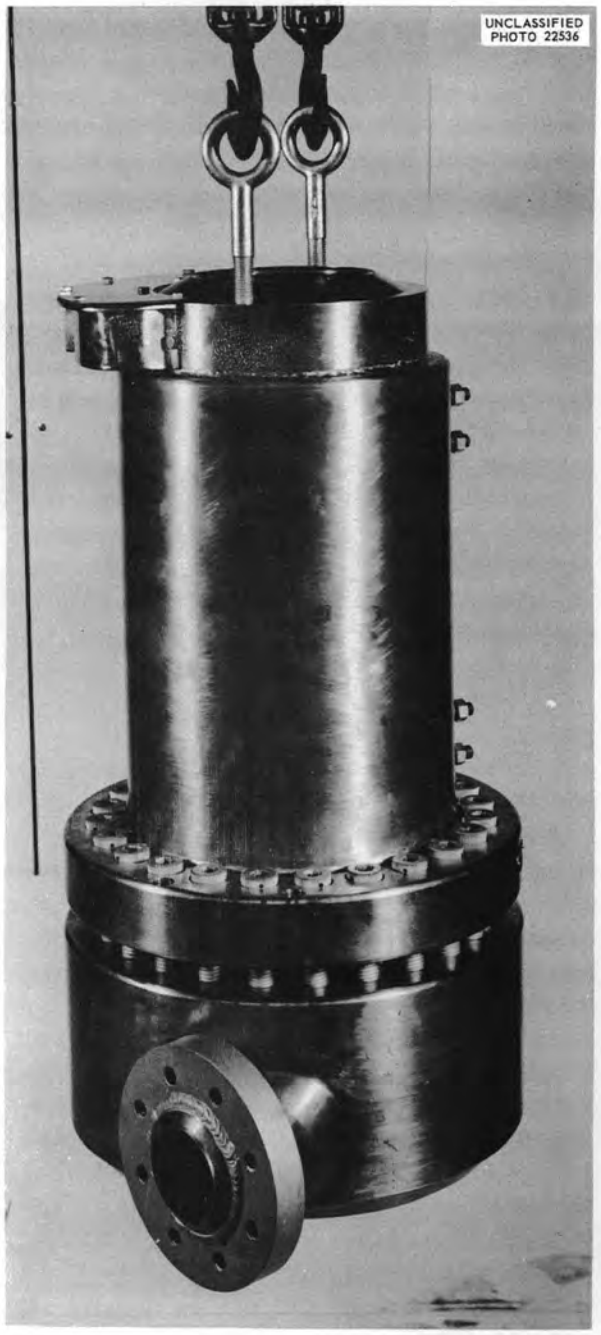

Fig. 1.24. Assembled Model 400A Pump.

[16] E. L. Youngblood, *Feed Pump Operating Characteristics*, ORNL CF-54-9-139 (Sept. 10, 1954).

[17] B. A. Hannaford, *Fluid Flow in HRT Pressurizer*, ORNL CF-54-9-178 (Sept. 24, 1954).

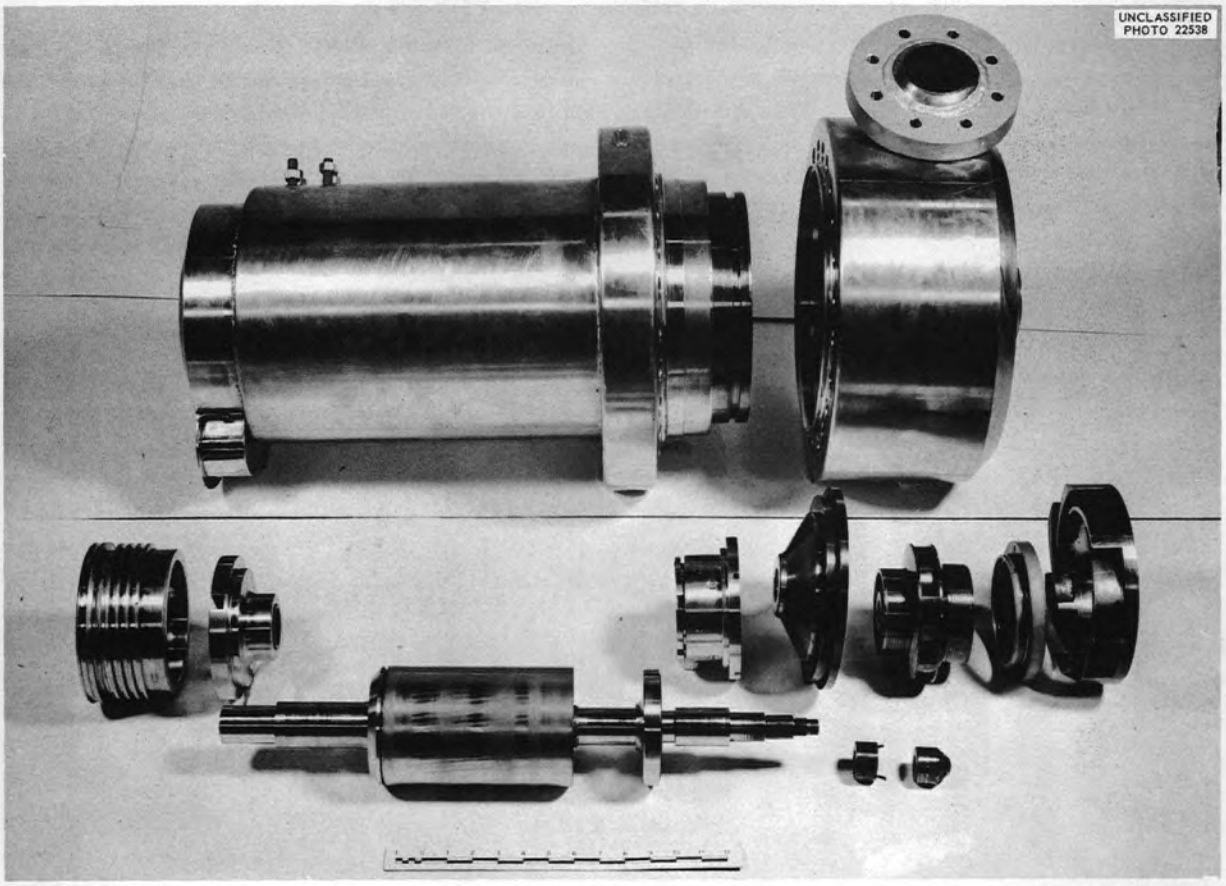

Fig. 1.25. Disassembled Model 400A Pump.

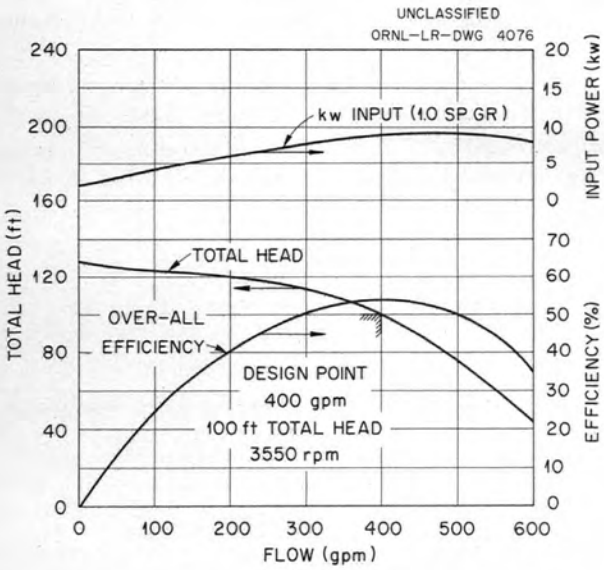

Fig. 1.26. Model 400A Pump Characteristics.

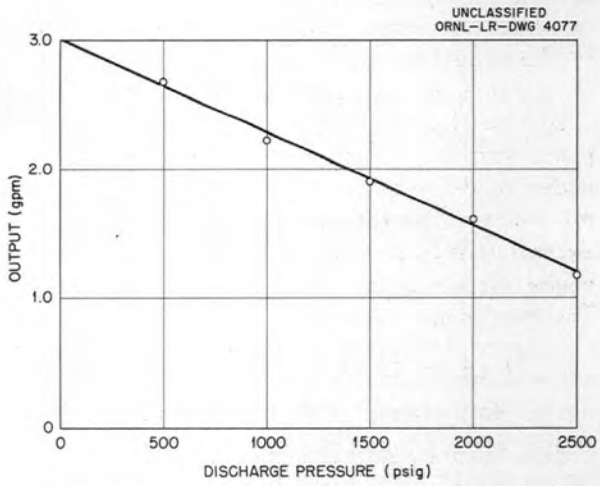

Fig. 1.27. Plot of Discharge Pressure vs Output for High-Pressure Feed Pump.

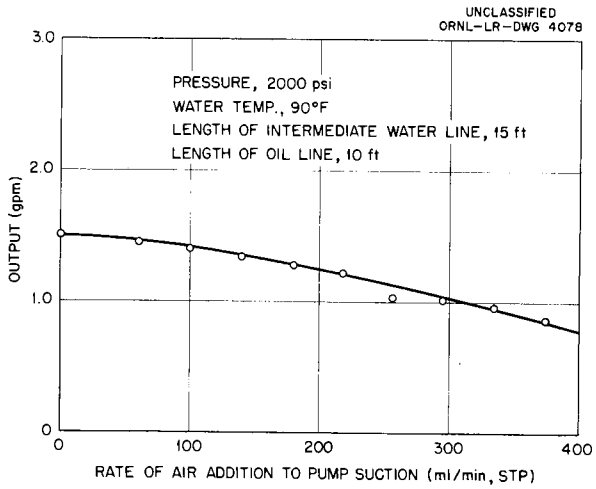

Fig. 1.28. Plot of Rate of Air Addition to Feed-Pump Suction vs Output.

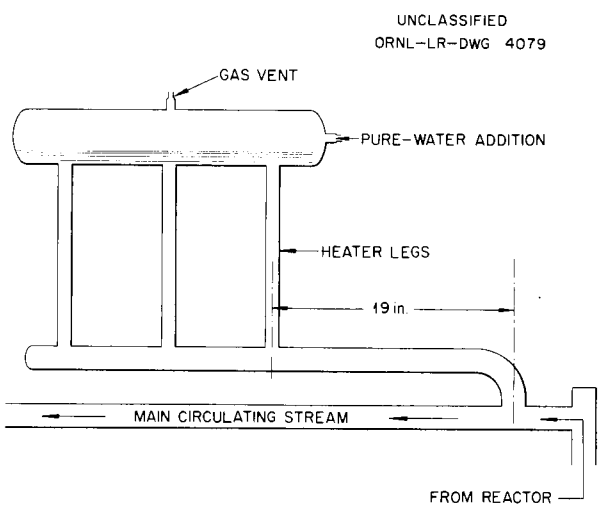

Fig. 1.29. Simulated HRT Pressurizer.

was found to extend about 18 in. into the lower horizontal leg of the pressurizer. A minimum length of 19 in. is required to prevent mixing with the heater legs. A pure-water addition of 5 gph appears to be sufficient to maintain pure water in the heater legs, provided that the 19-in.-length requirement is met. With a short horizontal leg, 30 gph was not sufficient to prevent mixing in the heater legs. The reactor pressurizers will be supplied with pure condensate at a rate of 10 gph.

The gas-collection rate seemed to be strongly dependent on the flow pattern of the main circulating stream. Five times as much gas was picked up when a long-radius elbow preceded the pressurizer as when a tee, which is recommended, was present. For the HRT geometry, about 3 cc of vapor per minute is expected.

Thoria slurry was found to settle in the lower horizontal leg of the pressurizer. Clean water injected at rates of up to 1 gpm and introduced in various locations was not effective in redispersing the solids.

1.4.7 Test of HRT Dump-Tank Evaporator and Entrainment Separator

P. H. Harley I. Spiewak

Comprehensive testing of the HRT dump-tank evaporator[18] and of the entrainment separator[19] has been completed. A full-scale steel mockup of one of the two 14-in. dump tanks was operated.

The data indicate that 75-psig steam will evaporate 1 gpm per tank; 33-psig steam is used for 0.5 gpm. The over-all heat-transfer coefficients were about 350 Btu/hr·ft^2·°F. Liquid throughput in the evaporator section is 36 gpm at 0.5-gpm evaporation and 79 gpm at the higher rate of 1 gpm. These rates are sufficient to keep the contents of the tank well agitated.

When the dump tank is nearly full, there is a tendency for surges of liquid to plug the vapor line, flooding the entrainment separator and creating physical bumping of the equipment. This tendency has been eliminated by installing suitable baffles and an additional vapor line leaving the dump tank.

For normal operation of the entrainment separator (designed as a centrifugal separator with a corrugated plate baffle and wire-mesh pads), the entrained salt concentration is below 1 ppm. For greater analytical sensitivity, phosphate salt was used as a substitute for uranyl sulfate in the test.

Four simulated dumps, averaging 30 gpm of liquid and 245 ft^3 (10 gpm) of steam at 150 psi for 1 min, were handled smoothly by the dump-tank–entrainment-separator system. At these high overloads, the entrainment separator was 99.75 to

[18] P. H. Harley and I. Spiewak, *Performance Test of HRT Fuel Solution Evaporator*, ORNL CF-54-8-232 (Aug. 13, 1954).

[19] P. H. Harley, *Performance Tests of HRT Fuel Solution Evaporator and Entrainment Separator*, ORNL CF-54-10-51 (Oct. 13, 1954).

99.97% efficient, but it is not believed that appreciable contamination will be added to the recombiner which follows the entrainment separator. A total of 1.2 to 12 g of uranium would penetrate the separator, of which amount an estimated 0.02 to 0.2 g would contaminate the catalyst pellets for each dump.

1.4.8 Mockup Loop

J. A. Hafford I. Spiewak
J. W. Skillern D. S. Toomb, Jr.

A mockup of critical HRT components was described in previous progress reports.[20,21] This system will test the engineering operation of the high-pressure loop and the let-down system.

All parts are now on hand or have an early delivery date. Assembly is progressing, and operation will begin during the next quarter.

The 80-kw test-model steam-condensing heat exchanger reported previously[20] has been completed and shipped. A report covering fabrication, inspection, and testing techniques will be issued shortly. This experience will aid in design and fabrication of the HRT heat exchangers.

The companion unit, an 80-kw electric boiler, is scheduled for shipment in late November.

1.5 CONTROLS AND INSTRUMENTS

J. N. Baird[22]
M. C. Becker R. L. Moore
A. M. Billings R. E. Toucey
J. R. Brown E. Vincens
J. C. Gundlach W. P. Walker[23]
K. W. West

1.5.1 General Design

Engineering flow sheets showing the HRT instrument applications to the fuel, blanket, and heat-removal systems have been completed. The core-system flow sheet is shown in Fig. 1.30; the blanket-system instrumentation is almost identical. A descriptive tabulation of all instrument items shown on the flow sheets has been issued with cost estimates.

A proposal for the HRT control circuit and operational procedure has been issued.[24] The report covers in detail the controls and interlocks necessary to prevent conditions which might result in damage to the reactor system.

The design criteria for connections inside the reactor shield have been formulated.[25] Electrical-power and thermocouple leads will be protected by waterproof conduit to within a few feet of their points of termination or measurement. Pressure seals will be used at the ends of the conduit, and the electrical-power lead will contain a disconnect mechanism for remote maintenance. On the control-room side of the main shield are located the two shielded instrument cells which will contain the majority of the reactor sensing elements. These isolated cells will eliminate radiation and water damages and afford easier maintenance.

The general configuration of the liquids-inventory system has been determined, and detailed design and procurement are proceeding. Dump tanks and condensate tanks will be suspended on pneumatic weigh cells.

Layouts of the control and auxiliary instrument rooms have been approved, and design of the supporting frames and cabinets has been completed.

1.5.2 Component Development and Testing

In pneumatic-control systems such as will be used for the HRT, it is necessary to convert some electrical signals to pneumatic output by means of an electropneumatic transducer. Such a device has been developed by the addition of a simple passive network to a standard Minneapolis-Honeywell thermocouple converter, and preliminary testing indicates that it performs satisfactorily. When used with an external oscillator, this instrument is capable of converting an electrical signal in the 1,000- to 10,000-cps frequency range to a modulated pneumatic output with $\pm \frac{1}{2}\%$ accuracy and 5-μv sensitivity. The ability to use higher frequencies on instruments such as the pressurizer level should eliminate the effect of temperature variations at the primary element.

[20] C. B. Graham *et al.*, *HRP Quar. Prog. Rep. April 30, 1954*, ORNL-1753, p 44.

[21] W. L. Ross and L. F. Goode, *HRP Quar. Prog. Rep. July 31, 1954*, ORNL-1772, p 42–43.

[22] Transferred to Instrumentation and Controls Division Nov. 1.

[23] Appointed Acting Section Chief effective Nov. 1.

[24] R. L. Moore, *HRT Control Circuit Proposal*, ORNL CF-54-9-175 (Sept. 28, 1954).

[25] W. P. Walker, *Instrument Design Criterion*, ORNL CF-54-10-173 (Oct. 12, 1954).

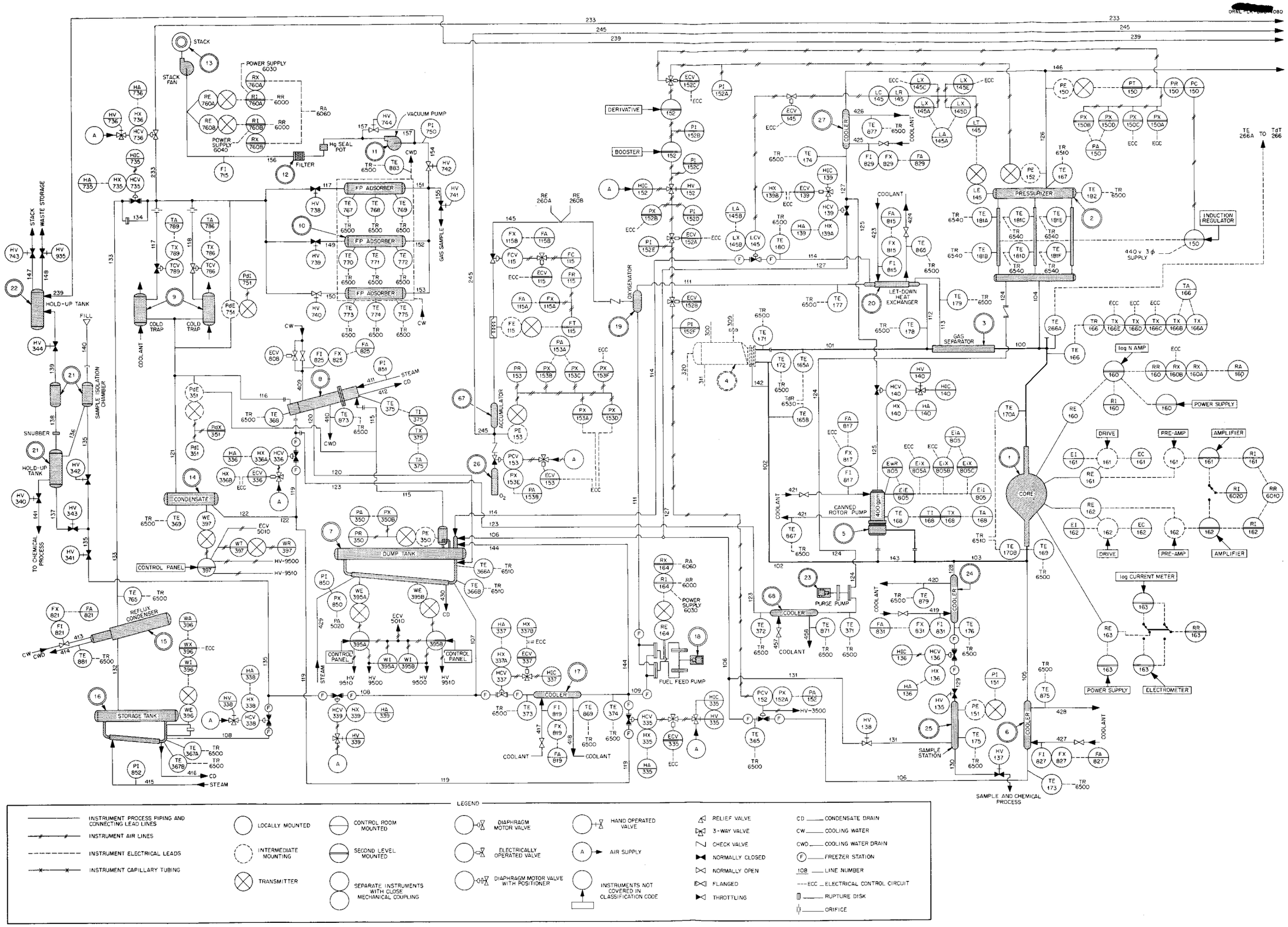

Fig. 1.30. Instrument Engineering Flow Sheet for Core.

[redacted] of the Remote Area Monitoring System (Jordan Electronic Mfg. Co., Inc.) has begun. This instrument should afford economy and simplicity to the problem of monitoring activities at several locations.

Corrosion data on the selected Chromel-Alumel thermocouple materials in aerated tap water indicate reasonable corrosion rates over a 500-hr period (see Sec. 5.1).

[redacted]

ORNL-LR-DWG 4081

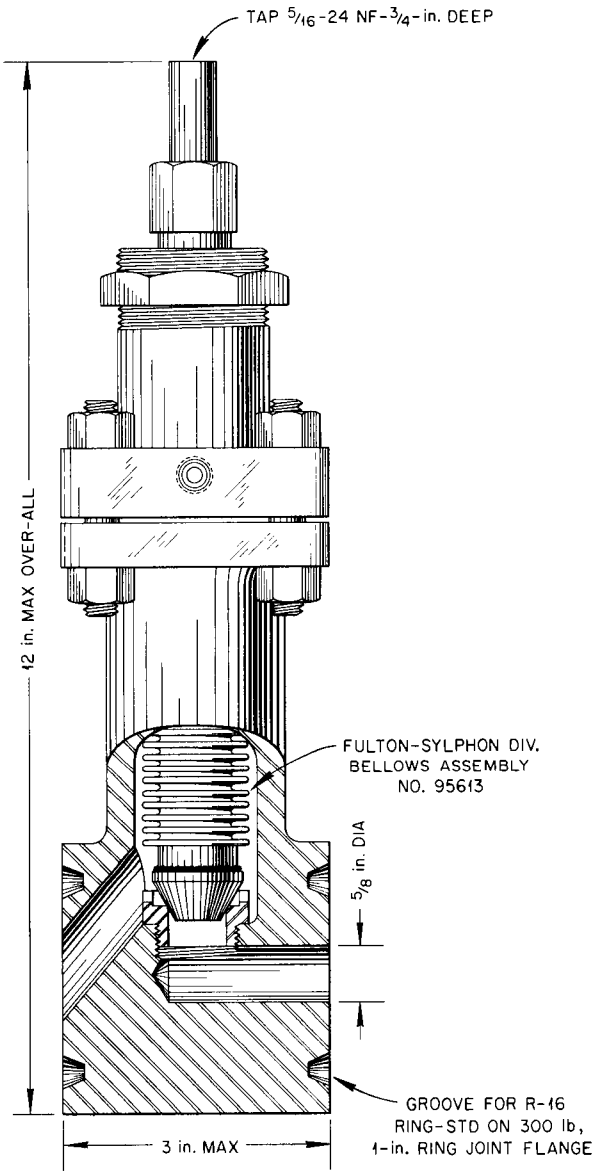

Fig. 1.31. One-half-inch 500-psi Valve.

1.5.3 Valves

Design has been completed and purchase requisitions have been issued for all HRT valves.

Figure 1.31 shows the valve which will be used in low-pressure process piping. It is a ½-in. 500-psi valve with integral flange face and has a stem seal which uses a 1⅛-in. Fulton-Sylphon bellows. The trim material for this valve is Stellite 6 and Stellite 12.

Shown in Fig. 1.32 is the ⅛-in. 2000-psi valve with an integral stainless steel, type 347, seat and with Stellite 6 overlay on the poppet. The bellows manufacturer has not been selected. This type of valve will be used in the sampler and to bleed gas from the circulating pumps.

Figure 1.33 shows the ½-in. 2000–500-psi valve using stacked 1⅛-in. Fulton-Sylphon bellows

UNCLASSIFIED
ORNL-LR-DWG 4082

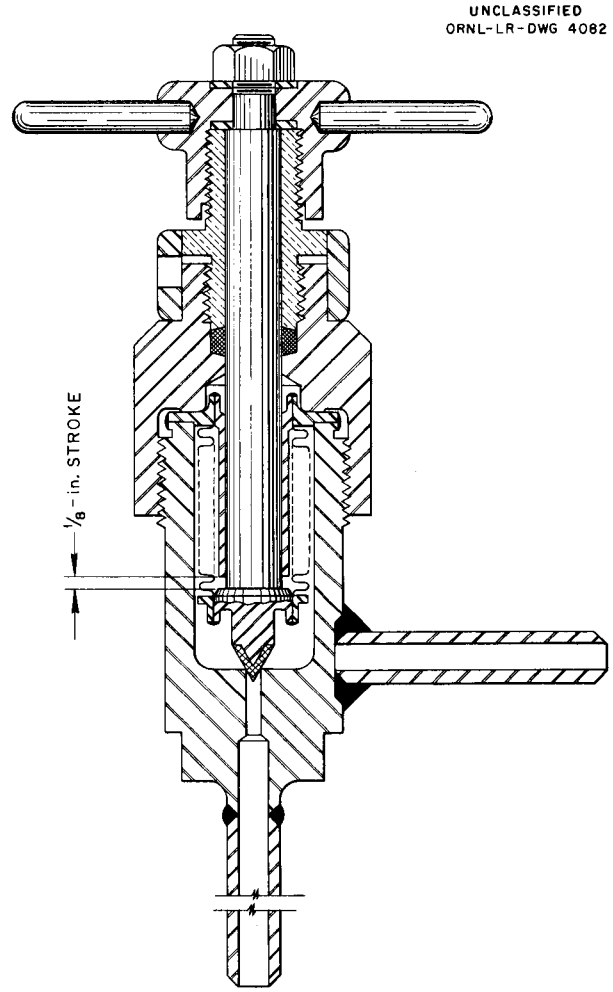

Fig. 1.32. One-eighth-inch 2000-psi Valve.

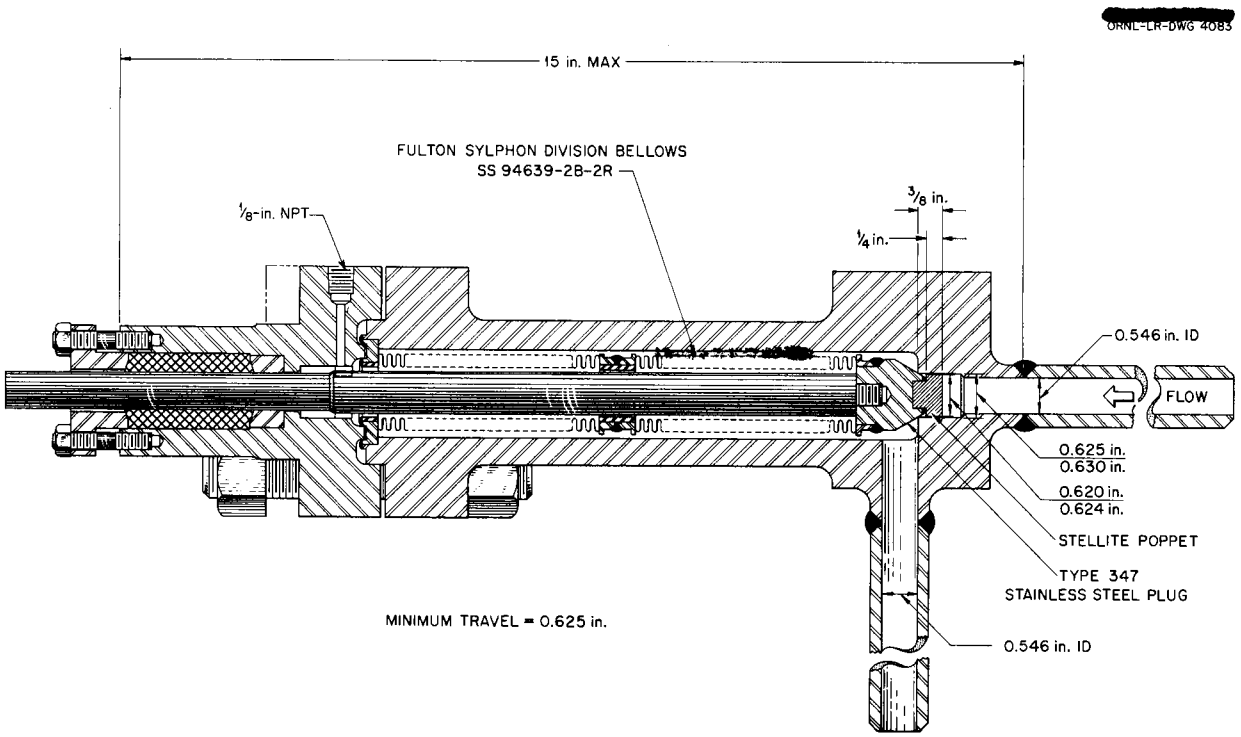

Fig. 1.33. One-half-inch 2000–500-psi Valve.

intended for use in the dump and let-down lines. Trim material is integral stainless steel, type 347, for the seat and seating surface of the poppet, with Stellite 6 for the throttling tip.

For throttling characteristics between the metering ranges of $\frac{1}{8}$- and $\frac{1}{2}$-in. valves, the $\frac{1}{2}$-in. valve will be used with a $\frac{1}{4}$-in. spline plug.

The results of the life tests performed on the stacked Fulton-Sylphon bellows at 600 psi and 250°C are given in Table 1.4. The $\frac{5}{8}$-in. movement is satisfactory for all design requirements.

In an attempt to find a suitable bellows for the $\frac{1}{8}$-in. 2000-psi valve, several $\frac{3}{8}$-in. Clifford bellows were tested; the results are given in Table 1.5. The results are considered as borderline, and additional testing is proceeding.

TABLE 1.4. RESULTS OF LIFE TESTS ON FULTON-SYLPHON BELLOWS AT 600 psi AND 250°C

Bellows No.	Stroke (in.)	Cycles Before Failure
1	$\frac{1}{2}$	114,000
2	$\frac{5}{8}$	14,678
3	$\frac{5}{8}$	10,065
4	$\frac{3}{4}$	8,338
5	$\frac{3}{4}$	3,382

1.5.4 Instrumentation Costs

The costs of all instruments and circuits required for the HRT have been estimated and are given in Table 1.6. The procurement of instrument items is approximately 60% complete. The electrical-service design for the building (engineering by K-25) is 95% complete.

TABLE 1.5. RESULTS OF TESTS ON CLIFFORD BELLOWS

Bellows No.	Pressure (psi)	Temperature (°C)	Stroke (in.)	Cycles Before Failure
1	1200	200	1/8	6,897
2	1350	200	1/8	9,674
3	2000	250	1/8	6,510
4	2000	250	1/8	5,711
5	2000	250	1/8	2,946
6	2000	250	3/32	11,953
7	2000	250	3/32	14,000

TABLE 1.6. ESTIMATED EQUIPMENT AND INSTALLATION COSTS OF HRT INSTRUMENTS AND CIRCUITS

	Equipment Cost	Installation Cost	Total
Reactor sensing elements	$ 35,000	$ 35,000	$ 70,000
Valves and operators*	75,000*	25,000	100,000
Nuclear instruments	15,000	5,000	20,000
Receivers and controllers	40,000	40,000	80,000
Steam system	14,000	14,000	28,000
	$179,000	$119,000	$298,000

*Includes spares.

Part II

THORIUM BREEDER REACTOR

W. C. Moore

[redacted]

2. CONCEPTUAL DESIGN

2.1 DESIGN PROGRAM OBJECTIVE

R. B. Korsmeyer

As previously outlined by Briggs and Edlund,[1] the objective of the TBR design program is to present the concept of a Th-U^{233} breeder power station in sufficient detail to provide the basis for detailed design by an architect-engineer. The first step in the program comprises an analysis of the relative effects of major process variables on the economics and characteristics of two-region thorium breeder reactors so that the optimum combination of values for the variables may be selected as the basis of design. The investigation of the process variables is nearing completion, and the results to date are presented in Sec. 2.2. From these results most of the major reactor characteristics have been determined; they are reported in Sec. 2.3, together with certain other engineering studies pertinent to the early phases of the program.

2.2 REACTOR ANALYSIS

M. C. Edlund, Section Chief

H. C. Claiborne M. Tobias
L. C. Noderer T. B. Fowler

2.2.1 Method and Conditions of Calculation

The data that were used for obtaining the [redacted] characteristics and cost factors are given in other reports.[2,3]

A schematic flow diagram of the system studied is shown in Fig. 2.1. As shown, the core will be processed by two methods. The liquid-solids separation plant, after precipitation of poisons, is estimated to be capable of removing 75% of the fission-product poisons effected by chemical processing.[4] Complete poison removal from the core solution (flow rate small compared with cycling rate through liquid-solids separation plant) carrying the precipitated poisons is effected in the Thorex plant. All processing of the slurry blanket will be done in the Thorex plant.

[redacted]

ORNL-LR-DWG 4084

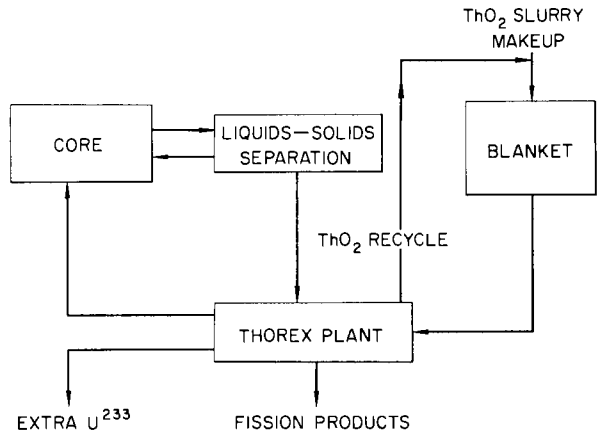

Fig. 2.1. Schematic Flow Diagram of Reactor System.

In order to produce uranium of high enrichment (about 95% U^{233}), the blanket stream will have to be processed for removal of the excess U^{233} (represented by breeding gain) before the core and blanket streams are mixed in the chemical processing plant. The core-stream enrichment will be only 25 to 30% U^{233}. By processing to remove protactinium, nearly 100% U^{233} could be produced. For these calculations, it was assumed that the uranium product would be that derived from the blanket mixture, that is, all protactinium decayed to U^{233} and mixed with the original uranium isotopes.

The different reactor systems were compared on the basis of a fixed amount of electrical power delivered to a network, since power is the main product. If power output were not held constant, the effect of the process variables would be masked by the effect of power level, the most important factor in unit cost calculations.

An electrical power output of 125 Mw was chosen as standard for one reactor, or 375 Mw for a three-reactor station. The parameter studies, other than those of temperature, were made for an average reactor temperature of 280°C. This was equivalent

[1] R. B. Briggs and M. C. Edlund, *A Preliminary Program for the Conceptual Design of the TBR*, ORNL CF-54-8-89 (Aug. 13, 1954).

[2] R. B. Briggs, *Aqueous Homogeneous Reactors for Producing Central-Station Power*, ORNL-1642 (May 4, 1954).

[3] H. C. Claiborne and M. Tobias, *Thorium Breeder Reactor Studies*, ORNL-1810 (to be issued).

[4] J. Halperin and R. W. Stoughton, *Some Effects of Transmutation Products on U^{233} Breeder Pile Operation*, ORNL-1368 (Sept. 29, 1952).

to 480.8 Mw of heat for a net station efficiency of 26.0%. The other net station efficiencies used in the study of the effect of different reactor temperatures were 21.1, 24.2, 27.1, and 28.1% for 200, 250, 300, and 320°C, respectively.[3]

The method of calculation consists of four main parts: (1) calculation of the uranium isotope concentrations in the blanket and the core by isotope balance equations for the particular blanket power selected; (2) two-group nuclear calculations to determine the critical concentration and the neutron balance, which yield, in turn, the core power and the ratio of resonance to thermal capture in the thorium; (3) unit cost calculations; (4) unit costs plotted vs total reactor power so that the costs at a particular total power could be used for comparison of the systems.

The parameters studied were core diameter, blanket thickness, blanket U^{233} concentration, thorium concentration, and core poisons for a reactor temperature of 280°C. The external power densities for the core and blanket systems were 20 and 14 kw/liter, respectively. The temperature study was carried out for only 1000 g of thorium per liter.

2.2.2 Results

The results shown in Tables 2.1–2.3 and in Figs. 2.2–2.5 have been normalized to 125 Mw (electrical) for two-region thorium power-breeder reactors operating at an average temperature of 280°C.

The effect of core poisons, which is related to the core processing cycle time, on relative unit cost and U^{233} production is shown in Fig. 2.2. The core poisons have little effect on the unit cost in the range of 4 to 10% with the minimum occurring near 7%. The gross breeding ratio (neglects processing losses) increases nearly linearly with reduction in poisons. Below 3% poisons, however, the net U^{233} production starts to decrease, since the highly increased chemical processing rate leads to significant uranium and protactinium losses. The same phenomenon would occur if the blanket U^{233} were lowered to small values. Figure 2.3 indicates that about 3 g of U^{233} per kilogram of thorium produces the lowest unit cost.

A breakdown of the unit costs and neutron balances for four reactors is shown in Table 2.1. The first one shown is fairly typical of all reactors

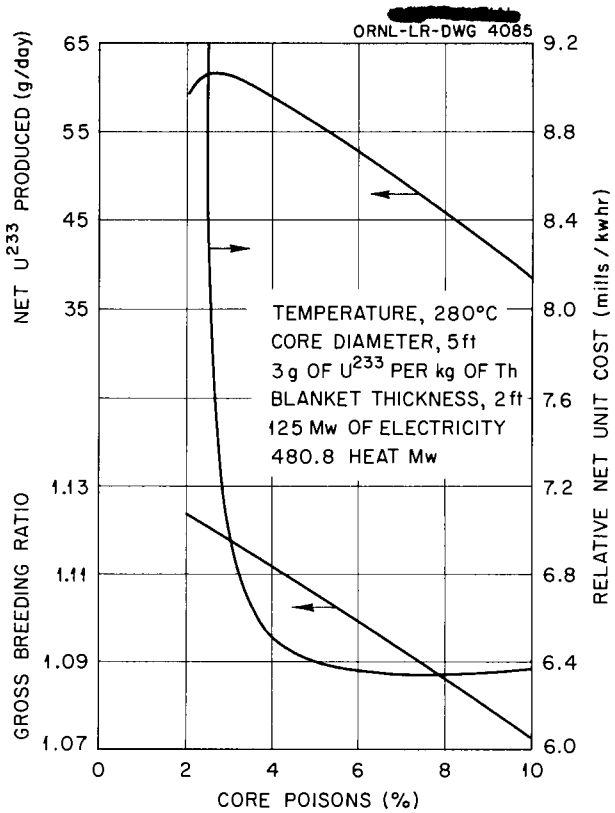

Fig. 2.2. Effect of Core Poisons on Relative Unit Cost and U^{233} Production.

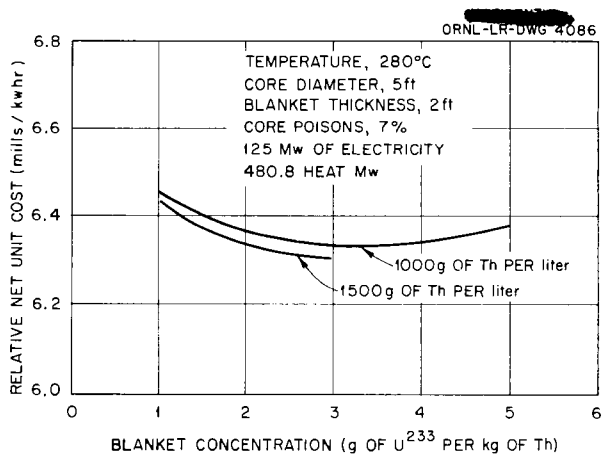

Fig. 2.3. Effect of U^{233} Blanket Concentration on Relative Unit Cost.

calculated for reasonable ranges of the parameters. The other three reactors indicate, in order, the effects of: very low core poisons (2.0%), reduction

TABLE 2.1. TYPICAL COST BREAKDOWN AND NEUTRON BALANCES

	Reactors			
Concentration, grams of Th per liter	1000	1000	500	1000
Core poisons, %	7.0	2.0	7.0	6.0
Group-3 poisons[4] cross section at 20°C, barns	40	40	40	18
Process Characteristics and Costs				
Core diameter, ft	5	5	5	5
Blanket thickness, ft	2	2	2	2
Grams of U^{235} per kilogram of Th in blanket	3	3	3	3
Blanket poisons, %	4.42	4.45	5.50	2.72
Blanket power, Mw	88	91	89	90
Core power, Mw	393	390	392	391
Net unit cost of power, mills/kwhr	6.33	16.8	6.53	6.23
Plant investment (less chemical processing), mills/kwhr	3.74	3.74	3.74	3.74
Fuel inventory, mills/kwhr	0.46	5.84	0.37	0.42
D_2O inventory, mills/kwhr	0.49	0.49	0.49	0.49
Fixed chemical processing, mills/kwhr	0.76	0.76	0.76	0.76
Blanket processing, mills/kwhr	0.24	0.24	0.20	0.24
Core processing, mills/kwhr	0.09	5.17	0.09	0.06
Operation and maintenance, mills/kwhr	0.75	0.75	0.75	0.75
Feed cost (D_2O and Th), mills/kwhr	0.18	0.18	0.18	0.18
Uranium (233 and 235) credit, mills/kwhr	0.37	0.34	0.05	0.41
Gross breeding ratio (233 and 235)	1.092	1.124	1.013	1.103
Net $U^{233} + U^{235}$ produced, g/day	48.8	59.1	6.7	55.3
U^{233} in product, weight fraction	0.956	0.956	0.937	0.959
U^{235} in product, weight fraction	0.0015	0.0015	0.0026	0.0014
Core system volume, liters	21,500	21,300	21,400	21,400
Blanket system volume, liters	15,400	15,400	15,200	15,300
Core concentration, g of U^{233} per kg of D_2O	2.54	2.38	2.44	2.48
Core concentration, g of U^{235} per kg of D_2O	0.34	0.33	0.38	0.30
Core concentration, g of U per kg of D_2O	9.32	8.74	9.90	8.39
Care Thorex cycle, days	199	2.31	194	335
Blanket Thorex cycle, days	131	129	87	130
Net thorium consumption, g/day	601	623	555	615
Flux at core wall, neutrons/cm^2/sec	1.00×10^{15}	1.10×10^{15}	1.36×10^{15}	1.10×10^{15}

TABLE 2.1. (continued)

Neutron Balance				
Absorptions in fuel				
U^{233} (core)	0.7984	0.7903	0.7928	0.7954
U^{233} (blanket)	0.2016	0.2097	0.2072	0.2046
U^{235} (core)	0.1184	0.1178	0.1350	0.1056
U^{235} (blanket)	0.0005	0.0005	0.0010	0.0005
Neutron losses (other than fuel)				
Core				
Poisons	0.0578	0.0164	0.0584	0.0488
U^{234}	0.1172	0.1165	0.1328	0.1044
U^{236}	0.0187	0.0186	0.0214	0.0166
Sulfur	0.0024	0.0024	0.0026	0.0022
Core tank	0.0305	0.0321	0.0396	0.0311
D_2O	0.0169	0.0179	0.0174	0.0173
Blanket				
Th (thermal)	0.8008	0.8330	0.8230	0.8128
Th (resonance)	0.3226	0.3268	0.2264	0.3220
Pa	0.0203	0.0218	0.0338	0.0208
Poisons	0.0081	0.0085	0.0104	0.0051
U^{234}	0.0019	0.0020	0.0032	0.0017
U^{236}	3×10^{-7}	4×10^{-7}	8×10^{-7}	3×10^{-7}
D_2O	0.0027	0.0028	0.0059	0.0027
Fast leakage	0.0385	0.0393	0.0508	0.0387
Slow leakage	0.0111	0.0113	0.0423	0.0112
Total absorptions and losses	2.5684	2.5677	2.6040	2.5415
Neutrons produced from U^{233}	2.3200	2.3200	2.3200	2.3200
Neutrons produced from U^{235}	0.2475	0.2472	0.2842	0.2217
Total neutrons produced	2.5675	2.5672	2.6042	2.5417
U^{233} breeding ratio (less processing losses)	1.083	1.106	0.982	1.093
U^{233} breeding ratio (with processing losses)	1.081	1.095	0.981	1.090

of thorium concentration to 500 g of thorium per liter in the blanket, and reduction in the group-3 poison[4] cross section from 40 to 18 barns. The higher cross section is a conservative value that has been used in previous studies; the lower value is the latest estimate for thorium-uranium reactors. Reducing the poison cross section by a factor of more than 2 generally reduces the net unit cost by 0.1 mill/kwhr and shifts the optimum core poisons from 7 to 6%. The core cycle time is the only factor that is appreciably affected.

The major results of the study on various parameters are shown in Fig. 2.4. It is immediately apparent that the net unit cost is very insensitive

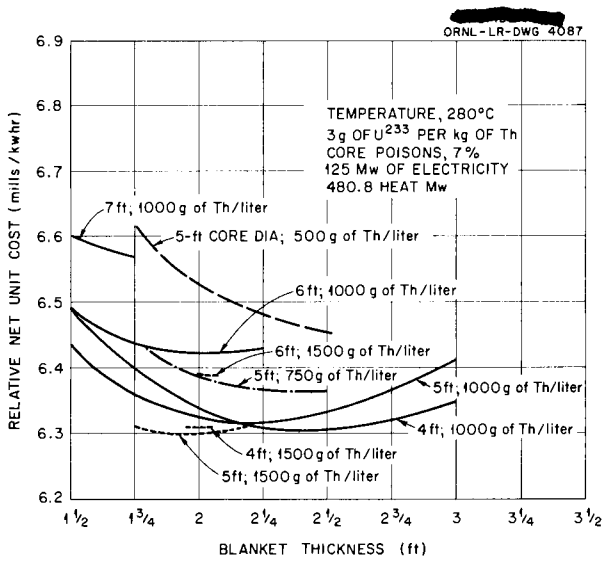

Fig. 2.4. Effect of Blanket Thickness on Relative Unit Cost.

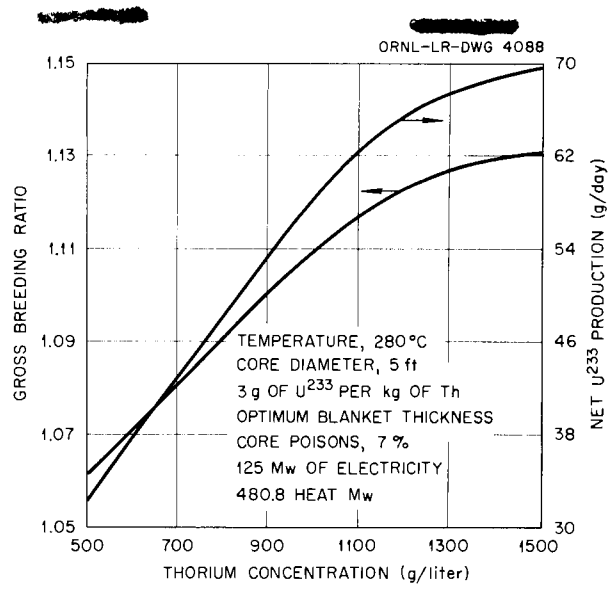

Fig. 2.5. Effect of Thorium Concentration on U^{233} Production.

to the parameters investigated; only 0.3 mill/kwhr separates the highest and lowest cost shown. This was not unexpected, since about 56% of the cost represents the fixed charges against the reactor plant and turbo-generator plant investment, and about 22% represents the operation and maintenance cost and fixed charges (investment and operating) on the chemical plant. The lowest unit cost results from using a thorium concentration of 1500 g/liter; however, the cost is only 0.02 mill/kwhr less than that for 1000 g/liter. An insignificant saving (0.01 mill/kwhr) is also indicated for the 4-ft core vs the 5-ft core. Such slight differences at this stage are too insignificant to warrant consideration in view of the probable extra engineering difficulties that would occur for such a high thorium concentration and high power density (near 400 kw/liter) resulting from the use of a 4-ft core. It was further indicated from this study that even if a thorium concentration as low as 500 g/liter and a core 6 ft in diameter had to be used, because of slurry problems and power density considerations, the unit cost would not be increased enough to preclude the possibility of economical generation of power.

Figure 2.5 shows the effect of thorium concentration on the breeding ratio and the net U^{233} production and further indicates that increasing thorium concentrations to greater than 1000 g/liter leads to little benefit.

The effect of temperature on cost is shown in Fig. 2.6. In this calculation a group-3 poison[4] cross section of 18 barns, rather than 40 barns, at 20°C was used. The indication is that little is to be gained by raising the average temperature over 280°C.

2.2.3 Effect of Substantial Errors in Some of the Two-Group Constants upon the TBR Calculations

Two-group constants which have been estimated for use in the TBR economic calculations were based on theoretical models possessing unavoidable inadequacies; as a result, there were uncertainties, believed to be of the order of 10 to 20%, in the values obtained. It was considered useful, therefore, to examine the effect of substantial changes (±50%) in the two-group constants for a typical case. While the study is not yet complete, the indications thus far are that the economic effects result almost entirely from altering the amount of credit obtained from excess fuel production. The largest effect thus far observed has been a difference of about 0.6 mill/kwhr (out of a total relative cost of about 6.4 mills) between two cases where combinations of extreme values were employed. Cases where only indi-

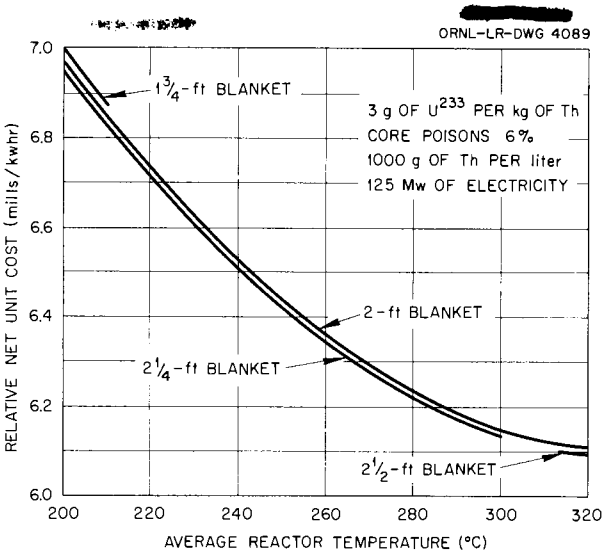

Fig. 2.6. Effect of Temperature on Relative Unit Cost.

vidual values were altered caused changes in the total cost of usually less than 0.1 mill. The critical mass and the breeding gain were much more strongly affected. Considerable changes in the core uranium concentration do not, however, lead to proportionally large variation in fuel inventory charges, since the latter contains a contribution of similar magnitude from other sources. The effects upon breeding gain are almost directly converted into changes in credit received for excess fuel production.

It seems reasonable, therefore, to conclude that, as long as about 85% of the power cost is tied up in factors unaffected by errors in the two-group constants, such errors are of secondary economic importance.

A summary of the results and constants used is presented in Table 2.2.

2.2.4 Comparison of Multigroup and Two-Group Breeder Reactor Calculations

Three thorium breeder reactors were calculated on the UNIVAC with the use of the 27-group Eyewash code in order to test the two-group method and constants. In general, the calculations show that the resonance fission in U^{233} accounts for from 10 to 15% of the total fissions and that the fast leakage is less by a factor of about 3 than that predicted by ignoring U^{233} resonances and inelastic scattering in thorium. These calculations predict about 15% less uranium in the core and a 2 or 3% increase in the breeding ratio. Caution, however, should be used in interpreting these results, since α for U^{233} was assumed to be constant, whereas it may be larger for the various resonances.

Direct comparison was hampered because the UNIVAC results were obtained for fixed uranium concentrations, yielding values of ν that were too small. Also, machine difficulties did not allow time to get concentrations for the proper value of ν. Therefore two-group uranium concentrations were later obtained with the use of the observed and the proper value of ν. These results, normalized to one fast neutron, are shown in Table 2.3. All reactors had a temperature of 280°C and had 1000 g of thorium per liter in the blanket with 2 g of U^{233} per kilogram of thorium.

2.3 ENGINEERING STUDIES

R. B. Korsmeyer

A. L. Gaines
P. N. Haubenreich
M. I. Lundin
R. G. McGrath[5]
J. R. McWherter[6]
W. F. Taylor[7]

2.3.1 Selection of Reactor Characteristics for Preliminary Design

As shown by the ORACLE calculations and other studies, the real cost of power will depend greatly on the capital investment, and this figure cannot be determined accurately until a power station is designed in considerable detail around a specific reactor. A study of this kind will also reveal the relative magnitude of all the engineering problems which must be solved and the direction in which further development is most profitable.

To this end, the major characteristics of a particular two-region reactor have been selected from the above-described ORACLE calculations with the restriction that proven components or systems be utilized in all possible cases. Where this is not presently possible, as is illustrated by the thorium slurry blanket system, a design most nearly approaching research experience will be selected. The major characteristics of the reactor are given in Table 2.4. A 5-ft-dia core was chosen, rather than a smaller one, because

[5] Westinghouse Electric Corp.
[6] Part-time employee.
[7] Pioneer Service & Engineering Co.

TABLE 2.2. EFFECT OF SUBSTANTIAL CHANGES[a] IN THE NUCLEAR CONSTANTS[b]

		C_T	C_X	B	$B(G)$	$G(U)$
Extrapolation distance, in.	7.62	6.2572	0.3879	1.0968	51.71	8.4
	15.24[c]	6.24	0.4173	1.1038	55.5	8.4
15.24	22.86	6.219	0.4294	1.1070	59	8.4
η	2.28					
2.32	2.36					
$\sigma_a(13)$	48.4					
96.8	145.2					
	106.2	6.1363	0.5288	1.1315	70.5	8.7930
τ_B	191.2	6.2103	0.4400	1.1096	58.6	8.4694
212.4	233.6	6.2483	0.3943	1.0984	52.58	8.3564
	318.6	6.3245	0.3062	1.0766	40.83	8.1812
	109					
τ_C	196.2					
218	239.8					
	327					
D_{1B}	0.745	6.2232	0.4048	1.1009	53.97	7.456
1.49	2.24	6.238	0.4235	1.1055	56.43	8.9915
D_{2B}	0.5865					
1.173	1.76					
D_{1C}	0.835	6.224	0.4332	1.1068	57.1	9.506
1.67	2.505	6.226	0.4097	1.1040	50.23	7.8063
D_{2C}	0.6152					
1.2304	1.846					
p_B	0.28					
0.56	0.84					
Combination case 1 (D's, τ's, p high; extrapolation distance low)		6.692	0.0102	1.0035	1.22	15.4
Combination case 2 (D's, τ's, p low; extrapolation distance high)		6.0804	0.5131	1.1278	68.42	3.5317

[a]The following properties were common to all the calculations performed:

Temperature, 280°C
W, grams of U^{233} per kilogram of thorium, 3
G_{02}, grams of thorium per liter, 1000
f_{pc}, poison fraction in core, 0.06
Reactor power, 480.8 Mw (125-Mw electrical output)
Core diameter, 5 ft
Pressure-vessel diameter, 9 ft
External power densities, kw/liter
Core system, 20
Blanket system, 40

[b]Symbols in column headings are defined as follows:

C_T = total power cost, mills/kilowatt-hour,
C_X = credit for excess fissionable material produced, mills/kilowatt-hour,
B = gross breeding gain, atoms of fissionable material produced before process losses per atom of fuel burned,
$B(G)$ = net grams of fissionoble material produced per day,
$G(U)$ = uranium concentration in core, grams of uranium per kilogram of heavy water.

[c]This row gives results for standard case. Underlined numbers are values chosen for parameters in standard case.

TABLE 2.3. COMPARISON OF MULTIGROUP AND TWO-GROUP BREEDER REACTOR CALCULATIONS

	Reactor with 4-ft-dia Core and 2-ft-thick Blanket			Reactor with 4-ft-dia Core and 3-ft-thick Blanket			Reactor with 5-ft-dia Core and 2-ft-thick Blanket		
	Eyewash	Two-Group	Two-Group	Eyewash	Two-Group	Two-Group	Eyewash	Two-Group	Two-Group
ν	2.2469	2.2469	2.5520	2.2464	2.2464	2.5520	2.2850	2.2850	2.5520
Residual thorium	0.1463	0.1339	0.1406	0.1494	0.1422	0.1500	0.1207	0.1110	0.1179
Residual U^{233}	0.0730	0	0	0.0731	0	0	0.0464	0	0
Fast leakage	0.0078	0.0223	0.0247	0.0014	0.0062	0.0071	0.0069	0.0183	0.0203
Slow thorium	0.3454	0.3411	0.3886	0.3532	0.3544	0.4032	0.3768	0.3735	0.4131
Slow uranium	0.4165	0.4896	0.4310	0.4165	0.4897	0.4310	0.4350	0.4814	0.4310
Slow leakage	0.0057	0.0078	0.0086	0.0010	0.0021	0.0023	0.0049	0.0067	0.0074
D_2O absorption	0.0053	0.0053	0.0063	0.0054	0.0054	0.0064	0.0093	0.0091	0.0103
Breeding ratio	1.0045	0.9702	1.2279	1.0265	1.0143	1.2834	1.0335	1.0066	1.2320
Concentration, g of U^{233} per liter	3.9459	4.6239	3.2808	3.9459	4.6247	3.2791	2.0987	2.4262	1.8668

of the uncertainty about engineering difficulties possibly associated with the higher power density and high concentrations for smaller cores. A net electrical capability of 100 Mw per reactor, in a three-reactor station containing its own fuel and blanket reprocessing facility, was set as the design base rather than the 125 Mw (electrical) per reactor used in most of the ORACLE calculations. Some adjustment in the values shown is to be expected as design proceeds.

2.3.2 Comparison of Two Methods for Starting Up the TBR

The ORACLE calculations have shown that the optimum steady-state blanket concentration is about 3 g of U^{233} per kilogram of thorium. At this concentration the power generated in the blanket will be nearly 20% of the total. One way of bringing the reactor up to steady-state operation is to begin with the blanket containing only D_2O and thorium and to delay chemical processing until the U^{233} has built up to the desired level. Another way is to load some U^{235} (or U^{233}) with the thorium in the blanket at startup. A study of the comparative costs of the two methods has shown that there is an economic advantage in having fissionable material in the blanket from the beginning.

If the TBR is started with 1000 g of thorium per liter and no uranium in the blanket, about five months at full core power will be required before the U^{233} concentration will reach the optimum level for steady-state operation. If chemical processing is begun at this point, the reactor must operate a total of at least seven months before uranium produced in the blanket will be available for sale or for feed to the core. Since the blanket power starts at a very low value and builds up gradually, the reactor power during the five-month period will be less than the capacity built into the heat-removal and -generating equipment. If, on the other hand, fissionable material is introduced into the blanket at startup, the blanket power can be held at the design level from the first. Extraction of uranium from the blanket can begin almost immediately so that the product will be available for core feed after only about two months.

An examination of the possible differences in cost between the two starting methods will show that after the initial seven-month period there will be no continued difference except for a possible difference in inventory charges on the U^{233} in the blanket. During the first seven months the items which will differ are: cost of core feed, cost of chemical processing, credit for excess U^{233} produced, income from power, and the inventory charges on U^{233}. Table 2.5 compares the first four items. The total difference between the two methods is $1,500,000, whereas the value

TABLE 2.4. REACTOR CHARACTERISTICS FOR PRELIMINARY DESIGN OF A 300-Mw STATION

(First Approximation)

Electrical capability (each of three reactors), Mw	100
Gross station efficiency, %	29.2
Net station efficiency, %	26.0
Operating pressure, psia	2000

Item	Core	Blanket
Reactor Construction		
Material	Zircaloy-2	20% stainless-steel-clad carbon steel
Wall thickness, in.	0.5	5.0
Thermal shield thickness, in.		4.0
Space between shield and vessel, in.		1.0
Pipe connections	Concentric	Straight-through
Inside diameter	5 ft 0 in.	10 ft 5 in.
Blanket thickness		2 ft 3 in.
Volume, liters	1855	13,200
Reactor Systems		
Operating temperature, °C (°F)		
Average	280 (536)	
Inlet	250 (482)	
Outlet	300 (572)	
System volume, liters	17,500	18,300
Fluid composition	UO_2SO_4-D_2O-$CuSO_4$	ThO_2-D_2O-(U)
U^{233}	2.53 g per kg of D_2O	3.00 g/liter*
U^{234}	6.28 g per kg of D_2O	0.12 g/liter*
U^{235}	0.34 g per kg of D_2O	0.004 g/liter*
U (total)	9.15 g per kg of D_2O	3.12 g/liter*
Thorium		1000 g/liter*
Inventory		
D_2O, kg	16,500	17,300
$U^{233} + U^{235}$, kg	43.1	55
Thorium, kg		16,540
Flux at core wall, neutrons/cm^2/sec	0.86×10^{15}	
Power density at core wall, kw/liter	66.0	
Mean power density in reactor, kw/liter	169	5.45
Power density in external system, kw/liter	20.0	14
Reactor power, Mw (heat)	313	72
Poisons, fraction	0.07	
Insoluble poisons, fraction	0.01	
Fraction of poisons removed, fraction	0.75	

TABLE 2.4. (continued)

Item	Core	Blanket
Reactor Systems		
Gross breeding ratio		1.1111
Net U^{233} produced, g/day		48.2
Total uranium produced, g/day		50.1
Circulation rate, gpm	24,000	
Maximum fluid velocity, fps	40	~50
G for D_2O decomposition, molecules of D_2 per 100 ev	1.67	
Rate of D_2 formation (no catalyst), lb mole/sec	0.109	
Rate of O_2 formation (no catalyst), lb mole/sec	0.054	
Gas dissolved		
In solution, g mole of D_2 per liter	0.105	
At outlet, g mole of O_2 per liter	0.052	
Volume of gas generated (D_2 + O_2) (wet)		
At 300°C and 2000 psia, cfm	144	
At STP, cfm	3510	
$CuSO_4$ concentration required for 100% recombination at 280°C and 2000 psia, g mole/liter	0.005	
Fraction of total gas production (no catalyst) required to hold Xe poison to ~1%	0.27	
Volume rate to hold Xe to ~1% at 300°C and 2000 psia, cfm	40	
Chemical Processing		
Filtration cycle, days	1.00	
Thorex cycle, days	200	150
Processing rate		
Fluid, liters/day	84.3	110
U^{233} + U^{235}, g/day	242	331
Total uranium, g/day	771	
Protactinium, g/day		~100
Thorium, kg/day		110
Cooling period to get $\leq 3\beta W/l$, days	94	55
Thorium feed rate, g/day		496
Thorex uranium inventory, kg	~24	~24
Thorex thorium inventory, kg		~6000

*At operating conditions.

of the uranium required to fill the blanket originally is about $1,000,000. It is evident that, no matter how inventory charges are reckoned, the method involving an initial loading of the uranium in the blanket is the more desirable of the two considered. This is because the steady-state blanket doubling time is less than the period required to establish the blanket fissionable-material inventory by breeding alone, thus yielding a net gain in U^{233} produced. In addition, there is some increase in revenue from the greater sale of power.

2.3.3 Xenon-Removal Problem

Calculations have been made to determine the poisoning effect of Xe^{135} in the TBR under various conditions of gas removal and handling. The xenon concentration in the reactor core can be significantly reduced by allowing part of the dissociated deuterium and oxygen to form bubbles and thus to strip xenon from the solution. The magnitude of the reduction depends on the rate at which bubbles form and the design of the system for handling the separated gas.

TABLE 2.5. COMPARISON OF SOME COST ITEMS DURING INITIAL SEVEN-MONTH OPERATING PERIOD

(Units are in Millions of Dollars)

[redacted]	With Uranium in the Blanket at Startup	Without Uranium in the Blanket at Startup
Costs		
Core feed	2.02	2.02
Blanket processing	0.03[a]	0.12[b]
	2.05	2.14
Credit		
U^{233} produced	0.00	1.24[c]
Electric power from blanket	0.43	0.67
	0.43	1.91
Net cost	1.62	0.23

[a]Two months.
[b]Seven months.
[c]Five months.

For a given rate of bubble formation, a system which lets down to low pressure for recombination gives the greatest reduction in Xe^{135} concentration, because the liquid returned to the main circulating system is practically free of xenon, an impossibility with high-pressure recombination. Figure 2.7 shows the xenon poison in the core at a core power level of 320 Mw (heat) as a function of bubble rate for a system in which the return stream contains no Xe^{135} at all.

Figure 2.8 represents a high-pressure recombination system. In such systems the concentration

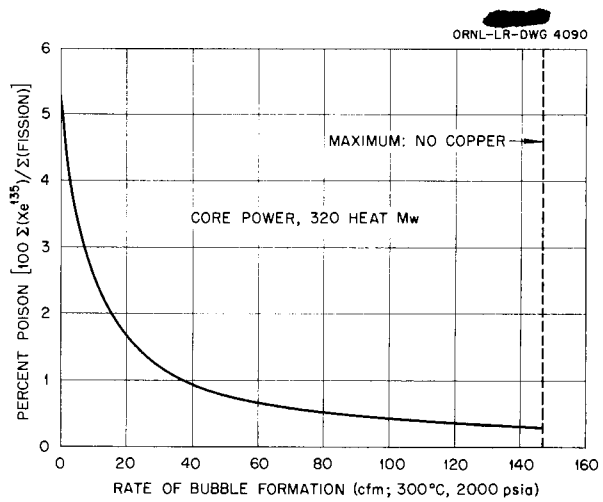

Fig. 2.7. Xenon Poisoning in the TBR with Low-[redacted]ure Recombiner.

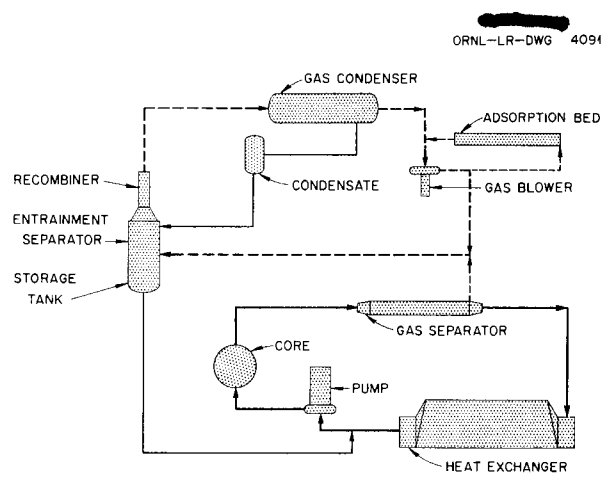

Fig. 2.8. High-Pressure Recombination System with Small-Void Gas Separator.

of xenon in the diluent gas tends to build up to relatively high levels. Unless some means is used to prevent this buildup, the stream of liquid returning from the storage tank will carry back to the core almost as much xenon as was stripped in the gas bubbles. The concentration can be kept low by passing part of the diluent gas through adsorption beds where the Xe^{135} is held up to allow it to decay (as shown). Figure 2.9 shows how the xenon poison is affected by the flow rate of gas to the adsorption beds. (The rates (cfm) shown are for the gas from which all Xe^{135} is removed. The same effect could be obtained by removing part of the Xe^{135} from a larger stream.) The particular system to which these results apply is one using a small-void gas separator with the radiolytic gases diluted after leaving the separator. (The system in Fig. 2.8 is of this type.) An alternative is a system incorporating a gas separator with a large void through which the diluent gas is circulated.[8] In this case there will be some direct transfer of xenon between the gas and the main body of the liquid in the separator. Furthermore, the rate of entrainment will be quite high even at low bubble rates. As a result, the reduction in xenon poisoning is generally less for the large-void systems. This is illustrated by Fig. 2.10.

[8] R. B. Briggs, *Aqueous Homogeneous Reactors for Producing Central-Station Power*, ORNL-1642, Fig. 5 (May 4, 1954).

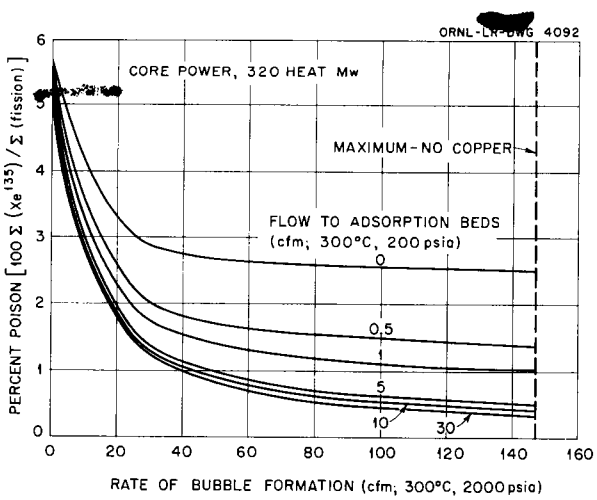

Fig. 2.9. Xenon Poisoning in the TBR with High-Pressure Recombiner and Small-Void Gas Separator. Entrainment equal to one-tenth the bubble rate.

2.3.4 Correlations of Engineering Data

For the purpose of securing consistent calculations on system optimization studies, a compilation of the accepted best information on engineering and thermodynamic data pertinent to TBR design has been undertaken. Although the data being compiled are available from various sources and in many forms, a graphic presentation in consistent engineering units will expedite design calculations.

To date, 10 graphs have been issued showing the density and cost relations for heavy water and solutions of uranyl sulfate in heavy water as a function of the temperature and the concentration of uranium in solution. The calculated costs of the fluids are based on the assumed values of $40 per pound of heavy water and $20 per gram of highly enriched uranium.

Information on the estimated costs of reactor system components is being compiled for use in TBR optimization studies. To date, the costs have been compiled for heat exchangers, reactor vessels, canned-rotor pumps, and stainless steel welding, bending, piping, and fittings in relation to size and types of construction. The cost figures are built up from actual materials quotations with labor, overhead, and profit added as

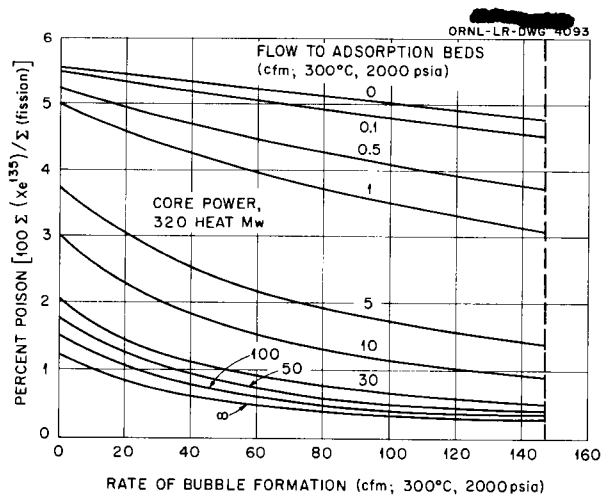

Fig. 2.10. Xenon Poisoning in the TBR with High-Pressure Recombiner and Large-Void Gas Separator. Entrainment, 500 gpm.

[redacted]

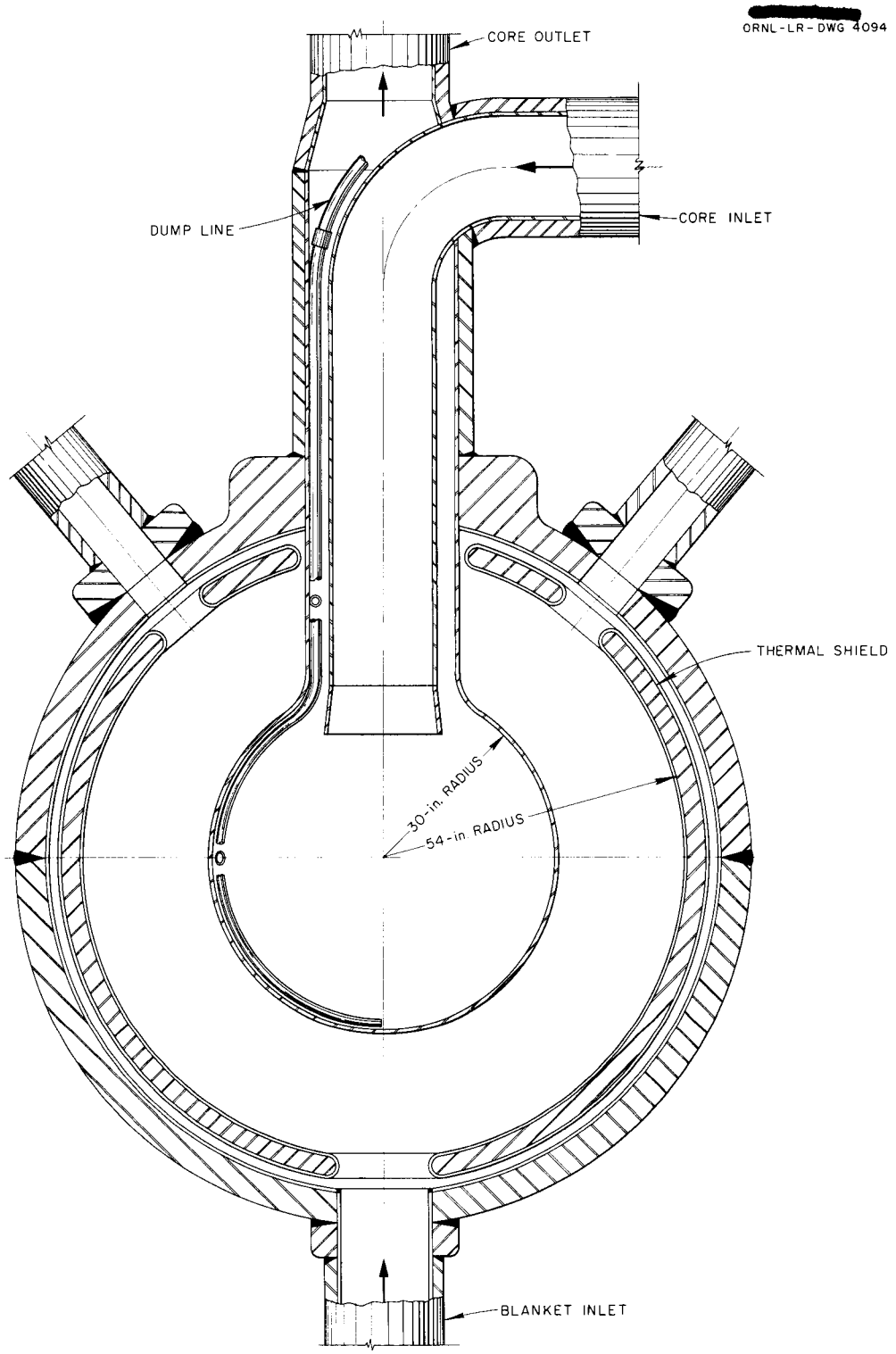

Fig. 2.11. Schematic View of Reactor Vessel with Thermal Shield.

percentages of materials costs. In addition, curves have been prepared so that approximate heat-exchanger dimensions could be estimated from the relations between the number of tubes that can be placed in a shell of given diameter and the tube size and spacing. At present a tube pitch of $\frac{5}{8}$ in. is required to permit seal welding of tube ends to the tube sheet. As welding techniques are improved, it should be possible to approach the TEMA (Tubular Exchanger Manufacturers Association) pitch of $\frac{15}{32}$ in.; at this pitch, up to 78% more tubes can be placed in a shell of a given diameter. The higher the surface-to-volume ratio of an exchanger can be made, the smaller the holdup becomes, with consequent reduction in the charges for the nondepreciable inventory.

2.3.5 Preliminary Study of Pressure-Vessel Design

Due to the relatively high radiation field existing at the outer surface of the blanket, the pressure vessel could be subject to large thermal stresses, caused by absorption of the radiation, which, added to the pressure stress, could exceed the allowable working stress for the vessel. The heat generation in the vessel wall is minimized by placement of a dense shield, such as several inches of steel, just inside the vessel. Since the shield is not a structural member, fairly high thermal stresses can be allowed in it and the temperature can be kept within suitable limits by circulation of part of the blanket fluid between the shield and vessel wall. A schematic diagram of such a reactor vessel and its thermal shield is shown in Fig. 2.11.

Calculations of the thermal and total stress for a carbon-steel vessel containing a 9-ft-dia blanket at 2500 psia pressure have been made by utilizing thermal shields of different thicknesses and without a shield, at core and blanket powers of 320 and 80 Mw (heat), respectively. Two limiting cases were assumed: the inner and outer surfaces of the vessel were at the same temperature (minimum stress); the vessel was completely insulated so that all flow of heat was inward to the blanket (maximum stress for insulated vessel). The thermal- and fast-neutron flux distribution in this reactor, determined previously,[9] is shown in Fig. 2.12. By use of this distribution the gamma flux incident on the thermal shield was determined, and from the neutron and gamma flux at the shield the contributions of each to heat generation in the shield and vessel wall were calculated.[10] The heat generation per unit volume in the steel vs the distance through the steel from the inside surface of the thermal shield is shown in Fig. 2.13. From this figure the thermal stress in the vessel wall was calculated for various shield and vessel thicknesses, and the results are shown in Figs. 2.14 and 2.15.

The pressure stress in the vessel wall was calculated for a pressure of 2500 psia and added to the thermal stresses to indicate the total stress in the vessel wall, as shown in Figs. 2.16 and 2.17.

[9] P. N. Haubenreich, *Preliminary Nuclear Calculations for the Thorium Breeder Reactor*, ORNL CF-54-8-61 (Aug. 13, 1954).

[10] J. R. McWherter, *Thermal Stress in the TBR Pressure Vessel*, ORNL CF-54-10-146 (Oct. 28, 1954).

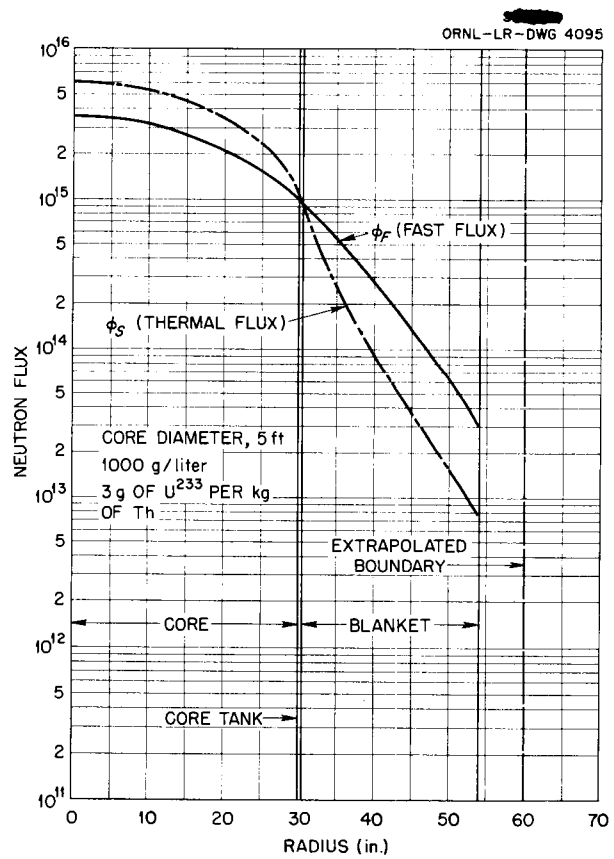

Fig. 2.12. Thermal- and Fast-Neutron Flux Distribution in Reactor.

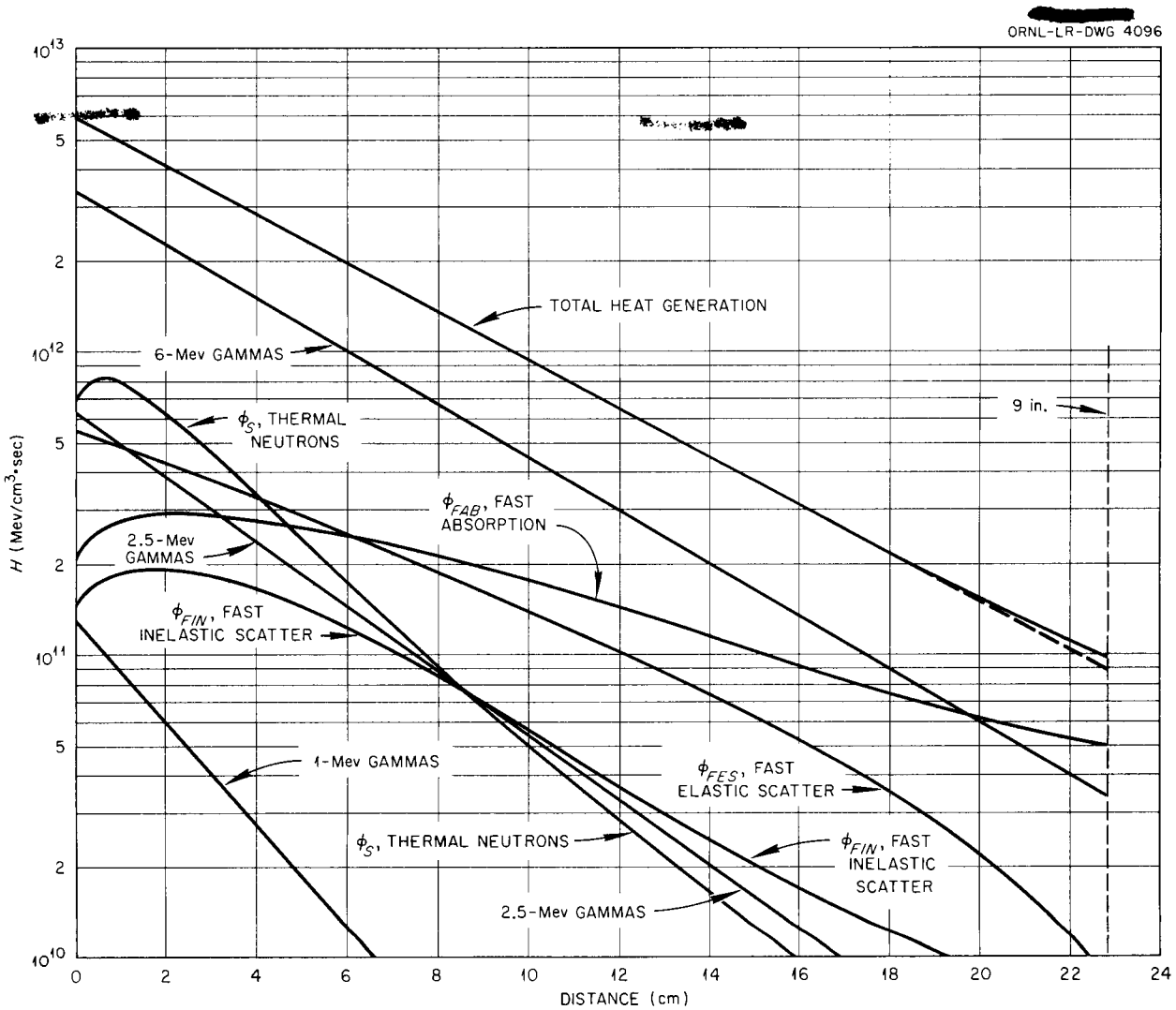

Fig. 2.13. Specific Heat Generation vs Thickness of Steel.

[redacted]

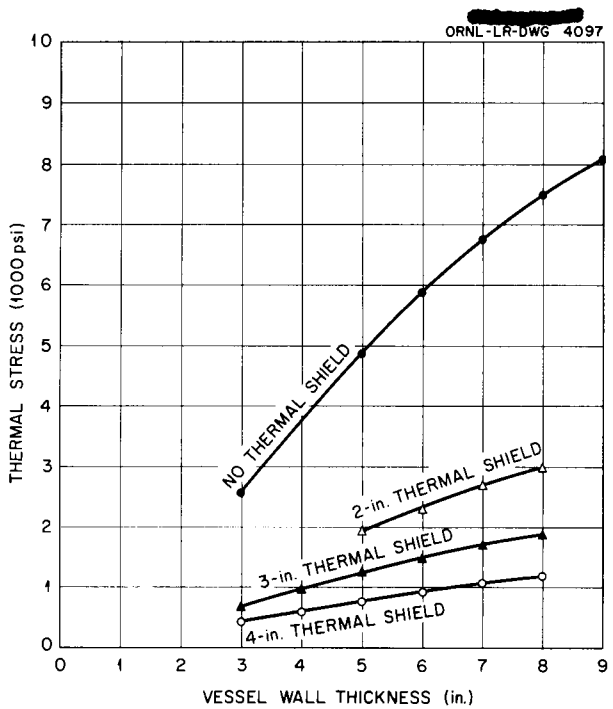

Fig. 2.14. Thermal Stress for Equal Vessel Wall Temperatures.

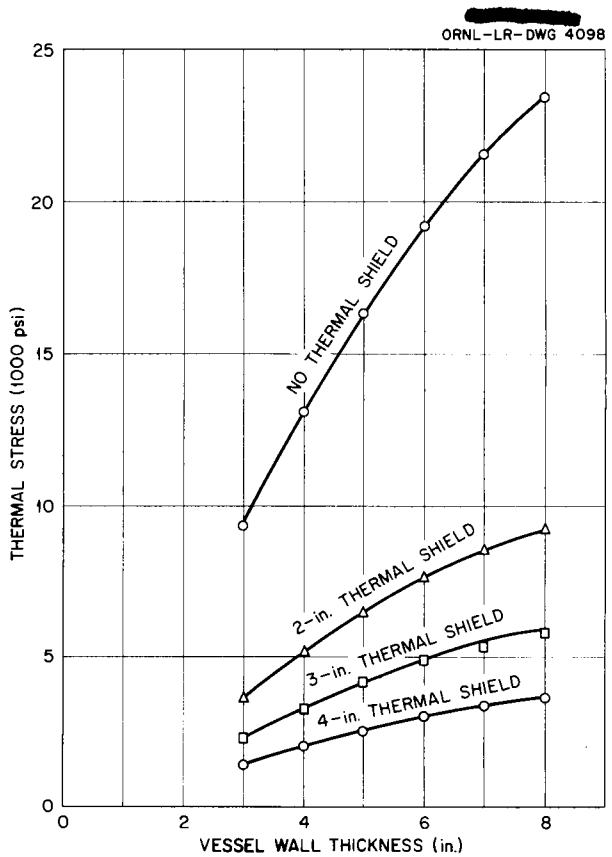

Fig. 2.15. Thermal Stress for Completely Insulated Vessel.

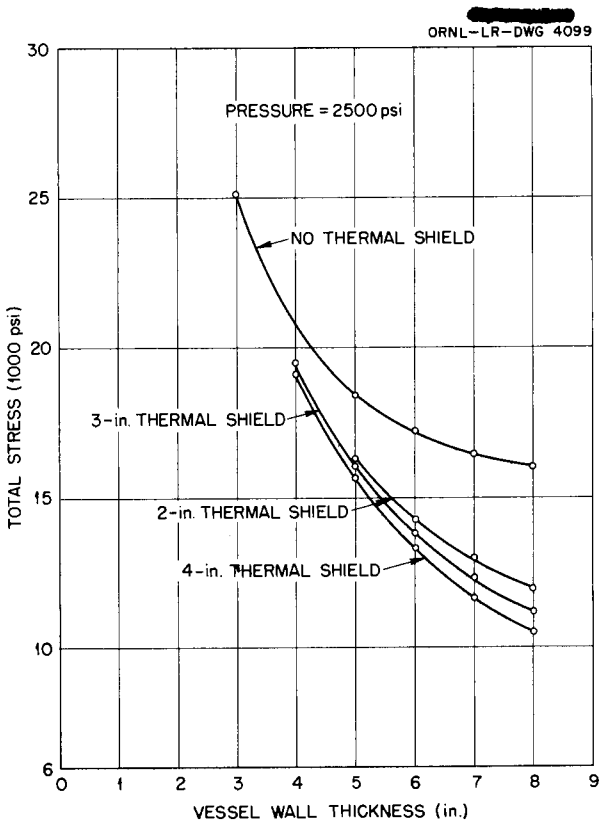

Fig. 2.16. Total Stress for Equal Vessel Wall Temperatures.

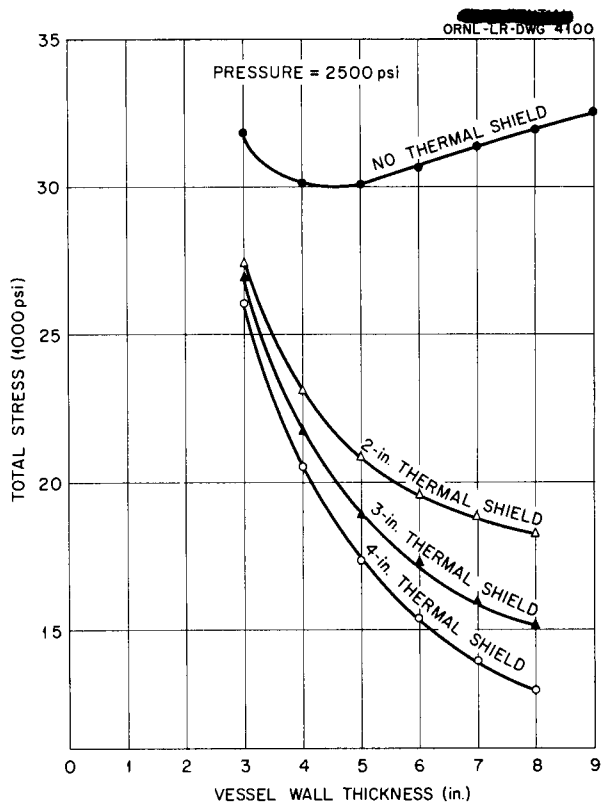

Fig. 2.17. Total Stress for Completely Insulated Vessel.

Part III

CORROSION

E. G. Bohlmann

3. PUMP-LOOP CORROSION TESTS

J. C. Griess H. C. Savage
R. S. Greeley F. J. Walter
R. E. Wacker R. M. Warner

3.1 PUMP-LOOP OPERATION AND MAINTENANCE

H. C. Savage F. J. Walter
R. M. Warner

3.1.1 Loop Status

(a) Solution. Fourteen dynamic test loops are available for corrosion tests. At present, multisample[1] loops A, K, and M are being used to conduct long-term corrosion tests.

Loop F has been used in an attempt to determine the minimum oxygen concentration necessary to stabilize uranyl sulfate solutions under various conditions. In order to circumvent the difficulties of building a 1-gpm let-down system, an attempt was made to control the oxygen concentration in the loop by regulating a flow of oxygen-saturated condensed steam from the pressurizer gas space to the main circulating system. Unfortunately, adequate oxygen-concentration control has not been attainable with this approach; so other systems will have to be investigated.

Loop L has been removed and cross sectioned for inspection. The interior walls of the main circulating pipe (1 ½-in. Schedule-80 IPS, type 347 stainless steel) showed no excessive or localized corrosion attack except in one small area immediately downstream from the corrosion sample holder. This loop also contained several standard 1 ½-in. tees, none of which was seriously corroded. Loop L had a cumulative operating time of more than 12,000 hr. Table 3.1 gives a condensed operating history. This loop has been replaced with a new multisample loop.[1]

Loop C has been removed and is being cross sectioned for examination. This loop contained a variety of fittings such as standard tees, elbows, pipe-bend sections with different radii, and saddle-weld tees.

(b) Slurry. In line with the interest in corrosion and/or erosion by thorium oxide slurries, two new loops are being designed for the study of slurry corrosion. Corrosion specimens and holders identical to the ones now used in uranyl sulfate corrosion tests[2] will be used. The major effort on the loop and sample-holder design has been to minimize the number of places for slurry to settle out. The general loop design is based on the experience of the REED Engineering Research Section. Figure 3.1 shows the design of the sample holder. A Plexiglas mockup of this sample holder has been built for flow testing. Figure 3.2 is an elevation of the proposed slurry loop. Present plans provide for each loop to contain five sample holders in parallel. The two slurry loops will replace solution loops B and C.

To investigate the adaptability of the present in-pile loop design[3] to the circulation of thorium oxide slurries, several attempts were made to pump thorium oxide slurry in an in-pile type of loop. Minor revisions made to the loop at the start of this phase of work included the removal of the in-line sample holder assembly, provision for a small stream of condensate (approximately 100 cc/hr) flow from the vapor space in the pressurizer to the back of the 5-gpm ORNL pump, and the addition of a ¼-in.-dia sampling connection in the pump discharge line.

The concentration of the slurry charged to the loop initially was 500 g of thorium per kilogram of H_2O; the slurry had been prepared from Lindsay No. 7 oxide and distilled water. Although the slurry was stirred with a small laboratory stirrer several hours prior to charging the loop, it was observed to settle very rapidly the instant that agitation was stopped. Simultaneously with filling the loop with thorium oxide, several hundred milliliters of distilled water was added to the rear of the pump. The loop was operated at 250°C and the pressurizer at 280°C.

Samples of the circulating slurry taken approximately 3 hr after the loop had reached operating temperature were found to be extremely low in

[1] H. C. Savage, R. A. Lorenz, and D. Schwartz, *HRP Quar. Prog. Rep. March 31, 1953*, ORNL-1554, p 48.

[2] H. C. Savage *et al.*, *HRP Quar. Prog. Rep. March 15, 1952*, ORNL-1280, p 46, Fig. 16 and p 61, Fig. 28.

[3] G. H. Jenks *et al.*, *HRP Quar. Prog. Rep. April 30, 1954*, ORNL-1753, p 81–83.

thorium oxide, indicating settling out of the thorium oxide.

After approximately 26 hr of operation, the loop instrumentation indicated that the pressurizer was completely plugged; so the run was discontinued. Examination of the loop after shutdown revealed that the major portion of the oxide charged to the loop had collected in the pressurizer and pressurizer-heater section as a caked plug. The core corrosion specimens in the core sample holder

TABLE 3.1. OPERATING HISTORY OF LOOP L (100A PUMP)

Solution	Gas	Temperature (°C)	Operating Time (hr)	Cumulative Operating Time Including Rinses (hr)
H_2O	O_2	250	194.3	208.1
0.17 *m* UO_2SO_4 + 0.1 *m* $CuSO_4$	O_2	250	45.9	254.0
H_2O	O_2	250	75.4	338.0
0.17 *m* UO_2SO_4 + 0.1 *m* $CuSO_4$	O_2	250	957.0	1,295.0
0.17 *m* UO_2SO_4	O_2 and CO_2	250	959.3	2,265.4
0.02 *m* UO_2SO_4	O_2	250	2039.3	4,357.1
0.02 *m* UO_2SO_4 + 0.05 *m* $CuSO_4$	O_2	250	1017.2	5,374.3
0.17 *m* UO_2SO_4 + 0.07 *m* HNO_3	O_2	250	100.0	5,482.7
0.02 *m* UO_2SO_4 + 0.006 *m* H_2SO_4	O_2	250	1465.2	6,947.9
0.17 *m* UO_2SO_4 + 0.04 *m* $CuSO_4$	O_2	250	400.5	7,348.3
0.17 *m* UO_2SO_4	O_2	225	900.1	8,251.2
0.004 *m* UO_2SO_4 + 0.002 *m* H_2SO_4	O_2	250	909.4	9,161.1
0.004 *m* UO_2SO_4 + 0.005 *m* H_2SO_4	O_2	250	1000.5	10,161.6
0.004 *m* UO_2SO_4 + 0.015 *m* H_2SO_4	O_2	250	969.0	11,130.6
0.015 *m* H_2SO_4	O_2	250	148.0	11,278.6
1.34 *m* UO_2SO_4	O_2	275	592.6	11,871.2
0.67 *m* UO_2SO_4	O_2	250	150.3	12,021.5

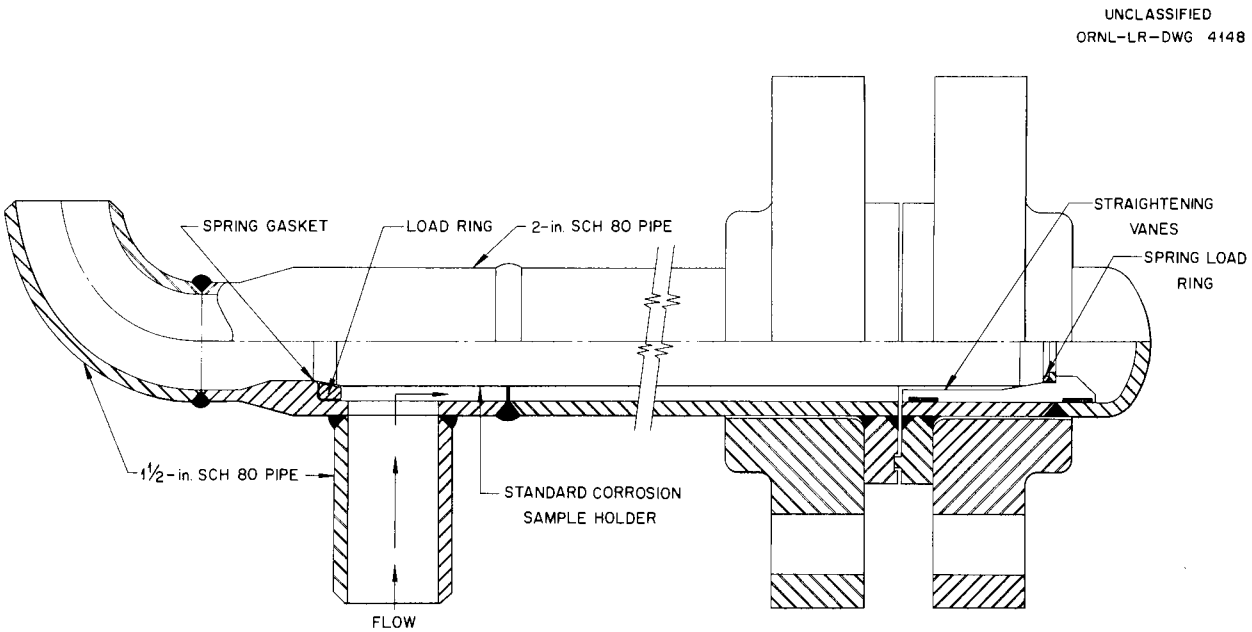

Fig. 3.1. Slurry-Loop Sample Barrel for Standard Corrosion Specimen Holder.

showed no appreciable weight loss or signs of corrosion.

During the first run the pressurizer lines had been connected to the high-pressure line (discharge line) of the pump. In order to obtain a higher flow rate through the pressurizer and thus reduce the possibility of plugging, its lines were connected across the core sample holder. Also, a flow restrictor in the form of a sharp venturi was installed in the pump to increase the pressurizer pressure relative to the pump suction pressure, thus assuring a flow of condensed vapor from the pressurizer to the back of the pump.

The second run was attempted with a slurry of Lindsay No. 7 oxide with a concentration of 1000 g of thorium per kilogram of H_2O which had been mixed in a small laboratory colloid mill for approximately 8 hr. This slurry did not settle out of solution rapidly when agitation was stopped.

At the start of the run, the pressurizer temperature and the loop temperature had approached 150 and 100°C, respectively, when the loop temperature-control instrumentation was found to be defective. All heating was stopped for approximately 2 hr to perform the necessary repairs. During this period it became apparent that the slurry in the loop was not circulating. When numerous attempts to relieve the situation failed, the run was stopped. During disassembly of the loop prior to cleaning, caked thorium oxide was found in the core sample holder and the pressurizer heater and pressurizer.

These tests have been terminated pending further study of thorium oxide slurries and the design requirements for maintaining circulation.

3.1.2 Westinghouse 100A Pumps

In a previous report[4] it was mentioned that two 100A pump rotor shafts had broken off near the impeller keyway. Subsequently, an additional shaft broke in the same fashion. Metallurgical and visual inspection of these fractures indicated that they were progressive-type failures which started at a stress-riser near the back of the impeller keyway. One of the failures occurred on a shaft that had been repaired by building up with weld deposit followed by machining to size. Another failure occurred on a titanium (Ti-150A) shaft.

In a previous report[5] it was noted that several Westinghouse 100A rotors had been repaired and returned to service by replacing the front stub

[4] H. C. Savage and F. J. Walter, *HRP Quar. Prog. Rep. July 31, 1954*, ORNL-1772, p 60.

[5] H. C. Savage and F. J. Walter, *HRP Quar. Prog. Rep. Jan. 31, 1954*, ORNL-1678, p 49.

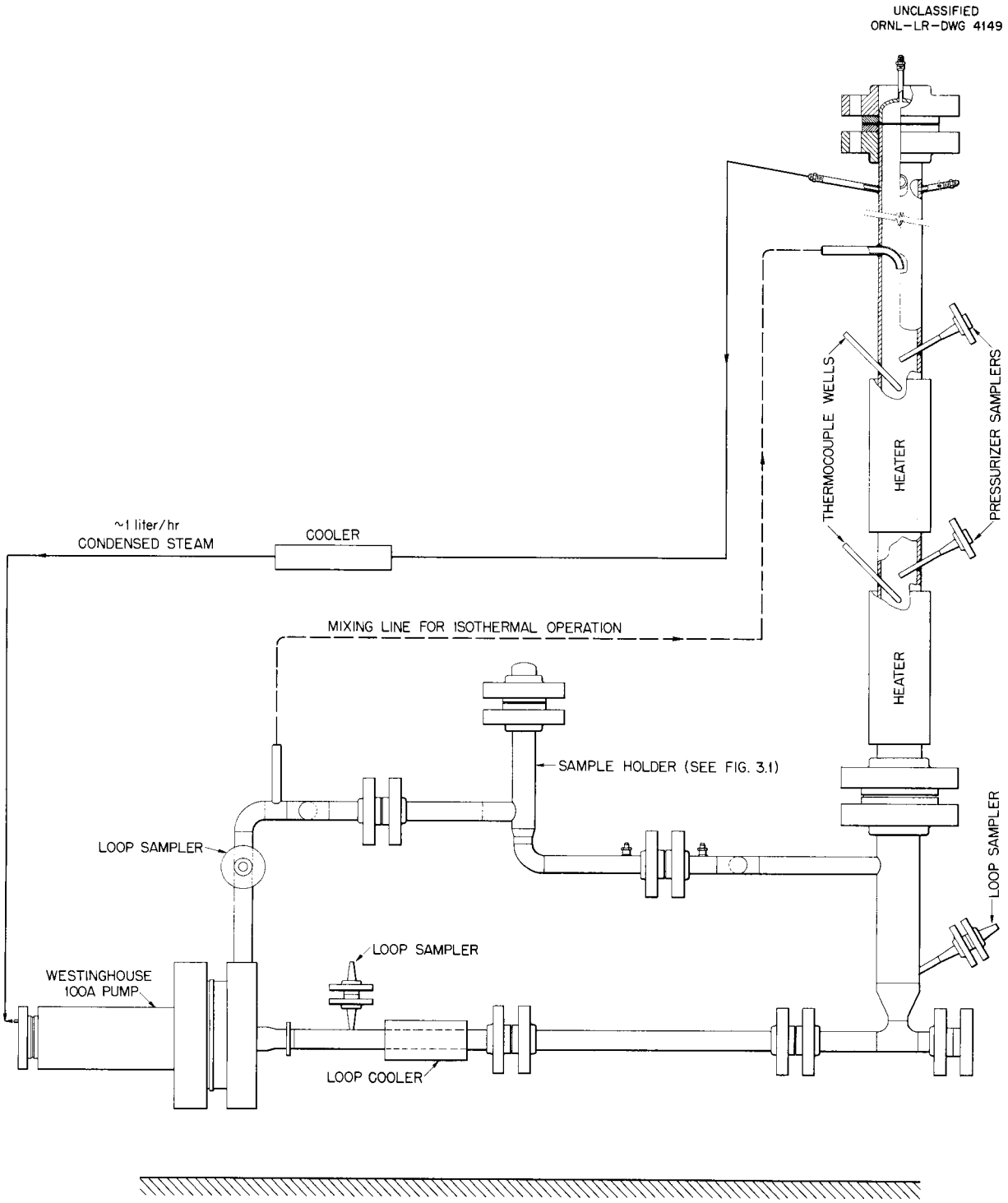

Fig. 3.2. Slurry Corrosion Test Loop.

shafts. These shafts were repaired by cutting off the old shaft and shrinking a new one into the shaft hub without replacing the shaft hub. All the rotors repaired in this manner failed after a short time in service (~40 to 1000 hr). In an attempt to locate the reasons for these failures, the cans were removed from the rotors, and it was discovered that the rotor-shaft hubs were loose where they had been shrunk into the iron core. To date, six rotors have failed because of loosening of the hub. An attempt has been made to remedy this situation by slightly changing the design of the shaft hub to give a more rigid support where it is shrunk into the core. All rotors are now being repaired to the new design as required.

3.2 RESULTS OF LOOP TESTS

J. C. Griess R. S. Greeley

3.2.1 Introduction

The corrosion resistance of several stainless steels to 0.06 *m* uranyl sulfate containing 0.006 *m* sulfuric acid has been determined at 200 and 225°C. The type of attack found under the above conditions generally paralleled the behavior observed at the same temperatures with other uranyl sulfate concentrations. Thus at both 200 and 225°C the heavy scale formed on the specimens contained at least some hydrated iron oxides, which apparently lacked the protective quality of the anhydrous oxide formed at higher temperatures. Also, the critical velocity was poorly defined at both temperatures, as was the case in both 0.02 and 0.17 *m* uranyl sulfate.

Attempts to dissolve iron and chromium oxides which had previously been deposited on titanium and zirconium corrosion specimens in uranyl sulfate solutions (as concentrated as 1.34 *m*) have proved to be unsuccessful. The specimens were mounted in the titanium loop and exposed to uranyl sulfate solutions flowing at 75 fps at 200 or 250°C, and even under these severe conditions weighable amounts of oxide were not removed either by chemical dissolution or by mechanical forces.

Several observations have been made concerning the desirability of having chromate ions present in the uranyl sulfate systems. Generally, the presence of hexavalent chromium in solution increased the critical velocity and minimized attack at flow rates less than the critical velocity.

The results of all the corrosion testing that has been completed during the past quarter are reported in tabular form (Table 3.2), and the more pertinent data are discussed in the following sections.

3.2.2 Results

(a) General Corrosion Rates. The average corrosion rates of pin-type corrosion specimens exposed in the loops during the past quarter are presented in Table 3.2. The presentation is the same as it has been in a number of previous reports,[6–12] and the same precautions given before should be exercised in using the data. All corrosion rates reported in Table 3.2 are average rates for the given exposure period. At flow rates less than the critical velocity, corrosion is not a constant rate process; the rate is usually high at the beginning of the exposure and decreases to a steady, usually low, rate after 50 to 200 hr. Thus the average rates given in Table 3.2 are greatly dependent on the duration of the test. The data at low flow rates, then, are of only limited value in an absolute sense but are of value for comparison of one alloy with another in a given run. At high flow rates the corrosion process usually occurs at a constant rate, and the data in Table 3.2 have a quantitative significane in these cases.

(b) Corrosion Testing in 0.06 *m* Uranyl Sulfate Containing 0.006 *m* Sulfuric Acid at 200 and 225°C. The corrosion of stainless steels has been studied previously[12] in 0.06 *m* uranyl sulfate containing 0.006 *m* sulfuric acid at 250°C. This study has been extended to other temperatures during the past quarter. Table 3.2 gives the pin data for runs E-29 through E-31 at 200°C and for runs I-13 through I-16 at 225°C.

---

[6] J. C. Griess, J. M. Ruth, and R. E. Wacker, *HRP Quar. Prog. Rep. Jan. 1, 1953*, ORNL-1478, p 63.

[7] J. C. Griess and R. E. Wacker, *HRP Quar. Prog. Rep. March 31, 1953*, ORNL-1554, p 49.

[8] J. C. Griess and R. E. Wacker, *HRP Quar. Prog. Rep. July 31, 1953*, ORNL-1605, p 74.

[9] J. C. Griess and R. E. Wacker, *HRP Quar. Prog. Rep. Oct. 31, 1953*, ORNL-1658, p 45.

[10] J. C. Griess and R. E. Wacker, *HRP Quar. Prog. Rep. Jan. 31, 1954*, ORNL-1678, p 50.

[11] J. C. Griess and R. E. Wacker, *HRP Quar. Prog. Rep. April 30, 1954*, ORNL-1753, p 61.

[12] J. C. Griess, H. C. Savage, and F. J. Walker, *HRP Quar. Prog. Rep. July 31, 1954*, ORNL-1772, p 59.

TABLE 3.2. CORROSION RESULTS OF PIN TYPE SPECIMENS

Run No.	Test Conditions					Pin Material	Number of Pins	Corrosion Rate (mpy)		
	UO_2SO_4 Concentration (m)	Temperature (°C)	Time (hr)	Additions	Flow Rate (fps ± 10%)			Minimum	Average	Maximum
C-41[a]	0.11	250	516	1000–2000 ppm O_2 0.016 m H_2SO_4	11	Type 304L stainless steel	2	8.6	10	12
						Type 347 stainless steel	9	6.0	9.4	12
						Type 309 SCb stainless steel	2	9.2	9.4	9.5
						Carpenter 20	1		14	
					22	Type 304L stainless steel	4	68	75	78
						Type 347 stainless steel	14	15	24	42
						Type 347 stainless steel[b]	4	86	98	110
						Type 309 SCb stainless steel	4	13	39	69
						Carpenter 20	2	44	64	84
C-42	0.11	250	493	1000–2000 ppm O_2 0.016 m H_2SO_4	11	Type 304L stainless steel	2	9.8	10	11
						Type 321 stainless steel	2	1.8	11	20
						Type 347 stainless steel	7	10	11	12
						Type 347 stainless steel[b]	1		4.8	
						Type 309 SCb stainless steel	2	10	11	11
					23	Type 304L stainless steel	5	19	66	82
						Type 321 stainless steel	3	22	46	82
						Type 347 stainless steel	11	16	24	34
						Type 347 stainless steel[b]	5	81	99	120
						Type 309 SCb stainless steel	4	17	48	75
C-43	0.11	250	506	1000–2000 ppm O_2 0.016 m H_2SO_4	11	Type 304L stainless steel	2	5.4	6.9	8.3
						Type 321 stainless steel	2	7.9	9.5	11
						Type 347 stainless steel	7	2.7	7.9	10
						Type 347 stainless steel[b]	1		2.3	
						Type 309 SCb stainless steel	2	9.5	10.3	11
					24	Type 304L stainless steel	5	35	48	63
						Type 316L stainless steel	2	74	80	85
						Type 318 stainless steel	2	52	56	60
						Type 321 stainless steel	3	26	41	63

TABLE 3.2. (continued)

Run No.	Test Conditions: UO_2SO_4 Concentration (m)	Temperature (°C)	Time (hr)	Additions	Flow Rate (fps ± 10%)	Pin Material	Number of Pins	Corrosion Rate (mpy): Minimum	Average	Maximum
C-43	0.11	250	506	1000–2000 ppm O_2 0.016 m H_2SO_4	24	Type 347 stainless steel	9	12	17	27
						Type 347 stainless steel[b]	2	45	59	73
						Type 309 SCb stainless steel	4	15	31	38
						Titanium–5% aluminum–2.5% tin	1[c]			
D-32–D-34[d]	0.02	275	142	1000–2000 ppm O_2 0.005 m H_2SO_4	16	Type 304L stainless steel	3	1.1	1.5	1.8
						Type 304 stainless steel[b]	1		2.0	
						Type 321 stainless steel	1		1.6	
						Type 347 stainless steel	4	1.9	2.1	2.6
						Type 347 stainless steel[b]	1		1.3	
						Type 309 SCb stainless steel	2	1.3	1.6	1.8
						Zircaloy-2	1[e]			
E-29	0.06	200	852	1000–2000 ppm O_2 0.006 m H_2SO_4	17	Type 304L stainless steel	4	11	12	14
						Type 318 stainless steel	1		7.7	
						Type 347 stainless steel	7	4.8	7.7	9.9
						Type 309 SCb stainless steel	2	8.7	9.9	11
					28	Type 304L stainless steel	5	17	19	22
						Type 304 stainless steel[f]	1		20	
						Type 316 stainless steel[b]	1		18	
						Type 318 stainless steel	2	18	19	19
						Type 322W stainless steel[g]	1		7.6	
						Type 322W stainless steel[b]	1		6.1	
						Type 347 stainless steel	8	17	20	22
						Type 347 stainless steel[b]	2	18	18	18
						Type 309 SCb stainless steel	3	17	18	19
						Miscro 4[i]	1		15	
						Titanium–3% aluminum–5% chromium	1[j]			

TABLE 3.2. (continued)

Run No.	Test Conditions: UO_2SO_4 Concentration (m)	Temperature (°C)	Time (hr)	Additions	Flow Rate (fps ± 10%)	Pin Material	Number of Pins	Corrosion Rate (mpy): Minimum	Average	Maximum
E-29	0.06	200	852	1000–2000 ppm O_2 0.006 m H_2SO_4	73	Type 304L stainless steel	3	21	23	26
						Type 316 stainless steel[b]	1		23	
						Type 318 stainless steel	1		34	
						Type 347 stainless steel	5	23	25	27
						Type 309 SCb stainless steel	2	23	25	26
E-30	0.06	200	507	1000–2000 ppm O_2 0.006 m H_2SO_4	16	Type 304L stainless steel	3	14	15	15
						Type 321 stainless steel	2	14	15	16
						Type 347 stainless steel	6	14	15	17
						Type 309 SCb stainless steel	2	13	13	13
						Platinum	1		0.13	
					27	Type 304L stainless steel	9	15	18	25
						Type 318 stainless steel	1		20	
						Type 321 stainless steel	3	15	17	18
						Type 347 stainless steel	10	17	19	21
						Type 309 SCb stainless steel	4	14	16	17
						Platinum	1		0.13	
					73	Type 304L stainless steel	4	20	21	21
						Type 321 stainless steel	1		22	
						Type 347 stainless steel	6	19	23	25
						Type 309 SCb stainless steel	2		20	
						Platinum	1		0.07	
E-31	0.06	200	250	1000–2000 ppm O_2 0.006 m H_2SO_4	16	Type 304L stainless steel	3	14	14	15
						Type 321 stainless steel	2	13	14	15
						Type 347 stainless steel	6	14	17	23
						Type 302B stainless steel	1		37	
						Type 309 SCb stainless steel	2	9.5	13	17
					27	Type 304L stainless steel	9	13	18	15
						Type 318 stainless steel	1		15	

TABLE 3.2. (continued)

Run No.	Test Conditions: UO_2SO_4 Concentration (m)	Temperature (°C)	Time (hr)	Additions	Flow Rate (fps ± 10%)	Pin Material	Number of Pins	Corrosion Rate (mpy): Minimum	Average	Maximum
E-31	0.06	200	250	1000–2000 ppm O_2 0.006 m H_2SO_4	27	Type 321 stainless steel	3	13	14	15
						Type 347 stainless steel	9	14	16	17
						Type 302B stainless steel	2	29	32	35
						Type 309 SCb stainless steel	4	10	11	12
					73	Type 304L stainless steel	4	15	17	21
						Type 321 stainless steel	1		20	
						Type 347 stainless steel	6	17	22	26
						Type 302B stainless steel	1		45	
						Type 309 SCb stainless steel	2	9.0	13	16
G-15[k]	0.06	250	200	~4000 ppm O_2; 0.005 m H_2SO_4	75	Type 347 stainless steel	1		72	
G-16[k]	0.06	250	200	~4000 ppm O_2; 0.005 m H_2SO_4 200 ppm Cr as $K_2Cr_2O_7$	75	Type 347 stainless steel	1		1.2	
I-13	0.06	225	937	2000–3000 ppm O_2 0.006 m H_2SO_4	15	Type 304L stainless steel	5	3.7	4.0	4.5
						Type 347 stainless steel	5	4.1	4.4	4.8
						Type 309 SCb stainless steel	4	2.3	4.3	5.1
					19	Type 304L stainless steel	12	4.5	15.5	33
						Type 318 stainless steel	2	5.6	8.8	12
						Type 347 stainless steel	13	2.1	6.8	11
					31	Type 304L stainless steel	12	43	51	70
						Type 318 stainless steel	2	34	45	55
						Type 347 stainless steel	13	6.2	18	47
					41	Type 304L stainless steel	12	46	53	63
						Type 318 stainless steel	2	52	59	66
						Type 347 stainless steel	13	15	32	47

TABLE 3.2. (continued)

Run No.	Test Conditions: UO_2SO_4 Concentration (m)	Temperature (°C)	Time (hr)	Additions	Flow Rate (fps ± 10%)	Pin Material	Number of Pins	Corrosion Rate (mpy): Minimum	Average	Maximum
I-14	0.06	225	382	2000–3000 ppm O_2 0.006 m H_2SO_4	15	Type 304L stainless steel	3	9.2	10	11
						Type 318 stainless steel	2	23	24	24
						Type 321 stainless steel	3	14	17	19
						Type 347 stainless steel	3	10	11	13
						Type 309 SCb stainless steel	3	11	12	13
					19	Type 304L stainless steel	10	7.0	11	15
						Type 318 stainless steel	2	16	20	24
						Type 321 stainless steel	2	16	21	26
						Type 347 stainless steel	12	8.8	13	17
						Type 309 SCb stainless steel	2	12	13	13
					31	Type 304L stainless steel	10	16	40	55
						Type 318 stainless steel	2	49	50	50
						Type 321 stainless steel	2	28	37	46
						Type 347 stainless steel	12	17	30	44
						Type 309 SCb stainless steel	2	36	42	48
					41	Type 304L stainless steel	10	37	50	61
						Type 318 stainless steel	2	45	46	47
						Type 321 stainless steel	2	40	44	48
						Type 347 stainless steel	10	24	44	65
						Type 309 SCb stainless steel	2	42	52	61
I-15	0.06	225	650	2000–3000 ppm O_2 0.006 m H_2SO_4	15	Type 304L stainless steel	3	4.3	5.4	6.9
						Type 304 stainless steel[b]	1		8.2	
						Type 321 stainless steel	3	7.3	7.5	8.0
						Type 347 stainless steel	3	5.4	5.9	6.4
						Type 347 stainless steel[b]	1		5.5	
						Type 309 SCb stainless steel	3	6.6	6.7	6.9
					19	Type 304L stainless steel	9	30	36	47
						Type 304 stainless steel[b]	1		39	
						Type 316L stainless steel	1		47	

TABLE 3.2. (continued)

Run No.	Test Conditions: UO_2SO_4 Concentration (m)	Temperature (°C)	Time (hr)	Additions	Flow Rate (fps ± 10%)	Pin Material	Number of Pins	Corrosion Rate (mpy): Minimum	Average	Maximum
I-15	0.06	225	650	2000–3000 ppm O_2 0.006 m H_2SO_4	19	Type 318 stainless steel	1		18	
						Type 321 stainless steel	2	14	18	21
						Type 347 stainless steel	11	6.5	18	51
						Type 347 stainless steel[b]	1		38	
						Type 309 SCb stainless steel	2	30	32	34
					32	Type 304L stainless steel	9	11	37	64
						Type 304 stainless steel[b]	1		33	
						Type 316L stainless steel	1		23	
						Type 318 stainless steel	1		28	
						Type 321 stainless steel	2	15	22	39
						Type 347 stainless steel	11	9.2	21	51
						Type 347 stainless steel[b]	1		48	
						Type 309 SCb stainless steel	2	29	32	35
					41	Type 304L stainless steel	10	36	42	52
						Type 316L stainless steel	1		58	
						Type 318 stainless steel	1		34	
						Type 321 stainless steel	2	35	39	42
						Type 347 stainless steel	12	9.7	31	71
						Type 309 SCb stainless steel	2	38	38	38
I-16	0.06	225	151	2000–3000 ppm O_2 0.006 m H_2SO_4	15	Type 304L stainless steel	3	15	17	19
						Type 321 stainless steel	3	20	24	27
						Type 347 stainless steel	3	18	22	27
						Type 309 SCb stainless steel	3	21	22	24
						Stellite 98M2	1		110	
						Stellite 6	1		140	
					19	Type 304L stainless steel	9	20	27	38
						Type 316L stainless steel	1		33	
						Type 318 stainless steel	1		34	
						Type 321 stainless steel	2	30	33	36

TABLE 3.2. (continued)

Run No.	Test Conditions					Pin Material	Number of Pins	Corrosion Rate (mpy)		
	UO_2SO_4 Concentration (m)	Temperature (°C)	Time (hr)	Additions	Flow Rate (fps ± 10%)			Minimum	Average	Maximum
I-16	0.06	225	151	2000–3000 ppm O_2 0.006 m H_2SO_4	19	Type 347 stainless steel	11	26	30	35
						Type 309 SCb stainless steel	2	28	28	28
						Stellite 3	1		110	
						Stellite 6	1		190	
					32	Type 304L stainless steel	9	35	37	40
						Type 316L stainless steel	1		35	
						Type 318 stainless steel	1		33	
						Type 321 stainless steel	2	35	46	56
						Type 347 stainless steel	11	32	38	42
						Type 309 SCb stainless steel	2	34	34	34
						Stellite 98M2	1		110	
						Stellite 6	1		190	
					41	Type 304L stainless steel	8	39	46	71
						Type 316L stainless steel	1		38	
						Type 318 stainless steel	1		45	
						Type 321 stainless steel	2	36	37	38
						Type 347 stainless steel	12	37	42	50
						Type 309 SCb stainless steel	2	39	39	39
						Stellite 98M2	1		160	
						Stellite 6	1		180	
J-38	0.11	300	1000	1000–2000 ppm O_2 0.016 m H_2SO_4	17	Type 304L stainless steel	2	0.66	0.75	0.83
						Type 347 stainless steel	9	0.71	0.78	0.92
						Type 309 SCb stainless steel	2	0.82	0.86	0.90
						Carpenter 20	1		0.87	
					75	Type 304L stainless steel	2	3.2	3.4	3.6
						Type 347 stainless steel	9	3.4	5.6	6.9
						Type 309 SCb stainless steel	2	2.6	2.7	2.7
						Carpenter 20	1		13	

TABLE 3.2. (continued)

Run No.	Test Conditions: UO_2SO_4 Concentration (m)	Temperature (°C)	Time (hr)	Additions	Flow Rate (fps ± 10%)	Pin Material	Number of Pins	Corrosion Rate (mpy): Minimum	Average	Maximum
J-39	0.11	300	6.4	1000–2000 ppm O_2 0.016 m H_2SO_4	16	Type 304L stainless steel	2	120	135	150
						Type 347 stainless steel	8	130	145	160
						Type 347 stainless steel[b]	2	130	140	150
						Type 309 SCb stainless steel	2	110	115	120
					75	Type 304L stainless steel	2	530	580	630
						Type 347 stainless steel	8	510	528	540
						Type 347 stainless steel[b]	2	650	765	780
						Type 309 SCb stainless steel	2	450	455	460
J-40	0.11	300	101	1000–2000 ppm O_2 0.016 m H_2SO_4	16	Type 304L stainless steel	2	11	12	12
						Type 347 stainless steel	8	10	12	13
						Type 347 stainless steel[b]	2	10	11	12
						Type 309 SCb stainless steel	2	11	11	11
					75	Type 304L stainless steel	2	98	104	110
						Type 347 stainless steel	8	34	266	380
						Type 347 stainless steel[b]	2	140	260	380
						Type 309 SCb stainless steel	2	74	78	81
J-41	0.11	300	192	1000–2000 ppm O_2 0.016 m H_2SO_4	16	Type 304L stainless steel	2	4.8	5.4	6.0
						Type 304 stainless steel[b]	1		7.0	
						Type 347 stainless steel	8	5.8	6.7	7.8
						Type 347 stainless steel[b]	1		6.7	
						Type 309 SCb stainless steel	2	5.4	5.7	6.0
					75	Type 304L stainless steel	2	51	52	52
						Type 304 stainless steel[b]	1		66	
						Type 347 stainless steel	8	120	125	140
						Type 347 stainless steel[b]	1		98	
						Type 309 SCb stainless steel	2		42	

FOOTNOTES FOR TABLE 3.2.

[a]After 135 hr the loop was shut down for 90 min to repair the oil pump.

[b]Cast.

[c]Specimen showed a weight gain of 0.8 mg after removal of iron and chromium oxide film. The specimen retained a film probably composed of oxides of titanium and alloying elements.

[d]The same samples were exposed in all three runs.

[e]Zirconium sample gained 1.2 mg by deposition of iron and chromium oxides; pin was not defilmed.

[f]Sensitized by treating for 24 hr at 1000°F.

[g]Malcomized.

[h]Precipitation hardened.

[i]Miscro 4 is a cast-iron alloy with the composition (wt %): Ni, 0.15%; Cr, 13.1%; Si, 1.41%; C, 0.07%.

[j]Titanium sample gained 0.2 mg because of deposition of iron and chromium oxides; pin was not defilmed.

[k]All-titanium loop.

At 200°C at low flow rates (~15 fps), type 347 stainless steel pins showed little or no corrosion after the first 500 hr of exposure, whereas type 304L pins showed a continuing corrosion rate of 5 mpy after the first 500-hr period of rapid corrosion. Both types 304L and 347 stainless steel pins had the same weight of film, and both had continuous oxide coatings. This behavior was identical to that observed at the 0.17 *m* uranyl sulfate concentration,[12] and, as previously stated, the reason for the observation is not known. At high flow rates (~75 fps) both alloys were free of film and both showed the same corrosion rate, approximately 25 mpy. The critical velocity was poorly defined but appeared to be about 20 fps.

At 225°C and 15 fps both types 347 and 304L specimens had uniform oxide coatings and both corroded at the same rate of about 1 mpy after an oxide film had formed. At 19 fps, however, these pins behaved differently; the type 304L pins corroded at an average rate of 13 mpy, and the type 347 pins corroded at an average rate of 3 mpy. The reason for the different rates was apparent when the specimens were examined. The type 304L pins were not completely covered with oxide films, but the type 347 pins had continuous films. In effect, then, the critical velocity was lower with type 304L stainless steel than with type 347. This fact was also observed in 0.17 *m* uranyl sulfate at 225°C.[12] At both 32 and 41 fps all pins were partially free of film and showed high average corrosion rates, but at both flow rates the type 304L pins had less film and a higher average corrosion rate than did the type 347 pins. At 225°C the critical velocity observed on type 347 stainless steel coupons was 30 fps. At the highest velocity on the coupons, the film-free corrosion rate was 51 mpy.

In the last quarterly report[12] the results obtained in 0.06 *m* uranyl sulfate at 250°C were given. Table 3.3 sums up the corrosion rates and critical velocities in 0.06 *m* uranyl sulfate containing 0.006 *m* sulfuric acid at 200, 225, and 250°C. From the table it can be seen that both the critical velocity and the film-free corrosion rate increased as the temperature was increased.

A series of runs with 0.06 *m* uranyl sulfate containing 0.006 *m* sulfuric acid at 320°C is in progress, and full discussion of the results will be postponed for a subsequent report. However, preliminary results indicate that a more adherent film is formed at 320°C than at any of the lower temperatures and that the critical velocity appears to be in excess of 50 fps. At flow rates less than the critical velocity the extent of corrosion during film formation appears to be lower than at temperatures between 200 and 250°C under the same flow conditions.

TABLE 3.3. CORROSION OF TYPE 347 STAINLESS STEEL IN 0.06 *m* UO_2SO_4 CONTAINING 0.006 *m* H_2SO_4

Temperature (°C)	Critical Velocity (fps)	Corrosion Rate (mpy)	
		At 15 fps	At 75 fps
200	20	<1	25
225	30	1	51
250	35	1	120

(c) Titanium-Loop Operations. The titanium loop, loop G, is ideally suited for certain experiments, because soluble corrosion products are not formed from the loop itself and because corrosion products originating from the loop are not deposited on other parts of the system. On the other hand, when uranyl sulfate solutions are circulated in stainless steel loops, all of the nickel and part of the chromium remain in solution; also, the insoluble corrosion products do not remain *in situ* but are transported throughout the system and deposit on all metal surfaces. For the above two reasons the interpretation of corrosion results in stainless steel systems is complicated, and it is frequently impossible to evaluate the effects of certain variables.

It has been mentioned previously that both titanium and zirconium corrosion specimens develop heavy scales of iron and chromium oxide when exposed to uranyl sulfate solutions in stainless steel systems. It was of interest to determine how stable the oxide films were to uranyl sulfate solutions which contained no corrosion products. Hence one titanium and one zirconium pin, each having about 10 mg of mixed iron and chromium oxides deposited on its surface as a result of a previous run in a stainless steel system, were exposed in the titanium loop. Both pins were exposed to 0.17 *m* uranyl sulfate flowing at 75 fps for 100 hr at 250°C and for 100 hr at 200°C. With the use of the same pins and exposure time, the

above procedure was repeated with 1.34 *m* uranyl sulfate at 200 and 250°C. After each run the specimens were weighed, and the results showed that in all cases no weighable quantity of film was removed from the pins either by chemical dissolution or by cavitation. Thus the high degree of chemical and mechanical inertness of the oxide film was demonstrated, and the results show that when film is removed from stainless steel under conditions such as previously described[11] cavitation cannot completely account for the observed results.

The titanium loop has also been used to demonstrate the desirability of maintaining chromate ions in uranyl sulfate systems even at low uranyl sulfate concentration. It has been shown previously that stainless steel pins exposed at 75 fps in 0.02 *m* uranyl sulfate at 250°C in a stainless steel loop lose very little weight (~10 to 15 mg), and then practically stop corroding. However, in these systems the chromate-ion concentration of the solution increased at an appreciable rate because of the large surface area of the stainless steel; consequently, it has not been possible to determine how important the chromium was in causing the very low corrosion rate. For that reason, one newly machined type 347 stainless steel pin was mounted in the all-titanium loop and exposed to 0.02 *m* uranyl sulfate containing 0.005 *m* sulfuric acid and about 1000 ppm of oxygen for 200 hr at 250°C. Because of the very small surface area of stainless steel, the source of chromium, it was expected that the chromium concentration in solution would remain low. At the end of the run the stainless steel pin was badly corroded and had lost 84.8 mg. The chromate concentration in solution at the end of the run was only 9 ppm. A second run was then made under the same conditions as the first except that the solution contained 200 ppm of chromium as potassium dichromate and a new pin was used. In the latter case the pin lost only 1.4 mg, and, visually, the corrosion damage was nil. These data clearly demonstrate not only the desirability but perhaps also the necessity of maintaining an adequate concentration of hexavalent chromium in solution if a low corrosion rate is to be achieved. Future experiments are planned in order to determine the chromate concentrations necessary to form protective coatings at several concentrations and temperatures.

3.2.3 Discussion

Most of the data presented in Table 3.2 are sufficiently clear to need no further explanation. However, some of the runs need clarification to explain the reasons for the conditions used and for the results observed. At the uranyl sulfate concentration of 0.11 *m* (25 g of uranium per liter at 25°C), 0.016 *m* sulfuric acid (~15 mole %) was added. The reason for the relatively large amount of sulfuric acid was to prevent the formation of a second liquid phase at temperatures as high as 320°C. Since it was originally planned to explore the 0.11 *m* uranyl sulfate concentration over the temperature range of 200 to 320°C, all runs that were made contained 0.016 *m* sulfuric acid. In runs C-41 through C-43 the acidified uranyl sulfate solution was circulated at 250°C. All three runs were terminated because of unplanned shutdowns of the loop. In one case there was a power failure; in another, the oil pump had to be replaced; and in the third, the 100A pump failed. It was coincidental that all three runs were of essentially the same duration, but the corrosion rates shown in Table 3.2 demonstrate the rather high degree of reproducibility that can be expected from one run to another. The data in these three runs also show that type 304L stainless steel had a lower critical velocity than did type 347 stainless steel. For example, at 11 fps, types 347 and 304L had the same average corrosion rates but at 24 fps, type 347 pins showed considerably lower corrosion rates than did the type 304L pins.

The series of runs J-38 through J-41 was completed under the same conditions as those for runs C-41 through C-43 except for the temperature, which was 300°C for the J runs. It can be seen from Table 3.2 that in run J-38 the average corrosion rates were much lower than in runs J-39 through J-41. In fact, the weight losses of the specimens were lower in J-38 than in the subsequent runs even though the exposure time was much longer. The reason for the abnormal results observed in run J-38 was the high concentration of hexavalent chromium formed in the loop solution very early in the run. For example, after one day's operation the chromium concentration of the solution was 200 ppm. As discussed in the last quarterly report,[12] chromate ions are very effective in decreasing the extent of corrosion and increasing the critical velocity. The source of the chromium

in this run was apparently the corrosion products present in the loop as a result of the previous run, J-37, in which 1.34 *m* uranyl sulfate was circulated at 200°C. During run J-37 corrosion damage was extensive, and large amounts of loosely adhering hydrated iron and chromium oxides were deposited throughout the loop. In run J-38 the uranyl sulfate solution at 300°C dissolved a large amount of chromium from the oxide and probably converted the hydrated oxide to the anhydrous form. In subsequent runs the chromate-ion concentration increased in a normal fashion, and the extent of corrosion was more nearly that to be expected on the basis of previous experience.

Since there is presently a minimum of interest in uranium concentrations as high as 0.11 *m*, further studies at this concentration are not anticipated. Although the studies were not carried to the point where definite corrosion rates were determined, the data indicated that the extent of corrosion was intermediate between that observed in 0.06 *m* and 0.17 *m* uranyl sulfate, as would be expected. Hence, reasonably reliable values of critical velocities and corrosion rates can be obtained by interpolation of the data obtained at other concentrations.

The inhibitory action of hexavalent chromium was demonstrated in the last quarterly report,[12] and the experiments carried out in the titanium loop further confirm the beneficial action of hexavalent chromium in uranyl sulfate–stainless steel systems. Previously reported corrosion data[9] have also shown that, in a given system, the critical velocity increases as the temperature is increased and that at flow rates less than the critical velocity the extent of corrosion is less at high temperatures than at low temperatures. Since the formation of soluble chromium also increased as the temperature was raised, it is conceivable that the improved corrosion resistance observed at high temperatures is a result of the increased rate of formation of hexavalent chromium in solutions at high temperatures.

When an entire stainless steel loop is considered as a whole and when the soluble corrosion products in solution are plotted at different temperatures after a fixed time as a function of temperature, curves, such as those shown in Fig. 3.3, are obtained. The points shown were obtained in 0.06 *m* uranyl sulfate solutions containing 0.006 *m* sulfuric acid after 200 hr of operation, but similar

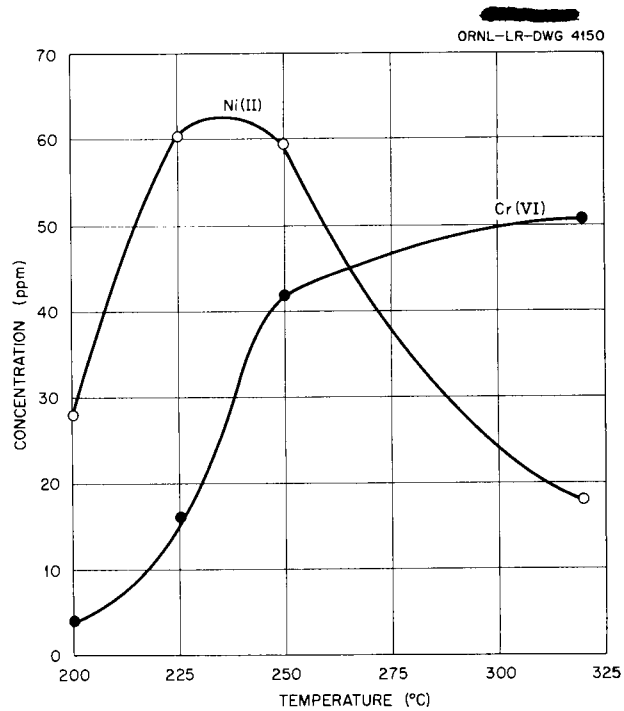

Fig. 3.3. Soluble Corrosion Products Found in 0.06 *m* Uranyl Sulfate Containing 0.006 *m* Sulfuric Acid After 200 hr Operation.

curves are obtainable after any period of operation and at concentrations ranging from 0.02 to 1.34 *m*. If the nickel concentration is used as a measure of the total corrosion in the system, it is seen that the total corrosion was less at high temperatures than at low and that the soluble chromium concentration was larger at the high temperatures. In other words, then, the chromium-to-nickel ratio increased as the temperature increased and the total corrosion decreased. Curves of the above type lend support to the belief that the improved corrosion resistance of stainless steel at the high temperatures is related to the higher concentrations of hexavalent chromium in solution at the higher temperatures.

Experiments are now in progress to determine the minimum oxygen concentrations necessary to stabilize uranyl sulfate solutions under different conditions. Very preliminary results have indicated that 40 to 70 ppm of oxygen is sufficient to stabilize 0.17 *m* uranyl sulfate at 250°C, and it is probable that much lower oxygen concentrations will be adequate. A full discussion of this work will be given in a future report.

Two loops were started on essentially lifetime tests during this past quarter. Each loop contains a solution 0.04 *m* in uranyl sulfate, 0.006 *m* in sulfuric acid, and 0.005 *m* in cupric sulfate. In loop K the solution is being circulated at 300°C and in loop M, at 250°C. Other tests now in progress have been designed to determine the effects of cavitation, oxygen concentration, and chromate-ion concentration on the corrosion of stainless steel by uranyl sulfate solutions.

3.2.4 IBM Corrosion File

R. E. Wacker

With the increasing amount of corrosion data, both dynamic and static, it became desirable that a method of filing the data be made available. An IBM card system was selected for this purpose. It has several advantages over any of the available punch-card systems, the main one being the speed with which cards may be sorted.

A standard IBM card, $3\frac{1}{4} \times 7\frac{1}{2}$ in., is used, with the corrosion data being punched on it. These cards consist of 80 columns of 12 digits each. Each column may be punched for one number or letter only. One card is punched for each individual piece of data. The data recorded on the card are: (1) environment, solution or mixture with concentrations; (2) source of the information; (3) conditions, including length of test, temperature, velocity, etc.; (4) the material tested with its metallurgical history; and (5) weight loss and type of attack. Several unused columns of the card are available for information not at present recorded. A minimum of coding is used, so the data may be used as taken from the card. To simplify and speed sorting, atomic numbers rather than symbols are used to designate elements and compounds.

With the use of the IBM machines, approximately 10,000 cards an hour may be sorted and the information from the desired cards may be tabulated in any desired order. To date, most of the dynamic loop data, approximately 10,000 items, have been incorporated into the file.

4. RADIATION CORROSION

G. H. Jenks
W. N. Bley
N. C. Bradley
S. F. Clark
W. E. Clark
H. O. Day
H. A. Fisch
D. N. Hess
B. O. Heston
H. C. Savage
D. T. Jones
R. A. Lorenz
J. R. McWherter
A. R. Olsen
M. D. Silverman
H. H. Stone
L. F. Woo
W. C. Yee

4.1 STATIC BOMB STUDIES

G. H. Jenks
S. F. Clark
W. E. Clark
H. O. Day
H. A. Fisch
B. O. Heston
D. N. Hess
D. T. Jones
J. R. McWherter
A. R. Olsen
M. D. Silverman
H. H. Stone
L. F. Woo
W. C. Yee

4.1.1 Zircaloy-2

(a) Introduction. Studies of the effect of irradiation on the corrosion of Zircaloy-2 by uranyl sulfate solution have been initiated. Three static (or bomb) in-pile exposures have been completed, and a fourth test is under way. Out-of-pile bomb-type corrosion studies have also been initiated. Six experiments are under way or have been completed.

The methods, techniques, and equipment employed in these studies were, in general, those which have been developed and used for similar studies with stainless steel.[1]

[1] C. H. Secoy *et al.*, *HRP Quar. Prog. Rep. April 30, 1954*, ORNL-1753, p 139.

The bombs for these studies were constructed of Zircaloy-2. The pressure fitting, which forms the bomb closures, and the capillary tubing attached to the fitting were of titanium. The material from which the bombs were fabricated was in the form of $\frac{3}{4}$-in. bar stock. Three different bars have been used. Each has been analyzed for various alloying elements and found to be of nominal composition. The analytical results are shown in Table 4.1. The bombs were used in the as-machined and as-welded condition, except for a 1-hr pretreatment with water at 250°C. This pretreatment occurred during the pressure testing which preceded each experiment.

Pin corrosion specimens, $\frac{1}{16}$ in. in diameter and 1.5 in. in length, were placed in each bomb. The material from which the pins were fabricated has been analyzed, and the results are shown in Table 4.1.

(b) Out-of-Pile Studies. A summary of the out-of-pile studies with Zircaloy-2 is given in Table 4.2. The results of oxygen-pressure measurements for experiments H-53, -54, -61, and -62 are shown graphically in Fig. 4.1. As indicated in Table 4.2, all the experiments except H-63 are continuing. The corrosion data presented in Table 4.2 and in

TABLE 4.1. RESULTS OF ANALYSES OF ZIRCALOY-2 STOCK COMPOSITION

Stock Material	Composition (wt %)							
	Sn	Cr	Ni	Fe	C	H	O	N
Bar U	1.10	0.12	0.08	0.37	0.16	0.0023	0.0026	<0.001
Bar V	0.89	0.08	0.05	0.16	0.17			
Bar W	1.22	0.10	0.05	0.16	0.16			
$\frac{1}{16}$-in. weld rod						0.0096	0.032	<0.001
Pins	0.93	0.08	0.05	0.28	0.025			

TABLE 4.2. SUMMARY OF OUT-OF-PILE CORROSION STUDIES OF ZIRCALOY-2

Bomb No.	Solution	Initial Oxygen Pressure (psi)	Exposure Temperature (°C)	Duration of Exposure (days)	Corrosion (mils)		Corrosion Rate (mpy)	
					Pin Data	O_2 Data	Current*	Over-all
H-63	0.17 *m* UO_2SO_4 0.02 *m* $CuSO_4$	300	250	7.5	0.015	0.014		0.5
H-53	0.17 *m* UO_2SO_4 0.02 *m* $CuSO_4$	300	250	55 *		0.053	0.26	0.35
H-54	0.34 *m* UO_2SO_4 0.04 *m* $CuSO_4$	300	250	34 *		0.017	0.15	0.18
H-55	0.17 *m* UO_2SO_4 0.02 *m* $CuSO_4$	300	290	19 *		0.016	0.20	0.30
H-61	0.17 *m* UO_2SO_4 0.02 *m* $CuSO_4$ 0.04 *m* H_2SO_4	300	250	14 *		0.0096	0.21	0.25
H-62	0.17 *m* UO_2SO_4 0.02 *m* $CuSO_4$ 210 ppm of Cr added as $K_2Cr_2O_7$	300	250	14 *		0.0054	0.10	0.14

*Test continuing.

Fig. 4.1 were calculated from the oxygen data with the usual assumptions that the oxygen disappearance is due only to the formation of metal oxide and that the corrosion is uniform over the surfaces of the bomb and pin specimens.

Experiment H-63, the first experiment with Zircaloy-2, was carried out to test the compatibility of Zircaloy-2 with titanium fittings and also the method in general. The bomb contained one Zircaloy-2 pin and one titanium pin. No difficulty was experienced, and the metals appeared to be compatible. Experiments H-53 and H-54 were designed as control experiments for the in-pile measurements. Tests H-61 and H-62 are being made to determine the effects of added acid and added chromate ion.

The present data show that the corrosion rates are low in all the systems and that there is little difference among systems. However, the data will be considered as tentative until the experiments are terminated and the bombs and contents have been examined.

(c) In-Pile Studies. The general procedure for carrying out an in-pile experiment was similar to that used in previous studies.[1] The bomb, after pressure testing, was charged with the corrosion test solution and with sufficient hydrogen peroxide to yield the desired pressure of oxygen upon thermal decomposition. The bomb was then closed and was installed in the exposure assembly. All in-pile exposures were made in hole HB-6 of the LITR, where bombs are rocked during exposure. The system usually was operated out-of-pile at the test temperature for at least a day before installation in the reactor. During reactor exposure the oxygen pressure was determined at frequent intervals, usually once a day, with the reactor at zero power, that is, with no fissioning in the test solution. The bomb was maintained at test temperature during these determinations. The duration of the exposure was governed by the initial pressure of excess oxygen and by the rate of loss of oxygen during exposure. The experiment was terminated when the oxygen

[redacted]

ORNL-LR-DWG 4151

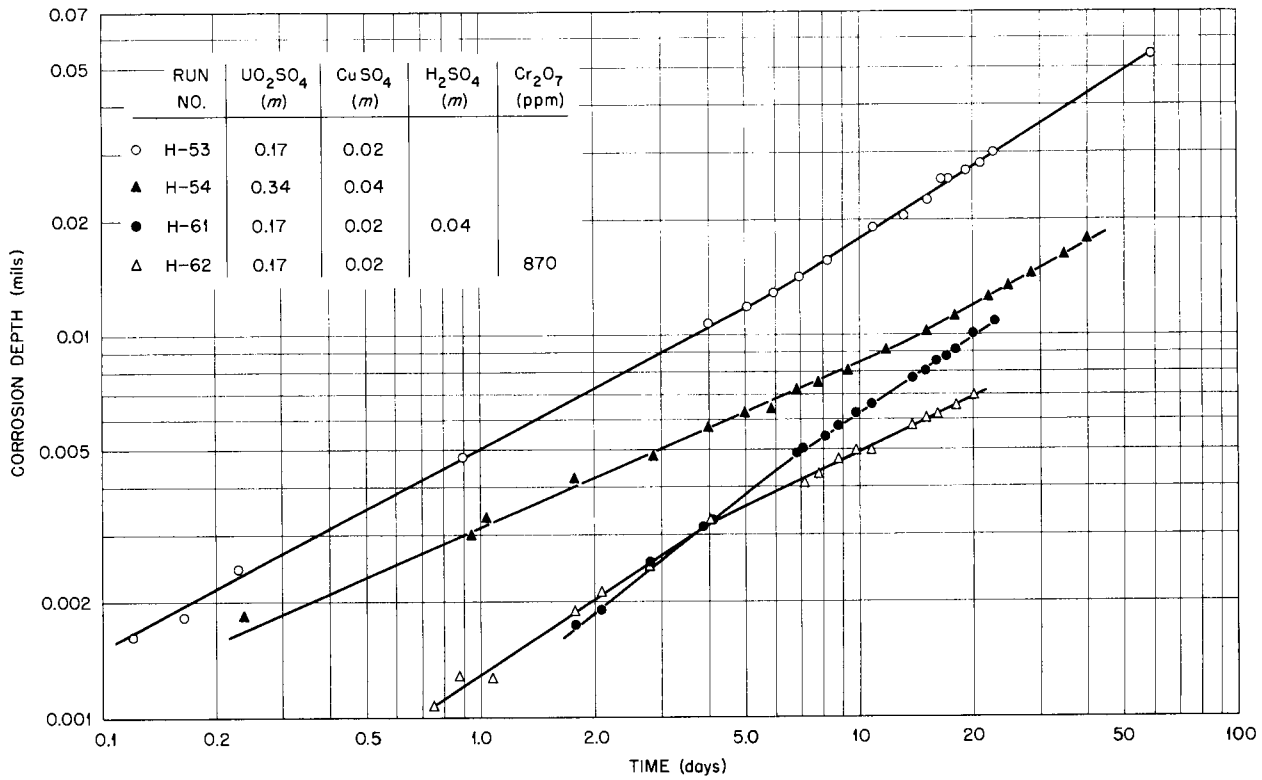

Fig. 4.1. Out-of-Pile Corrosion of Zircaloy-2 in UO_2SO_4 Solution at 250°C.

pressure had decreased to about 50 psi. Each experiment is described in more detail in the following sections.

H-57. – The experimental conditions for run H-57 and for other in-pile studies are listed in Table 4.3. The uranium in the solutions was 93% U^{235}. The pressures of excess oxygen are those measured at 250°C. The power densities are discussed in another section of this report. In experiment H-57 the charged bomb was not heated prior to installation in the reactor. Full reactor power of 3 Mw was utilized during the entire radiation exposure time. The reactor was down for several hours each time a pressure measurement was made. It was also down for a period of 32 hr at one point in the experiment to enable a determination of the rate of oxygen consumption in the absence of radiation.

The results of oxygen-pressure measurements are shown graphically in Fig. 4.2. The calculated total corrosive penetration in mils is plotted along the ordinate. The accumulated radiation time in units of 3 Mwhr of LITR operation is plotted along the abscissa. The slope of the line through the points for H-57 corresponds to a corrosion rate of 9.3 mpy, or 0.026 mil/day. The corrosive penetration during the 32 hr of reactor shutdown amounted to 0.010 mil. This result suggests that some significant amount of corrosion occurred during the times the reactor was down for pressure measurements. However, in the absence of information regarding the amount of corrosion during these times, it has been assumed for the present that this corrosion rate was negligible compared with the rate under irradiation.

Bomb H-57 has been opened, and the bomb and contents were examined. The pins were covered with a heavy tan-colored film, and all had gained in weight. If it is assumed that the weight gains were due to the formation of ZrO_2 and that all the oxide remained on the pins, the indicated penetration from the measured weight gains is 0.112 mil, compared with 0.135 mil based on oxygen uptake.

The bomb has been visually inspected, while in

TABLE 4.3. IN-PILE CORROSION TESTS OF ZIRCALOY-2

Bomb No.	Solution	Test Conditions		
		Initial Excess Oxygen (psi)	Exposure Temperature (°C)	Power Density at 3 Mw (w/ml)
H-57	0.16 *m* UO_2SO_4 0.02 *m* $CuSO_4$	300	250	5.2
H-58	0.15 *m* UO_2SO_4 0.02 *m* $CuSO_4$	560	250	4.9
H-59	0.31 *m* UO_2SO_4 0.036 *m* $CuSO_4$	370	~250	9.5
H-60	0.15 *m* UO_2SO_4 0.02 *m* $CuSO_4$ 0.04 *m* H_2SO_4	560	250	~5

a hot cell, through a $ZnBr_2$ window. The top and bottom portion appeared to be covered with a film of the type found on the pins. The middle section of the bomb was dark in color. Preliminary metallographic examination has been made of some of the bomb surfaces. No evidence of nonuniform corrosion was found.

A precipitate was found in the solution from the bomb. By analysis, this precipitate contained 7.5 mg of uranium, or about 4% of that initially present in solution. No reliable analysis for zirconium was made.

The pH of the solution had dropped from the initial 2.5 to 1.75. The copper concentration was 31% below the original concentration. Only a trace of zirconium was in solution. The uranium in solution plus that in the precipitate left about 10 mg of the original uranium unaccounted for.

The oxide film from one of the pins in this bomb was analyzed for zirconium and uranium and was found to contain these elements in a mass ratio of 4:1. The oxygen data indicated that 82 mg of zirconium had been oxidized. Hence, as much as 20 mg of uranium could have been in the film, which would then completely account for the original uranium.

It should be mentioned that a loss of copper from solution was also indicated by the pressures of radiolytic H_2 and O_2 during the exposure. The steady-state pressure of this gas mixture was about 350 psi at the start of radiation. During the experiment, the pressure increased in a regular fashion with total radiation time to 460 psi. This increase in steady-state pressure, if effected by copper concentration change alone, would indicate that the concentration of copper in solution had decreased by about 24% during exposure. The discrepancy between this value and that obtained from copper analysis may be accounted for by the uranium precipitation, also indicated by analysis.

H-58. – This experiment was in most respects a duplicate of H-57. The initial oxygen pressure was about twice that in H-57. As before, however, the reactor was held at zero power for 30 hr for a portion of the experiment. Following the period at zero power, the reactor was operated at 1.5 Mw for a total radiation time of 90 Mwhr and then returned to full power.

The pressure of radiolytic H_2 and O_2 in this bomb was initially about 315 psi. Again, this pressure increased with total radiation time to about 570 psi at the end of the experiment. The increase in this case indicates a loss from solution of about 45% of the copper. The results of the oxygen-pressure measurements are shown in Fig. 4.2. The slope of the line through the points is nearly the same as the slope for H-57 and corresponds to a corrosion rate of 9.2 mpy.

During the time the reactor was at 1.5 Mw, the corrosion rate was roughly one-half that observed when the reactor was at 3 Mw. As plotted with time units of 3 Mwhr of reactor operating time, the

data obtained at the two different powers fall roughly on the same straight line. The corrosive penetration during the period at zero power was 0.005 mil.

The pins from this bomb were found to have decreased in weight. They were also different in appearance from those in H-57. The color in this case may be described as "coppery." On the assumption that no oxide remained on the pins, the measured weight losses yield a value of 0.26 mil penetration during exposure. This agrees well with the value of 0.28 mil penetration calculated from

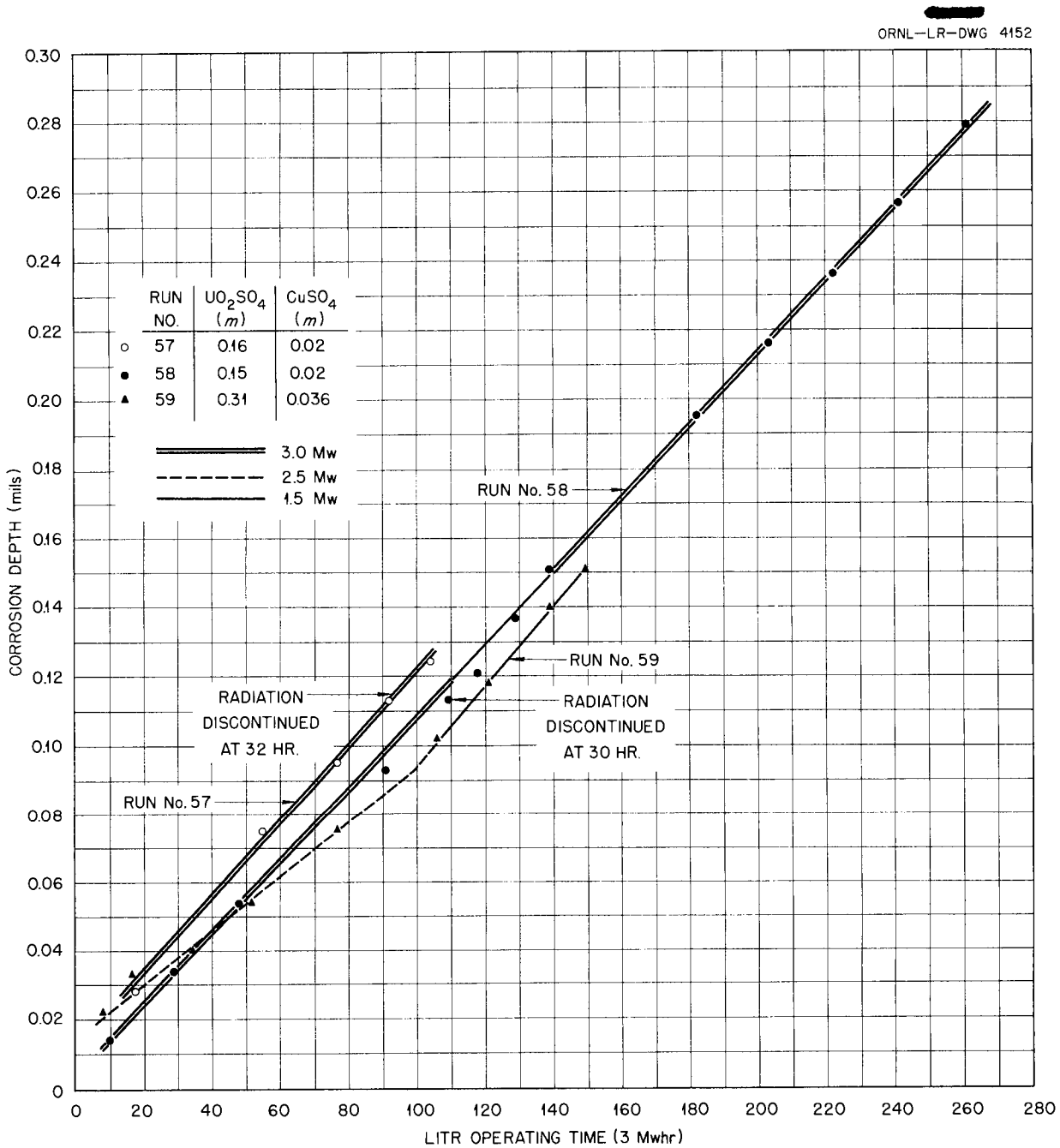

Fig. 4.2. In-Pile Corrosion of Zircaloy-2 in UO_2SO_4 Solution at 250°C.

oxygen uptake and tends to confirm the assumption of no film on the pins.

As before, the bomb surfaces were viewed through a $ZnBr_2$ window. The surfaces exhibited a uniform thin film appearance. A heavy precipitate was observed in the bottom of the bomb but has not been examined. Solution analyses have not yet been obtained.

H-59. – As shown in Table 4.3, the solution for this experiment contained twice as much uranium as that in H-58. The fission power density at a given reactor power was probably twice that in H-58. The maximum reactor power utilized during this experiment was 2.5 Mw. Provisions for cooling the bomb proved to be inadequate for operation at higher power levels. Actually, cooling was inadequate for operation at 2.5 Mw, and during part of the exposure at this power the bomb temperature exceeded the control temperature by as much as 10°C. The latter portion of the experiment was with a reactor power of 1.5 Mw. The steady-state pressure of radiolytic H_2 and O_2 was initially 220 psi when the reactor was at 1.5 Mw. This pressure increased to 305 psi at the end of the experiment. A loss of 28% of the initial copper is indicated. The results of oxygen-pressure measurements are shown in Fig. 4.2. The corrosion rates in this system were no greater than those in H-57 and H-58, although the power density was appreciably greater.

(d) Power Densities for In-Pile Experiments. The thermal-neutron flux which prevails within an empty bomb in experimental assembly HB-6 had been determined previously by means of cobalt activation. The value found for the flux was 4.8×10^{12} neutrons/cm^2/sec when the reactor was operating at 300 kw. From this value, Noderer[2] has calculated power densities of 7.8 and 15.1 kw/liter, respectively, for bomb solutions at 25°C containing 40 and 80 g of U^{235} per kilogram of water. A comparable value for the solution containing 40 g/kg had been calculated and employed by members of this group. Based on these calculated values, the power densities at operating temperature for the three in-pile experiments at an LITR power level of 3 Mw were the following:

Experiment	Power Density (w/ml)
H-57	5.2
H-58	4.9
H-59	9.5

A more direct determination of the power density for experiment H-58 has been made by radiochemical analysis for the total number of fissions which occurred during exposure. This analysis was carried out by E. I. Wyatt of the Analytical Chemistry Division. The method is that of separating fission-product cesium from the solution and comparing the activity of this cesium with that from a total-fission standard. The value determined in this manner for the total fissions per milliliter was 1.94×10^{17}. The exposure period was 785.4 Mwhr of reactor operation. The value for the fission power density during exposure at 250°C is, then, 4.94 w/ml when the reactor power is 3000 kw. This is in good agreement with the value calculated from the neutron flux. A total-fission analysis of the solution from experiment H-59 is planned.

4.1.2 LITR Experimental Facilities

The radiation-corrosion group has available for in-pile exposures horizontal holes HB-5 and HB-6 in the LITR. Past experiments in HB-5 have been made with stationary bombs. Hole HB-6 is equipped for experiments in which the bomb is rocked during exposure. The more consistent and interpretable results of the HB-6 experiments have shown the desirability of this change. Therefore hole HB-5 is presently being equipped for similar rocking-type experiments. The assembly of bomb holder, heater, and cooler in the new equipment is identical to that in hole HB-6, but the other portions of the equipment have been redesigned. A complete description of the modified setup will be given in the next quarterly progress report.

4.1.3 MTR In-Pile Experiment

The desirability of carrying out radiation-corrosion studies at higher power densities than those available in the LITR has long been recognized. Suitable high-power densities can be generated in the MTR, and an experimental facility in that reactor is available for such an experiment.

Conceptual-design studies have been initiated for a radiation-corrosion experiment employing the MTR facility. The experiment is presently visualized as being similar to the LITR bomb experiments. However, it is not immediately clear whether an experiment of this type will be suitable

[2] L. C. Noderer, *In-Pile Test Loop and HB-6 Bomb Power Density*, ORNL CF-54-9-238 (Sept. 21, 1954).

with the higher power densities which are anticipated. One apparent problem is that of heat removal. Very large temperature gradients between the solution and the wall of the bomb can be predicted at a power density of, say, 50 w/ml in a bomb of the present design. Experiments are under way to establish heat-transfer coefficients for such a bomb system and to determine the effect of thermal gradients on corrosion in the absence of radiation.

4.2 IN-PILE LOOP

G. H. Jenks H. C. Savage

4.2.1 LITR Operations

R. A. Lorenz D. T. Jones
G. H. Jenks N. C. Bradley
W. N. Bley H. C. Savage

During the past quarter the in-pile loop development program was brought to a successful conclusion with the very satisfactory performance of loop DD during a 465.5-hr in-pile run in beam hole HB-4 of the LITR. A total of 1137.3 Mwhr was logged by the LITR during this run. The operation of the loop while in the reactor was very smooth, the run was terminated as originally scheduled, the loop package was withdrawn without difficulty, and the loop is now in the dismantling facility being prepared for metallurgical examination of the corrosion specimens. The assembly and testing of loop DD prior to the first actual in-pile experiment are described in Sec. 4.2.2.

The success of the in-pile loop development permits the experimental radiation-corrosion program to be expanded to include studies of fissioning solutions in the presence of radiation gradients and velocity gradients and under a wider variety of environmental conditions than is possible with the static-bomb-test program.

4.2.2 HB-4 Mockup

W. N. Bley H. C. Savage
N. C. Bradley R. M. Warner

In-pile loop CC, previously described,[3] was disassembled in the remote-handling facility at X-10. The disassembly is described in Sec. 4.2.5a. The pump, pressurizer, and pressurizer heater from loop CC are being examined in detail. Metallurgical examination of sections cut from the pressurizer and pressurizer-heater line showed no evidence of stress-corrosion attack.

The pump was disassembled. The Stellite 98M2 journal bushings and Graphitar No. 14 bearings were in good condition, and there was no measurable wear. This pump had run in loop CC for approximately 420 hr with uranyl sulfate solution at 250°C and 1000 psia pressure. The pump impeller was corroded to a considerable extent on the outer edge, particularly around the discharge holes (see Fig. 4.3). Triangular-shaped pits previously observed on corrosion specimens from the 100A pump test loops[4] were also present. This is the first incident of such corrosion attack in an in-pile loop system. The fact that additional hydrogen and oxygen gas was injected into the loop during the recombination studies may have resulted in cavitation. In addition, the uranyl sulfate solution in the loop was changed several times during the run, resulting in removal of chromate. The presence of chromate in the circulating solution has been found to inhibit corrosion attack. In all other known conditions the run in loop CC was similar to run AA-7 (described in Sec. 4.2.3) in which corrosion was very low with no pitting of the test specimens or excessive corrosion of the pump impeller. Further tests will be made to determine the effect of these and other factors on corrosion in the in-pile loops.

As noted in Sec. 4.2.1, in-pile loop package DD was completed during the past quarter and run in the installation at beam hole HB-4 of the LITR. As

[3] G. H. Jenks *et al.*, *HRP Quar. Prog. Rep. July 31, 1954*, ORNL-1772, p 83-87.

[4] J. C. Griess and R. E. Wacker, *HRP Quar. Prog. Rep. April 30, 1954*, ORNL-1753, p 76-77.

UNCLASSIFIED PLATE 1241

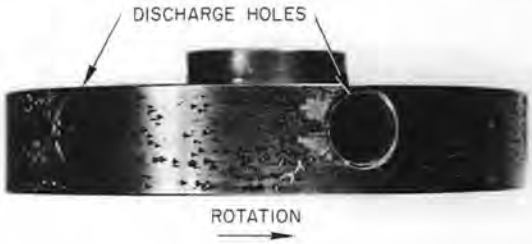

Fig. 4.3. Pump Impeller, Loop CC.

for all in-pile loops, the material (type 347 stainless steel) used in the construction of the loop was controlled and the Heliarc welds were inspected both by Dy-Chek and x-ray examination. In addition, the pressurizer assembly was stress-relieved at 950°F for 4 hr as a result of the transgranular cracks found in the pressurizer of loop BB.[5] Loop DD contained type 347 stainless steel corrosion specimens in Zircaloy-2 holders in both the in-line and core positions and Zircaloy-2 impact specimens in the core position.

The initial testing of loop DD consisted of a hydraulic pressure check at 1200 psi followed by a leak check with a helium leak detector. When no leaks were detected, the loop was connected to the shield plug by means of the plug connector, and all service lines (thermocouples, pressure and drain lines, electrical leads) were connected. At this point an operational check of the loop was made; then the loop container was installed around the loop and welded to the container head through which all service lines pass. The container was pressure tested at 500 psi to ensure that any leaks or ruptures of the loop during operation would be contained.

The loop assembly with shield plug was then installed in the beam-hole liner in the mockup, where a check was made of the water-seal gasket at the outer edge of the loop and plug assembly. The gasket was leaktight to the cooling water used in the annulus loop container and hole liner. The loop was given a standard cleanup pretreatment with trisodium phosphate solution at 100°C, followed by 5% nitric acid at 100°C. After operation with water and oxygen for 24 hr at 250°C, the loop was filled with natural-uranium uranyl sulfate solution (0.17 *m*) containing 0.031 *m* copper sulfate and 0.0085 *m* sulfuric acid and run for another 24 hr at 250°C and 1000 psia.

The loop assembly performed entirely satisfactorily during the testing and pretreatment and after removal was delivered to the LITR for additional calibration and testing of the instruments and equipment at hole HB-4 prior to installation in the LITR.

As a result of some difficulties encountered in the assembly of loop DD, two design changes are being made and incorporated in future loops. One problem was in obtaining leaktight seals in the loop-container head through which the thermocouple and electrical leads pass. Another problem was making a satisfactory solder-joint connection in all the cooling-water, container-vent, and air lines passing through the loop connector. These joints must be easily broken for separation of the loop and shield plug after operation in the LITR. The connections have been redesigned to make them easier to fabricate and more reliable.

Two additional in-pile loops, EE and FF, have been built. Loop FF, containing Zircaloy-2 corrosion specimens, is now being assembled in the in-pile mockup and will be installed in beam hole HB-4 at the LITR as soon as possible, replacing loop DD.

4.2.3 Loop Package Testing

H. C. Savage

Three additional runs (AA-5, AA-6, and AA-7) were made in one of the in-pile development loops as part of the program to improve the operation of the 5-gpm pump.

Type 347 stainless steel coupons in titanium holders were exposed to the conditions given in Table 4.4 in both the core and in-line position. As seen in Table 4.4, run AA-5 was interrupted after approximately 60 hr of operation because the pump bearing failed; before the failure occurred, the loop had operated for about 580 hr (runs AA-1 to AA-5). The pump contained Stellite 98M2 journal bushings with Graphitar No. 14 bearings of an old design. A new pump with an all-metal (Stellite 98M2) journal-bearing combination was installed. After an operation of approximately 10 hr, the journal-bearing combination failed, and the run was terminated. An Allis-Chalmers hydraulic bearing pump was then installed, and run AA-6 was made. However, bearing failure occurred after about 7 hr of operation, and this run was terminated.

Before starting run AA-7, the 5-gpm pump rotor and housing were modified to allow a bearing-thrust-load check and adjustment after installation in the loop. Type 17-4 PH stainless steel, hardened, journal bushings were installed as replacements for Stellite 98M2 journal bushings with Graphitar No. 14 bearings. The use of type 17-4 PH stainless steel will eliminate the introduction of cobalt (alloying element in Stellite 98M2) into the circulating solution, as a result of corrosion of the Stellite, if the temperature in the pump cavity rises

[5] G. H. Jenks *et al.*, *HRP Quar. Prog. Rep. July 31, 1954*, ORNL-1772, p 82.

[redacted] TABLE 4.4. OPERATING HISTORY OF RUNS AA-5 THROUGH AA-7

Run	Solution	Operating Conditions				Remarks
		Time (hr)	Temperature (°C)	Pressure (psia)	Gas	
AA-5	3 wt % Na_3PO_4	5	100	~100	Helium	Interrupted after 59 hr because of Graphitar bearing failure; new pump with all-metal (Stellite 98M2) journal-bearing combination installed, and run resumed
	5 wt % HNO_3	24	100	~100	Helium	
	Water	30	250	1000	Helium	
	Water	4	100	~100	Helium	Terminated at end of additional 8.8 hr because journal-bearing combination failed; Allis-Chalmers hydraulic bearing pump installed
	Water	2.5	250	1000	Oxygen (~500 ppm)	
	0.17 *m* UO_2SO_4 + 0.013 *m* $CuSO_4$ + 0.0085 *m* H_2SO_4	2.3	250	1000	Oxygen (~500 ppm)	
AA-6	Water	7	200	~500	Helium	Terminated because of hydraulic pump bearing failure
[redacted]						
AA-7	5 wt % HNO_3	4.7	100	~100	Helium	
	Water	95.5	250	1000	Oxygen (~500 ppm)	
	0.17 *m* UO_2SO_4 + 0.031 *m* $CuSO_4$ + 0.0085 *m* H_2SO_4	478	250	1000	Oxygen (150 to 500 ppm)	

for any reason. A reduction in fabrication cost should also result from the change in material.

The last portion of run AA-7 was made with 0.17 *m* uranyl sulfate solution containing 0.031 *m* copper sulfate with 0.0085 *m* sulfuric acid. Solution velocity past the test specimens was approximately 10 to 45 fps. This run was terminated after 478 hr for examination of the pump bearings and test specimens. The test coupons in the core position showed no velocity effect. The total corrosion of the specimens was less than 0.3 mg/cm^2 on each specimen, corresponding to an average corrosion rate of about 0.2 mpy. This low corrosion rate was also shown in the nickel analyses – the concentration of nickel in solution reached approximately 20 ppm after 100 hr of operation and increased very slowly to approximately 38 ppm at the end of the run. Based on the increase of the nickel concentration in the solution, the average over-all corrosion rate was about 0.14 mpy. The cobalt concentration of approximately 10 ppm during the entire run was probably a contaminant in the loop from previous runs with Stellite 98M2 bearings. The results of the chemical analyses of solution samples taken during the run are plotted in Figs. 4.4 and 4.5. The oxygen and carbon dioxide (from the Graphitar bearings) concentrations are plotted in Fig. 4.6. That no oxygen addition to the loop was required during the run confirms the low over-all system corrosion rate.

Examination of the type 17-4 PH journal bushings and Graphitar No. 14 bearings revealed no visual or measurable wear.

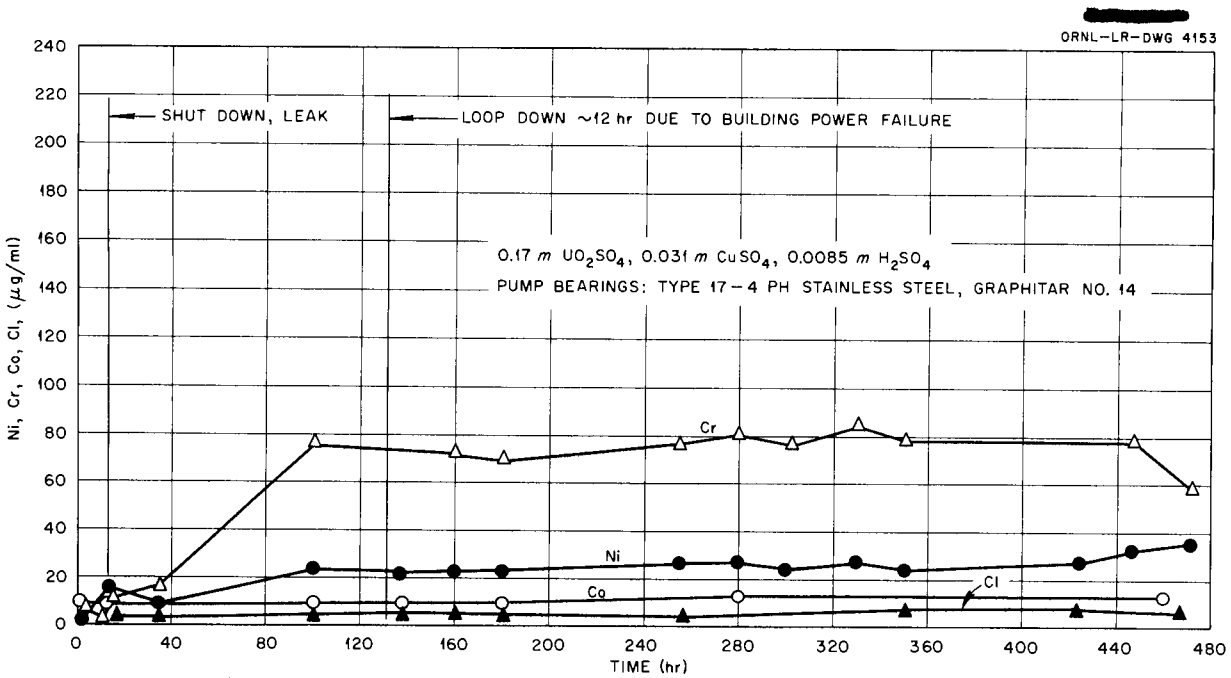

Fig. 4.4. Chemical Analyses (Cr, Ni, Co, Cl), Run AA-7.

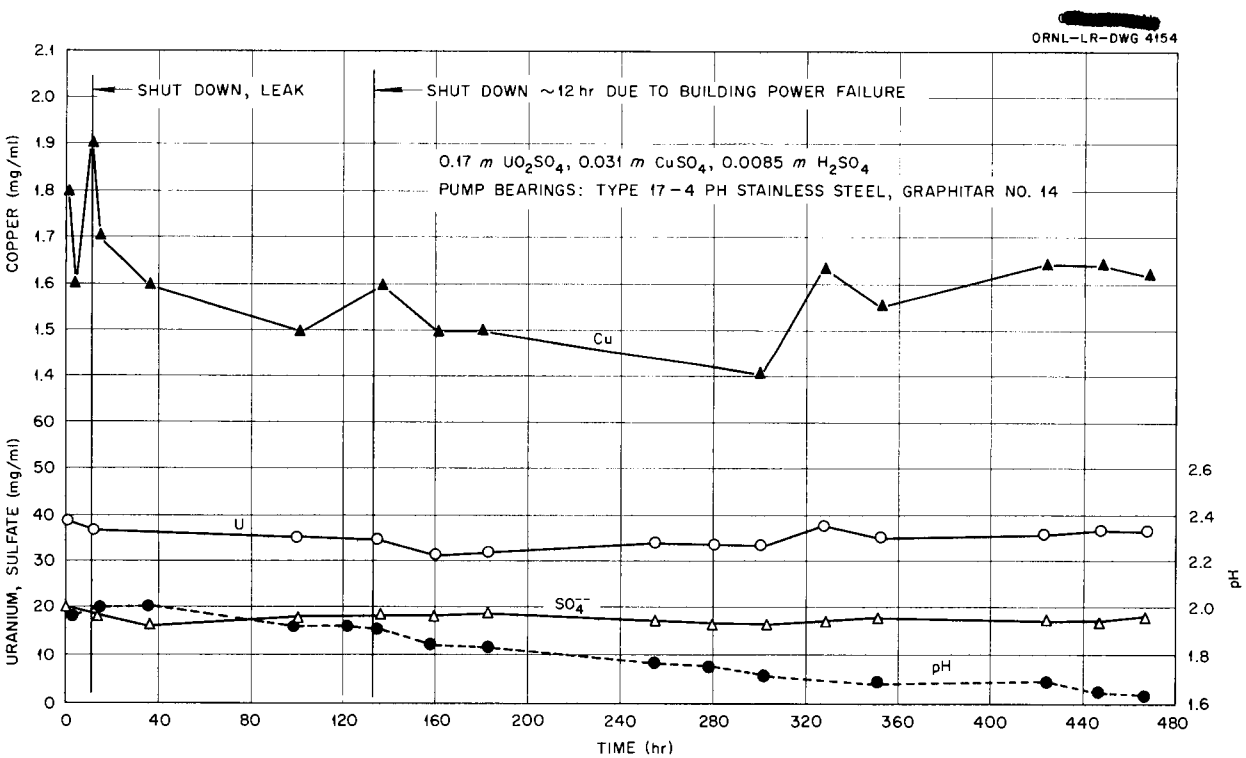

Fig. 4.5. Chemical Analyses (Cu, U, SO_4^{--}), Run AA-7.

[redacted]

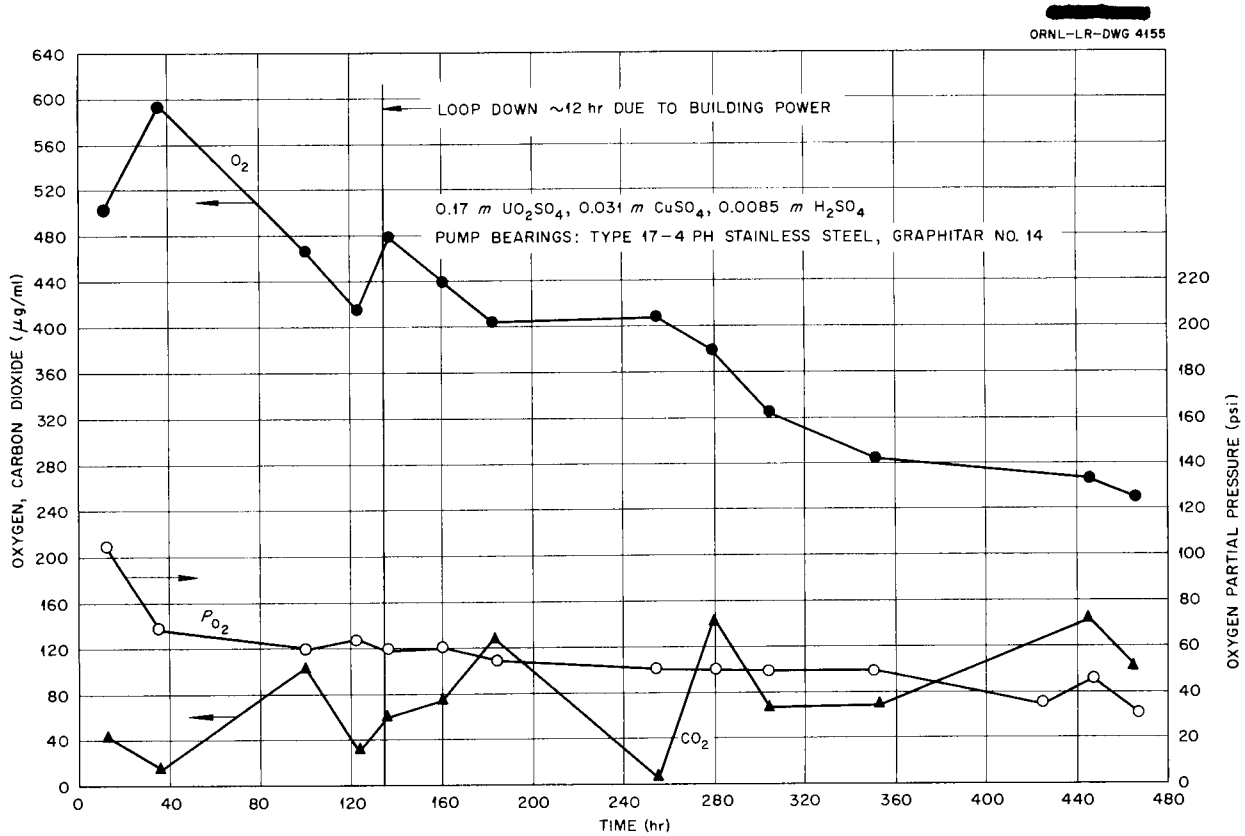

Fig. 4.6. Oxygen and Carbon Dioxide Concentration, Run AA-7.

4.2.4 In-Pile Pumps

W. N. Bley D. T. Jones
H. C. Savage

(a) ORNL Pump for HB-4 Loop Package. As a result of the pump test made in run AA-7 (described in Sec. 4.2.3), hardened type 17-4 PH stainless steel journal bushings are now being used in the in-pile loop circulating pumps.[6] This substitution has eliminated the introduction of cobalt into the circulating solutions from the Stellite 98M2 journal bushings previously used. Graphitar No. 14 bearings are being used with the type 17-4 PH stainless steel. The pumps in loops EE and FF contain the hardened type 17-4 PH stainless steel–Graphitar No. 14 journal-bearing combination.

Two pumps incorporating "outboard" bearings and double thrust surfaces have been built. One of the pumps was run for 140 hr in a test using an all-metal (Stellite 98M2–Stellite 98M2) journal-bearing combination. This combination was selected to determine whether the new type of bearing assembly was an improvement over the present design in which bearing failure occurred with this combination. The bearing thrust load was virtually eliminated prior to the start of the test by drilling appropriate hydraulic balance holes through the impeller eye. The pump operated quite satisfactorily during the run, which was terminated for inspection of the bearings. Some thrust-bearing wear was found even though the thrust load had been reduced to less than 5 lb. It is believed that the thrust-bearing surfaces are running partially dry. An attempt is being made to correct this by drilling small radial holes through the journal bushing at the junction of the radial and thrust surface to provide a forced feed of liquid to the thrust surfaces. If this proves to be satisfactory, the pump will be equipped with pure, sintered, aluminum oxide bearings and journals. Additional

[6] G. H. Jenks, R. A. Lorenz, H. C. Savage, and D. T. Jones, *HRP Quar. Prog. Rep. April 30, 1954*, ORNL-1753, p 81-93.

tests have shown that this material has excellent corrosion resistance in uranyl sulfate solution up to 250°C (cf. Sec. 5.3).

(b) Pump Development for Future In-Pile Loop. The status of pump development by two contractors, Byron Jackson Co. and Allis-Chalmers Mfg. Co., is reported below.

Byron Jackson Co. – This pump, of the canned-rotor centrifugal type with sleeve-type bearings, for operation at 2000 psi, is similar to the ORNL 5-gpm pump and is designed to fit inside a 6-in. beam hole. Except for journal material, the design of the pump was complete at the time of the last report.[7] A decision has been made to use journals of sintered aluminum oxide. The bearings are of the same material. The Byron Jackson Co. is willing to assume responsibility for the mechanical operation of this bearing combination.

Allis-Chalmers Mfg. Co. – This pump is the canned-rotor centrifugal type with hydraulic floating bearings for 2000-psi service, designed to fit inside a 6-in. beam hole. Bearings surfaces of the initial pump will be of type 347 stainless steel pretreated with chromic acid. Allis-Chalmers believes that the oxide coating will form a satisfactory bearing. Construction of the pump has been stopped as a result of delays in negotiating a cost-plus contract with the manufacturer.

4.2.5 Radioactive-Specimen Evaluation

D. T. Jones A. R. Olsen

(a) Loop Dismantling Facility. As mentioned previously, the centrifugal dust-collecting system, for removal of radioactive particles liberated during disassembly of an in-pile loop, as originally installed and operated in the dismantling cell, was inefficient.[8] A filter in the exhaust was considered necessary to ensure complete removal of radioactive particles. However, it has been found that the introduction of low-pressure steam to the intake of the collecting centrifuge markedly improves the separation. Only extremely fine air-borne particles pass the separator. An exact measure has not been made of the efficiency of separation, but it is believed to be above 95%. No filter will be used during the dismantling of the first active loop. Tests for activity in the exhaust plenums will be made during this operation. The results will determine filter requirements in future operations.

The test of dismantling procedures in this cell has been completed by using loop CC. This facility is considered to be ready for receiving the first active loop assembly.

Tests have also been completed of that portion of the dismantling procedure which employs the facilities of the Solid State Division. Because of the limited availability of these facilities for test operations, only the two sample assemblies from loop CC were dismantled. Very little difficulty was encountered. It is believed that the other portions of the loop, with the exception of the pump, can be handled readily. The pump will require unique remote manipulation.

(b) Corrosion Examinations of Loop CC. The pressurizer, pressurizer heater, sampling-line filter, and pump were removed from the loop in the dismantling facility for inspection. The impact samples from the core were transferred to the HRP Metallurgy Group for testing. The corrosion specimens were examined by use of remote procedures. The scrubbed weights indicated low corrosion rates in the mockup operation. However, triangular-shaped pits were noted on two coupons from the high-velocity region of both sample holders. Defilmed weights were not obtained.

(c) Corrosion-Examination Facility. Construction of this facility is about 50% complete. Delays in material deliveries have slowed construction so that the new tentative completion date is December 1, 1954. This date is tentative because no firm delivery date has been obtained on the cutting-bridge mechanism.

[7] G. H. Jenks *et al.*, *HRP Quar. Prog. Rep. July 31, 1954*, ORNL-1772, p 88.

[8] J. J. Hairston, D. T. Jones, and A. R. Olsen, *HRP Quar. Prog. Rep. July 31, 1954*, ORNL-1772, p 89.

5. LABORATORY CORROSION STUDIES

E. L. Compere
J. L. English G. E. Moore

5.1 CORROSION OF THERMOCOUPLE WIRES BY FILTERED WATER AT ROOM TEMPERATURE

J. L. English

Five different types of thermocouple wires were exposed singly and in two-metal combinations to aerated filtered city water at room temperature for a total of 200 hr. The single specimens of Chromel and constantan showed no weight change after the 200-hr period. Of the three thermocouple combinations tested, the Chromel-Alumel thermocouple exhibited the most satisfactory corrosion performance as determined by visual examination and the corrosion behavior of the respective control specimens for this combination. The iron-constantan thermocouple was the least satisfactory, corrosionwise, of the three combinations tested.

The test environment was selected to simulate exposure conditions in the HRT when the reactor cell is flooded with water during down times for inspection and maintenance operations. Since flooding of the cell would mean, for one thing, contact of the water with thermocouple leads to various reactor components, information was needed on the corrosion behavior of different thermocouple combinations in order that the most corrosion-resistant thermocouple could be used for the desired applications.

The thermocouple combinations included copper-constantan, Chromel-Alumel, and iron-constantan. The members of each pair were tested singly as well as in combination. The single-component specimens consisted of 7-in. lengths of the wires rolled into ½-in.-long coils of different diameters, the diameter serving for identification purposes. The combination-type specimens were prepared by taking 22-in. lengths of the wires, rolling into ½-in.-dia coils, and fusion-welding two ends of the desired wires onto a 3-in. square plate of ¼-in.-thick type 347 stainless steel. The ends of the wires were welded approximately ⅛ in. apart on the stainless steel plate.

All specimens were placed in a glass vessel containing 10 liters of aerated tap water at room temperature. The specimens were examined at 100-hr intervals, two in number. The water was replaced at the end of each 100-hr period. The initial water pH was 7.5; the final water pH at the end of each 100-hr exposure averaged 8.3 ± 0.1.

There were no measurable weight changes on the single Chromel and constantan specimens after 200 hr; the metal surfaces in each case remained bright and shiny. Weight losses on the Alumel, copper, and iron specimens were 0.6, 1.1, and 11.2 mg/cm^2, respectively, after the 200-hr exposure. The Alumel and the copper specimens were uniformly covered with a very thin, semidull, light-gray film, while the iron specimen exhibited voluminous rust-colored corrosion products which were removed easily with light brushing. The surface beneath the removed corrosion products had a heavily etched appearance.

The specimens which were welded to the stainless steel plates showed similar behavior to that of the control specimens, and there were no indications, visually, at least, of an accelerated corrosion attack due to the coupling with large masses of stainless steel.

As-removed weight losses and corrosion rates for the single control specimens are listed in Table 5.1. Photographs showing the appearance of the control specimens and the combination specimens after 100 hr of exposure are included in Figs. 5.1 through 5.4.

5.2 TAP-WATER CORROSION OF CARBON-STEEL NUTS

E. L. Compere

Exposure of stressed stainless steel bolts with carbon-steel nuts, of the type proposed for possible HRT flange use, to Oak Ridge city tap water for one month at room temperature resulted in the development of voluminous iron rust on the nut. Type 316 stainless steel bolts stressed to 20,000 psi were used as a stand-in for type 347 stainless steel bolts, which were not available at the time. A weight loss corresponding to a uniform corrosion of 1.2 mils was observed on the nut (16 mpy) with general unlocalized attack. An exposed bolt-nut assembly required 50 ft-lb to loosen it, while a similar unexposed bolt and nut equally stressed

TABLE 5.1. AS-REMOVED WEIGHT LOSSES ON THERMOCOUPLE CONTROL SPECIMENS EXPOSED IN FILTERED WATER AT ROOM TEMPERATURE

Material	After 100-hr Exposure		After 200-hr Exposure		Specimen Appearance
	Weight Loss (mg/cm^2)	Corrosion Rate (mpy)	Weight Loss (mg/cm^2)	Corrosion Rate (mpy)	
Chromel	0	0	0	0	Bright; shiny
Copper	0.6	2.1	1.1	2.1	Dull-gray film
Alumel	0.6	2.1	0.6	1.1	Dull-gray film
Iron	7.8	34.3	11.2	25.0	Heavy rust film
Constantan	0	0	0	0	Bright; shiny

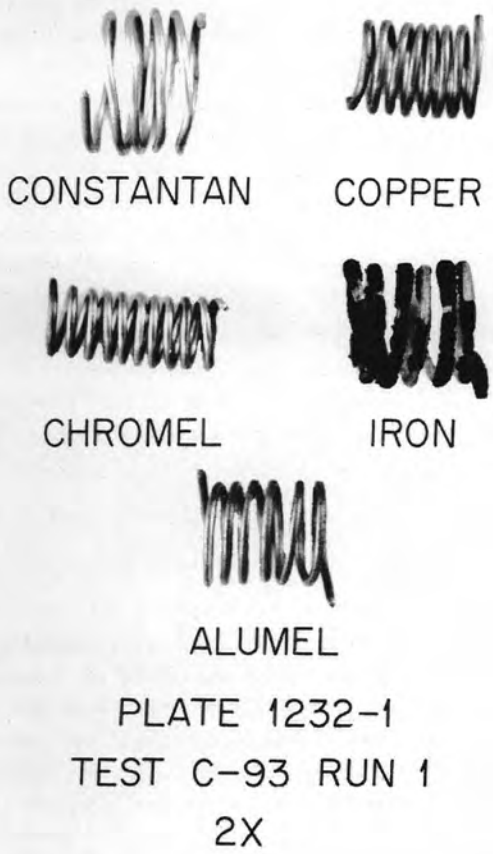

Fig. 5.1. Appearance of Thermocouple Control Specimens After 100 hr in Aerated, Filtered City Water at Room Temperature. Reduced 21%.

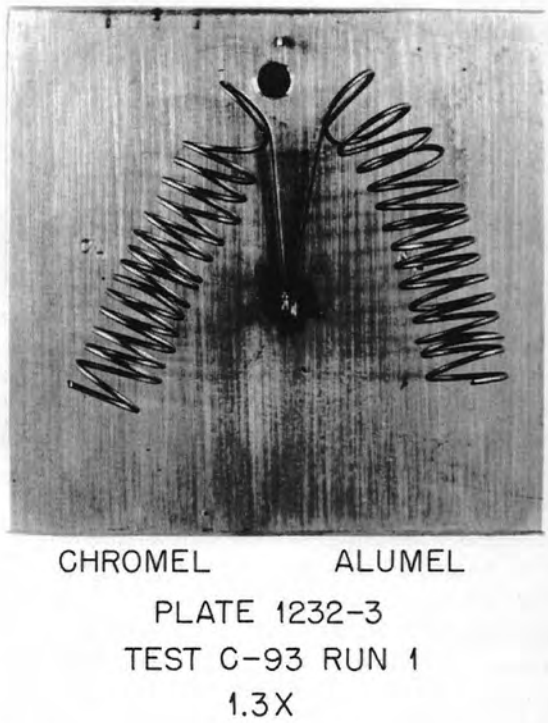

Fig. 5.2. Appearance of Chromel-Alumel Couple After 100 hr in Aerated, Filtered City Water at Room Temperature. Reduced 27%.

IRON CONSTANTAN
PLATE 1232-4
TEST C-93 RUN 1
1.3X

Fig. 5.3. Appearance of Iron-Constantan Couple After 100 hr in Aerated, Filtered City Water at Room Temperature. Reduced 26%.

CONSTANTAN COPPER
PLATE 1232-2
TEST C-93 RUN 1
1.3X

Fig. 5.4. Appearance of Copper-Constantan Couple After 100 hr in Aerated, Filtered City Water at Room Temperature. Reduced 25%.

required 60 ft-lb, indicating that no galling occurred as a result of the exposure.

5.3 CORROSION OF ALUMINUM OXIDE BEARING MATERIAL BY URANYL SULFATE SOLUTION

J. L. English E. L. Compere

Aluminum oxide has been under consideration as a bearing material for the small canned-rotor pumps such as are used in the HRP in-pile loop program. As is shown in Table 5.2, very low corrosion rates (0–4 mpy) have been observed when disks of Al_2O_3 were exposed to 0.17 *m* uranyl sulfate solution at various temperatures in the range 150 to 250°C. Although the white material acquired a light mottled stain in the course of exposure, presumably as a pickup of corrosion products of the stainless steel autoclave, no further damage has been noted on the surface of the specimens. The total exposure time was 915 hr in one case and 300 hr in the other.

5.4 CORROSION OF STELLITE-TYPE 347 STAINLESS STEEL COUPONS

J. L. English E. L. Compere

The severe corrosion of the Stellite part of the let-down valve from the HRE mockup suggested that electrochemical coupling of Stellite and type 347 stainless steel might result in an increased rate of corrosive attack by uranyl sulfate solutions. A series of 100-hr tests of different types of couples between type 347 stainless steel and the respective Stellites 6, 12, and 98M2 in oxygenated 0.17 *m* uranyl sulfate solutions (with and without added 0.01 *m* cupric sulfate) at 100°C is reported below.

In addition to specimens of the uncoupled steel and respective Stellite, duplicate steel-Stellite couples were prepared variously: press fit, shrink fit, mechanically clamped couples, and, in the case of Stellites 6 and 12, as torch hard-faced and

TABLE 5.2. CORROSION OF ALUMINUM OXIDE BEARING MATERIAL BY URANYL SULFATE SOLUTION

Material: Al_2O_3 disk
Container: Stainless steel autoclave
Solution
B-86: 0.17 *m* UO_2SO_4
D-1: 0.17 *m* UO_2SO_4 and 0.01 *m* $CuSO_4$
pH: 2.4
Atmosphere: 150-psi oxygen

Run Period	No. B-86 Temperature (°C)	No. B-86 Cumulative Time (hr)	No. B-86 Cumulative Weight Loss (mg/cm²)	No. B-86 Incremental Rate (mpy)	No. D-1 Temperature (°C)	No. D-1 Cumulative Time (hr)	No. D-1 Cumulative Weight Loss (mg/cm²)	No. D-1 Incremental Rate (mpy)
1	150	118	0.31	2.4	200	100	0.42	3.9
			Smooth white				Smooth white	
2	150	218	0.49	1.7	200	200	0.69	2.5
3	150	314	0.67	1.7	250	300	0.81	1.1
							Slight yellow stain	
4	150	414	0.79	1.1				
			Brown stain					
5	150	515	0.90	1.0				
6	175	615	0.92	0.2				
7	200	715	0.97	0.5				
8	225	815	0.82	1.4 (gain)				
			Light mottled stain					
9	225	915	0.89	0.6				
	Over-all average rate			0.9				2.5

Heliarc hard-faced material. The couples employed and the results observed are given for Stellite 98M2 in Table 5.3, for Stellite 12 in Table 5.4, and for Stellite 6 in Table 5.5.

Exposure was carried out in six 1500-ml, type 347 stainless steel autoclaves, with 1000 ml of 0.17 *m* uranyl sulfate solution, with or without 0.01 *m* cupric sulfate, being charged. Each autoclave contained a complete set of the test specimens of the given Stellite and steel. Exposure was to the solution phase. The autoclaves were pressurized to 150 psig with oxygen gas and heated to 100°C.

The first 50 hr of exposure, for some of the autoclaves containing torch hard-faced materials, showed solutions less acid than the original, and with high levels of corrosion products. It was therefore decided to replace the solution in all the autoclaves with fresh material after each exposure period.

No particular coupling effect was observed for Stellite 98M2 (Table 5.3). There was a generally light attack of 0.7 to 3 mpy on the Stellite, with the corrosion rate decreasing as the exposure continued. In general, there was no particular effect that could be attributed to the copper.

On Stellite 12 (Table 5.4), in general, a very low rate of corrosion was observed, 0.1 mpy or less, except in the case of certain torch hard-faced specimens, where the Stellite 12 had been laid onto a type 347 stainless steel rod, subsequently cut into ¼-in.-thick wafers, and exposed to the solution as indicated. These specimens showed pronounced localized attack with blisters at the Stellite-steel interface, with localization indicating

TABLE 5.3. CORROSION OF ELECTROCHEMICAL COUPLES BETWEEN STELLITE 98M2 AND TYPE 347 STAINLESS STEEL BY URANYL SULFATE SOLUTIONS AT 100°C

Container: Autoclaves Nos. 4 and 8 (type 347 stainless steel)
Duration: 1000 hr
Atmosphere: 150-psi oxygen
Solution
Autoclave No. 4: 0.17 *m* UO_2SO_4[a]
Autoclave No. 8: 0.17 *m* UO_2SO_4[a] and 0.01 *m* $CuSO_4$[a]

Specimen	Tested in Autoclave No. 4		Tested in Autoclave No. 8	
	Average Weight Loss (mpy)	Appearance	Average Weight Loss (mpy)	Appearance
Stellite 98M2 only	1.3 (decrease[b])	Slight tarnish	1.4 (decrease[b])	Unchanged
Clamped couple	0.14 (decrease[b])	Slight tarnish on Stellite in crevice	0.13 (decrease[b])	Unchanged
Stellite 98M2	0.7		0.7	
Type 347 stainless steel	0.05		0.04	
Shrink-fit couple[c]	0.7 (decrease[b])	Slight tarnish	2.7 (decrease[b])	Even attack
Stellite 98M2	1.1		3.1	
Type 347 stainless steel	0.02		2.2	
Shrink-fit couple[d]	0.7 (decrease[b])	Tarnish in crevice	0.5 (decrease[b])	Unchanged
Stellite 98M2	1.6		1.3	
Type 347 stainless steel	0.13		0.04	

[a]Solution changed at the end of 50, 100, 200, and 500 hr.
[b]Decreasing rate with time.
[c]Stellite/steel area ratio: 2.2.
[d]Stellite/steel area ratio: 0.73.

a true penetration rate of perhaps 10 to 20 times the weight-loss rates observed. Penetration rates in pits and blisters could probably be expected to be about 200 mpy. A second, apparently similar, set of specimens from another source did not show any significant attack. Rates were substantially the same for Stellite 12 in the copper-containing solutions.

Torch hard-facing of Stellite 6 on type 347 stainless steel resulted in very severe pitting of the Stellite, sometimes perforating the Stellite layer. This amounted to over 100 mils in less than 1000 hr. The actual pitting penetration rate must have been at least 10 times that given by the weight-loss rates listed in Table 5.5. Heliarc hard-facing and various mechanical types of couple showed little intensification of attack due to coupling. The rates in copper-containing solutions were slightly higher in the most severe cases.

In general, it is concluded from this study that coupling, as such, does not particularly affect the corrosion rate of Stellite coupled to stainless steel in oxygenated 100°C, 0.17 *m* uranyl sulfate solution. Copper sulfate in such solutions shows only a very slight effect. Torch hard-facing can give rise to very serious pitting attack, but Heliarc hard-facing and some specimens of torch hard-facing are relatively unattacked. Due caution apparently should be exercised where hard-facing with Stellite is concerned.

5.5 CHLORINE IN GRAPHITAR

G. E. Moore E. L. Compere

The object of the present investigation was to determine the average chlorine content of Graphitar No. 14, which is used for bearings in canned-rotor pumps, and to investigate methods for chlorine removal. Any chlorine present might be transferred

TYPE 5.4. CORROSION OF ELECTROCHEMICAL COUPLES BETWEEN STELLITE 12 AND TYPE 347 STAINLESS STEEL BY URANYL SULFATE SOLUTIONS AT 100°C

Container: Autoclaves Nos. 6 and 5 (type 347 stainless steel)
Duration: 1000 hr
Atmosphere: 150-psi oxygen
Solution
Autoclave No. 6: 0.17 *m* UO_2SO_4[a]
Autoclave No. 5: 0.17 *m* UO_2SO_4[a] and 0.01 *m* $CuSO_4$[a]

Specimen	Tested in Autoclave No. 6		Tested in Autoclave No. 5	
	Average Weight Loss[b] (mpy)	Appearance Before Defilming	Average Weight Loss[b] (mpy)	Appearance Before Defilming
Type 347 stainless steel only	0.05	Slight golden stain	0.05	Slight golden stain
Stellite 12 only	0.5[c] (gain)	Red-brown film	0.05	Bright; no film
Press-fit couple		Slight tarnish		Bright
Stellite 12 only	3[c] (gain)		5[c] (gain)	
Type 347 stainless steel only	0.07		0.04	
Torch hard face Stellite 12 on type 347 stainless steel rod; sectioned	12 (decrease[d])	Severe blisters, cracks, and localized etch on Stellite	26	Severe blisters, cracks, and localized etch on Stellite
Torch hard face Stellite 12 on type 347 stainless steel rod; sectioned (second source)	0.03 (500 hr)	Dull brown tarnish	0.02 (500 hr)	Slight etch near interface

[a]Solution changed at the end of 50, 100, 200, and 500 hr.
[b]Defilmed.
[c]$mg/dm^2/day$.
[d]Decreasing rate with time.

to the circulating solution. The presence of even very small concentrations of halides in uranyl sulfate solutions is known to cause vapor-phase pitting of stainless steels under some conditions[1] (incomplete data not yet reported). The concentration of chlorine which has caused pitting in other tests would have been attained in in-pile loop solutions if all the chlorine indicated to be present in Graphitar bearings by early analyses had been leached out.

Apparently the first suggestion that chlorine might be present in Graphitar No. 14 came as a result of the discovery by G. H. Jenks[2] of about 13 ppm of chlorine in a solution 0.17 *m* in uranyl sulfate and 0.01 *m* in cupric sulfate when Graphitar was irradiated at 100°C in a Co^{60} gamma source. Subsequent chemical analyses of the Graphitar indicated that 1000 to 4000 ppm of chlorine was present.[3] Solutions from development runs in the in-pile loop program showed 14 and 30 ppm of chlorine, which was presumed to have originated in the Graphitar No. 14 bearings of the pump.[3,4]

As an attempt to remove chlorine from Graphitar, gamma irradiation by a Co^{60} source was tried, since it was under these conditions that chlorine in the solution was originally observed. Two levels

[1]J. C. Griess and R. E. Wacker, *HRP Quar. Prog. Rep. April 30, 1954*, ORNL-1753, p 78.

[2]G. H. Jenks *et al.*, *HRP Quar. Prog. Rep. Jan. 31, 1954*, ORNL-1678, p 65.

[3]G. H. Jenks, R. A. Lorenz, H. C. Savage, and D. T. Jones, *HRP Quar. Prog. Rep. April 30, 1954*, ORNL-1753, p 81–94.

[4]G. H. Jenks *et al.*, *HRP Quar. Prog. Rep. July 31, 1954*, ORNL-1772, p 84–86.

TABLE 5.5. CORROSION OF ELECTROCHEMICAL COUPLES BETWEEN STELLITE 6 AND TYPE 347 STAINLESS STEEL BY URANYL SULFATE SOLUTIONS AT 100°C

Container: Autoclaves Nos. 3 and 7 (type 347 stainless steel)
Duration: 1000 hr
Atmosphere: 150-psi oxygen
Solution
Autoclave No. 3: 0.17 *m* UO_2SO_4[a]
Autoclave No. 7: 0.17 *m* UO_2SO_4[a] and 0.01 *m* $CuSO_4$[a]

Specimen	Tested in Autoclave No. 3		Tested in Autoclave No. 7	
	Average Weight Loss[b] (mpy)	Appearance Before Defilming	Average Weight Loss[b] (mpy)	Appearance Before Defilming
Stellite 6 only	0.02	Mottled brown film	0.01	Brown spots
Clamped couple		Brown film		Brown film
Stellite 6 only	0.03		0.04	
Type 347 stainless steel only	0.00		0.01	
Press-fit couple		No crevice attack		Golden tarnish
Stellite 6 only	1.2[c] (gain)		2.0	
Type 347 stainless steel only	0.13	Brown spots	0.5	
Heliarc hard face one side; Stellite 6 on type 347 stainless steel	0.13[c] (gain)	Brown film	0.05[c] (gain)	Brown film
Heliarc hard face two sides; Stellite 6 on type 347 stainless steel	0.03	Brown film	0.01	Brown film
Torch hard face one side; Stellite 6 on type 347 stainless steel	34	Very deep pits; perforated Stellite	110 (accelerated[d]) (stopped at 500 hr)	Heavy pitting; perforated Stellite
Torch hard face two sides; Stellite 6 on type 347 stainless steel	220 (stopped at 200 hr)	Very heavy pitting	720 (stopped at 100 hr)	Very heavy pitting

[a]Solution changed at the end of 50, 100, 200, and 500 hr.
[b]Defilmed.
[c]$mg/dm^2/day$.
[d]Rate accelerating with time.

of gamma flux were used, one of about 10,000 r/min and the other of about 2000 r/min.

The Graphitar samples were immersed in redistilled water at room temperature during the irradiations. The samples were then analyzed for chlorine, together with control samples from the same bearing.

The initial results of the analyses were very inconsistent and indicated that samples from the same bearing varied from 100 to 34,000 ppm of chlorine, independent of the treatment to which the material had been subjected. These initial analyses were made by a volatilization and absorption technique. Modification of the method led to the conclusion that there was actually not enough chlorine present to detect; the estimated sensitivity of the modified method was about 50 ppm.

Concurrent with these analyses, results from the use of a Parr bomb (ignition of sample in the presence of sodium carbonate in bomb, adsorption in sodium hydroxide, and titration of the chloride) confirmed only that much smaller amounts of chlorine were present in Graphitar No. 14 than the earlier results indicated. No detectable amount of chlorine was found except in one sample of a Graphitar No. 14 bearing for which two independent analytical laboratories reported 200 and 200 to 400

ppm of chlorine. The estimated limit of detection by the Parr method was about 15 ppm.

Since neutron activation analysis appeared to be ideally suited to the Parr type of determination, samples were submitted for chlorine determination by this technique. On the above bearing material analyzed by the Parr technique, activation analysis gave 15 ppm, and on another sample of Graphitar gave checks of 25.4 and 25.5 ppm of chlorine.

Samples of Graphitar No. 14 that had been exposed for 122 days to the 2000 r/min gamma flux were also analyzed for chlorine by use of the neutron activation method. On four samples the values for the concentration of chlorine were 105 ± 4, 124 ± 4, 158 ± 4, and 99 ppm; the first three analyses were in duplicate. The distilled water in which these samples had been immersed during their irradiation showed 7.6 ± 0.1 ppm of chlorine by ionic chemical analysis. This corresponds to a removal of approximately 15 ppm of chlorine from the Graphitar.

Fifteen new Graphitar No. 14 bearings were procured and were machined to size. The dust from the machining of each bearing was collected and submitted for neutron activation analysis. The analyses were carried out in duplicate and gave a precision of about ±10%. The chlorine content ranged from 65 to 230 ppm, with an average of 139 ppm of chlorine. In addition to the chlorine, sodium and manganese activities were found that probably represented a few ppm of these species as impurities. An unidentified short-lived activity was also observed; antimony was suspected.

As a final check on a possible source of chlorine contamination, the oil used in machining the bearings was submitted for analysis. Direct chemical analysis showed less than 1 mg of chlorine per liter in new and used oil. Neutron activation analysis showed 22.3 and 23.8 mg of chlorine per kilogram of new oil and 429 and 457 mg of chlorine per kilogram of used oil. The used oil was taken from a waste tank and had been used on many materials other than Graphitar.

These results indicate that the concentration of chlorine in Graphitar No. 14 by several different methods of analysis is of the order of 100 to 200 ppm, which is at least a factor of 10 below the original estimate. For the approximately 200 g of Graphitar present as bearing material in either the Westinghouse 100A or in-pile loop pumps, this amount corresponds to 20 to 40 mg of chlorine. If all this chlorine were leached from the bearing, a concentration of about 20 to 40 ppm in the in-pile loop solution could result.

In view of the reduced chlorine concentration of the Graphitar indicated by the above analytical investigation and the likelihood, suggested by further experience, that the chlorine concentrations encountered in the initial tests mentioned above actually resulted from unrecognized contamination, this investigation has been terminated.

5.6 SMALL-SCALE DYNAMIC-CORROSION PROGRAM

G. E. Moore E. L. Compere

5.6.1 General Studies

At the end of the last quarter the emphasis in the small-scale dynamic-corrosion program was shifted from studies of uranyl sulfate solutions to those of thorium oxide slurries. Consequently, the attention this quarter was directed to some preliminary aspects of the effect of circulating thorium oxide slurries in stainless steel toroids. Among the factors considered were the effects of slurry and oxygen concentration on the rate of attack on various metals, the effect of flow at 250°C on the nature of the slurry, and the ability of the toroid technique to distinguish between slurries of different abrasive character. However, the primary objective of these studies has been to evaluate the experimental technique and equipment rather than to obtain quantitative data on these variables.

The four-toroid rotator was operated for 920 hr in experiments designed to define the effects of the slurry and oxygen concentrations on type 347 stainless steel, titanium 75A, and Zircaloy-2. Also, it was possible to gain some indication of the effect, on the slurry, of circulation in the toroids.

All runs were carried out with Ames, 100-mesh, screened thorium oxide in distilled water at 250°C at a bulk-slurry velocity of 26 fps. New, type 347 stainless steel toroids fabricated from $\frac{3}{8}$-in. schedule-40 pipe were used. The general experimental arrangement was the same as that described previously.[5]

Since no completely satisfactory method for defilming titanium or Zircaloy-2 has yet been developed, the as-removed, scrubbed weights for these metals are given. The stainless steel specimens were all

[5] E. L. Compere and G. E. Moore, *HRP Quar. Prog. Rep. July 31, 1954*, ORNL-1772, p 104.

electrolytically defilmed. The weight changes have been recorded in Table 5.6 as losses (–) or gains (+) in milligrams per square decimeter per day on the assumption that there was uniform attack of the exposed area of the specimen. When more than one value for a specified set of experimental conditions was obtained, the average value was recorded.

The effect of oxygen concentration was studied by using a helium atmosphere above the slurry to eliminate oxygen. Concentrated (30%) hydrogen peroxide was added to the slurry in other runs to provide, by thermal decomposition, oxygen concentrations greater than atmospheric. The concentrations of oxygen were estimated from the calculated oxygen partial pressure and oxygen solubility data in water.[6]

During these early runs some difficulty in sampling the slurry for analysis was encountered. Nominal slurry concentrations of about 100, 200, 500, and 1000 g of thorium per kilogram of water at room temperature were prepared either by adding distilled water to weighed thorium oxide or by diluting a previously prepared slurry mixture with distilled water. A liter or less of each slurry stock solution was prepared, and 20-ml portions were used in each toroid. Analysis of the slurry concentration after each run often varied widely (±60%) for the same slurry stock solution. Since the sampling of the slurry stock solution was accomplished more readily than that from the toroid after a run, the analyses of the original stock solution are believed to be a more reliable estimate of the actual slurry concentration. In most cases these results were within 10% of the calculated concentration. Due to this difficulty in sampling, nominal slurry concentrations (grams of thorium per kilogram of water) are used in Table 5.6 and are believed to represent the actual slurry concentration within about ±20%.

Table 5.6 shows that the general level of attack as observed in these toroid runs and under the conditions so far studied is rather low. The estimated accuracy of the results varies from about ±1 to ±10 mg/dm^2/day, depending upon the experimental conditions. In the more recent experiments all weighings were performed on a semimicro balance in order to improve the precision. Even so, the time per run (120 to 240 hr) and the exposed area (about 1 cm^2) tend to make the apparent level of the attack of the same magnitude as the precision in a majority of the observations.

The correlation of these results with those obtained from pump loops is unknown. The results

[6]H. A. Pray, C. E. Schweickert, and B. H. Minnich, *Ind. Eng. Chem.* **44**, 1146 (1952).

TABLE 5.6. SUMMARY OF SAMPLE PIN CORROSION RESULTS OBTAINED FROM CIRCULATING THORIUM OXIDE (AMES) SLURRIES IN TYPE 347 STAINLESS STEEL TOROIDS AT 250°C AND 26 fps RELATIVE VELOCITY

Sample Pin	Nominal Slurry Composition (g of Th per kg of D_2O)	Weight Change (mg/dm^2/day) for O_2 Concentration (ppm)				
		0	35	85	450	1500
Type 347 stainless steel (defilmed)	100			–4	0	
	200	–2	–9	–6	0	–2
	500	–11			–2	
	1000	–71	–39	–16	–5	
Titanium 75A (as-removed, scrubbed)	100			+1	+10	
	200		+21	+11	+22	
	500	+3			+3	
	1000	+16	0	–2	+7	
Zircaloy-2 (as-removed, scrubbed)	100			+6	+10	
	200			–6	+11	
	500	0			+1	
	1000	+19			+4	

in toroids with uranyl sulfate showed greater corrosion at lower velocities than in pump loops under similar bulk velocity conditions, however.[5]

Within the limitations of the data, the number of pins (two or four) in each toroid had no apparent effect on the results. The agreement between pins of the same type within each set of conditions also appeared to be adequate.

With type 347 stainless steel a definite and pronounced effect both of oxygen concentration and slurry concentration was observed. The effect of the slurry concentration was most pronounced in the absence of oxygen (helium atmosphere); increasing the slurry concentration increased the corrosion rate. The effect was apparent at 35 and 85 ppm of oxygen and possibly at 450 ppm also. Increasing the oxygen concentration gave decreasing corrosion rates at slurry concentrations of 1000 g of thorium per kilogram of water and probably also at the 500-g level. At lower slurry concentrations the results are not clearly discernible because of the general low level of attack.

Both electropolished and as-machined type 347 stainless steel specimens were used; the electropolished specimens yielded results consistently 10 to 50% lower.

The weight changes with titanium 75A and Zircaloy-2 are generally low and show no definite trends with slurry or oxygen concentration. Ordinarily, a small weight gain was observed.

In the absence of oxygen the type 347 stainless steel pins were generally quite darkened in some areas and very brightly polished in other areas. In the presence of oxygen a general golden film was observed. Titanium and Zircaloy-2 generally showed interference tints under all conditions. However, the specimens themselves were not always uniformly attacked. In the more concentrated slurries the pins often showed a localized attack at their root end, which is also the area where solids would be expected to centrifuge. Attack in the form of a V-shaped groove was observed on the upstream face of some pins; in at least one case the weight loss could be attributed completely to this area and corresponded to a uniform rate of 72 mpy. From the results so far obtained, it is not possible to assign this localized attack either to the geometry and conditions unique to the toroid or to a phenomenon to be encountered generally in circulating slurries in any mechanical system.

Of interest also is the behavior of the slurry in these experiments. In no case was it possible to pour a slurry containing 1000 g of thorium per kilogram of water from the toroid at the completion of a run. In every case it was necessary to rinse out the toroid with water in order to remove the slurry. However, it is believed that circulation of the slurry was achieved during the run, because consistent weight-loss increases were obtained with type 347 stainless steel as the slurry concentration was increased. In addition, a flow pattern on the corrosion specimens was observed. Two runs were made in which the concentration of the slurry was 500 g of thorium per kilogram of water; with the one that had operated under a helium blanket no trouble was experienced in removing the sludge, although the particles seemed to cling to glass more than is usual. In the other case, in which about 450 ppm of oxygen was present, only a small amount of a thick slurry sludge could be poured out, and it coated the glass completely. This material did not flow at all up to 270°C, when a small portion of it was sealed into a quartz tube and slowly rocked while being heated.

In the absence of oxygen the slurry became black in color on circulation in the toroid, was magnetic, and analyzed very high in iron, nickel, and chromium. Iron(II) and chromium(III) were present by qualitative analysis. In some cases the slurry became black when 35 to 80 ppm of oxygen was present. However, 450 ppm of oxygen appeared to be satisfactory for maintaining a white slurry.

Four additional rotators of this same type are now being set up and should provide additional experimental facilities some time during the next quarter.

The furnace for the 20-toroid rotator has been fabricated and installed, and the unit is now ready for operation. Some preliminary experiments will be required to test the completed assembly for satisfactory performance.

5.6.2 Comparison of Thoria Slurries

Toroids may find useful application for quality control in slurry production or for evaluating material prepared by different techniques. The results of one toroid run have shown that it is possible to distinguish between two different slurries, since they showed significantly different corrosion results.

The corrosion behavior of type 347 stainless steel in 100-mesh, screened Ames thorium oxide slurry was compared with that of Lindsay No. 7 thorium oxide slurry to determine whether a significant difference could be detected. Slurry concentrations of 500 g of thorium per kilogram of water were used with a calculated 450-ppm oxygen concentration added initially as hydrogen peroxide. The toroids were run for 110 hr at 250°C and at a bulk-slurry velocity of 26 fps. Each toroid contained two as-machined and two electropolished type 347 stainless steel corrosion pin specimens. Four toroids were rotated simultaneously on one rotator, each slurry being run in duplicate.

At the completion of the run the slurries were removed and examined. In all cases they were somewhat creamy and settled relatively slowly. The analytical results obtained from these slurries are summarized in Table 5.7. The type 347 stainless steel corrosion pins were electrolytically defilmed and weighed; these results are summarized in Table 5.8.

The fact that the iron content was considerably greater for the Lindsay No. 7 slurries in toroids B and D than for the Ames slurry in toroid C (Table 5.7) suggests that there was a greater attack on the stainless steel system in toroids B and D. On the other hand, the Ames slurry in toroid A shows not only a high iron content but also relatively high and out-of-proportion nickel and chromium concentrations. It is believed that the results obtained in toroid A are due to the previous operating history of the toroid, as will be explained below.

The variance in the pin weight-loss rate (Table 5.8) between toroids has been analyzed by means of the *t*-test whereby it was found that there was a significant difference in corrosion rate on type 347

TABLE 5.7. ANALYTICAL RESULTS ON AMES AND ON LINDSAY NO. 7 THORIUM OXIDE SLURRIES IN TYPE 347 STAINLESS STEEL TOROIDS

Oxygen Concentration: 450 ppm
Temperature: 250°C
Bulk-Slurry Velocity: 26 fps
Duration: 110 hr

Slurry	Toroid	Composition (mg/g)				pH	Filtrate			
		Th	Fe	Ni	Cr		pH	Chloride (mg/liter)	Sulfate (mg/liter)	Ions*
Ames	A	323	0.682	0.364	0.162	6.15	6.1	7		465
		314	0.657	0.350	0.170					
	C	291	0.349	0.057	0.052	5.40	6.0	6		186
		295	0.362	0.053	0.041					
			0.428							
			0.428							
Lindsay No. 7	B	344	1.07	0.185	0.147	6.10	6.4	8		55
		342	1.03	0.188	0.136					
	D	372	0.686	0.115	0.088					
		367	0.684	0.120	0.096	6.4	6.3	9		72
Ames (original)		320	0.008	<0.005	0.004	8.3	6.4	5	27	54
		322	0.004	<0.005	0.003					
Lindsay No. 7 (original)		277	<0.005	<0.005	<0.003	8.9	7.0	4	40	10
		150	<0.005	<0.005	<0.003					

*Based on specific conductivity; arbitrary units.

TABLE 5.8. COMPARISON OF CORROSION RESULTS OBTAINED IN TOROIDS ON TYPE 347 STAINLESS STEEL BY AMES AND BY LINDSAY NO. 7 THORIUM OXIDE SLURRIES

Thorium Concentration: 500 g of Th per kg of H_2O
Oxygen Concentration: 450 ppm
Temperature: 250°C
Bulk-Slurry Velocity: 26 fps
Duration: 110 hr

Slurry	Toroid	Pin Weight Loss ($mg/dm^2/day$)*	Arithmetic Mean ($mg/dm^2/day$)	Standard Deviation	95% Confidence Interval of Mean
Ames	A	−5.9	−5.8	1.0	1.6
		−4.6			
		−5.2			
		−7.4			
	C	+0.9	−0.2	2.0	3.1
		+2.4			
		−2.2			
		−2.0			
Lindsay No. 7	B	−11	−12	2.7	4.3
		−14			
		−15			
		−8.5			
	D	−10	−7.2	2.4	4.0
		−4.2			
		−9.0			
		−5.7			
Ames	A and C		−3.0	3.2	2.8
Lindsay No. 7	B and D		−9.7	3.4	3.0

*Metal weight loss of 5.5 $mg/dm^2/day$ corresponds to a uniform corrosion rate of 1 mpy. Weight gains imply adhering metal oxide, and the above factor does not apply.

stainless steel between the Ames and Lindsay slurries at the 99% confidence level. Table 5.8 shows that the mean corrosion rate by the Lindsay slurry was about three times larger than the mean rate shown by the Ames slurry. The analysis of variance also showed that although there was probably no significant difference between the two Lindsay slurries, there was a difference between the results from the two toroids of Ames slurry which was statistically significant at the 99% level.

Table 5.8 also shows that there was almost as much dispersion between the Ames slurry in toroids A and C as there was between the mean of the two Ames slurries and the Lindsay slurry. It is believed that this difference between the Ames slurries can be explained in the following manner: The four toroids had been used previously to obtain the results described in the preceding section on the effect of slurry and oxygen concentration. Toroid A had been operated exclusively in the absence of oxygen prior to this run, whereas the other toroids had been used with slurries containing no less than 85 ppm of oxygen. It appears

that this difference in operating history may have affected the results in toroid A and consequently caused the dispersion in the corrosion results with the Ames oxide. A repeat run is being planned.

In spite of the dispersion within the results with the Ames oxide, however, it was possible to distinguish between these two oxides on the basis of their corrosion rates on type 347 stainless steel pins by using the toroid technique.

Part IV

ENGINEERING DEVELOPMENT

J. A. Lane

6. DEVELOPMENT OF FUEL-SYSTEM COMPONENTS

C. B. Graham

J. S. Culver
D. M. Eissenberg
C. H. Gabbard
L. F. Goode
J. N. Baird, Jr.[1]
D. S. Toomb, Jr.[2]
R. J. Kedl
W. L. Ross
J. G. Smith
I. Spiewak
E. L. Youngblood
J. L. Redford[2]

6.1 RECOMBINER DEVELOPMENT

D. M. Eissenberg
R. Goodman
A. L. Johnson
I. Spiewak
J. L. Redford

The electrical control and power circuits of the high-pressure recombiner loop[3] were completed during the past quarter. The system was helium leak-tested, and all leaks were eliminated.

The electrolytic cells have been operated at atmospheric pressure and have given no trouble. The system was brought to nominal operating conditions of 1000 psi, 250°C, and 0.5-cfm diluent-gas recirculation. After final testing at this condition, the electrolytic cells will be tested at high pressure and the experimental program will be started.

6.2 DUMP-VALVE TEST LOOP

J. G. Smith
I. Spiewak
D. S. Toomb, Jr.

A loop for testing the performance and useful life of dump valves and trims is being designed (Fig. 6.1) and will be constructed of equipment already available. This equipment permits valve operation on soup at reactor temperature, pressure, and flow rate, but the volume dumped is limited to the 15-gal capacity of the high-pressure storage. It is planned

[1] Instrumentation and Controls Division.

[2] Instrumentation and Controls Section.

[3] C. B. Graham *et al.*, *HRP Quar. Prog. Rep. April 30, 1954*, ORNL-1753, p 53–58.

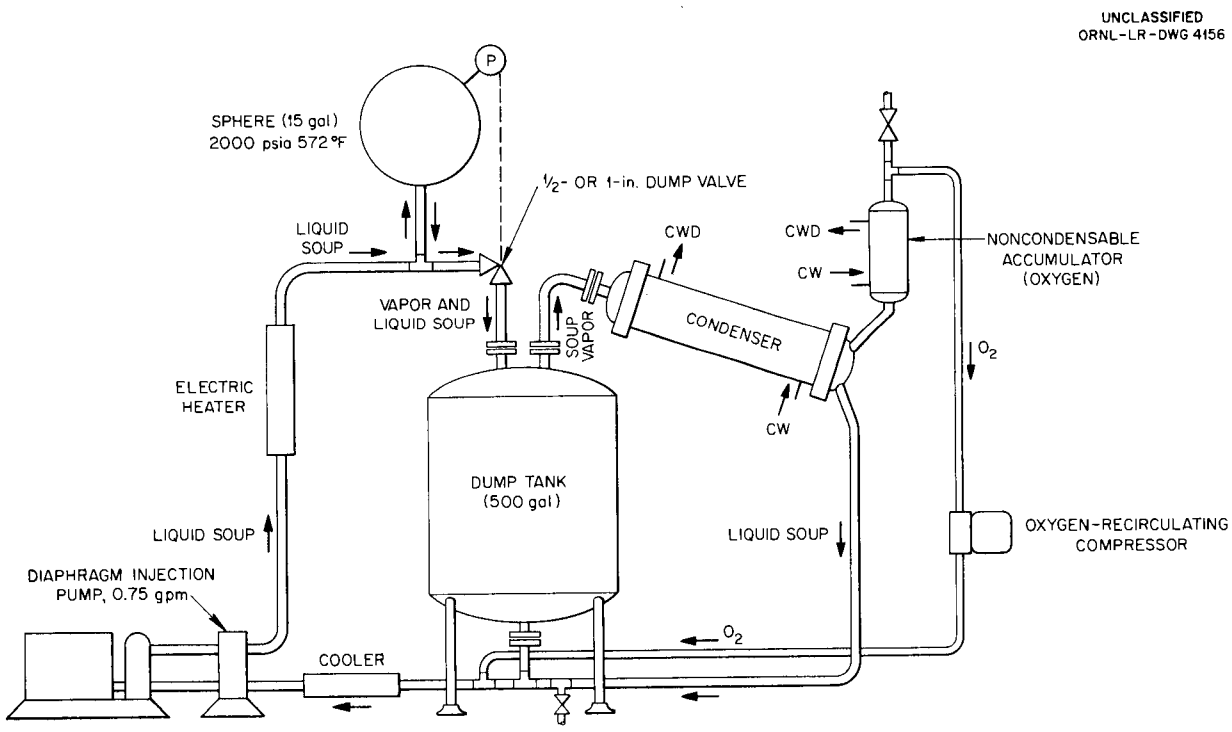

Fig. 6.1. Fuel-Valve Test Loop.

that additional high-pressure storage capacity will be purchased for future enlargement of the system.

The loop will be instrumented so that when the high-pressure system is full the dump valve will open. The feed pump will work continuously, allowing one dump every 20 to 25 min.

6.3 SMALL REACTOR COMPONENTS

6.3.1 Allis-Chalmers 500-gpm Pump and 20-cfm Gas Circulator

W. L. Ross R. J. Kedl

Negotiations are continuing with the Allis-Chalmers Mfg. Co. for the construction of the 500-gpm canned-rotor pump and the 20-cfm canned-rotor gas circulator. The contract has been delayed slightly because of a change in the specifications. Originally, hollow-wire conductors were to be used for the pump stator, and low-pressure water was to be circulated through the conductors for cooling. However, the terminal box for this system was large, complicated, and expensive; so it was decided that solid-wire conductors would be used with an auxiliary cooling system. This decision is also a result of the manufacturer's opinion that hollow conductors would not be desirable in future large pumps.

6.3.2 ORNL Gas Circulator

W. L. Ross R. J. Kedl
C. C. Hurtt A. B. Daffron

Tests of the ORNL gas circulator[4] (assembly drawing, Fig. 6.2) are continuing. The circulator has been calibrated at three frequencies. Figure 6.3 shows flow vs developed head for frequencies of 60, 80, 100, and 120 cps. Operational experience with the circulator is summarized in Table 6.1. A series of 30 starts and stops has also been performed. After these tests, the bearings showed

[4] C. B. Graham *et al.*, *HRP Quar. Prog. Rep. July 31, 1954*, ORNL-1772, p 109.

TABLE 6.1. OPERATIONAL DATA FOR ORNL GAS CIRCULATOR

Frequency (cps)	Synchronous Speed (rpm)	Run Time (hr)
60	3600	350
100	6000	38
120	7200	120

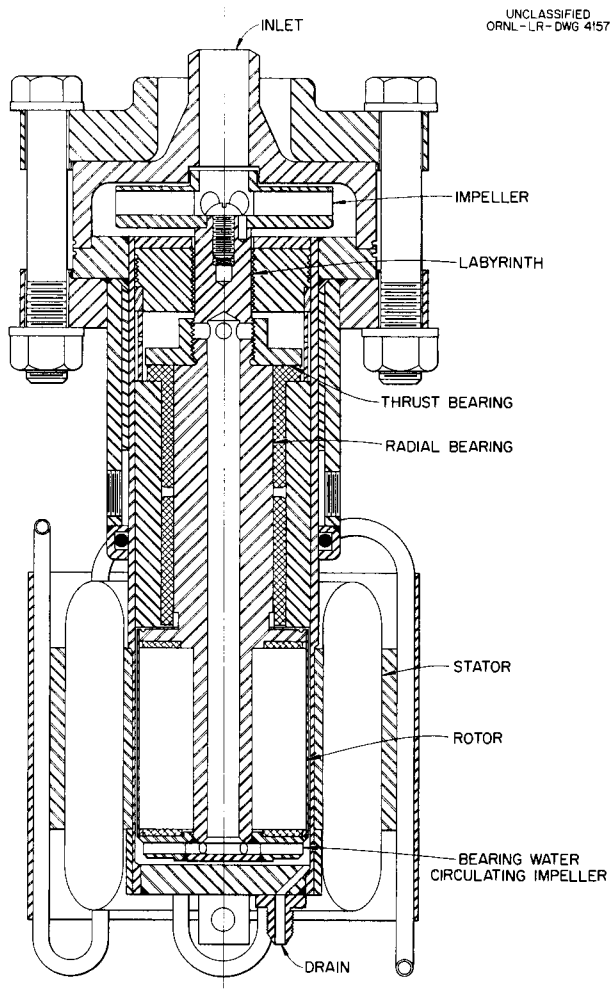

Fig. 6.2. ORNL Canned-Rotor Gas Circulator.

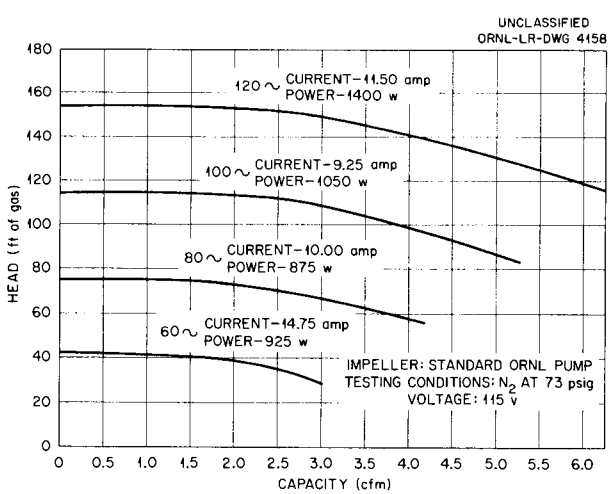

Fig. 6.3. ORNL Gas-Circulator Characteristics.

practically no wear. None of the other circulator parts showed signs of wear.

It has been found that the circulator will not operate satisfactorily for extended periods of time when it is circulating completely noncondensable gas, since the shaft will gradually throw out of the bearing chamber the liquid necessary for proper bearing operation. The bearings then will begin to run dry. If part of the gas is condensable, it will refill the cool bearing chamber as fast as the liquid is thrown out.

6.3.3 ORNL 5-gpm Pump

C. C. Hurtt A. B. Daffron
W. L. Ross

An ORNL 5-gpm pump has continued to operate in an endurance test to determine the life expectancy of the various parts. This pump has run for a total of about 4500 hr while circulating water at a temperature of 250°C. Approximately 200 start-and-stop operations have been accumulated, with about one-half the operations occurring during one short test period.

The pump has been disassembled and examined after 100, 1100, 2100, 2700, and 3700 hr. During disassembly, after 2700 hr of operation, the head of the impeller screw was damaged. The screw was replaced with a new one, which unfortunately had a loose fit in the threads. After 2 hr of operation, excessive pump noise dictated a shutdown. Examination revealed that the impeller screw had worked loose and that this allowed the impeller to rub on the pump scroll. The radial-bearing surface was worn excessively. The impeller, scroll, labyrinth seal, and shaft were rubbed and worn to a slight extent. None of the other examinations revealed any unusual or severe wear on any of the pump parts; therefore the bearing and impeller screw were replaced, and operation has continued.

The pump stator has operated for a total of 6400 hr without failure. The stator is cooled with copper water coils on the iron laminations and has class A insulation on the windings. The pump is continuing in endurance-test operation with the use of 250°C water exposed to helium pressure.

During the report period the pressure drops required for various flows of water through a 5-gpm pump with the pump stopped were measured in order to aid in determining the feasibility of using the 5-gpm pump to fill the HRT blanket vessel at low pressure. One proposal suggests that an ORNL pump be placed in the suction line of the blanket feed pump so that the blanket system may be filled by the 5-gpm pump rather than by the lower capacity feed pump.

The pressure-drop measurements were taken by using water flow in standard $\frac{3}{4}$-in. pipe with pressure taps 3 in. from the pump suction and 3 in. from the discharge. Figure 6.4 shows the pressure drop through an ORNL pump for flows of from 1.5 to more than 5 gpm. At a flow of 2 gpm through the blanket feed pump, an ORNL pump in the suction line would require about 1 in. of water-pressure loss.

6.4 LARGE REACTOR COMPONENTS

6.4.1 50-Mw Main Fuel Heat Exchanger

L. F. Goode W. L. Ross

Negotiation of the contract for the 50-Mw main fuel heat exchanger has been completed, and work is proceeding under the contract.

Development in tube-joint welding in which manual techniques are used is nearing completion. Mockup tube sheets, each containing seven $\frac{3}{8}$-in. tubes (0.049-in. wall thickness) on a $\frac{5}{8}$-in. triangular pitch, have been prepared, with the use of the most promising welds to date, and will be corrosion tested.

A series of corrosion studies has been performed on weldments (fabricated by the Foster Wheeler Corp.) containing various percentages of ferrite; details of the studies are reported in Sec. 9.2.1.

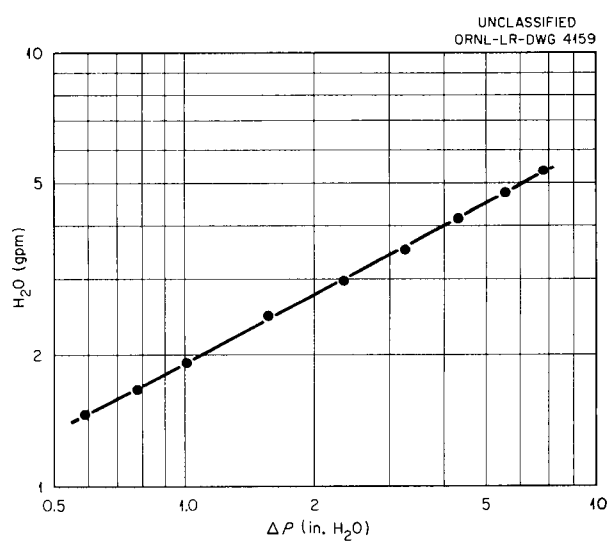

Fig. 6.4. Pressure Drop vs Water Flow Through an ORNL Pump (When Stopped).

As a result of the studies, the allowable ferrite content for welds in contact with the primary fluid has been raised to 8%. This change in specification has somewhat simplified the welding program. Economic and time savings are anticipated.

Investigation of tube-testing methods is continuing. Arrangements are being made with Magnetic Analysis Corp., Long Island City, New York, to inspect approximately 11,000 ft of $\frac{3}{8}$-in. (0.065-in. wall) HRT heat-exchanger tubing with their high-frequency flaw detector. Sperry Products Inc., Danbury, Connecticut, will develop a special reflectoscope search unit for $\frac{3}{8}$-in.-dia tubing, and evaluation of the ultrasonic inspection methods will continue. RCA has demonstrated an x-ray television technique which, although in the early development stages, shows considerable promise; it will be investigated further.

6.4.2 Large Heat Exchanger

L. F. Goode W. L. Ross
K. E. Estes

In the course of the study of large heat exchangers,[5] the design shown in Fig. 6.5 has been submitted. It is believed that this 300-Mw unit represents the maximum-size heat exchanger of its type that can be considered practicable at the present time. Cost and material-procurement studies of this and similar units are proceeding.

During this period, cost information on tube-sheet machining, tube-joint preparation and welding, stainless steel tubes, steam-drum fabrication, and other heat-exchanger construction and testing costs have been supplied to the REED Engineering Design Section by Foster Wheeler Corp.

A single U-tube heat exchanger is being built to obtain heat-transfer data. Figure 6.6 shows the heat exchanger which will be installed on a Westinghouse 400A pump test loop. Flow rate and soup concentrations in the tube will approximate the conditions contemplated for the heat exchangers of the large reactors. A velocity of 20 fps and a concentration of 6 g of uranium per kilogram of solvent have been tentatively selected as the operating conditions desired.

The water on the outside of the tube will form steam which will be condensed by the cooling water in the jacket around the steam space of the exchanger. At equilibrium conditions the heat input to the cooling water will equal the heat loss of the solution if heat loss through the insulation is disregarded. With adequate insulation, results should check fairly closely. The results obtained will be used to calculate the over-all heat-transfer coefficient. These values will be plotted as a function of time.

Two carbon-steel strips are to be placed in the shell of the heat exchanger to determine whether the large amount of stainless steel area with the small amount of carbon-steel area sets up any galvanic action which might cause severe corrosion and/or deposit scale on the heat-transfer surface. This area is approximately 10:1, based on the wetted surface. This is in line with the ratio of stainless steel to carbon steel in the HRT heat exchanger, as well as that expected in large heat exchangers.

6.5 4000-gpm LOOP[6]

C. H. Gabbard R. G. Meza
W. B. Krick D. S. Toomb, Jr.

On September 3, the 4000-gpm loop was started on water without incident. The ensuing period has been devoted to debugging components and adjusting instrument settings for smooth operation.

The loop operates at 1000 psi and heats to 250°C in about 2 hr. Temperature and pressure regulation is good, and unplanned shutdowns have virtually been eliminated.

Initial operation was on an 8 hr per day basis, which was later increased to 16 hr per day. This increase in operating time allowed thermal cycling of the loop flanges, which will be checked for leaks during a planned shutdown before UO_2SO_4 is added to the system.

After 160 hr of operation, the loop was shut down to repack the feed pump. A new type of Teflon seal with Chevron packing will be installed in an effort to reduce leakage through the packing.

The system was dumped by two methods to establish a guide for future operation. First, normal procedure was used in which the water is let down through a $\frac{1}{4}$-in. valve into the flash tank, which is equipped with a condenser to take care of the steam. This dump took about 20 min to reduce the system pressure to 200 psi. The second test was

[5] C. B. Graham *et al.*, *HRP Quar. Prog. Rep. July 31, 1954*, ORNL-1772, p 110.

[6] J. R. McWherter *et al.*, *HRP Quar. Prog. Rep. Nov. 15, 1951*, ORNL-1221, p 18.

UNCLASSIFIED
ORNL-LR-DWG 4160

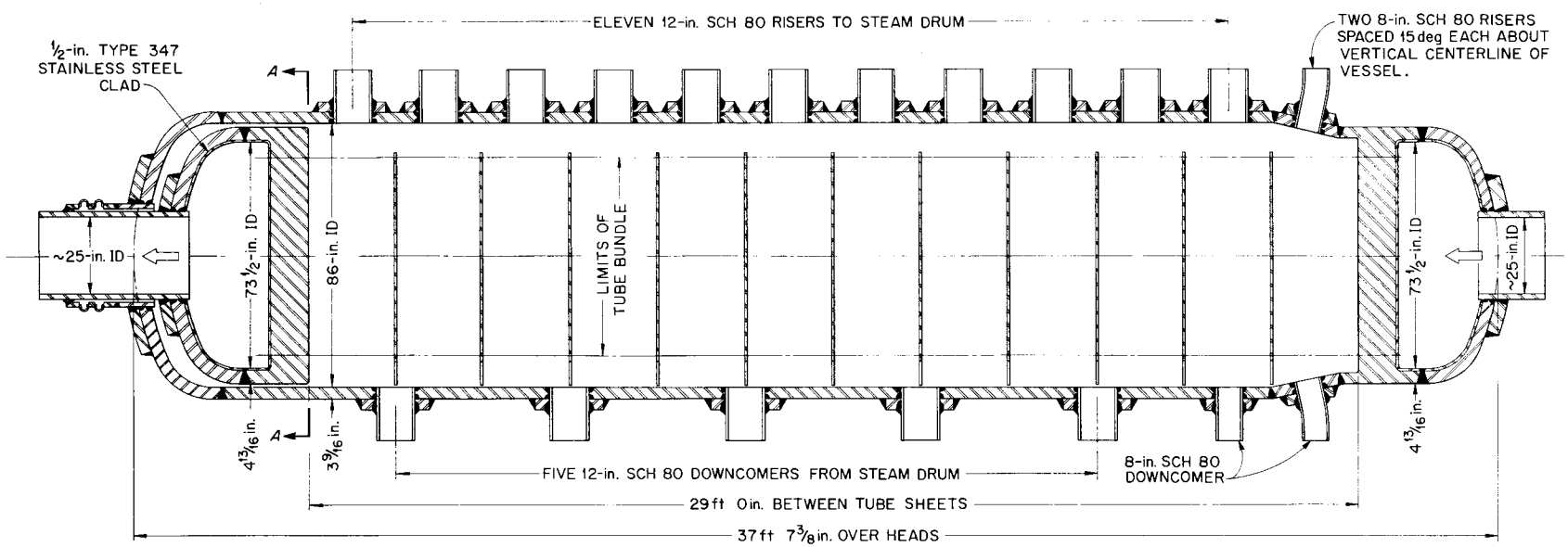

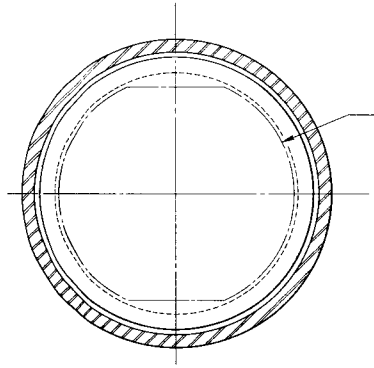

SECTION A-A

NOTES:

DIMENSIONS ARE APPROXIMATE.

UNIT CONSTRUCTED OF CARBON STEEL SA 212 GRADE "B" AND SA105 GRADE "II" WITH TYPE 347 STAINLESS STEEL IN CONTACT WITH PRIMARY FLUID PER 1952 ASME SECT. VIII UNFIRED.

Fig. 6.5. Large Heat Exchanger.

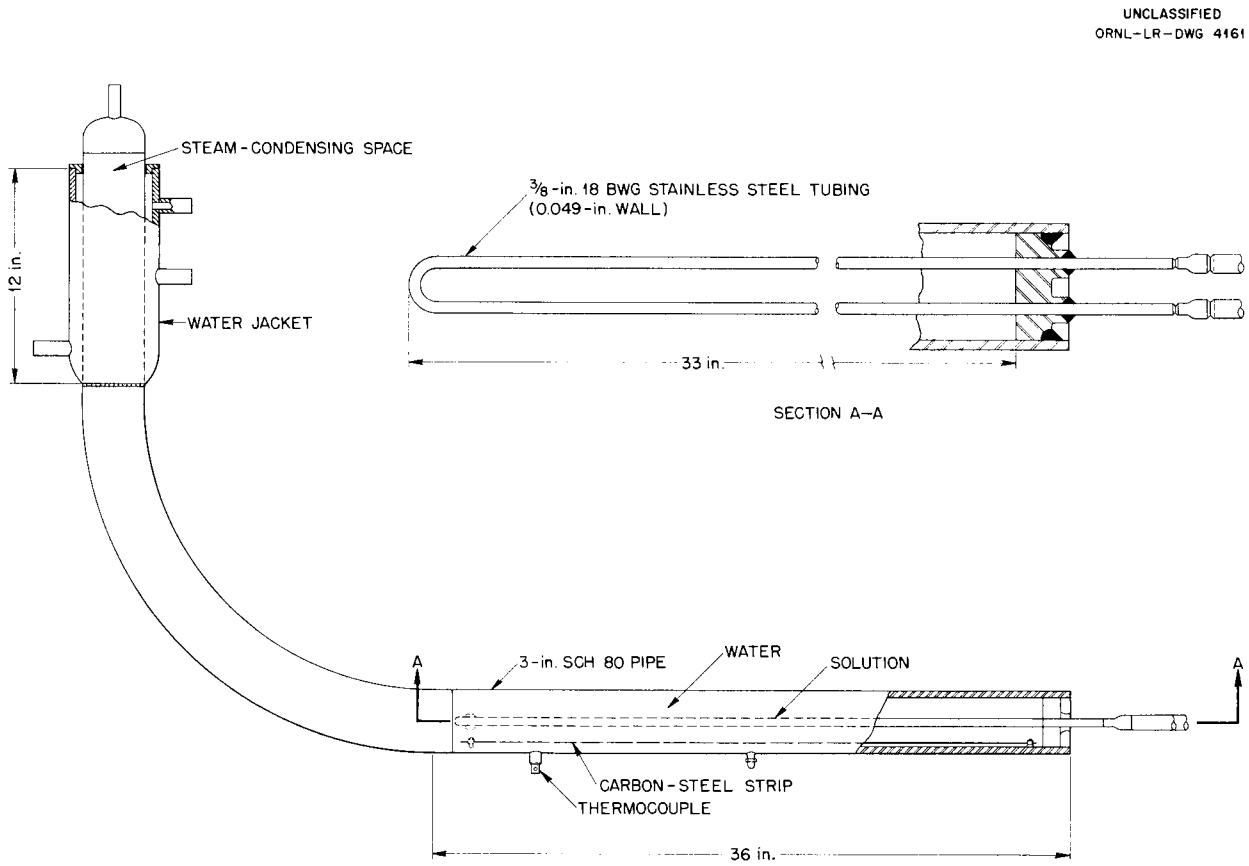

Fig. 6.6. Test Heat Exchanger.

a test panic dump through a ½-in. air-operated valve. This dump took only 10 min. Due to the rapid discharge, without benefit of cooling in the dump tank, most of the exhausted liquid was discharged into the vent and drain system. Although no damage to equipment occurred, this mode of dumping would not be used except in a dire emergency.

In addition to the leak test previously mentioned, it is planned to take water samples for corrosion data and to calibrate the oxygen system so that actual O_2 concentration in the high-pressure system will be known by the O_2 flow rate.

Before the UO_2SO_4 solution is added, the loop will be thoroughly checked, and pump parts and other components which might suffer severe corrosion will be weighed, measured, or photographed for comparison after running. In the early stages of runs with UO_2SO_4, the amount of contaminant present in the condensate stream circulating through the canned-rotor pump motor will be measured.

Two of the stainless steel O-ring gaskets will be replaced with new ones which have been gold plated so as to attain ease of tightening and to observe their corrosion effect.

6.6 SLURRY-INJECTION PUMP LOOP

J. M. Baker E. L. Youngblood
D. S. Toomb, Jr.

The injection pump loop which was operated on ThO_2 slurry, as reported previously,[7] was charged with thoria from another source, with the result that erosion rates greatly increased. It has been suggested that ORNL-manufactured thoria slurry, because of a lower calcining temperature, may be less erosive.

[7] R. N. Lyon *et al.*, *HRP Quar. Prog. Rep. Jan. 31, 1954*, ORNL-1678, p 90.

A run recently completed on Lindsay No. 8 thoria in a concentration of 500 g/liter completely destroyed the trim in the throttling valve used to reduce the pressure from 1000 psi to atmospheric. The trim material was the same as that used in the previous test (Stellite 6 plug and Stellite 12 seat). The time required was 50 hr to erode the valve so that it would no longer hold pressure when completely shut off. This compares with 63 hr on the previous test with the same concentration of slurry.

The ball checks, made of Star J metal, acquired a frosted appearance in contrast to the usual mirror finish. The pump diaphragm showed almost no erosion as a result of running on the Lindsay No. 8 oxide.

New trim, identical in every respect with that run on the Lindsay oxide, has been placed in the valve, and a test will be made with a slurry containing thoria, produced at ORNL, at a concentration of 500 g/liter.

7. DEVELOPMENT OF BLANKET-SYSTEM COMPONENTS

R. N. Lyon

S. G. Bankoff
P. R. Crowley
D. G. Davis
R. B. Gallaher
W. Q. Hullings
A. S. Kitzes
B. A. Kress
C. G. Lawson
L. E. McTaggart
R. H. Nimmo
L. F. Parsly
J. D. Perret
W. B. Plummer
M. Richardson
D. G. Thomas
D. S. Toomb
P. C. Zmola

7.1 SLURRY-COMPONENT DEVELOPMENT

A. S. Kitzes

P. R. Crowley
W. Q. Hullings
B. A. Kress
C. G. Lawson

7.1.1 5-gpm Pumps

A 5-gpm, all-stainless-steel, canned-rotor pump developed by the Allis-Chalmers Mfg. Co. as a slurry pump was tested with a slurry containing 1000 g of thoria per kilogram of water at 250°C. The pump, designed to deliver 5 gpm with a head of approximately 35 ft, has special stator windings to permit operation at temperatures up to 750°F. All the bearings are the fluid-piston type. The radial bearings of stainless steel are an integral part of the rotor and run against a hollow, stationary, stainless steel shaft as the journal. The balance of thrust forces is maintained by the relative flow of liquid between the impeller shrouds and the front and back walls of the pump casing.

A slurry containing 1000 g of thorium per kilogram of water was circulated with this pump at 250°C for 79 hr. Inspection of the pump after shutdown revealed that the stationary hollow shaft and rotor chamber were partially filled with solids. As a result, the impeller was pushed forward against the front of the pump casing. No difficulty was encountered in restarting the pump once it was stopped, even though the rotor chamber contained solids.

The pump is now being modified so that water injection can be used to keep the bearings flushed of solids at all times.

7.1.2 Westinghouse 200A Slurry Pump

Delivery of the Westinghouse 200A pump, described in the previous progress report,[1] is scheduled for November 12, 1954. The design of the pump is such that metal pump parts in all regions of high velocity and/or turbulence can be fabricated from, or lined with, titanium.

7.1.3 Pressurizer Studies

Various schemes for pressurizers suitable for use in the HRT are being studied. These include:

1. the present loop design in which the entire circulating stream passes through the lower part of the pressurizer,
2. a sloping horizontal pressurizer in which only a small fraction of the circulating fluid passes through the pressurizer,
3. a vertical pressurizer fed at the top by a mixture of slurry and steam. (This mixed stream is obtained by heating a small bypass stream from the main circulating loop. This results in a net downward flow in the pressurizer and tends to maintain the pressurizer at the same slurry concentration as the rest of the system.)

Preparatory to the pressurizer studies at the elevated temperatures and pressures, a low-temperature loop, partially constructed of glass, is being used to observe flow patterns in mockups of pressurizer prototypes.

7.1.4 Pressure-Vessel Studies

Results of tests in an 18-in.-dia plastic mockup of the HRT pressure vessel still indicate that the slurry is homogeneous in flowing through the system. However, two inlets were modified so that the fluid enters tangentially and sweeps across the bottom of the vessel to pick up the solids which have settled during a long shutdown. To redisperse the solids after a long shutdown, a minimum inlet velocity of 10 fps was found to be necessary. Using one outlet from the blanket

[1] R. N. Lyon *et al.*, *HRP Quar. Prog. Rep. July 31, 1954*, ORNL-1772, p 114–131.

vessel, various modifications are being investigated to eliminate stagnant areas found to exist just above the top of the core vessel.

The steel mockup of the blanket vessel described previously[1] is assembled, and testing with slurry should begin by December 1, 1954.

7.2 HRT BLANKET MOCKUP

L. F. Parsly
L. E. McTaggart R. H. Nimmo
W. B. Plummer

The work of designing a full-scale slurry mockup, previously reported[1] as being done by a group at K-25, has been transferred, with the men, to ORNL.

The flow sheet for the mockup has been established and is shown in Fig. 7.1. After the various possibilities were reviewed, it was decided to use steam pressurization and to provide a positive flow of slurry through the pressurizer in order to ensure that solids would not accumulate in the lower part. A continuous bleed of steam is let down to low pressure to purge the vapor space of noncondensable gases and to supply water for purging the pump motor, instrument connections, etc. The pressurizer has been located on the suction side of the main circulating pump so that the pump head will be available for forcing the bypass stream through the pressurizer heater and into the pressurizer.

For design purposes, the bypass stream has been set at 2% of the main-stream flow. The steam let-down rate has been based on the requirement of diluting 10% of the radiolytic decomposition gases produced at a power level of 1000 kw to below the explosive limit, and it is assumed that the balance of the gases will be recombined catalytically on the ThO_2, or an incorporated catalyst, at operating conditions. At the above bypass and vaporization rates, approximately 5% of the water in the bypass stream will be vaporized.

In addition to the uncertainty regarding the reliability of ThO_2 as a recombination catalyst, the best location of the pressurizer tie-in to the circulating loop has not been fixed. The proposed arrangement locates the tie-in an appreciable distance from the reactor, and some question exists as to whether a pressure increase sufficient to damage the core will occur during a power surge. The Reactor Analysis Section is calculating the transient pressure effects which are expected. If it turns out that the pressurizer tie-in must be placed as close to the reactor outlet as possible, it will be necessary to shift the main circulating pump upstream of the heat exchanger or to provide an auxiliary pump for the bypass stream.

Layout studies have been made, and it has been determined that the reactor piping layout can be duplicated without sacrificing accessibility for maintenance during testing and substitution of alternative components in the mockup. Therefore, the piping will duplicate that in the reactor.

The status of design and procurement is as follows:

Construction drawings for the slurry heat exchanger have been completed.

Design calculations and preliminary sketches for the other equipment are essentially complete, and requisitions for most of the material have been issued.

Instrument and valve requirements have been determined, and these items will be requisitioned in the near future.

Arrangements have been made with the Engineering Development Section to have the main circulating pump available when required for installation in the mockup. Prior to its use in the mockup, the pump will be tested by the Engineering Development Section.

7.3 SLURRY-CIRCULATION STUDIES

A. S. Kitzes
R. B. Gallaher

During the past quarter, additional data have been collected concerning the resistance of type 347 stainless steel to slurry attack at 250°C. Two loops, previously described,[2] were in operation with slurries of various thorium oxide preparations. In all runs the loops were pretreated for 15 to 90 hr by circulating water containing 500 ppm of oxygen at 250°C to develop a protective oxide film on the stainless steel. During the slurry runs the initial oxygen concentration was varied from 200 to 600 ppm.

The ThO_2 slurries with oxygen were circulated without difficulty, and the concentrations have been essentially constant except for one run (S-51), in which, for the first time, the solids accumulated in the pressurizer as a soft cake. The cause for

[2] R. N. Lyon *et al.*, *HRP Quar. Prog. Rep. Oct. 31, 1953*, ORNL-1658, p 127–128.

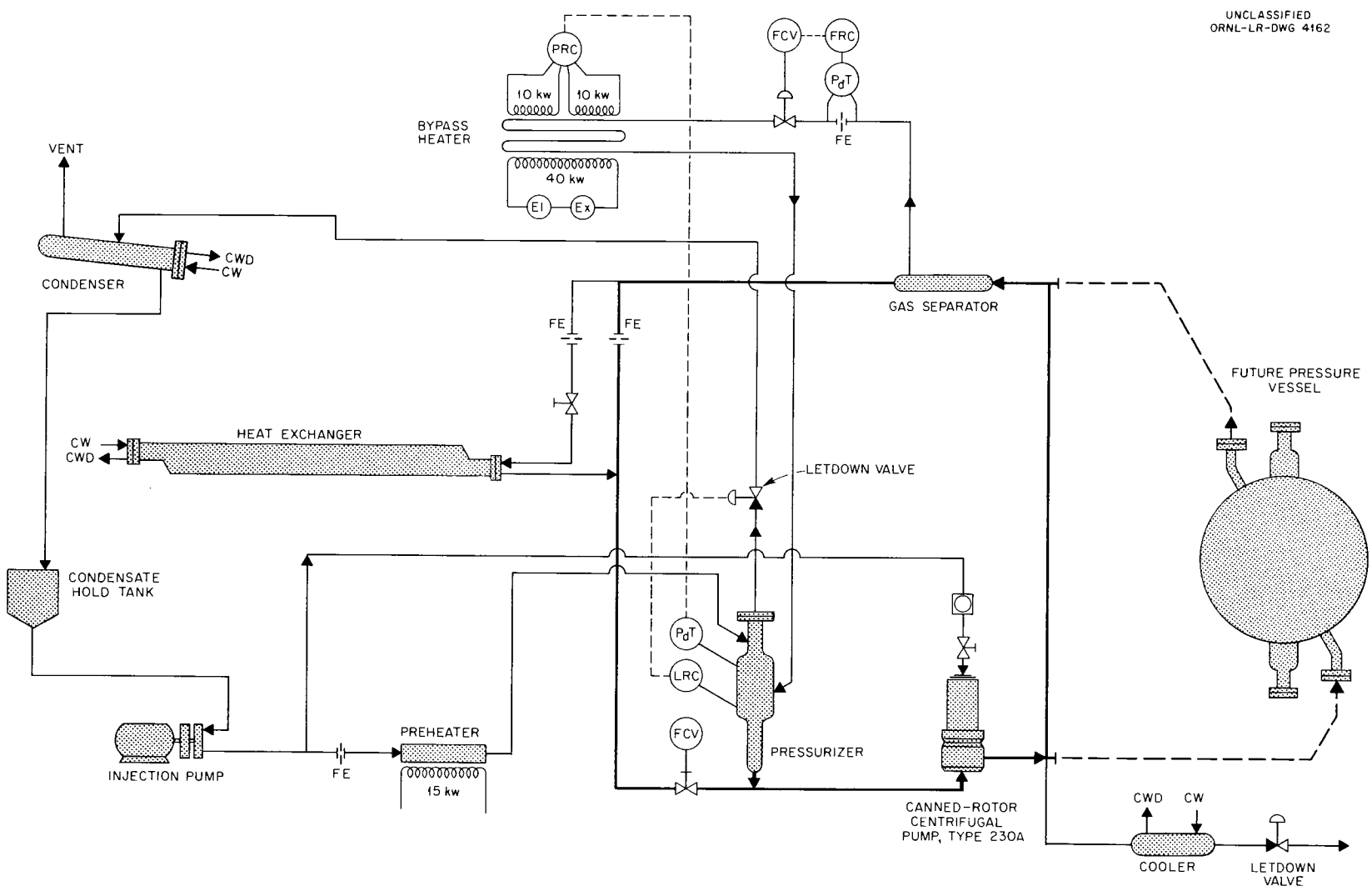

Fig. 7.1. Flow Sheet – HRT Blanket Mockup.

the accumulation in the pressurizer is still unknown. The oxide used in S-51 was prepared from the formate and contained 15 mg of sulfate per gram of solids as the major impurity.

In the previous report,[1] the resistance of type 347 stainless steel to thorium oxide slurry attack at 250°C was stated to have been greatly improved by oxygenation during the run, attack being reduced by a factor of 4. The rate of increase of the Fe:Th ratio, a measure of the rate of attack, was reduced from 1.95 mg/g for the first 100 hr for an unoxygenated slurry (S-45) to 0.5 mg/g for a slurry containing oxygen (S-49).

Table 7.1 is a summary of the runs which were made to determine the corrosion-erosion resistance of type 347 stainless steel to slurries of various thorium oxide preparations containing oxygen. The oxygen, metered into the cold pressurizer at the beginning of the run and whenever the run was interrupted, was distributed throughout the system by the water used to flush the Graphitar bearings. This water, obtained by condensing steam from the pressurizer, was injected into the motor end of the pump. Very little oxygen, if any, entered the circulating stream by diffusion down through the pressurizer, because of the net upward flow of water below the surface.

Prior to each run the systems were pretreated by circulating water containing 500 ppm of oxygen at 250°C for 15 to 90 hr. After this pretreatment, the stainless steel was covered with a golden-brown film, whereas a thin yellow film appeared on the titanium parts.

In run S-51, oxide prepared by calcining the formate at 650°C was used to prepare the slurry. Oxide calcined from the oxalate at 900°C (Lindsay Chemical Co.) was used in runs S-52, T-43, and T-45. The ORNL Chemical Technology Division supplied the oxide used in run S-53; this material was prepared from the oxalate initially calcined at 375°C for 4 hr and then calcined again at 650°C for 8 hr. In run T-46 the oxide was obtained from Lindsay and was prepared by calcining the oxalate at 650°C in one step. The oxides used in runs S-53 and T-46 were obtained by precipitating the oxalate according to the procedure recommended by McBride[3] and then calcined as noted.

Both runs S-51 and S-52 were loaded to give a thorium concentration of 1000 g per kilogram of water at room temperature. After 22 hr of circulation at 250°C, the thorium concentration in run S-51 decreased by 20% and continued to drop during the entire course of the run to an average concentration of 550 g/kg. The concentration of thorium in run S-52 remained essentially constant during the entire run (see Note below).

Inspection of the system at the termination of run S-51 revealed that the solids had accumulated and formed a soft cake in the pressurizer. Previous to run S-51, slurries of various thorium oxide preparations have been circulated at 250°C under a variety of environmental conditions for an accumulated time of over 7000 hr without large accumulations forming in the pressurizer, although some fluctuations in the concentration have usually been observed.

Note: At 250°C, almost one-half the fluid in the loop is held in a relatively stagnant condition in the pressurizer. Although baffles are provided in the pressurizer to prevent a vertical vortex from forming, gamma-radiation measurements along the outside of the pressurizer indicate varying accumulations of solids in this stagnant region, due, presumably, to varying degrees of swirling and eddying into the upper part of the pressurizer. It is believed that this accounts for the fluctuations in concentration as indicated by samples withdrawn during the runs. The initial adjustment of solid distribution is believed to account for the large concentration change which takes place in many of the runs; for example, see run S-52, which changed from 1790 g/kg at 1 hr to 1045 g/kg at 18 hr and then remained essentially constant. The loading for this run was intended to give a concentration of 1000 g/kg in the circulating slurry.

Reference to Table 7.1 reveals the following differences between these two runs:

1. The sulfate content of the slurry was considerably higher in run S-51 (12,000 ppm as loaded) than in run S-52 (approximately 200 ppm).
2. The room-temperature pH of the slurry dropped from 7.4 to 4.4 in 187 hr in run S-51, whereas the pH remained essentially at 9.0 in run S-52.
3. The Fe:Th ratio in milligrams per gram, a qualitative measure of the rate of attack of the stainless steel by the slurry, increased much more rapidly in run S-52 than in S-51 (5.20 mg/g in 189 hr, as compared with 0.37 mg/g for run S-51).

It has not been established whether these differences caused the caking observed in run S-51. Of the three differences, the high sulfate content of

[3] D. E. Ferguson, *et al.*, *HRP Quar. Prog. Rep. Jan. 31, 1954*, ORNL-1678, p 85.

TABLE 7.1. CIRCULATION OF THORIUM OXIDE SLURRIES AT 250°C WITH WESTINGHOUSE 100A PUMP; COMPARISON OF OXIDES PREPARED BY DIFFERENT METHODS WITH OXYGEN ADDITIONS

Sample No.[a]	Circulation Time (hr)	Solids[b]									Filtrate			Gas Analysis			
		Th (g/kg)	Fe (ppm)	Ni (ppm)	Cr (ppm)	Ti (ppm)	SO_4 (ppm)	pH	Fe (mg)/Th (g)	Cr (mg)/Th (g)	pH	Ni (ppm)	SO_4 (ppm)	Volume of Gas (ml)	O_2 (ppm of slurry)	CO_2 (ppm of slurry)	H_2 (ppm of slurry)
S-51-0	2	1150	60	<5	25	<20	12,200	7.1	0.04	0.01	6.4	<1	5	23.5	176		0
1	22	942	97	<5	17	39	8720	5.4	0.10	0.018	5.7	1	500				
2	97	720	182	<5	49	53	7980	4.8	0.25	0.068	4.9	7					
3	116	700	171	13	58			4.7	0.24	0.083	4.8	4					
4	117[c]	800	159	23	36			4.8	0.20	0.045	4.9	4					
5	139	632	165	24	45	38	6720	4.6	0.26	0.071	4.7	5					
6	187	627	232	31	41	<20	7000	4.4	0.37	0.065	4.4	7					
7	256	564	267	30	55	<20	5720	4.2	0.47	0.097	4.2	6					
8	304	534	307	26	57	<20	4300	3.8	0.57	0.10	3.9	8	30				
9	328	552	327	31	59	<20	5120	3.7	0.59	0.11	3.8	7	75				
S-52-0	1	1790	161	40	70		100	9.6	0.09	0.04	9.2	<1	10				
1	18	1045	678	110	204		100	8.6	0.65	0.20	7.9	<1	8	19.9	173		0
2	42	1045	1200	134	330	145	100	8.7	1.15	0.31	8.6	<1	13				
3	65	1000	1535	117	293	145	100		1.54	0.29	7.6	<1					
4	139	1000	3900	534	485	<20	244	8.7	3.90	0.49	8.4	<1	10				
5	189	1295	6700	956	1810	<20	285	9.0	5.20	1.40	8.5	<1	15				
S-53-0	1	400	29	44	7	<20	3700	8.2	0.07	0.02	8.1	<1	44	29.2	340		0
1	69	582	141	107	59	<20	5300	6.7	0.24	0.10	7.2	4	75				
2	116	560	169	83	80	<20	4600	6.2	0.30	0.14	6.5	9	100				
3	165	571	211	113	73	<20	5300	5.9	0.37	0.13	6.3	11	96	51.4	450		0
4	237	580	258	131	84	64	5100	5.3	0.45	0.15	5.6	14	98				
5	307	525	219	149	29	69	5000	5.0	0.42	0.06	5.1	16	74	49.9	340		
T-42-0	1	237	205	36	47	20	3530	1.95	0.96	0.20	1.95	25	1100	44	520		0
1	18	237	1330	180	342	20		2.25	5.6	1.45	2.25	118					
T-43-0	1	243	29	10	262	20		5.1	0.12	1.08	6.0	1		44	520		0
1	18	236	146	5	305	28		5.4	0.62	1.29	5.7	2					
2	42	255	285	39	390	39		5.8	1.12	1.53	5.8	13					
3	67	218	315	39	360	49		5.5	1.44	1.65	5.6	1					

TABLE 7.1. (continued)

Sample No.[a]	Circulation Time (hr)	Solids[b]									Filtrate			Gas Analysis			
		Th (g/kg)	Fe (ppm)	Ni (ppm)	Cr (ppm)	Ti (ppm)	SO_4 (ppm)	pH	Fe (mg)/Th (g)	Cr (mg)/Th (g)	pH	Ni (ppm)	SO_4 (ppm)	Volume of Gas (ml)	O_2 (ppm of slurry)	CO_2 (ppm of slurry)	H_2 (ppm of slurry)
T-43-4	138	207	454	68	297	20		6.7	2.19	1.92	6.5	1					
5	141	243	550	90	377	20		5.5	2.26	1.96	5.7	1					
6	158	236	591	91	390	20		5.2	2.50	2.07	5.3	1					
T-45-0	1	260	36	<5	420	<20		6.5	0.14	1.6	6.5	<1					
1	90	300	540	36	580	<20	<100	5.1	1.80	1.9	5.8	<1	16				
2	114	312	673	107	482			5.1	2.16	1.5	5.6	<1					
3	115	293	642	119	462	26	<100	5.9	2.19	1.6	6.0	<1	25	80	980		0
4	133	298	704	123	610	<20	<100	5.7	2.36	2.1	6.1	1	19				
5	157	270	720	123	556	<20	289	5.6	2.66	2.1	5.8	<1	25				
6	182	228	678	105	394	<20	475	5.2	2.97	1.7	5.6	<1	33				
7	279	283	1090	68	560	<20	232	4.9	3.85	2.0	5.2	<1	23				
8	326	275	1215	99	562	37	588	5.0	4.40	2.1	5.3	2	25				
9	413	214	1310	202	532	<20	100	4.7	6.10	2.5	5.0	5	41				
10	485	237	1770	269	260	71	237	4.7	7.50	1.1	5.0	1	42				
11	581	245	2510	346	288	141	181	4.7	10.2	1.2	4.9	8	10				
12	633	214	2500	360	280	125	100	4.3	11.7	1.3	4.6	11	<10	58	720		0
T-46-0	1	326	44	9	61	<20	290	9.5	0.14	0.19	10.4	<1	<10				
1	19	300	384	77	255	<20	252	9.2	1.28	0.83	7.8	<1	<10	54	605		0
2	43	307	670	115	292	<20	267	8.7	2.18	0.95	8.4	<1	<10				
3	91	282	879	155	299	<20	185	8.8	3.11	1.06	8.2	<1	<10	69	318		0
4	140[d]	228	890	155	270	<20	125	9.2	3.90	1.18	8.5	<1	<10				

[a]Run S-51 – oxide prepared from formate calcined at 650°C;
Run S-52 – oxide prepared by Lindsay Chemical Co. from oxalate calcined at 900°C;
Run S-53 – oxide prepared by ORNL Chemical Technology Division from oxalate calcined at 375°C and then at 650°C;
Run T-42 – oxide prepared by Lindsay Chemical Co. from oxalate calcined at 900°C; 20 ml of concentrated H_2SO_4 added;
Run T-43 – oxide prepared by Lindsay Chemical Co. from oxalate calcined at 900°C; 2 ml of concentrated H_2SO_4 and 6 g of CrO_3 added;
Run T-45 – oxide prepared by Lindsay Chemical Co. from oxalate calcined at 900°C; 9 g of CrO_3 added;
Run T-46 – oxide prepared by Lindsay Chemical Co. from oxalate calcined at 650°C.

[b]Based on total slurry.

[c]Checked for leak; none found.

[d]Sampled cold after loop was shut down because of leak; sample may not be representative.

the slurry in run S-51 could possibly be one of the contributing factors for caking, since thorium sulfate does form a hydrate, $Th(SO_4)_2 \cdot 9H_2O$, which is stable at temperatures up to 400°C. Additional runs are planned to investigate the effect of thorium sulfate on the pumping characteristics of oxide slurries.

A type 347 stainless steel rod $\frac{3}{8}$ in. in diameter was suspended axially by means of two spiders through the throat of a venturi tube in order to measure velocity effects in both runs. In run S-51 a golden-brown film was formed on the rod in the low-velocity regions and a much thinner, yellowish film was apparent in the high-velocity (approximately 45 fps) region. There was a net loss of 39 mg in the weight of the rod. Correspondingly, the rod lost 243 mg in weight in run S-52, and it was covered with a black oxide film in the low-velocity region. In the high-velocity region the rod was pitted, and no film was evident by visual observation.

To study the oxygen effect as a function of the pH of a slurry, concentrated sulfuric acid (run T-42), sulfuric and chromic acid (run T-43), and chromic acid (run T-45) were added to the slurries to adjust the pH of the slurries prepared from Lindsay oxide from 9 to 6. The slurries were prepared at room temperature by adding the amount of acid determined by laboratory titrations to fresh slurries to lower the pH from 9 to 6 at room temperature. In run T-42, the pH of the slurry dropped from 9 to 2 when the slurry was circulated at 250°C; this caused severe corrosive attack on the stainless steel (Table 7.1). The run was stopped after 18 hr because of this apparent high corrosion rate. In run T-43, a slurry containing 240 g of thorium (as Lindsay oxide) per kilogram of water, 500 ppm of oxygen, 6 g of CrO_3, and 2 ml of concentrated H_2SO_4 was circulated at 200°C for 158 hr. The run was stopped because the sample valve failed to close after a sample was drawn and slurry was discharged to the atmosphere. Run T-45 duplicated T-43 except that an additional 3 g of CrO_3 was added instead of the 2 ml of H_2SO_4. The results of these two runs are shown in Table 7.1. For the first 158 hr the iron buildup in the solids, a measure of the attack rate, was essentially the same in both runs, T-43 and T-45. The Fe:Th ratio increased from 0.0 to 2.6. However, when run T-45 was continued for an additional 475 hr, the Fe:Th ratio continued to increase and gave no indication of leveling off as found in previous runs.[1] Inspection of the components after shutdown of run T-45 revealed that the areas most severely attacked by the slurry were the pump and flow restrictor. The impeller lost 17 g in weight, and the flow restrictor lost 0.7 g. The stainless steel thrust pads on the thermal spacers were also badly attacked, especially the one near the discharge of the pump, a region of high turbulence. The pipe walls, however, were covered with a golden-brown oxide film. Although the impeller lost weight, it was not pitted and it was covered with a yellow-brown film which could not be removed by light hand scraping. A black oxide film had also been deposited on the face of the front impeller. The film was easily removed for chemical analysis, and it was found to contain 58% Th, 1.2% Fe, 4.3% Ni, 27.4% Cr, and 0.3% Mn.

Because of the severe attack on the thermal-spacer weld pads, it is difficult to interpret the chemical results for run T-45 and to ascertain whether or not the oxygen effect is a function of the pH of the slurry. As soon as the stainless steel weld pads are replaced with titanium to minimize the attack at these points, the run will be repeated.

As indicated above, runs S-53 and T-46 were carried out in order to compare oxides prepared by two different suppliers using essentially the same method. The circulating systems were, however, different; in loop S the pump impeller, flow restrictor, and the rod through the throat of the venturi tube were all of titanium, whereas in loop T these parts were of stainless steel. Also the loadings in the two loops were slightly different because of the limitations imposed by the difference in pump impellers. The analytical data for the two runs are presented in Table 7.1. Inspection of the data reveals several interesting features:

1. The sulfate concentration in run S-53 was higher than in run T-46, probably because of differences in the thorium nitrate starting material from which the oxalate was initially precipitated.

2. The pH values in run S-53 were initially lower than in run T-46 and during the run continued to decline toward a value of 5.0, whereas the pH values in run T-46 remained above 8.5.

3. The sampled concentrations of slurry in run S-53 were substantially higher than the concentration initially loaded; coincidentally, gamma-radiation examination of the pressurizer revealed

the presence of a region of low density (water) above a region of higher density (slurry). No concentration increase or region of low density in the pressurizer was found in run T-46. A 94% recovery of solids after run S-53 eliminated the possibility of an error in loading the system.

4. The attack in run T-46 was much more severe than in run S-53 (as measured by the increase in iron and chromium contents of the solids). However, the nickel contents of the solids were not significantly different, and the nickel content of the filtrates from run S-53 was higher than that from run T-46.

Interpretation of the data is, at this point, still tentative, pending examination of the results of additional runs which are in progress. However, the presence of the high sulfate concentration in the run S-53 slurry may account for most of the observed phenomena. Thorium sulfate, upon hydrolysis in water at elevated temperatures, produces thorium oxide and sulfuric acid. This acid would reduce the pH of the slurry. Reduction of the pH and the presence of the electrolyte may have been responsible for the change in slurry properties in run S-53, permitting settling in the quiet region of the pressurizer to a higher bulk density and thus raising the concentration in the circulating stream. Attack on stainless steel in regions of high velocity and/or turbulence has always been more pronounced by slurries having a high pH, such as the slurry in run T-46. Moreover, loop T, as noted above, contained stainless steel instead of titanium parts in the high-velocity regions. A check run (S-54), now in progress, contains slurry prepared from the same oxide used in run T-46. After the initial behavior of this slurry is established in loop S, thorium sulfate solution will be added to give a sulfate concentration of 2000 ppm and the effect on subsequent behavior will be noted.

7.4 MECHANICAL PROPERTIES OF SLURRIES

D. G. Thomas
J. D. Perret R. Buxton[4]

Because of the large room-temperature yield stresses of settled, pumped, and unpumped slurries,[1] a short-term program has been undertaken to characterize the properties of the pumped slurries with the expectation that this study will give a means of controlling slurry properties.

[4]On loan from Analytical Chemistry Division.

7.4.1 Viscous Properties of Pumped Thoria

The stiff consistency, at room temperature, of many pumped thoria slurries is in marked contrast to the consistency of unpumped thoria suspensions and is obviously undesirable in a circulating system. The apparent viscosity of several pumped slurries has been measured with a Brookfield viscometer.

Apparent viscosity, μ_p, is arbitrarily defined as the reading in centipoises obtained with a Brookfield viscometer at a particular rotational velocity, p. Other fluid viscosities are described in the following manner: For a Newtonian fluid,

$$-\frac{dV_r}{dr} = \frac{g_c \tau_r}{\mu} .$$

For a Bingham plastic,

$$-\frac{dV_r}{dr} = \frac{g_c}{\eta}(\tau_r - \tau_y) , \qquad |\tau| \geqq |\tau_y| ;$$

$$-\frac{dV_r}{dr} = 0 , \qquad |\tau| < |\tau_y| .$$

For an Ostwald–de Waele plastic (usually referred to as a pseudoplastic),

$$-\frac{dV_r}{dr} = \frac{g_c \tau_r^n}{\mu_0} ,$$

where

r = distance from the center of rotation,
V = linear velocity in the circumferential direction,
τ = shear stress,
τ_y = stress required to produce yield,
η = modulus of rigidity,
μ = viscosity,
μ_0 = Ostwald–de Waele coefficient.

The interpretation of Bingham plastic data from a cylindrical viscometer, such as a Brookfield, is rather involved. An analysis shows, however, that if τ_y is large, so that $r_{cup} > (\tau_s r_s/\tau_y)$, the data will approximate the following expression:

$$\tau_s \approx \tau_y + \sqrt{2\eta/g_c} \times \sqrt{\tau_s \omega_s} ,$$

where τ_s is the shear at a spindle of radius r_s, and ω_s is the angular velocity of the spindle. Thus a straight line approximating the dota when plotted as τ_s vs $\sqrt{\tau_s \omega_s}$ will have a slope of about $\sqrt{2\eta/g_c}$ and will intersect the τ_s oxis at approximately τ_y.

Data obtained from a pseudoplastic, when plotted as ω_s vs τ_s on log-log paper, will approximate a straight line of a slope n and intersect $\omega_s = 1$ at $(n-1)(\mu_0/g_c)$.

The Brookfield viscometer has only four possible speeds; hence the measurements were made over a limited range of shear rates. Figure 7.2 gives the stress-strain curves for slurries from run S-49[1] and runs S-51 and S-52 (see Sec. 7.3). It is seen that these slurries are either Bingham plastics or extreme pseudoplastics. The apparent viscosity of these slurries was quite high; for example, the apparent viscosity of run S-49 slurry containing 730 g of thoria per liter was 43,000 centipoises at the lowest spindle speed (6 rpm). However, the coefficient of rigidity, η, is seen from Fig. 7.2 to be essentially zero within the range and accuracy of the measurements, since the apparent viscosity rapidly decreases as the shear rate increases.

[5]V. Kohlschütter and A. Frey, *Z. Elektrochem.* **22**, 145 (1916).

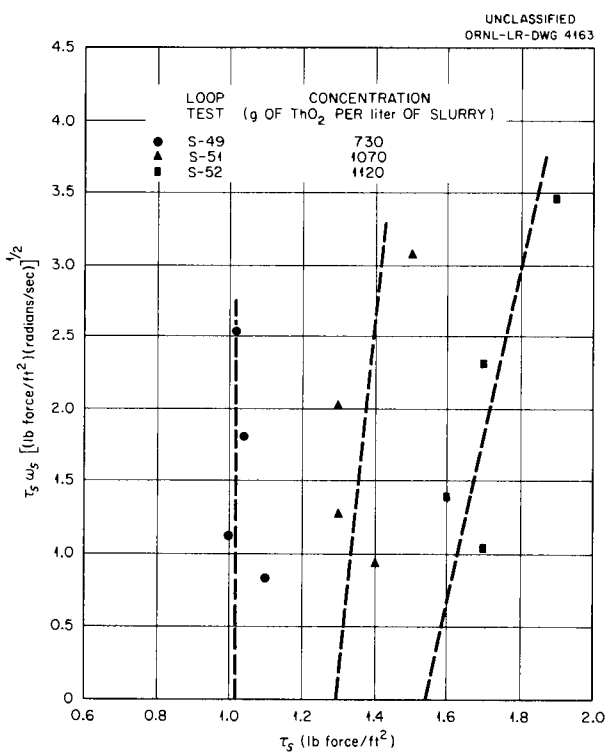

Fig. 7.2. Stress-Strain Diagram for Various Pumped Slurries. τ_s, shear stress at spindle; ω_s, angular velocity of spindle.

7.4.2 Mechanism of Viscosity Increase upon Pumping

Kohlschütter and Frey[5] reported that thoria, prepared by igniting the oxalate, readily formed a colloidal solution in water after treatment with dilute acid. Maximum colloidal solubility was obtained when the oxalate was heated at 500 to 600°C; above 700°C a noncolloidal product was obtained. Peptization was also effected by halogen acids, HNO_3 and H_2SO_4. These results were confirmed by boiling a sample of Lindsay thoria with HNO_3 and then removing the acid by washing with

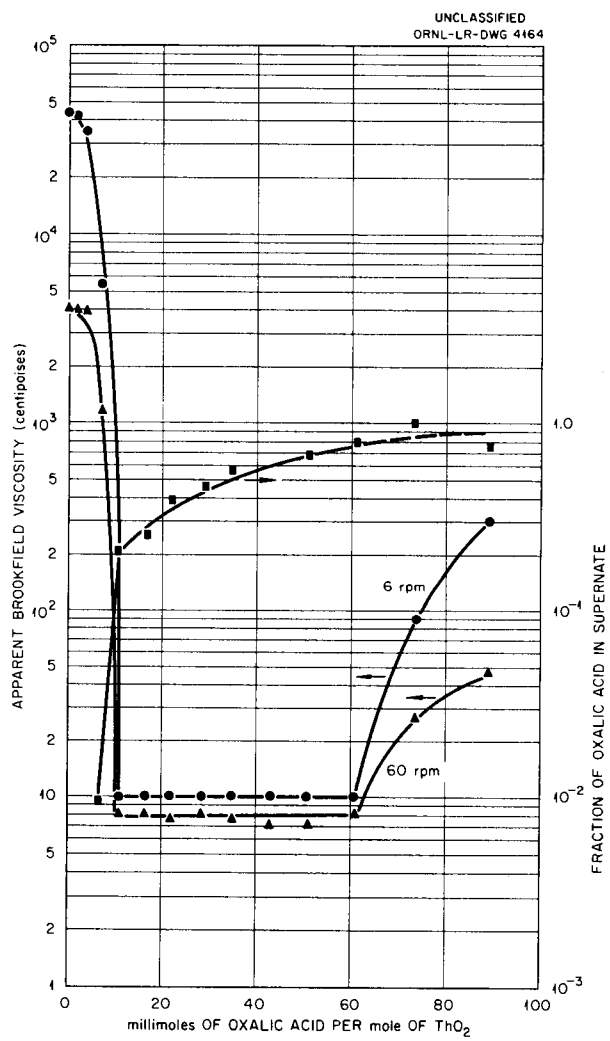

Fig. 7.3. Effect of Oxalic Acid on Apparent Viscosity of ThO_2 Slurries. Run S-49, 730 g of ThO_2 per liter of slurry.

water. The particles peptized at a pH less than 3, which resulted in a stable suspensoid of low viscosity. The pH was increased to above 3 by using additions of ammonium hydroxide, the viscosity increasing by a factor of 10 as the pH was changed from 2 to 11.

It was also found that mechanical agitation of Lindsay thoria in a Waring blender produced a high-viscosity slurry with a settling rate much lower than that of a freshly prepared slurry.

7.4.3 Addition of Dispersing Agents

A number of possible dispersants were screened in order to determine whether there was an appreciable decrease in the viscosity of the pumped slurries.

A rather striking effect was found upon addition of oxalic acid (Fig. 7.3). Upon the addition of approximately 10 mmoles of oxalic acid per mole of thoria, the viscosity immediately dropped to 7 to 10 centipoises and remained at this value over a fivefold concentration range. At higher oxalic acid concentrations the viscosity again increased. As shown in Fig. 7.4, the slopes of the stress-strain curves on a log-log plot were essentially unity in the low-viscosity range, which indicates that the slurry reverted from a non-Newtonian fluid to a Newtonian fluid. The oxalic acid was practically quantitatively adsorbed on the thoria particles (Fig. 7.3) until the low-viscosity range was reached, and then further adsorption was small. Other carboxylic acids were tried in order to test the effect of structure. Malonic acid was equally effective, citric acid was much less effective, and formic acid had practically no effect.

Sodium silicate (water glass) and Calgon (sodium hexametaphosphate), both of which are well-known dispersing and sequestering agents, were found to reduce the viscosity, although not so effectively as oxalic acids. The action of electrolytes such as H_2SO_4, HCl, H_3PO_4, and NaOH were also tested, but no appreciable effect was found. However, McBride (see Sec. 10.4) reports the dialysis of sodium silicate into run S-49 slurry overnight from a 0.13 wt % sodium silicate $[Na_2O(SiO_2)_{3.25}]$ solution. This treatment reduced the viscosity to a few centipoises. The effect of direct addition of sodium silicate $[Na_2O(SiO_2)_{3.25}]$ was then reexamined, and it was observed that hours and, in one case, days were required to reach steady state

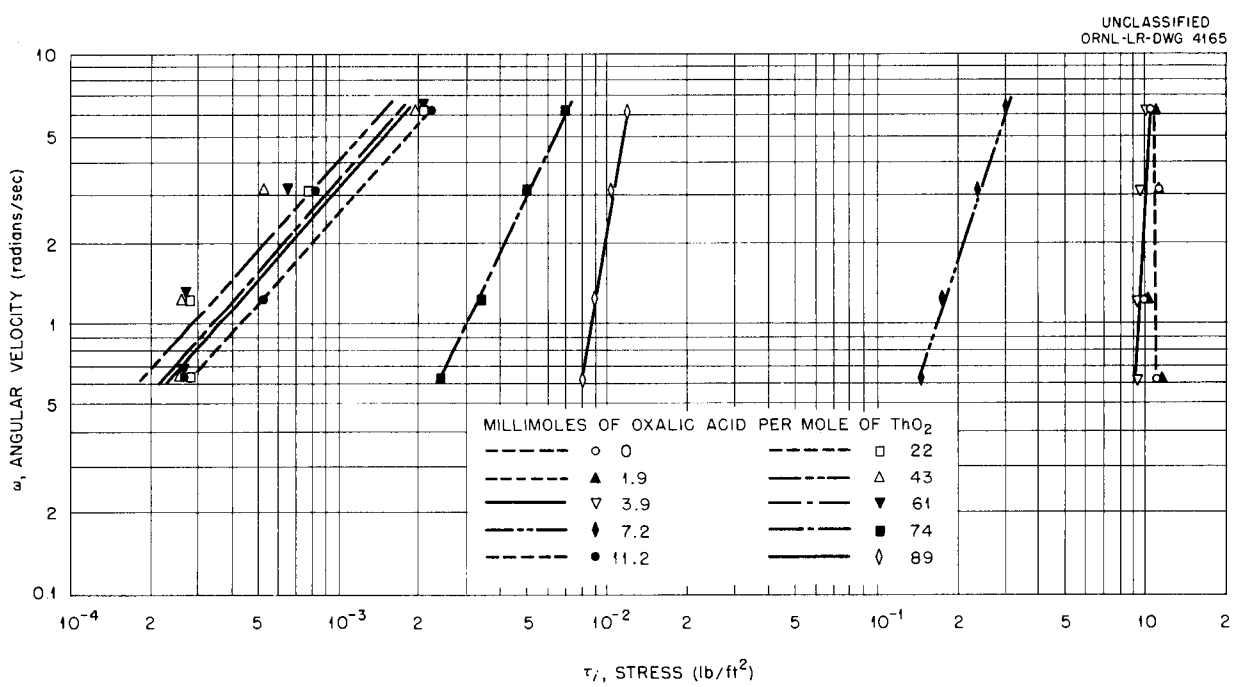

Fig. 7.4. Effect of Oxalic Acid on Stress-Strain Curves of ThO_2 Slurry. Run-49, 730 g of ThO_2 per liter of slurry.

(Fig. 7.5). The relatively slow action of sodium silicate, as compared to oxalic acid, is as yet unexplained. The Calgon curve was redetermined, and similar results were obtained.

Table 7.2 gives typical data obtained with various pumped slurries. It will be observed that an apparent correlation appears between the attack on stainless steel in the loops, as indicated by the iron, nickel, and chromium contents, the amount of sodium silicate (but not the amount of oxalate) required to reduce the viscosity to about 20 centipoises, and the sulfate content of the slurry. This apparent correlation is being investigated further to determine its consistency.

The thermal stability of the electrolyte-treated slurry was tested by heating the treated slurry in a stainless steel bomb at 280°C, cooling, and then checking the viscosity. At the end of 90 hr the bombs were opened for the first time, and it was found that the Calgon-treated slurry had precipitated, whereas the sodium silicate–treated material was easily resuspended and was still quite fluid. The silicate-treated slurry was recharged to the bomb and remained there for 380 hr, when the test was discontinued. There was no change in the slurry property during the test period. Further tests in which the pH of the silicate-treated slurry was lowered below 5 with HCl, H_3PO_4, and Cr_2O_3 have shown that both HCl- and Cr_2O_3-treated slurries are thermally stable, whereas the H_3PO_4-treated slurry was precipitated. Tests are continuing on the effects of electrolytes in an attempt to understand the mechanism, as well as to provide information that may be useful with a high-temperature system.

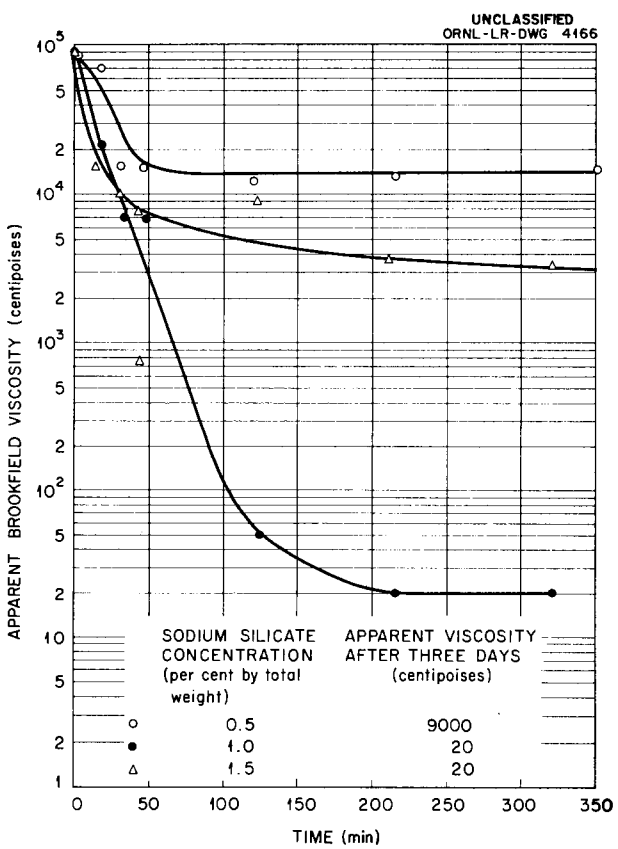

Fig. 7.5. Effect of Time and Sodium Silicate Concentration on Apparent Viscosity (6 rpm) of ThO_2 Slurry. Run S-49, 730 g of ThO_2 per liter of slurry.

7.4.4 Effect of Calcining Temperature

Another approach to the problem of preventing a viscosity increase is to reduce the hydration rate by reducing the surface area and/or the concentration of active centers. This can be accomplished by a high-temperature calcining operation. Kilogram quantities of Lindsay thoria are being calcined by the Ceramics Laboratory at 900, 1200, and 1500°C. Slurries of these materials will be charged to the small loops and tested for abrasiveness and viscosity buildup.

7.5 BOILING STUDIES

P. C. Zmola
R. V. Bailey[6] H. A. MacColl
M. Richardson

7.5.1 Vapor Transport in the Mixture

A method of calculating vapor transport and presenting experimental data has been developed in which the liquid and vapor velocities, and hence the relative or vapor slip velocities, enter explicitly. While, at present, the manner in which the physical properties of the liquid and vapor enter the calculations is somewhat unclear, it has been possible to show that the slip velocity in a circulating (dynamic) system can be predicted from information obtained from natural-vapor-rise (static) systems.

It is experimentally observed that in static systems the vapor velocity, U, based on the entire cross-sectional area of the test region can be

[6]Consultant, Tulane University.

represented by

$$(1) \qquad U = U_s \frac{f}{1 - f} ,$$

where U_s is a constant and f is the fraction vapor in the region of interest. On the premise that the velocity of the vapor relative to the liquid, u_r, should be the same in static and dynamic systems, the expression for the slip velocity is

$$(2) \qquad u_r = \frac{U}{f} - \frac{U_0}{1 - f} = \frac{U_s}{1 - f} ,$$

where U_0 is the liquid velocity based on the total cross-sectional area of the test section. Accordingly, for a dynamic system the vapor velocity is given by

$$(3) \qquad U = (U_s + U_0) \frac{f}{1 - f}$$

$$= (U_s + U_0) \frac{x}{1 - x} \times \frac{\rho_f}{\rho_g} ,$$

where ρ_f and ρ_g are liquid and vapor densities, respectively, and x is the steam quality. Representative experimental data shown in Fig. 7.6, obtained by Bailey at Tulane University from an air-water system 2 in. in diameter and 10 ft high, indicate that the postulation of slip velocity being independent of the circulation velocity is valid. This is at variance with results obtained previously.[7] Results of volume boiling experiments are in agreement with Eq. 3 modified to account for a distributed vapor generation.

[7] E. Schmidt, P. Behringer, and W. Schurig, *Forsch. Gebiete Ingenieurw.* 5, 104 (1934).

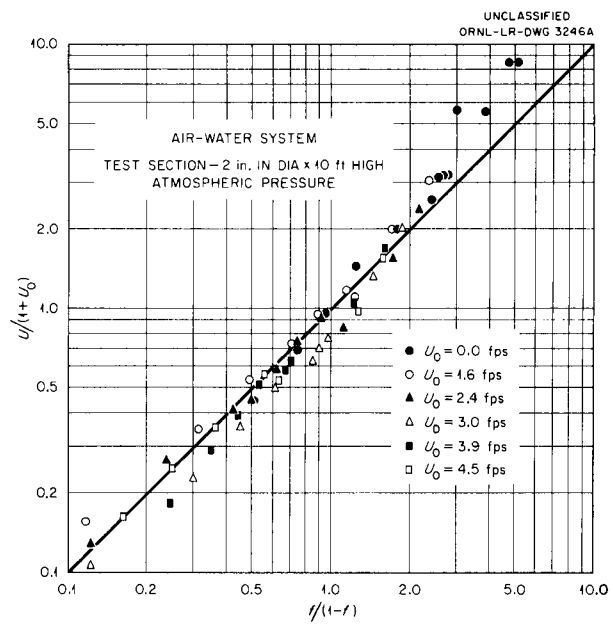

Fig. 7.6. Comparison of Experimental Results with Eq. 3. Data obtained by Bailey at Tulane University.

TABLE 7.2. TYPICAL DATA OBTAINED WITH VARIOUS PUMPED SLURRIES

Run No.	Origin of Material	Calcining Temperature (°C)	Room-Temperature Slurry Properties: Chemical Analysis (mg per gram of slurry)						Electrolyte Required to Lower Viscosity to Approximately 20 centipoises	
			Fe	Ni	Cr	SO_4^{--}	Concentration $\left(\frac{\text{grams of } ThO_2}{\text{liter of slurry}}\right)$	Initial Viscosity* (centipoises)	Oxalic Acid $\left(\frac{\text{millimoles}}{\text{mole of } ThO_2}\right)$	Sodium Silicate (wt %), Based on Slurry Weight
S-49	Formate	650	0.55	0.063	0.090	1.65	730	43,000	10	1.0
S-51	Formate	650	0.219	0.027	0.032	4.33	1070	64,000	17	1.5
S-52	Lindsay	900	1.92	0.282	0.548	0.29	1120	54,000	10**	<0.1
T-45	Lindsay	900	7.70	0.84	1.13	<0.39	1670	30,000	8	<0.1
T-46	Lindsay	650	2.20	0.62	0.35	0.28	980	30,000	34	<0.1

*Viscosity measured at 6 rpm on Brookfield viscometer.

**Viscosity was lowered to approximately 1000 centipoises and then was changed very little when an additional 90 millimoles/mole was added.

One manner of including the influence of pressure and physical properties in the foregoing analysis is to express U_s in Eq. 1 as

$$U_s = \frac{C}{\kappa_f \sqrt{\rho_g}} , \tag{4}$$

where κ_f is the kinematic viscosity of the liquid and C is a constant. This equation is in agreement with data[6] for steam-water mixtures at pressures from 1 to 40 atm as well as with atmospheric-pressure, static, air-water data from Tulane. However, static-system results from Tulane in which air was bubbled through methanol and glycerin as well as water indicate that the gas velocity is independent of the viscosity of the liquid. Work at Tulane is continuing on determining the influence of these and other physical properties.

Experimental work has been continued at the Laboratory with the 6 × 6 in. natural-circulation apparatus. The vapor chest has been increased from 5 ft^3 to about 10 ft^3 to prevent splashing into the reflux condenser. Density distribution and circulation flow-rate measurements were obtained for the following three arrangements of the apparatus:

1. test section open and unrestricted outlet to the vapor chest,
2. test section open and corrugated-plate vapor separator of 0.75 ft^2 projected area at outlet,
3. masonite spacers in test section to give six parallel channels approximately 1 × 6 in. in cross section and unrestricted outlet to the vapor chest.

These data have not been completely analyzed; however, it appears that the effect of diameter is considerably weaker than the interpretation of past experiments had indicated and that power-removal capability is almost independent of the system diameter.

The behavior of a boiling ThO_2 slurry has been studied in a small natural-circulation apparatus preparatory to loading slurry into the larger circulating systems to determine the vapor-transport properties of the mixture. In order to obtain quantitative information on vapor transport, it is necessary to devise a method of measuring the density of a boiling mixture in which the liquid component contains a gamma emitter. At present, instrumentation is being assembled to measure the attenuation of gamma rays from a monoenergetic source at the source energy. Other techniques are possible and will be explored if necessary. As might be expected, the boiling slurry behaves, qualitatively, very much like a boiling liquid, with the exception of settling in low-velocity regions.

7.5.2 Vapor Separation

Essentially all the work on vapor separation is being conducted by The Babcock and Wilcox Co. under subcontract. Two types of separators have been investigated. Corrugated-plate-type separators were found to permit considerable entrainment of vapor in the downcomer liquid at steam rates per unit surface considerably below those of interest in boiling-reactor applications, although pressure drop through these units was quite low. Because of the entrainment limitation, further work on this type of separator was discontinued. The greatest effort, as in the past, has been devoted to modification of existing types of centrifugal separators to obtain high flow rates of relatively low vapor-fraction mixtures with the attendant pressure drop through the unit as low as possible. Also being studied is the pressure drop in the manifolding necessary for application to a boiling reactor. Experimental work is being conducted with both an air-water apparatus at atmospheric pressure and a steam-water apparatus at pressures from 25 to 100 psia.

7.5.3 Density Transients Due to a Power Pulse

Studies of the density change of a boiling liquid with time, under conditions of a power pulse, carried on by the University of California at Los Angeles under subcontract, were concluded during this quarter. The growth rate of a single bubble in a superheated liquid was calculated.[8] By utilizing this relation the density-time behavior of an ensemble of bubbles subject to a uniform power pulse was computed by taking into consideration both the growth of existing bubbles and the formation of new bubbles. The calculations compared favorably with experimental results.[9] Utilization of the expression for the

[8] H. K. Forster and N. Zuber, *J. Appl. Phys.* 25, 474 (1954).

[9] R. P. Lipkis and N. Zuber, *Measurement and Prediction of Density Transients in a Volume Heated Boiling System*, paper presented at Reactor Heat Transfer Information Meeting, Brookhaven National Laboratory, October 18–19, 1954.

density change requires a rather detailed knowledge of the state of the system and so, in a sense, is the obverse of highly integrated boiling-reactor experiments such as the ANL Borax or ORNL Water Boiler tests. To the extent to which comparison is possible, the results of all these experiments are at least in qualitative agreement. A final report on the work has been prepared.[10]

[10] M. L. Greenfield, R. P. Lipkis, N. Zuber, and C. Lui, *Studies on Density Transients in Volume Heated Boiling Systems*, Report 54-77, Department of Engineering, University of California at Los Angeles, October 1954.

8. EXPERIMENTAL VALVE PROGRAM

J. N. Baird, Jr.[1]
A. M. Billings R. L. Cauble
R. D. Cheverton T. H. Mauney

Three of the 2000-psi sealing bellows ordered for the ½-in. experimental valves[2] have been received. Two other bellows have been shipped to valve manufacturers for incorporation into experimental valves. The two makes of welded-diaphragm, type 347 stainless steel bellows are shown in Fig. 8.1.

The smaller bellows was made by Breeze Corporations, Inc., Newark, New Jersey. It contains 96 convolutions, each of which consists of a convex diaphragm 0.031 in. thick and a concave diaphragm 0.025 in. thick. The bellows, exclusive of end pieces, has a free length of 8.8 in. and an approximate spring rate of 425 lb per inch of deflection. According to the manufacturer, this bellows has withstood external pressurizing of 3600 psi without deformation and 3750 psi with only slight deformation. The manufacturer believes that, by forming the diaphragms under higher hydraulic pressures, the bellows can be made to

[1] Instrumentation and Controls Division.

[2] J. N. Baird, Jr. *et al.*, *HRP Quar. Prog. Rep. July 31, 1954*, ORNL-1772, p 45.

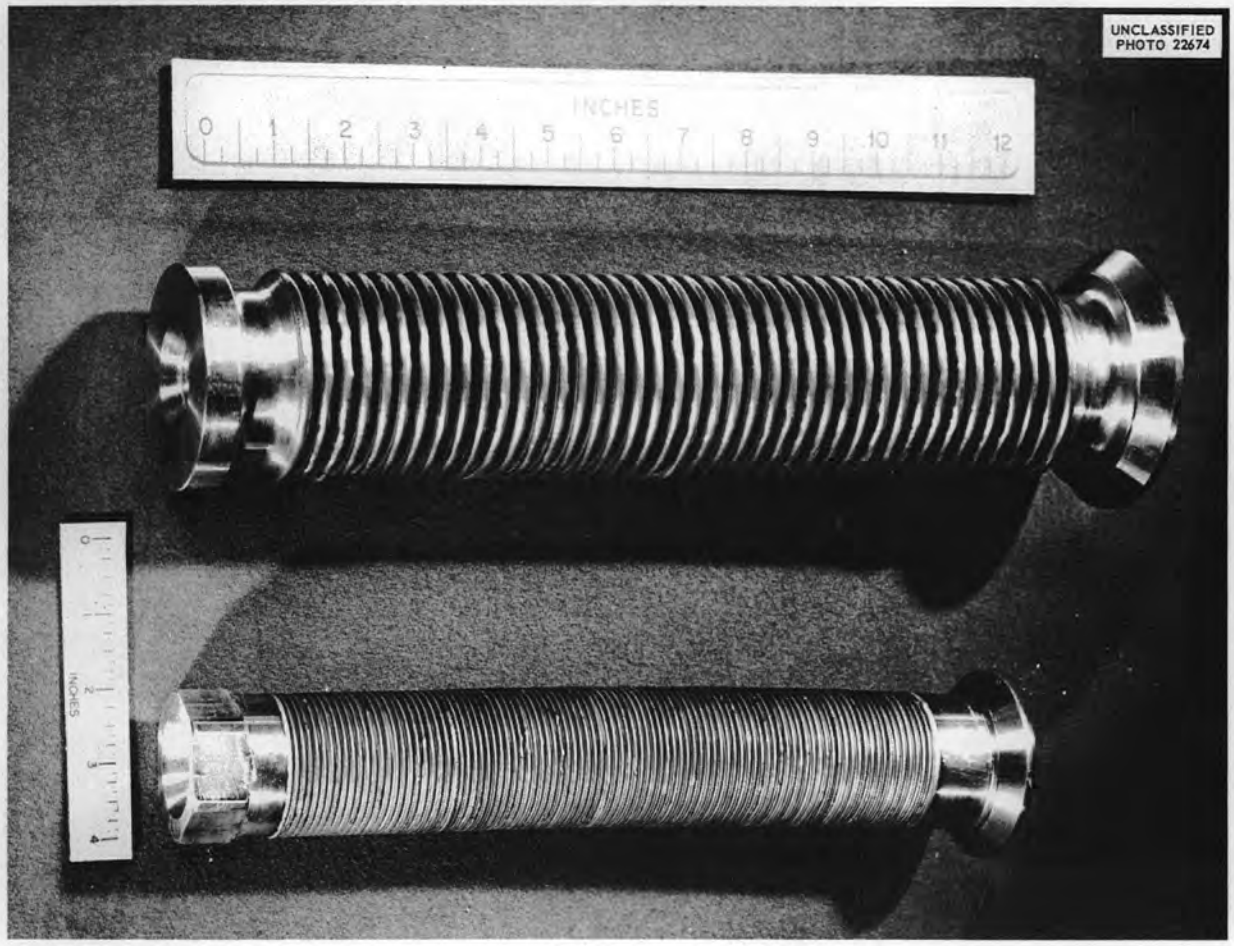

Fig. 8.1. Welded-Diaphragm, Type 347 Stainless Steel, 2000-psi Bellows.

withstand 3750 psi satisfactorily. The bellows then could withstand the full proof pressure of the all-welded HRT piping system.

The larger bellows in Fig. 8.1 is made by Flexall Division, Process Engineering, Inc., Somerville, Massachusetts (formerly Badger Fire Extinguisher Co.). It has 39 active convolutions, each one consisting of a convex stack of four plies, each ply being 0.015 in. thick, edge-welded to a concave stack of three plies, also 0.015 in. thick. Despite the rather cumbersome size of the Flexall bellows, it is designed to take a $\frac{3}{4}$-in. valve stem (as is the Breeze bellows). Unfortunately, this Flexall bellows has not withstood static tests. Figure 8.2 shows untested and tested Badger bellows. The right-hand bellows distorted nonuniformly when externally pressurized by the manufacturer at 2000 psi with the bellows under $\frac{1}{2}$-in. compression. A second bellows was similarly distorted when pressurized at only 1000 psi. The manufacturer admits that this design is faulty and, at his expense, is constructing another bellows, substituting a single diaphragm 0.062 in. thick for the four-ply members now used.

A $\frac{1}{2}$-in. valve body constructed in the ORNL shops and designed to utilize the Breeze bellows is shown in Fig. 8.3. An adapter plate which fastens to the high-tensile tie bolts will support a very large pneumatic operator.

The valve is very heavily constructed because of the basic idea behind the design, namely, that if wire drawing or other damage should occur to the valve seat, the valve stem can be driven with sufficient force to deform the seat plastically and reshape it, thus presumably restoring it to a leaktight condition. The pneumatic pressure to

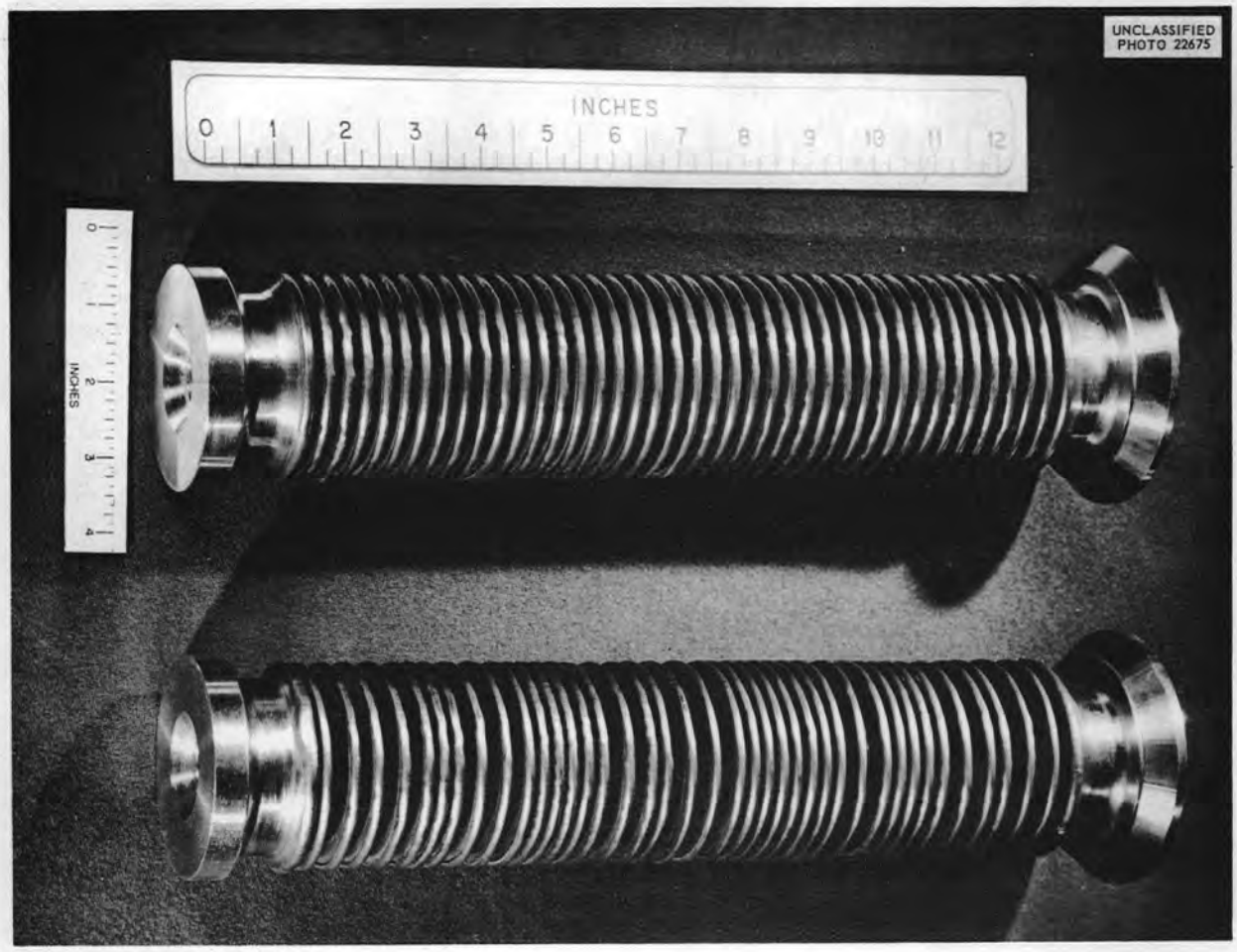

Fig. 8.2. Badger Bellows, Before and After Pressurization.

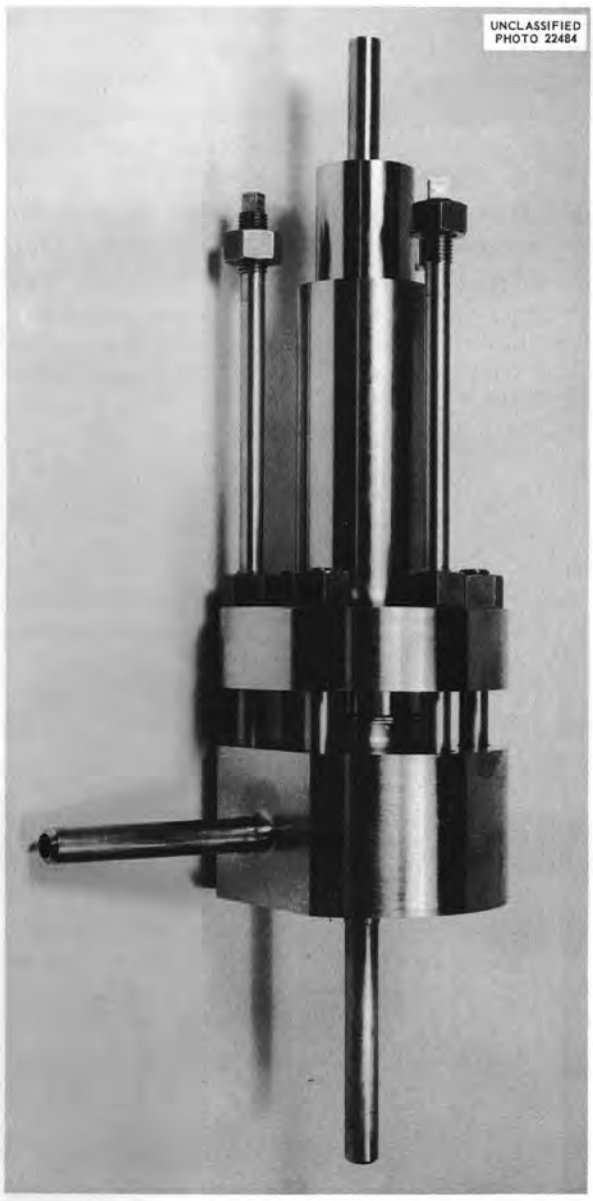

Fig. 8.3. ORNL-Constructed ½-in., 2000-psi Valve.

the actuator would be reduced thereafter so that valve operation would continue with closing forces smaller than those required for reshaping of the seat.

Four sets of replaceable trim have been made in the ORNL shops for this experimental valve. In one set, a 60-deg plug faced with Stellite works against a type 347 stainless steel, 62½-deg seat in an arrangement which would produce something approaching a line-mating surface. In a second set, both the seat and the Stellite-faced plug have the same face angles and thus produce a finite area of contact. A third set employs a gasketing effect, produced by a gold ring (in a groove cut in the plug) which works against a ridged seat. The fourth set comprises a plug with a flat face which makes normal contact with a raised seat. This flat-plate trim represents a suggested technique.[3]

A Breeze bellows is being assembled into the valve body, and tests will be run on each set of trim for leaktightness before and after cycling, and to check the feasibility of reshaping the seat. Thereafter, cycling tests will be conducted on the bellows itself.

Experimental ½-in. valves incorporating the Breeze bellows are expected to arrive as follows: from Kieley & Mueller, Inc., three weeks; from The Annin Co. and from Associated Valve & Engineering Co., twelve to fifteen weeks. Atwood and Morrill Co. is making a 1-in. version of this valve, plus a spare for possible emergency use as a blanket dump valve.

[3]G. H. Pearson, *The Design of Valves and Fittings*, 1st ed., Chap. 3, Sir Isaac Pitman and Sons, Ltd., London, 1953.

9. METALLURGY

E. C. Miller
W. J. Fretague W. O. Harms
T. W. Fulton W. J. Leonard
J. J. Woodhouse

9.1 WELDING DEVELOPMENT

9.1.1 Welding Development on 1-in. Carbon-Steel Plates Clad with Type 347 Stainless Steel

W. J. Leonard

The pressure vessel in the HRT design is to be a spherical outer container of 4-in. carbon-steel plate, clad with type 347 stainless steel on the interior, with an internal diameter of approximately 5 ft. The design is such that the final girth weld must be made from the outside only, rather than by the more common back-chipping method which allows welding from both sides. Where the welding must be done from the carbon-steel side only, one suggested procedure is to fill the root and groove with stainless steel weld metal to a point above the interface between the carbon steel and stainless steel, followed by an intermediate layer of a few passes of a material such as ingot iron, low-carbon steel, type 308 stainless steel, or type 310 stainless steel, and to complete the weld with low-hydrogen, mineral-coated, carbon-steel electrodes. Another variation of this sequence consists in using a thin strip insert of low-carbon steel, in lieu of laying down welding passes, as the intermediate layer between the stainless steel and carbon-steel weld metal.

To evaluate several variations of these proposed welding sequences, a 1-in.-thick plate of ASTM A201 grade A carbon steel, with a 20% cladding of type 347 stainless steel, was obtained. The root face and groove were prepared by machining test specimens to accommodate the preplaced wire used in the Electric Boat Heliarc welding method.[1] Previous work indicated the desirability of using this method, rather than manual Heliarc welding in conformance with HRP welding specifications, to obtain closer control of root penetration and weld soundness.

Six welds of this type were made in these specimens by using the Heliarc welding method described with type 347 preplaced wire. Amperage was varied from 140 maximum to 90 minimum for different weld-metal passes; travel speed of the electrode was varied from 1 to $4\frac{1}{2}$ in. per minute. These manipulations allowed control of the heat input per pass, thus regulating the resulting penetration and dilution. At each amperage level used, a heat input over a certain critical value resulted in cracking of the root pass. At a 140-amp welding current a minimum welding speed of 4 in. per minute must be maintained to secure a sound root pass. At 90 amp a speed of 1 in. per minute or greater resulted in sound welds. At lower amperages, travel speed is less critical because of greater dissipation of the total heat percentagewise by the base plate. All passes that cracked were ground out and rewelded, so eventually all plates had sound root passes.

These welds were completed up to the carbon-steel and stainless steel interface by filling with coated-electrode type 347 stainless steel. The balance of the weld groove was finished by using the various types of special techniques mentioned earlier. The completed weldments were radiographed. All welds, which were made by using welding rod exclusively to fill the groove, were sound when they were radiographed. The welds which had a plate insert between the stainless steel weld metal and carbon-steel weld metal did not result in a sound joint. All exhibited sufficient porosity to result in rejection, based on the ASME Boiler Code 1952, Section VIII, Weld Porosity Standards.

These plates are being sectioned for various mechanical tests of plate specimens, as well as metallurgical examination for soundness of the weld and microconstituents present in the weld area.

9.2 METALLURGY OF CORROSION

9.2.1 Dynamic Corrosion of Austenitic-Stainless-Steel Weld Specimens

W. O. Harms

Previous tests[2] have indicated that the presence of ferrite may have a deleterious effect on the

[1] T. A. Risch and A. E. Dohna, *Welding J. (NY)* 33, 670 (1954).

[2] W. J. Fretague, *Met. Semiann. Prog. Rep. Oct. 10, 1954*, to be published.

corrosion resistance of austenitic stainless steels in uranyl sulfate solutions. Since the data in this regard have not been entirely consistent, a more systematic approach to the problem was attempted. All-weld-metal specimens ranging in ferrite content from 0 to 12% were tested by the Dynamic Corrosion Group in oxygenated 0.17 *m* uranyl sulfate at 250°C and at velocities of 15 and 30 fps for 200 hr. These specimens were machined from the top half of ½-in. weld pads deposited in type 347–buttered carbon-steel plate by using the argon-shielded tungsten-arc process under the following conditions: 200 to 220 amp, 12 to 16 v, and average travel speed of 4 in. per minute. The samples were prepared by a subcontractor, the Foster Wheeler Corp., at the request of the Engineering Development Section. Specimens of wrought-annealed type 347 stainless steel and Armco type 17-4 PH, a precipitation-hardening type of stainless steel, were included in the test for comparison. The chemical compositions of the weld pads from which specimens were machined are listed in Table 9.1.

The results of runs M-23 and M-24 are shown in Table 9.2. Included in the main line in run M-23 was a chromized tube bundle consisting of seven tubes, ⅜-in. OD and 0.049-in. wall thickness, which underwent severe corrosion attack causing abnormally high concentration of hexavalent chromium ion in the solution. Since this is known to inhibit attack in uranyl sulfate, it was believed that the results of run M-23 required confirmation. Run M-24 was undertaken for this purpose, and it was observed that, although relative behavior was similar in both runs, differences were much more pronounced in the check run. After 200 hr at the lower velocity no significant differences in corrosion resistance were observed. However, at the higher velocity, marked differences were noted. The fact that alloy No. 4, containing only 3.5 to 4.5% ferrite, and the fully austenitic Composition H showed the least corrosion resistance demonstrated that the ferrite content alone is not the controlling factor in 0.17 *m* uranyl sulfate under the conditions of these tests, although the spread in chromium content of the weld samples complicates any comparison. It was interesting to note that the high-carbon type 307 Mn and the wrought-annealed type 17-4 PH stood up as well as wrought-annealed type 347 in these environments.

9.2.2 Stress-Corrosion Cracking of Austenitic Stainless Steels

Two simulated HRT tube-to-tube-sheet assemblies, in which the ⅜-in.-OD, 0.049-in.-wall, type 347 stainless steel tubes had been expanded by a rolling operation, by 0.006 and 0.0015 in., respectively, were tested in boiling magnesium chloride solutions. In addition, as-received tubes were tested for comparison. Cracks were observed after 5 hr in the expanded end of the 0.006-in. rolled specimen, near the surface of the 1-in. tube sheet. After 10 and 15 hr, tubes in this assembly

TABLE 9.1. CHEMICAL COMPOSITIONS OF WELD PADS USED IN STUDY OF THE EFFECT OF FERRITE ON CORROSION RESISTANCE

Alloy	Chemical Composition (wt %)							
	C	Mn	Si	P	S	Ni	Cr	Cb + Ta
High-carbon type 307 Mn	0.80	4.86	0.77	0.031	0.026	9.10	18.20	
Composition H	0.17	3.80	0.54	0.022	0.032	12.40	18.30	0.65
4	0.050	1.63	0.65	0.024	0.016	11.22	18.74	0.54
Composition P	0.11	1.70	0.54	*	*	9.50	19.60	0.61
1	0.05	1.58	0.41	0.022	0.013	10.25	20.15	1.00
3	0.063	1.68	0.28	0.026	0.014	11.27	21.28	0.73
2	0.041	1.64	0.47	0.033	0.014	10.35	19.71	1.05

*Not determined.

TABLE 9.2. DYNAMIC CORROSION OF AUSTENITIC-STAINLESS-STEEL WELD METAL CONTAINING VARYING AMOUNTS OF FERRITE

Alloy[a]	Ferrite in Weld[b] (%)	Weight Loss (mg/cm^2)			
		Run No. M-23[c]		Run No. M-24[c]	
		14.0 fps	28.4 fps	15.5 fps	30.5 fps
High-carbon type 307 Mn	None	2.8	4.2	2.7	9.3
		1.5	1.6	3.6	8.0
Composition H	None	2.5	13.8	3.5	51.5
		2.5	3.8	3.5	18.2
4	3.5–4.5	1.5	11.8	4.1	134.8
		1.2	11.6	4.2	154.9
Composition P	6.0–6.5	1.7	3.1	2.3	10.2
		1.9	2.5	2.8	8.8
1	6.5–7.5	2.1	3.2	2.9	24.7
		1.2	2.9	2.4	15.2
3	7.5–8.5	1.1	2.4	1.3	6.2
		1.2	2.2	1.9	5.9
2	11.5–12.5	5.9	2.8	2.0	8.0
		5.9	2.7	2.0	6.7
Wrought-annealed type 347		1.3	12.7	5.7	4.6
		2.6	2.5	2.0	8.8
		1.4	11.8	5.8	5.8
		0.9	1.3	2.0	5.5
Wrought-annealed type 17-4 PH		0.7	1.3	1.4	8.2
		0.7	1.0	1.3	2.7

[a]See Table 9.1 for the chemical compositions of the weld deposits.

[b]Ferrite content determined by Magne-gage measurements.

[c]Conditions of runs M-23 and M-24: 0.17 *m* uranyl sulfate, 250°C, 200 hr. Rapid corrosion of a chromized tube bundle in the main line of run M-23 caused abnormally high concentration of Cr^{6+} in solution and correspondingly lower corrosion losses on specimens.

showed many cracks in those areas where the rollers had scored and dug into the inside surface of the tubing. On the other hand, the 0.0015-in. rolled material showed only a few minor superficial cracks even after 15 hr. No cracks were observed in the as-received tubing. This indicates that the use of the lighter expansion lessens the susceptibility to a stress-corrosion failure.

9.3 PROPERTIES OF TITANIUM AND ZIRCONIUM ALLOYS

W. J. Fretague

9.3.1 Commercial Titanium

Impact tests have been completed on specimens machined from an unalloyed-titanium dynamic-corrosion-loop specimen holder whose loop-exposure

history is presented in Table 9.3. In addition to the tabulated exposures, the holder was cathodically defilmed frequently in inhibited 5% sulfuric acid at room temperature.

To serve as a basis for comparison, 12 multiple-break impact specimens were machined from the same lot of material in the as-received condition and impact tested. Results are plotted in Fig. 9.1. The data indicate that the loop exposure, chemical or thermal, or the cathodic defilming, or a combination, has embrittled the material, raising the impact transition temperature from approximately 100 to above 200°C. Previous attempts to embrittle unalloyed titanium by cathodic treatment[3] in H_2SO_4 and by loop exposure to simulated HRP environments[4] have not embrittled the specimens. Vacuum-fusion analyses for hydrogen show no difference within the limits of experimental error (0.0084 wt % hydrogen in the as-received condition, 0.0082% after exposure). Representative samples, taken from the impact specimens and examined by x-ray diffraction, indicated the possible existence of an additional unidentified phase in the loop-exposed samples. This is being studied further. Metallographic samples are also being examined for evidence of a second phase in the microstructure of the exposed specimen.

Additional impact tests have been performed on unalloyed titanium, exposed to the loop environment described in Table 9.4, in the swaged-and-machined condition, to study the effect of cold work on the possibility of hydrogen adsorption by titanium, as might be indicated by impact behavior. Data are plotted in Fig. 9.2. A comparison of unexposed as-swaged material[3,5] with swaged-and-vacuum-annealed material does not reveal any effect on impact properties attributable to speci-

[3] W. J. Fretague, A. R. Olsen, R. G. Berggren, and J. J. Woodhouse, *Met. Semiann. Prog. Rep. Oct. 10, 1953*, ORNL-1625, p 9–10 and Fig. 5.

[4] W. J. Fretague, *Met. Quar. Prog. Rep. Oct. 31, 1952*, ORNL-1437, p 41.

[5] W. J. Fretague, A. R. Olsen, and R. G. Berggren, *Met. Semiann. Prog. Rep. April 10, 1953*, ORNL-1551, p 13–15 and Fig. 12.

TABLE 9.3. DYNAMIC-CORROSION-LOOP HISTORY OF UNALLOYED-TITANIUM SPECIMEN HOLDER

HRP Loop Run No.	Solution: Uranium Concentration as UO_2SO_4 (g of U per liter)	Solution: Additions	Temperature (°C)	Time (hr)
I-3	40	0.042 *M* H_2SO_4 200-psi O_2	250	1036
F-20	300	200-psi O_2	250	117
D-1	300	50 ppm of Tc 200-psi O_2	250	101
D-2	300	200-psi O_2	250	100
H-15*		1.0 *M* HCl 1.4 *M* H_2SO_4 0.2 *M* H_2O_2 Alkyl pyridine inhibitor 200-psi He	85	4
H-16	25	200-psi O_2	250	200
H-17	25	200-psi O_2	250	400
				1958

*Decontamination run.

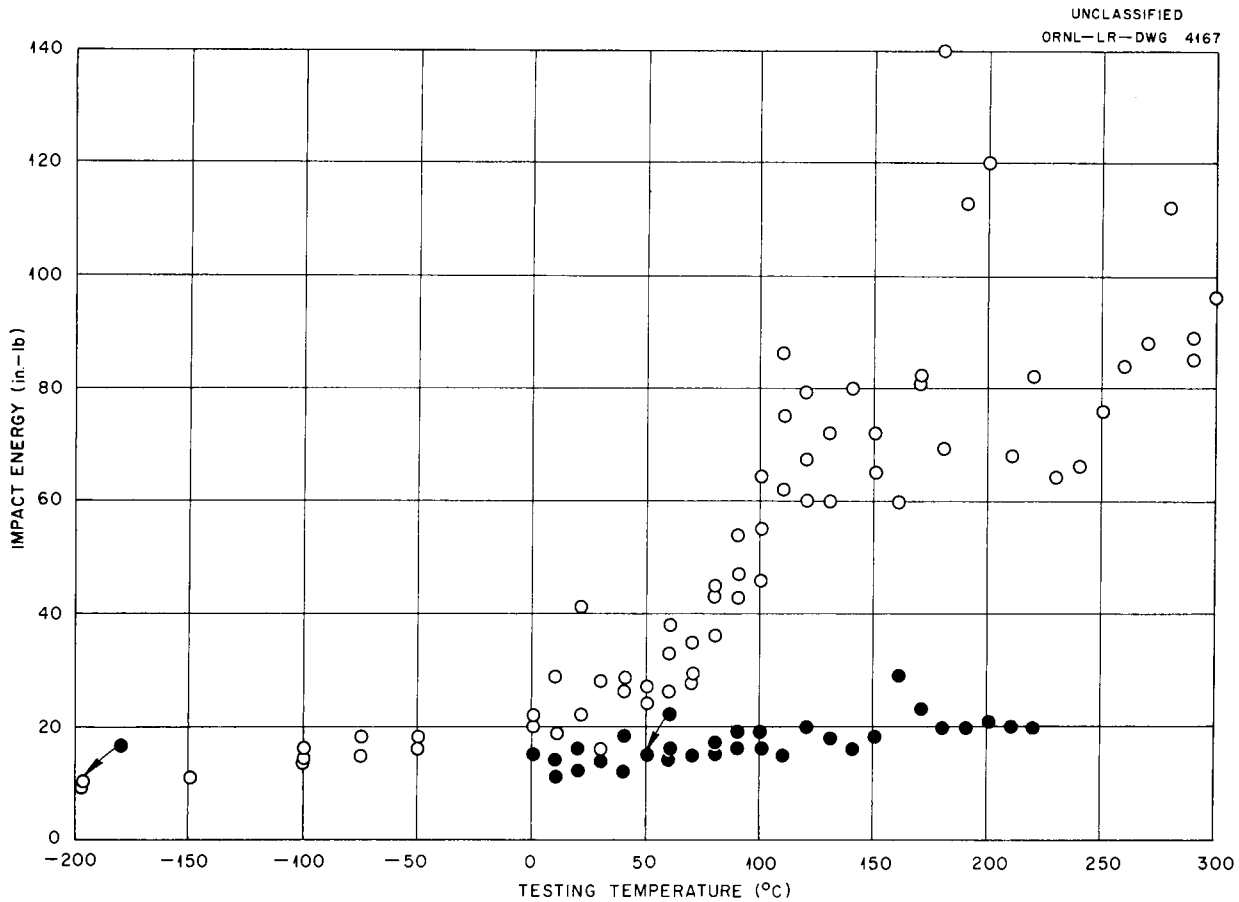

Fig. 9.1. Data on Impact Energy vs Testing Temperature; Material, Titanium (RC-70).

men treatment prior to exposure or attributable to the corrosive environment.

Four multiple-break impact specimens of the same lot of material, but vacuum annealed, were impact tested after exposure to the loop environment described in Table 9.5. Data are plotted in Fig. 9.3. Again, no significant difference in the impact behavior of these specimens as compared with similar specimens, not annealed, exposed under similar conditions,[5] was observed.

Samples from the titanium-pressurizer section of an all-titanium loop that failed in service[6] were analyzed for hydrogen by the vacuum-fusion method at Battelle and at ORNL. The results are presented in Table 9.6. No as-received material was available that could be positively identified as being a section of the tube that failed in the loop. Specimens representative of the same size, source, and manufacturing practice, but not necessarily the same piece, analyzed 0.0109 wt % (BMI), 0.0113 wt % (BMI), and 0.011 wt % (ORNL). These results indicate that, although the temperature at the point of failure was sufficiently high, approximately 800 to 900°C, to transform the structure into the beta phase, the corrosion reaction up to this transformation temperature did not introduce an appreciable amount of hydrogen into the titanium.

To check further the possibility of having lowered the transformation temperature of the unalloyed titanium in the pressurizer tube section by picking up contaminants (O_2, N_2, H_2, etc.) during loop exposure, sections of the pipe adjacent to the rupture were heat treated in Vycor capsules under a partial pressure of purified argon to 704, 826, and 934°C and examined metallographically. No evidence of transformation was apparent in the

[6] E. C. Miller *et al.*, *HRP Quar. Prog. Rep. July 31, 1954*, ORNL-1772, p 136.

704°C sample, whereas the other two contained alpha transformed from the beta phase. This is further confirmation of the hydrogen-analysis results – that the loop exposure had no appreciable effect on the transformation behavior of the titanium and that the pressurizer failure must have occurred at some temperature above 700°C.

9.3.2 Bureau of Mines Titanium

Impact specimens exposed to HRP loop environment in run G-9 in UO_2SO_4 (containing 300 g of uranium per liter) + 50-psi O_2 (added at room temperature), at 300°C, for 427 hr were impact tested. The resultant data, Table 9.7, compared with impact

TABLE 9.4. LOOP HISTORY OF SWAGED-AND-MACHINED UNALLOYED-TITANIUM IMPACT SPECIMENS (Ti-75A, Heat L782, REED Item 24)

HRP Loop Run No.	Solution		Temperature (°C)	Time (hr)
	Uranium Concentration as UO_2SO_4 (g of U per liter)	Additions		
A-67	15	0.006 *M* H_2SO_4	310–320	977

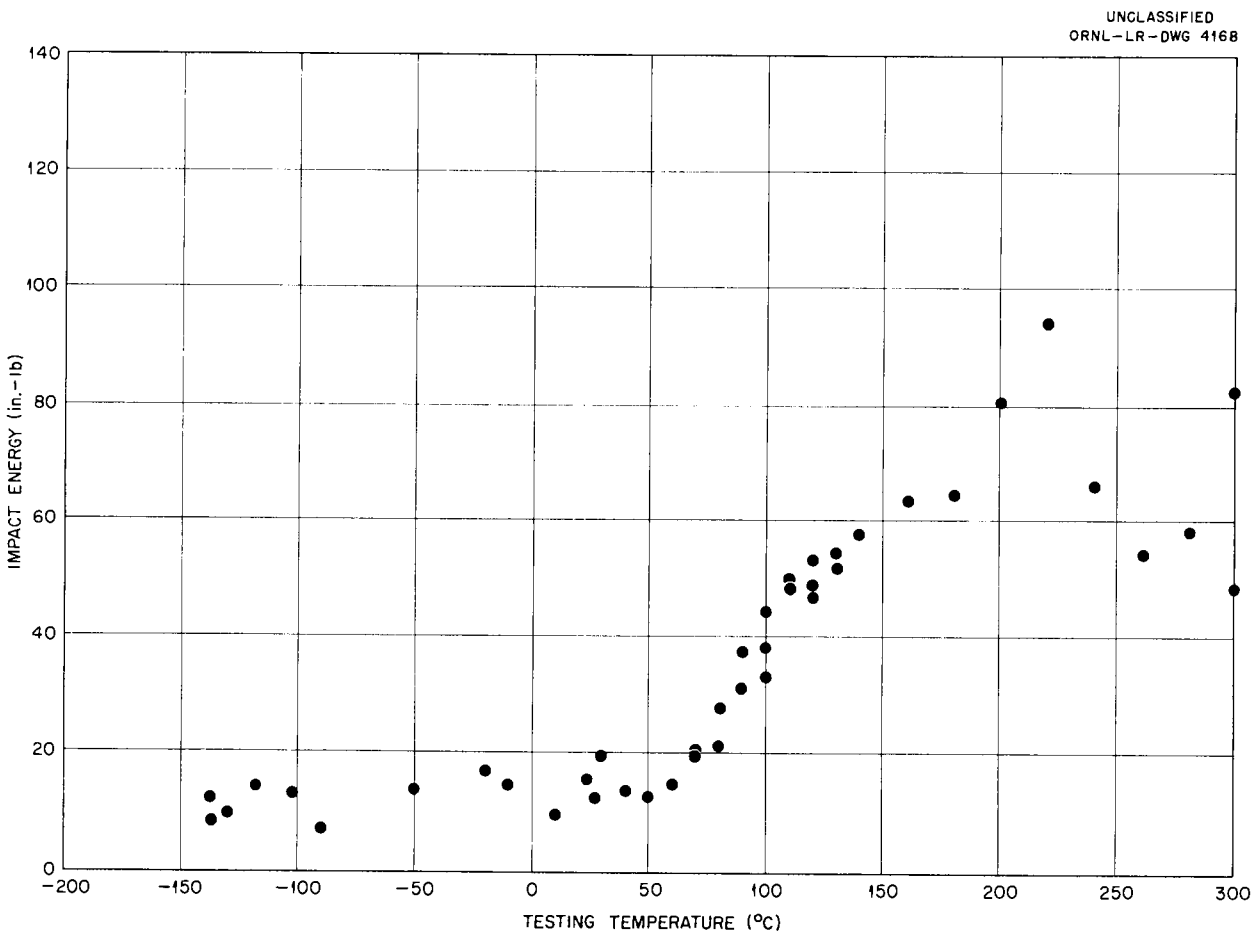

Fig. 9.2. Data on Impact Energy vs Testing Temperature; Material, Titanium 75A, Heat L782, REED Item No. 24.

data on unexposed vacuum-annealed Bureau of Mines titanium,[7] show no substantial effect of the corrosive environment on the impact properties of the exposed samples under the test conditions; that is, in neither set of tests were any of the samples broken by the impact.

[7] W. J. Fretague and J. O. Betterton, *HRP Quar. Prog. Rep. July 31, 1953*, ORNL-1605, p 121.

9.3.3 Zirconium Alloys

(a) Zircaloy-2. Room-temperature, notched, slow-bend tests (loading rate 1 in. per minute) were

TABLE 9.5. LOOP HISTORY OF VACUUM-ANNEALED UNALLOYED IMPACT SPECIMENS

HRP Loop Run No.	Solution: Uranium Concentration as UO_2SO_4 (g of U per liter)	Solution: Additions	Temperature (°C)	Time (hr)
G-11	300 (1.34 *M*)	0.3 *M* H_2SO_4 1000 ppm O_2	300	150

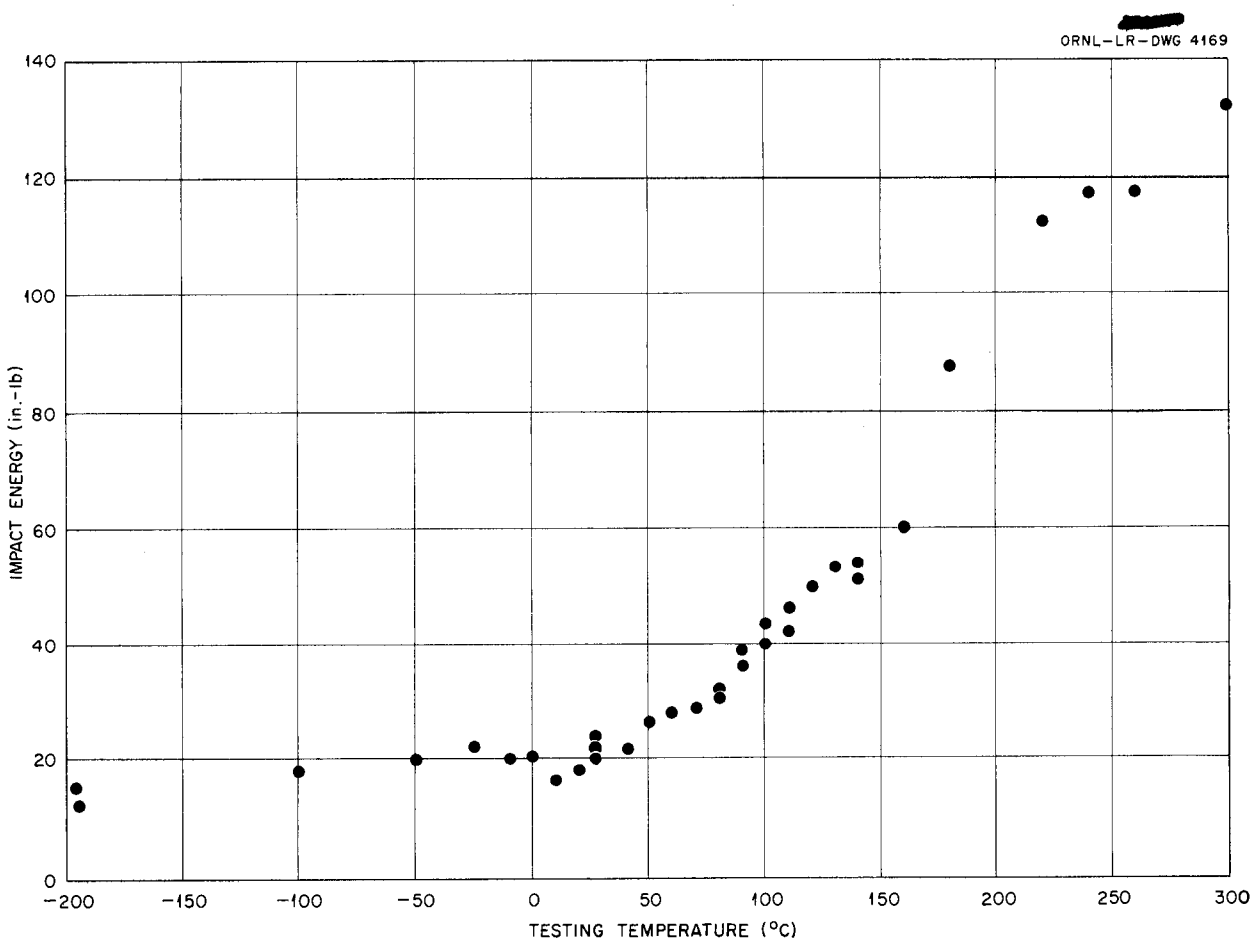

Fig. 9.3. Data on Impact Energy vs Testing Temperature; Material, Titanium 75A, Heat L782, REED Item No. 24.

TABLE 9.6. HYDROGEN IN UNALLOYED TITANIUM FROM RUPTURED PRESSURIZER TUBE

Laboratory Performing Analysis			
Battelle Memorial Institute		Oak Ridge National Laboratory	
Location	Hydrogen content (wt %)	Location	Hydrogen content (wt %)
Ruptured section	0.0083; 0.0089	Ruptured section	0.0086
Section adjacent to failure	0.0061; 0.0061	Section adjacent to failure	0.0048*
		Section away from failure	0.0064

*This sample was smaller in size (0.7 g) than the other samples (1.2 to 1.9 g), and this probably accounts for the difference between results obtained by the different laboratories.

TABLE 9.7. IMPACT DATA FOR HIGH-PURITY BUREAU OF MINES TITANIUM SPECIMENS EXPOSED IN HRP LOOP RUN G-9

Specimen No.	Temperature (°C)	Impact Energy (in.-lb)	Remarks
B2-1	27	125	Threaded end*
	27	148	Did not break
	−197	182	50% fracture
B2-2	27	100	Threaded end*
	27	144	50% fracture
	−197	178	50% fracture
B3-1	27	100	Threaded end*
	27	133	60% fracture
	−197	142	75% fracture
B3-2	27	128	60% fracture
	−197	156	60% fracture

*The ends of the specimens, threaded to hold them in the loop specimen fixture, extended below the point of impact of the striking hammer of the impact tester, and the deformation of the threads on impact gives rise to some error in the readings.

performed on four Zircaloy-2 specimens, cut from plate rolled from ingot 610D 441 RFB 4/5 BK. Specimens were 1/2 in. wide by 1 3/8 in. long by plate thickness and contained a 45-deg notch, 0.040 in. deep, with a 0.005-in. radius at the root of the notch, located centrally in the 1 3/8-in. dimension and parallel to the 1/2-in. dimension. Load-deflection curves were obtained for each specimen, and the area under the curve from zero to maximum load was calculated. These values are recorded as energy (in.-lb) in Table 9.8. Specimens Z2A1 and Z2B1 have the 1 3/8-in. dimension perpendicular to the rolling direction of the plate, and specimens Z2A2 and Z2B2 were prepared with the 1 3/8-in. dimension parallel to the rolling direction of the plate. Side bend specimens (5/16 in. by plate thickness by 1 3/8 in.) are being prepared and will be tested to check the reported[8] 180-deg bend around a 1-in.-dia rod.

TABLE 9.8. NOTCHED SLOW-BEND TESTS OF ZIRCALOY-2 PLATE

Plate No.	Specimen No.	Energy to Maximum Load (in.-lb)
Z2A	1	27.30
	2	22.80
Z2B	1	25.80
	2	28.05

[8]Newport News Shipbuilding & Dry Dock Co., Newport News, Virginia, *Report on the Physical Behavior of Zircaloy-2 Plate Material Rolled by Bureau of Mines from Ingot 610D 441 RFB 4/5 BK*, April 8, 1954, p 4.

Part V

CHEMICAL ENGINEERING DEVELOPMENT

F. R. Bruce

10. SLURRY FUEL AND BLANKET STUDIES

D. E. Ferguson
J. P. McBride
L. E. Morse
J. T. Roberts
W. L. Pattison
W. K. Eister
E. O. Nurmi
G. R. Williams
W. M. Woods
R. O. Payne
J. L. Patton

10.1 PREPARATION OF THORIUM DIOXIDE

Thorium dioxide of sufficient purity to meet tentative specifications for homogeneous reactor blanket use has been made in 5- to 10-kg lots. Thorium oxalate is precipitated from a 1 *M* solution of mantle-grade thorium nitrate by adding solid oxalic acid. The oxalate is washed two or more times by slurrying with water at 70°C and filtering. The washed material is air-dried and is then calcined, in a bed 1 to 1.5 in. deep, at 370°C to constant weight (about 5 hr) and then at 650°C for 3 hr. With minor additions and modifications the equipment used for this process could be used to produce thorium dioxide from thorium formate. Type 316 or 347 stainless steel and glass are suitable for equipment that comes in contact with thorium nitrate solution, nitric acid, or oxalic acid. As indicated by the purity of the thorium dioxide product, Vitreosil (fused silica), Alundum, or aluminum is suitable for the trays holding the material in the 370°C calcination, and Vitreosil, Alundum, or nickel for the 650°C calcination.

The chief impurities in the ThO_2 product were 2000 ppm of sulfate and 1000 ppm of alkaline earths. These impurities were present in the thorium nitrate used as starting material. The material shrank to about one-third its original volume during the 370°C heating, but practically no shrinkage occurred in the 650°C heating. The thorium dioxide produced (300 lb) is being evaluated in the 100-gpm pump loops (see Secs. 7.3 and 7.4).

10.2 GAS-RECOMBINATION STUDIES

A thorium oxide slurry blanket in a large-scale thermal power breeder in which approximately 10 kw of fission heat per liter of slurry is generated may be expected to produce about 4.5 moles of hydrogen and oxygen per liter of slurry per hour with a *G* value (molecules of hydrogen formed per 900 ev of fission energy absorbed) of 0.8 (see Sec. 10.3). The use of an internal catalyst to promote the recombination of this gas would greatly simplify the blanket design by eliminating the necessity for a high-pressure recombiner. It is the ultimate objective of the gas recombination studies to develop an internal catalyst for use in thorium oxide slurries which would not adversely affect desirable slurry properties. Of more immediate need is a slurry catalyst for use in the in-pile irradiation studies of thorium oxide slurries containing enriched uranium.

Studies on combination of oxygen and hydrogen gas were made with several thorium oxide slurries and with slurries of mixed oxides of thorium and uranium and of thorium and copper. Pure thorium oxide slurries exhibited some catalytic activity, combining about 0.05 mole of hydrogen per liter of slurry (530 g of thorium per kilogram of water) per hour at 300°C with a hydrogen partial pressure of 500 psi (excess oxygen pressure). The presence of 4 to 8% uranium oxide in the thorium oxide approximately doubled the combination rate. The addition of 0.1 *m* cupric oxide to the thorium oxide increased the combination rate to 1.7 moles of hydrogen per liter of slurry per hour, a rate which should be sufficient to maintain at the homogeneous reactor design pressure of 2000 psi a slurry blanket dissipating 6 kw of fission heat per liter at 300°C.

The combination studies were carried out in stainless steel bombs (20 ml volume, 10 ml of slurry used) vigorously agitated to minimize diffusion effects. Oxygen and hydrogen were added in stoichiometric ratio at room temperature, and the bomb was heated to 300°C. The decrease in pressure was followed by means of a water-filled capillary connected to the bomb and a Baldwin cell, which in turn actuated a recorder.

A plot (see Fig. 10.1) of the decrease in pressure per time interval vs the average pressure in the interval yielded a straight line, indicating a first-order dependence on pressure as in the case of homogeneous catalysis in aqueous solutions.[1]

[1] H. F. McDuffie *et al.*, *Reactor Sci. Technol.* **4**, No. 2, 23-42 (1954) (TID-2013).

The slope of the line (k_π) is characteristic of the slurry at the temperature and under the specific geometric conditions of the experiment. If it is assumed that the perfect gas law holds in the vapor phase and that the slurry and gas phases are always in equilibrium, the moles of hydrogen, n, removed from the system per liter of slurry per unit time, t, may be calculated from the equation

$$\frac{\Delta n}{\Delta t} = k_\pi \times \frac{pV_g}{RT} \times \frac{1000}{V_s},$$

where V_g and V_s are the volumes of the gas and slurry, respectively, in cubic centimeters and p is the hydrogen partial pressure. This equation accounts only for the change in the gas phase, since, under the experimental conditions of interest, only a small fraction of the total hydrogen in the system is present in the slurry phase. Table 10.1 gives the rate of hydrogen combination with oxygen in the presence of the various slurries. It is apparent from the data that both uranium and copper enhance catalytic activity over that exhibited by either the thorium oxide or copper oxide slurries alone. Other metal oxides can be expected to have a similar effect, and experiments are planned in which the effect of the addition of silver oxide, platinum, palladium, and rhodium on the catalytic activities of slurries will be determined.

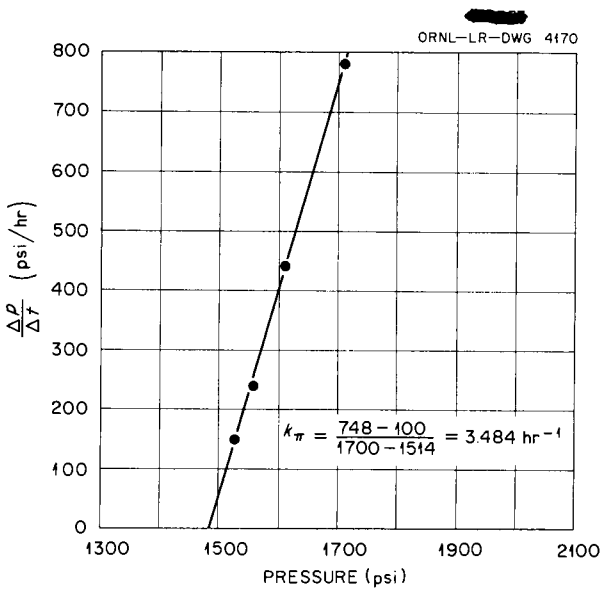

Fig. 10.1. Treatment of Experimental Data for Catalytic Oxidation of Hydrogen at 300°C by Thorium Oxide Slurry (530 g of Thorium per Kilogram of Water) Containing 0.1 *m* CuO.

10.3 SLURRY-IRRADIATION STUDIES

A thorium oxide–uranium oxide slurry containing 530 g of thorium and 40 g of U^{235} per kilogram of water has been irradiated for six days at a flux of

TABLE 10.1. CATALYTIC OXIDATION OF HYDROGEN BY METAL OXIDE SLURRIES

Conditions: 300°C; hydrogen partial pressure 500 psi, excess oxygen; 530 g of thorium per kilogram of water

Slurry	Preparation	H_2 Combination Rate (moles/liter/hr)
Ames ThO_2	Calcination of oxalate above 650°C	0.01
ThO_2	Calcination of oxalate at 600°C	0.04
ThO_2	Pyrohydrolysis of oxalate at 250°C; dried at 350°C	0.045
ThO_2 + 4% UO_3	Pyrohydrolyzed $ThO_2 + UO_3$	0.1
ThO_2 + 8% UO_3	Pyrohydrolyzed $ThO_2 + UO_3$	0.08
ThO_2 + 0.025 *m* CuO	Pyrohydrolyzed $ThO_2 + Cu(OH)_2 \cdot CuCO_3$*	0.25
ThO_2 + 0.1 *m* CuO	Pyrohydrolyzed $ThO_2 + Cu(OH)_2 \cdot CuCO_3$*	1.7
0.1 *m* CuO**	$Cu(OH)_2 \cdot CuCO_3$*	0.9

*$Cu(OH)_2 \cdot CuCO_3$ decomposed to CuO in water at high temperatures.
**No ThO_2.

about 7×10^{11} neutrons/cm^2/sec, corresponding to a fission heat generation of about 1 kw per liter of slurry. During the irradiation of the slurry and gas phase, temperatures were 290 to 300°C and 200 to 250°C, respectively. Radiolytic gas pressures in excess of steam varied between 1000 and 2000 psi and inversely with the gas phase temperature. Analysis of the gas production data indicated a G value of about 0.8 and a recombination rate approximating the hydrogen-oxygen combination rate observed in the presence of a similar slurry in out-of-pile studies (see Table 10.1).

The slurry was irradiated in a stainless steel bomb (20 ml volume, 10 ml of slurry) equipped with a remotely operated dash-pot type of stirrer. A stainless steel capillary connection permitted a continuous record of the pressure to be obtained. As the irradiation progressed, the operation of the stirrer became increasingly labored and stopped completely after four days in the reactor. No marked change in radiolytic gas pressures was observed in the absence of stirring. The contents of the bomb will be inspected to determine the cause of the stirring difficulty.

Under the temperature conditions of the experiment the walls of the gas phase were continually wetted with condensing vapors, preventing the formation of dry areas and possible "hot spots" for initiation of hydrogen and oxygen explosions.

A previous experiment utilizing a thorium oxide slurry containing 4% enriched uranium as the oxide was terminated by rupture of the radiation bomb, presumably the result of an internal explosion. In that experiment the gas-phase temperature was 10 to 20°C greater than that of the slurry phase (270°C). The gas recombination rate observed prior to the explosion was an order of magnitude greater than had been observed in out-of-pile studies with a similar slurry. It is presumed that the explosion occurred as the result of local overheating of some solid surface in contact with the gas phase, promoting a spontaneous reaction of the radiolytic gases.

Facilities for opening the radiation bombs and examining their contents are being developed. Further experiments using slurries containing enriched uranium are planned for both the ORNL Graphite Reactor and the LITR. Particular attention will be paid to the difficulty encountered in stirring the slurry under irradiation. Gas recombination catalysts are being developed for use in the in-pile studies at high fission densities.

10.4 DEFLOCCULATION OF THORIUM OXIDE SLURRIES

The marked increase in viscosity and decrease in settled bulk density of slurry solids noted in a thorium oxide slurry subjected to an extended pumping test (Run S-49)[2] prompted an examination of a sample of the material in an effort to ascertain the factors contributing to the alteration of the slurry. The major cause of the phenomenon appeared to be a degradation of the particles and subsequent flocculation of the fragments. The addition of a deflocculating agent, 0.01 m $Na_2O(SiO_2)_2$, dispersed the flocs and restored the fluidity of the system.

The thorium oxide slurry (made up from oxide prepared by a 650°C calcination of thorium formate) had been pumped for 1500 hr at 250°C in loop S and cooled to room temperature. It was found to contain solids of a low bulk density (about 750 g of thorium per liter) compared with the original material and to exhibit, at this concentration of thorium, plastic flow properties of a high yield point and high viscosity.

Sedimentation particle-size analyses were obtained on samples of dilute suspensions (<0.5% ThO_2) of the slurry to which 0.005 M $Na_4P_2O_7$ had been added to disperse the aggregates. Circulation in the loop was found to degrade the oxide from an average particle size of >26 μ to <2.5 μ, more than a thousandfold reduction in volume.

X-ray diffraction patterns, obtained on the original slurry and on an undried sample of the pumped material, indicated both the original and the pumped material to be crystalline and to be composed of structural units of 0.06 to 0.1 μ in size. If anything, the pumped material contained slightly larger fundamental crystals. Background scattering was substantially the same for both the original and the pumped material.

Subjecting a suspension of the pumped slurry to an extended dialysis in water (48 hr) failed to improve its properties, indicating that the increase in viscosity during pumping was probably not the result of the liberation of ionic species from the degraded slurry.

The efficiency of several dispersants was determined by adding the dispersant to a suspension of the pumped material containing 50 g of thorium per liter, agitating overnight, and allowing the

[2] R. N. Lyon *et al.*, *HRP Quar. Prog. Rep. July 31, 1954*, ORNL-1772, p 114.

system to stand for an extended period of time. The higher the density of settled solids after extended settling, the greater the dispersion or defloccu-lation. The most efficient dispersants, the settling time, and the density of the settled solids are given in Table 10.2.

The sodium silicate was selected as being the dispersing agent most likely to be thermally stable in water at high temperature, and an additional experiment was carried out in which the concen trated pumped slurry (700 g of thorium per liter was placed in a dialysis bag, submerged in 0.13% $Na_2O(SiO_2)_{3.25}$, and dialyzed overnight in ar agitated system. At the end of the dialysis the fluidity of the concentrated suspension was ap-proximately that of water. Analysis of the dispersec slurry showed it to contain sodium and silicon ir a 1:1 ratio and 0.01 *m* concentrations.

TABLE 10.2. EFFECT OF INORGANIC SALTS ON THORIUM OXIDE SLURRY FLOCCULATION

Dispersant	Settling Time (hr)	Settled Density (g of thorium per liter)
None	70	400
0.5% Calgon	72	1280
0.004 *m* $Na_4P_2O_7$	68	1250
0.08% $Na_2O(SiO_2)_{3.25}$	66	960
0.01 *m* Na_2CO_3	51	1500

10.5 THORIUM HYDROXIDE STUDIES

Electron-diffraction studies of thorium hydroxide prepared from thorium formate by the addition of ammonium hydroxide have shown that the hydroxide as precipitated, or when dried, or when autoclaved at 250°C in water is crystalline, although x-ray diffraction studies made previously[3] on similar materials had indicated them to be amorphous. The average size of the microcrystalline structural units of the freshly precipitated material was <50 Å, and that of the autoclaved material was 200 Å, although the agglomerates were considerably larger (>10 μ).

[3]D. E. Ferguson *et al.*, *HRP Quar. Prog. Rep. July 31, 1954*, ORNL-1772, p 142.

[redacted]

11. PLUTONIUM-PRODUCER BLANKET PROCESSING

D. E. Ferguson
R. E. Leuze
R. H. Rainey
W. E. Tomlin
J. M. Delozier
O. K. Tallent

The objective of processing the uranyl sulfate solution blanket of the plutonium producer is to remove plutonium and possibly neptunium as rapidly as possible in order to minimize Pu^{240} buildup. During this quarter the study of the chemistry of plutonium and neptunium under simulated reactor conditions has included plutonium solubility determinations, study of PuO_2 dissolution, measurement of the adsorption of plutonium on stainless steel, on titanium, and on zirconium, PuO_2 particle-size determinations, and measurement of the adsorption of neptunium on MnO_2.

11.1 SOLUBILITY OF Pu(IV) IN URANYL SULFATE SOLUTIONS

The solubility of Pu(IV) in 1.3 *m* UO_2SO_4 at 250°C increased rapidly with an increase of free acid, as shown in Fig. 11.1. The curve represents an approximate average of the data and shows that only 0.05 *m* sulfuric acid increases the plutonium solubility by a factor of 3. Plutonium solubilities of 100 mg per kilogram of water were obtained with 0.40 *m* sulfuric acid.

11.2 DISSOLUTION OF PuO_2

After the PuO_2 has been physically concentrated in a small volume of uranyl sulfate solution and removed from the blanket system, the next operation in processing is recovery of the D_2O by evaporation and heating of the UO_2SO_4 cake for several hours at 200°C. The presence of neptunium and fission-product activity may make it impossible to limit the maximum drying temperature to 200°C. In order to determine whether calcined material can be readily dissolved, a slurry of PuO_2 in 1.1 *m* UO_2SO_4 was evaporated to dryness in a quartz boat and then heated at 825°C for 2 hr. Dissolution of both the uranium product and PuO_2 was obtained by heating the residue in concentrated nitric acid containing ammonium hexanitratocerate for 30 min at 90°C. A small amount of undissolved residue apparently contained no plutonium or uranium. Firm flow-sheet conditions will be established at a later date.

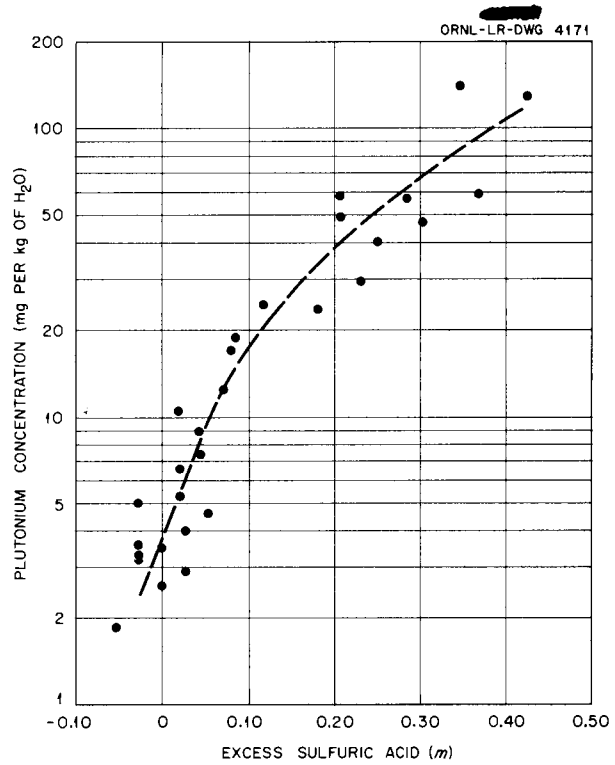

Fig. 11.1. Effect of Sulfuric Acid Concentration on Solubility of Pu(IV) in 1.3 *m* Uranyl Sulfate at 250°C.

11.3 ADSORPTION OF PLUTONIUM ON STAINLESS STEEL, TITANIUM, AND ZIRCONIUM

Results of studies on adsorption of plutonium on metal surfaces confirmed previous results[1] for stainless steel but not for titanium. After nine cycles of adding 1.25 *m* UO_2SO_4 solution containing 105 mg of plutonium per kilogram of water [91% Pu(IV)], heating to 250°C for 12 hr, removing the solution and precipitate, and rinsing with water, two type 347 stainless steel containers had adsorbed plutonium to the extent of 0.06 and 0.11 mg/cm^2 and two titanium vessels had adsorbed

[1] D. E. Ferguson *et al.*, *HRP Quar. Prog. Rep. July 31, 1954*, ORNL-1772, p 143.

0.18 and 0.21 mg/cm^2 with no indication that equilibrium had been reached. Plutonium adsorption on a zirconium container appears to have reached equilibrium at about 0.03 mg/cm^2. These values were determined by material-balance calculations, with the plutonium not found either in solution or in the precipitate assumed to be adsorbed on the metal walls. This series of experiments is still in progress. At the completion of the test series the amount of plutonium adsorbed will also be determined by analyses of descaling solutions. Of the total amount of plutonium used, it is estimated that 45% was adsorbed on the stainless steel, 60% on the titanium, and 12% on the zirconium.

The stainless steel vessels used were made from 8-in. lengths of ¼-in. IPS pipe, the titanium vessels were made from 8-in. lengths of 0.625-in.-ID tube, and the zirconium vessel was made from an 8-in. length of 0.44-in.-ID tube. With the stainless steel vessels 5 ml of 1.25 *m* UO_2SO_4 containing 105 mg of plutonium per kilogram of water was used, 10 ml was used with the zirconium vessel, and 15 ml with the titanium vessels. Loose caps were placed on all vessels so that they were exposed to the atmosphere in the autoclave. After being heated for 12 hr at 250°C in an atmosphere of 150-psi oxygen and 150-psi hydrogen, the solutions were cooled and removed along with any precipitate. This was followed by a water rinse, but no attempt was made to remove the adherent scales.

Plutonium buildup on the metal walls during the nine cycles is shown in Fig. 11.2. The last three runs show that no additional plutonium was adsorbed on the zirconium, indicating an approach to equilibrium. Plutonium is continuing to be adsorbed on both titanium and stainless steel. The duplicate titanium tests check quite well. The difference in behavior of the two stainless steel vessels can be explained by the fact that concentration of the uranyl sulfate by evaporation in runs 2 and 3 resulted in corrosion, and the protective film was broken in vessel 2, causing corrosion in subsequent runs.

The amount of plutonium remaining in solution in the stainless steel vessels after being heated to 250°C for 12 hr varied considerably, with an average value of about 25 mg of plutonium per kilogram of water found in solution. This high

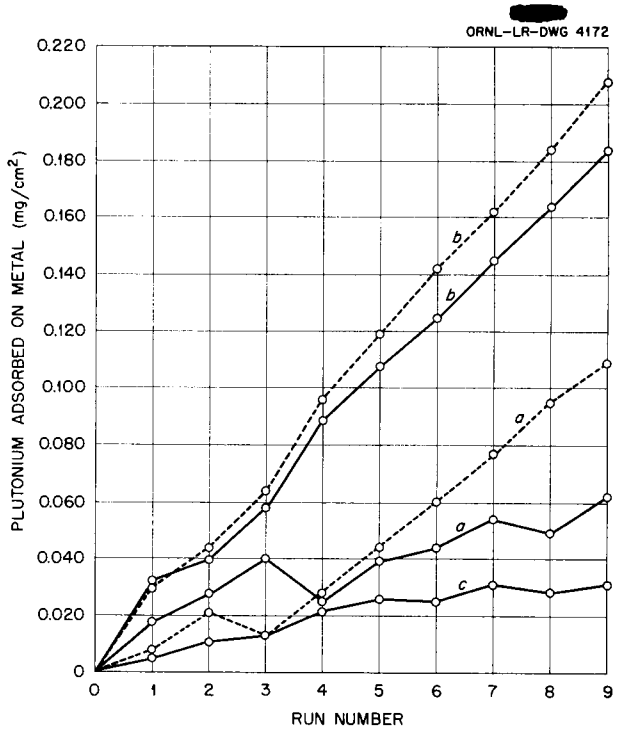

Fig. 11.2. Adsorption of Plutonium on (*a*) Type 347 Stainless Steel, (*b*) Titanium, and (*c*) Zirconium from 1.25 *m* Uranyl Sulfate Solution Containing 105 mg of Plutonium per Kilogram of Water by Heating Solution at 250°C for 12 hr.

solubility was obtained because the plutonium in the stainless steel vessels under an atmosphere of 175 psi of O_2–175 psi of H_2 was oxidized to the soluble Pu(VI). This behavior was not observed in the titanium and zirconium vessels. Further investigation is necessary to determine the reason for this behavior.

11.4 PARTICLE SIZE OF PuO_2

Analyses of two PuO_2 precipitates indicated that particle size in the reactor blanket will range from 0.25 to 1.5 μ. Less than 0.1 wt % of the precipitates studied was smaller than 0.25 μ, and less than 10 wt % was smaller than 0.5 μ. The bulk of the material was between 0.5 and 1 μ. Although it is not yet possible to determine precisely how this precipitate will behave in a hydroclone separator, results with ThO_2 indicate that no difficulty will be encountered in the separation (see Sec. 12.2) of the 0.5-μ particles.

11.5 NEPTUNIUM CHEMISTRY

In a single experiment, when a solution containing 0.7 g of Np(IV) per kilogram of water was added to 1.35 *m* uranyl sulfate containing 1.1 *m* sulfuric acid, the neptunium valence remained unchanged at room temperature. However, when heated for 8 hr at 250°C, the neptunium was completely oxidized to Np(V). In a similar experiment in which the solution contained 0.02 *m* ferrous sulfate, the neptunium remained as Np(IV) when heated to 250°C. As expected, no precipitation was noted at this acidity.

Of several materials tested, manganese dioxide was found to be the best adsorbent for trace amounts of neptunium from uranyl sulfate solution. Three treatments removed 90% of tracer neptunium from 0.1 *m* uranyl sulfate solution. Although the manganese dioxide also removed some uranium from solution, the manganese dioxide can be presaturated with uranium without appreciably decreasing its effectiveness for neptunium removal. The adsorbed neptunium and uranium can be eluted with 8 *N* nitric acid at room temperature. The manganese dioxide capacity for neptunium adsorption is not known, but a low capacity will rule out its use as a means of removing neptunium from the plutonium-producer blanket solution.

11.6 DETERMINATION OF REACTOR NEUTRON CAPTURE CROSS SECTION OF Np^{239}

A preliminary value for the capture cross section of Np^{239} is 80 ± 20 barns (see Sec. 16).

Plutonium from the uranium irradiated for 8 and 16 days in the LITR has been recovered, purified, and transferred to the Chemistry Division. The quantities of plutonium recovered were 10.8 and 22.4 mg, respectively. This completes the plutonium-recovery work for Np^{239} cross-section studies. Table 11.1 presents a summary of the recovery work.

TABLE 11.1. PRODUCTION* AND ISOLATION** OF PLUTONIUM FOR Np^{239} CROSS-SECTION DETERMINATION

Number of Slugs	Weight of Uronium (g)	Amount of Plutonium (mg)	Amount of Plutonium Isolated (mg)
6	1160	4.9	3.2
6	1160	9.7	7.4
4	773	13.2	11.0
2	382	12.7	8.9
1	193	13.1	10.8
1	193	27	22

*Depleted uranium (0.03% U^{235}) irradiated in LITR at an average flux of 2.8×10^{13} neutrons/cm^2/sec.

**Plutonium isolated by TBP extraction followed by fluoride precipitation.

12. FUEL AND THERMAL-BREEDER BLANKET PROCESSING

D. E. Ferguson
R. A. McNees
S. Peterson
W. B. Howerton
W. K. Eister
M. E. Whatley
P. A. Haas
R. W. Horton
J. R. Engel
V. L. Fowler
H. E. Goeller
W. E. Unger
W. L. Carter
H. O. Weeren
A. M. Rom
H. E. Williamson
C. E. Guthrie
F. C. McCullough

12.1 FISSION-PRODUCT AND CORROSION-PRODUCT CHEMISTRY

The behavior of cerous sulfate in simulated fuel solution at 280°C was studied under dynamic conditions in a circulating loop (10 liters volume) test. The solubility of $Ce_2(SO_4)_3$ in simulated homogeneous reactor fuel (0.02 *m* UO_2SO_4, 0.005 *m* H_2SO_4) was about 0.006 g per kilogram of H_2O. This is in agreement with the value of 0.004 g per kilogram of H_2O at 270°C obtained in static experiments (10 to 1000 ml volume).[1]

When rare-earth sulfates, traced with Nd^{147}, were coprecipitated at 270°C with iron and chromium hydrous oxides, they did not redissolve immediately when the solution was rapidly cooled to room temperature. Separation of the rare earths from the fuel solution along with iron and chromium oxides by centrifugation at room temperature therefore may be possible. The amount of $Nd_2(SO_4)_3$ in solution under these conditions was 0.04 g per kilogram of H_2O.

As much as 80% of the iodine was removed from a simulated fuel solution by heating the solution, in the neighborhood of 300°C, and contacting the gas phase, which contained oxygen, above it with silver wire (see also Sec. 14.2). The initial oxidation state of the iodine had no effect on the amount removed.

12.1.1 Rare-Earth Solubility

Corrosion test loop D was modified for use in the solubility studies by providing means for taking filtered samples of solution from the loop, as well as unfiltered samples, while in operation. The filter consisted of a length of heavy-wall stainless steel tubing packed with crushed quartz held in place by means of perforated metal disks at each end of the quartz packing. The tube was inserted in the loop in such a fashion that the liquid being filtered was at the same temperature as the liquid circulating in the loop.

Operation of the 10-liter-volume loop was started with 7.5 liters of a simulated rare-earth-free fuel solution (0.02 *m* UO_2SO_4, 0.005 *m* H_2SO_4) and brought to 280°C. After a few hours, when operation had become stable, 2.5 liters of simulated fuel containing rare earths was added at a rate of 50 ml/hr. This solution was 0.02 *m* in UO_2SO_4 and 0.005 *m* in sulfuric acid, contained 1.0 g of mixed rare-earth sulfates per liter, and was spiked with Ce^{144} tracer. Both filtered and unfiltered samples of the loop contents were taken at intervals. The rates of sampling and feed addition to the loop were the same.

The cerous sulfate in solution at 280°C increased to 0.012 g per kilogram of H_2O during the first 12 hr of rare-earth solution addition. The value rapidly dropped to 0.006 g per kilogram of H_2O after 12 hr, where it remained essentially constant for the next 24 hr while the rest of the rare-earth solution was being added. After all the rare-earth solution had been added, the loop was held at 275 to 280°C for 20 hr. During this time the cerous sulfate in solution dropped to 0.004 g per kilogram of H_2O. In the following period of 24 hr the temperature was gradually lowered to 200°C, and the solubility of $Ce_2(SO_4)_3$ increased to 0.005 g per kilogram of H_2O.

When the loop was opened for inspection, it was found that the filter tube was broken off. This apparently happened at about the fourteenth hour of the spike addition, since a difference in Ce^{144} content between filtered and unfiltered samples was observable up to this time but thereafter no difference could be seen. Some filtering action was obtained, however, since samples of filtered material contained no solid corrosion products, while unfiltered samples always contained enough corrosion-product solids to make an opaque dispersion when thoroughly mixed.

[1] D. E. Ferguson *et al.*, *HRP Quar. Prog. Rep. July 31, 1954*, ORNL-1772, p 151.

Eight hours after the Ce^{144} spike addition had been started, the distribution of activity in the unfiltered samples between solid and liquid phases was about 1 to 1. At the conclusion of the run the activity distribution was 12 to 1 in favor of the solid. When some of these solids were treated with simulated fuel solution at 100°C, several hours was required to get appreciable amounts of cerium back into solution.

12.1.2 Coprecipitation of Rare Earths with Other Elements

Results of further rare-earth precipitation studies indicated that operation of the hydroclones at low temperatures and pressures may be possible. Earlier work[2] had shown that rare-earth sulfates which had been precipitated from simulated fuel solution by heating the solutions in quartz tubes redissolved quickly when the temperature was lowered. However, when rare earths were coprecipitated by heat with hydrolyzed corrosion products in the loop test (Sec. 12.1.1), re-solution was very slow.

In experiments on the dissolution characteristics of the precipitates, sulfates of various metals (iron, chromium, magnesium, or aluminum) were added to simulated fuel solutions containing rare-earth sulfates traced with either Ce^{144} or Nd^{147}. Ten-milliliter samples of the mixed solutions were sealed in quartz tubes and heated to 270°C in an autoclave for 6 hr and then slowly cooled to room temperature. Analysis of liquid samples that had been decanted from the solids showed that in no case was any significant amount of the rare earths removed from the solution by this method. Further tests with more of the same types of solutions showed that the amount of neodymium remaining in solution when the solutions were filtered at 270°C was not significantly lower than when no additives or corrosion products were present.

However, when simulated fuel solutions containing rare-earth sulfates and either iron or chromium sulfate or mixtures of the two were heated to 270°C, cooled rapidly, and centrifuged at room temperature, the liquid decanted from the solids contained only a fraction of the rare earths originally in the solution. When Nd^{147} tracer was used, the amount of neodymium sulfate in solution after cooling rapidly from 270°C and centrifuging was only 0.04 g per kilogram of H_2O. A mixture of iron and chromium sulfates gave better rare-earth separation than either alone. Results of preliminary experiments indicate that aluminum gives less separation than the iron-chromium mixture, but magnesium may give significantly more.

12.1.3 Iodine Removal

Work on the distribution of iodine between its several possible valence states showed that, in 0.02 *m* UO_2SO_4 solutions containing iodate and 25% excess sulfuric acid, at 300°C free iodine was in equilibrium with iodate. As would be expected, no iodide was present. Since free iodine was found in solution, an equilibrium amount of iodine would be expected in the gas phase, and processing the vapor phase above reactor solutions for iodine removal would introduce little or no contamination into the fuel solution. Silver-impregnated Alundum chips were held in the gas phase above simulated fuel solutions containing iodine in various oxidation states, and the solutions were heated to 250°C for 6 hr in sealed quartz tubes inside a pressurized vessel. The gas phase in the quartz tube contained 15-psi oxygen, provided by the decomposition of hydrogen peroxide which was added before the tubes were sealed. Qualitative observations indicated that iodine was extensively removed from solution and deposited in the Alundum chips. The iodine concentrations used were in the range of 10^{-1} to 10^{-3} g of iodine per kilogram of water, the range expected in the HRT.

12.2 ENGINEERING STUDIES

12.2.1 Hydroclone Liquid-Solid Cyclone Separators

In earlier studies[3] the efficiency of the DorrClone TM-3 0.4-in.-dia unit hydroclone fell off rapidly with feed rates below 0.5 gpm (15 gpm per stage of 32 units). For removing PuO_2 from the blanket of a homogeneous plutonium-producing reactor and precipitated fission products from the TBR, a cascade (see Fig. 12.1) of three stages of hydroclone separators will be necessary to obtain the desired concentration. While the performance of the 0.4-in.-dia hydroclone is satisfactory for the first two stages, the feed rate to the final stage

[2] W. K. Eister *et al.*, *HRP Quar. Prog. Rep. April 30, 1954*, ORNL-1753, Figs. 124–127.

[3] D. E. Ferguson *et al.*, *HRP Quar. Prog. Rep. July 31, 1954*, ORNL-1772, p 153.

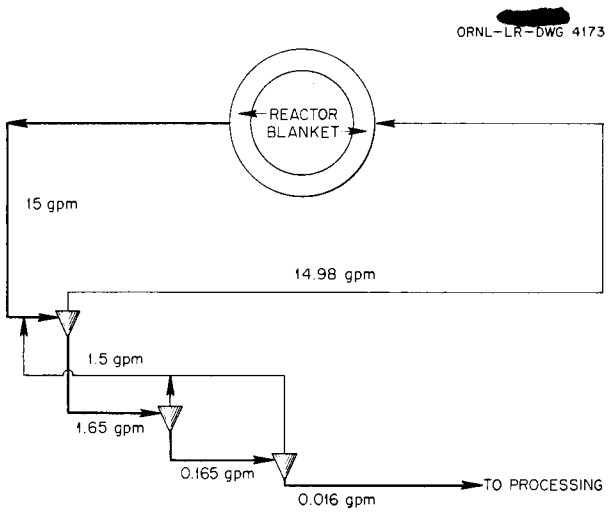

Fig. 12.1. Proposed Hydroclone Coscade for Plutonium-Producer Blanket.

is about 0.1 gpm, which is below the minimum capacity for efficient operation of the 0.4-in.-dia hydroclone.

As part of the development work on production of more satisfactory hydroclones for use in processing the homogeneous reactor fluids to remove solid particles, hydroclone units of 0.5- and 0.25-in. diameter (Fig. 12.2) have been made and tested. Both conical and cylindrical hydroclones have been studied with various sizes of feed inlets and overflows. Results of the experiments with 0.5-in.-dia hydroclones (see Table 12.1) confirm the previous conclusions with 0.4-in.-dia units that, although separation efficiencies of about 90% can be obtained at feed rates of 0.8 to 1 gpm, units of this size will be unsatisfactory for rates below 0.5 gpm. Conical units were more effective than cylindrical ones, but cylindrical hydroclones of greater length may give comparable efficiencies.

In preliminary tests with the conical 0.25-in.-dia hydroclones, 1.5 in. long, efficiencies up to 95% were obtained at feed flow rates of 0.2 gpm, with 10% of the liquid stream reporting to the underflow. In similar runs with a 3.5-in.-long unit, separation efficiencies of 80 to 85% were obtained, which indicate the existence of an optimum length for a given diameter, probably in the vicinity of 1.5 in. for this case. Based on these tests, the 0.25-in.-dia hydroclone is capable of effecting twice the clarification of the 0.5-in.-dia unit.

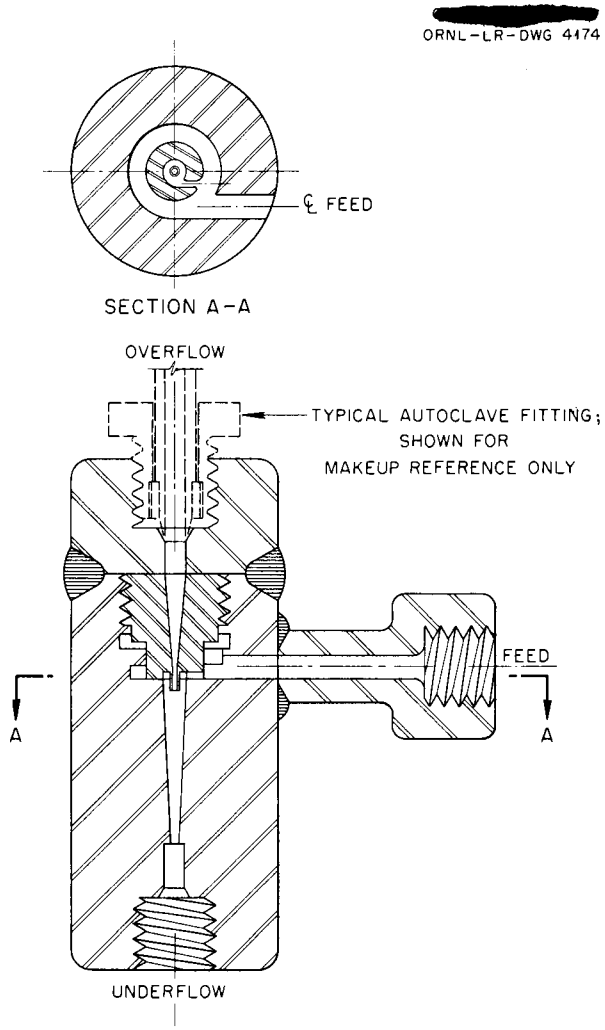

Fig. 12.2. Proposed High-Pressure 0.25-in.-dia Hydroclone.

Particle-size analyses of samples of the thorium dioxide slurry fed to the 0.5-in.-dia hydroclone and collected from the underflow and overflow did not show the high degree of classification characteristic of larger diameter hydroclones (3 in. or greater in diameter). The particle-size distribution curves of the feed, overflow, and underflow were similar in appearance down to about 0.7 μ. The analysis used is based on a settling-rate curve plotted from data obtained by activation analysis techniques, and, when the bulk of the material is above 1.0 μ, accuracy below this size is somewhat limited.

Because of the small size of the feed inlets and overflows, the 0.25-in.-dia hydroclones are susceptible to plugging. This difficulty could be overcome in reactor operation by removing any very large particles (~200 μ) with a large-diameter hydroclone and sending the overflow, or part of it, to the small units.

Copies of the TM-3 unit are being fabricated of stainless steel and titanium for use in high-pressure loop tests.

12.2.2 High-Pressure Test Loops

Loop A, designed for testing sampling devices and physical properties of the solids in the fuel

TABLE 12.1. EFFICIENCY OF 0.5-in.-dia HYDROCLONE SEPARATOR

Feed material studied: Suspension of thorium dioxide in water, 25 wt % of whose particles* were less than 1 μ in diameter; 10% liquid to underflow

Cyclone Type	Length (in.)	Inlet Diameter (in.)	Overflow Diameter (in.)	Feed Rate (gpm)	Solids to Underflow (%)
Conical	3.5	0.0625	0.0515	0.5	85
		0.0625	0.0515	0.8	92
		0.0625	0.0625	0.5	84
		0.0625	0.0625	0.8	89
		0.0937	0.0515	0.5	78
		0.0937	0.0515	0.8	88
		0.0937	0.0625	0.5	91**
		0.0937	0.0625	0.8	89
		0.0937	0.0625	1.0	91
		0.0937	0.0925	0.5	82
		0.0937	0.0925	0.8	93
		0.0937	0.0925	1.0	95
		0.125	0.0625	0.8	85
		0.125	0.0625	1.0	86
Cylindrical	1.6	0.0937	0.0625	0.8	78
		0.0937	0.0625	1.0	80
	3.6	0.0937	0.0625	0.8	85
		0.0937	0.0625	1.0	92
	1.6	0.125	0.0625	0.8	57
		0.125	0.0625	1.0	70
	3.6	0.125	0.0625	0.8	69
		0.125	0.0625	1.0	78
	1.6	0.125	0.0925	0.8	54
		0.125	0.0925	1.0	59
	3.6	0.125	0.0925	0.8	65
		0.125	0.0925	1.0	73

*Particle-size analysis for material used:

Particle Diameter (μ)	Amount of Solid Less Than This Size (wt %)
8.70	100.0
5.50	90.9
2.76	70.7
1.53	48.9
1.01	25.7
0.75	10.9
0.62	4.7

**Questionable accuracy.

solution, was placed in operation in September. It has been operated for 50 hr with a solution containing 5 g of uranium (as uranyl sulfate) per liter and for 50 hr with a solution of the same uranium concentration plus 0.5 g of neodymium per liter at 250°C and 1000 psi. Modifications of the equipment will be made to permit operation at 300°C and 2000 psi as soon as a high-pressure pump becomes available.

Both filtered and unfiltered samples of the loop contents have been removed and analyzed, but results are inconclusive because of uranium precipitation and corrosion-product contamination of samples. These difficulties were caused by small gas-phase leaks in Bourdon tubes, one in a pressure alarm switch and one in a pressure gage, which allowed the oxygen atmosphere to bleed off; otherwise, the mechanical operation of the system has been satisfactory during this time.

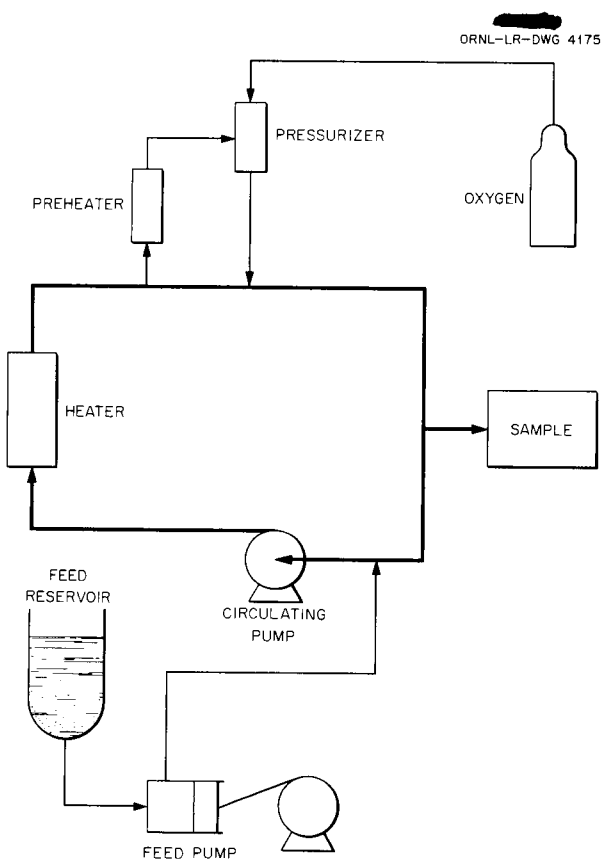

Fig. 12.3. Loop A, Schematic Drawing.

Loop A (see Fig. 12.3) is a completely welded, stainless steel, circulating, ½-in. IPS pipe loop using an ORNL 1000-psi 5-gpm pump. It is fitted with a solids-separating sampler.

Loop B (see Fig. 12.4) design is complete, and shop fabrication of components is about 80% complete. The loop is scheduled to be in operation by January 1955. Operation of loop B will permit dynamic study of the chemistry of fission-product precipitation and the effects of temperature cycling and attrition on the separability of the precipitates, and will demonstrate the effectiveness and performance of hydroclones under the simulated conditions of reactor operation.

Loop B is a figure-eight loop that will provide temperature cycling in simulation of the reactor heat-exchanger loop. It will be continuously fed with a solution of rare earths to simulate the fission products formed by fissioning uranium in the reactor core. The loop slurry can be drawn off continuously to feed a hydroclone solid-liquids separator. The clarified overflow will be returned to the loop; the underflow can be either returned to the loop or diverted to a receiver for evaluating the hydroclone performance.

The loop and the HRT are compared in Table 12.2.

TABLE 12.2. COMPARISON OF LOOP B WITH HRT FUEL SYSTEM

Item	HRT	Loop B
Total volume, liters	500	25
Circulation rate, gpm	400	5
Fluid velocity, fps	18	3.9
Temperature cycle, sec	19	40 to 100
Temperature cycle range, °C	50	50
Residence time	3.5 days	40 min to 27 hr
Hydroclone feed rate, gpm	0.6 to 1	0.2 to 1
Solids concentration, mg/liter	80	10 to 100
Nominal temperature, °C	300	300
Nominal pressure, psi	2000	2000

[redacted]
ORNL-LR-DWG 4176

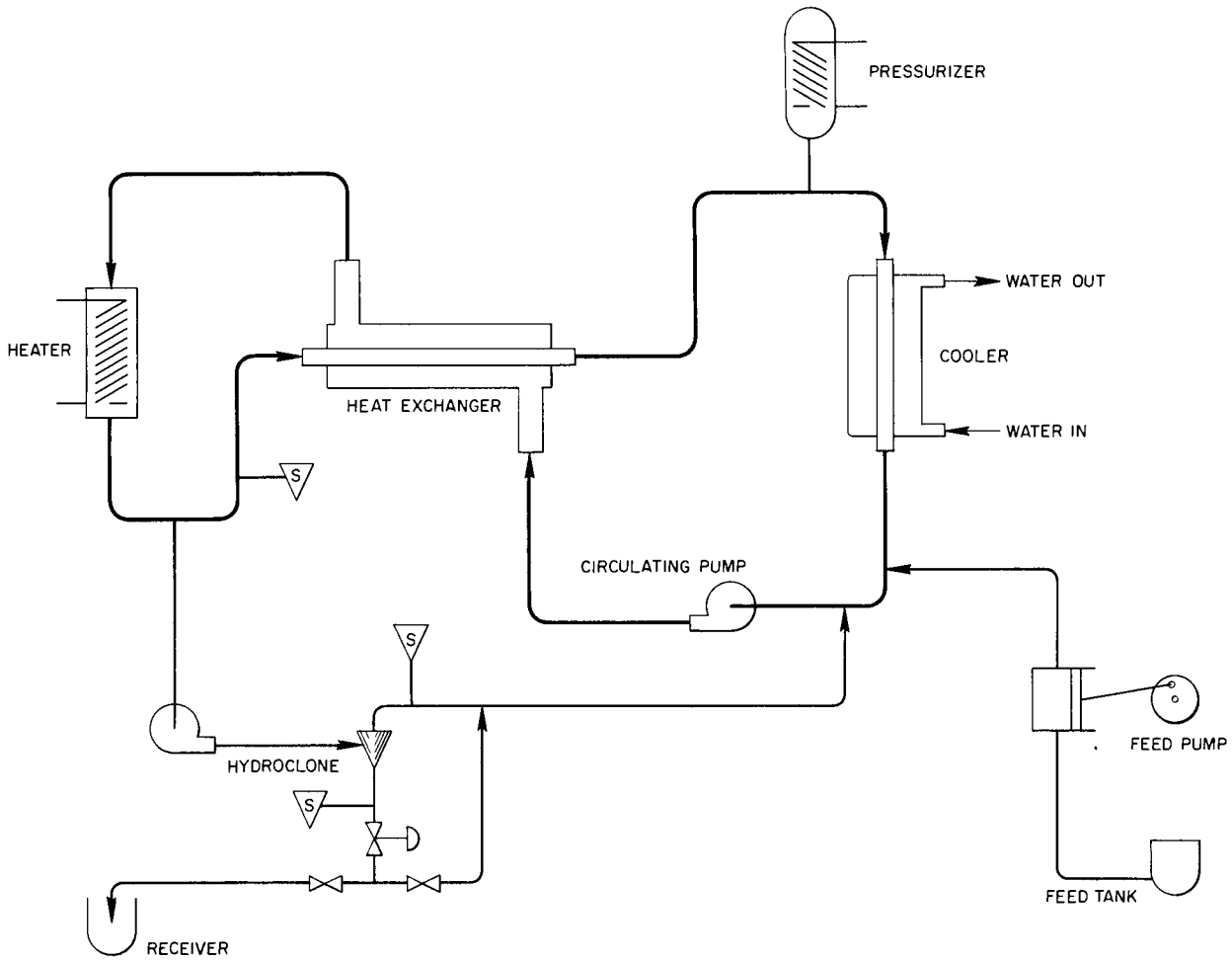

Fig. 12.4. Loop B, Schematic Drawing.

13. DECONTAMINATION OF THE HRE

D. E. Ferguson
D. O. Campbell C. W. Green

On zirconium, titanium, and types 347 and 304L stainless steel specimens that had been in the HRE circulating-fuel system during most of its operation, niobium and zirconium accounted for more than 95% of the radioactivity remaining after decontamination with several cycles of 8 *m* nitric acid followed by alkaline-tartrate-peroxide solution. This remaining activity could be removed only by removing the corrosion film from the metals. In the zirconium and titanium specimens the ratio of radioactive niobium to zirconium was about 3:2, the ratio expected from the HRE at that time; both stainless steels had a niobium-to-zirconium ratio of 4:1, which indicated that the stainless steel had selectively adsorbed niobium or that zirconium was selectively removed during decontamination.

Zirconium and titanium resisted further decontamination because they could not be descaled easily by the usual methods. The stainless steels could be descaled and further decontaminated by a factor of greater than 100 by 1.2 *m* HCl–1.8 *m* H_2SO_4 reagent, by concentrated sulfuric acid at about 150°C in a few minutes, by 3% HF–20% HNO_3 in about six days at room temperature, or by from 1 to 5% oxalic acid at 70°C, which replaced the rust-red oxide with a gray γ-Fe_2O_3 film, in 5 to 20 hr, depending on the concentration. The oxalic acid is less corrosive in use than the mineral acids, and it can be destroyed with hydrogen peroxide, leaving a noncorrosive waste to be stored.

14. WORK OF VITRO LABORATORY[1]

14.1 PILOT-PLANT MODIFICATIONS

The equipment originally set up to study the calcium fluoride process is being modified so that the precipitation of rare-earth sulfates in a circulating loop system at high temperature can be studied. Provisions are being made to permit the collection of samples of such precipitates in amounts large enough for study of the physical properties of the solids. It is intended that this equipment will be used to study the behavior of other fission and corrosion products as well as rare earths.

14.2 IODINE REMOVAL

When simulated fuel solutions containing either iodide or iodate were heated to 310°C for 45 min and then cooled, the solutions contained free iodine. Iodine was partially removed from the solutions when stainless steel coupons were in contact with them during the heating. Unpassivated coupons were severely oxidized; passivated coupons were also oxidized but less severely.

When metallic silver, as wire or silver-impregnated Alundum pellets, was contacted at 310°C with a simulated uranyl sulfate fuel solution containing iodate, most of the iodine was removed from solution, but substantial amounts of silver were dissolved (1.34 and 1.46 g of silver per kilogram of water in two separate experiments). Treatments at 100°C did not remove the iodine.

When silver wire was contacted with the vapor, containing oxygen, above a simulated fuel solution at 310°C for 45 min with an initial iodate concentration of 0.2 g per kilogram of H_2O and heated to 310°C for 45 min, 80 to 85% of the iodine was removed from solution. Eighty per cent of the iodine initially present as iodate (0.2 g per kilogram of H_2O) was removed by heating the solution to 310°C for 45 min with a length of silver wire in the vapor phase only. Silver dissolution to the extent of 50 and 0 ppm was experienced in two separate tests.

[1] W. A. Bain, *HR Fuel Reprocessing Quar. Prog. Rep. Oct. 30, 1954*, KLX-1732.

Part VI

SUPPORTING CHEMICAL RESEARCH

E. H. Taylor

15. RADIATION CHEMISTRY STUDIES

J. W. Boyle H. A. Mahlman

15.1 REACTOR IRRADIATIONS OF CHROMATE SOLUTIONS

Because uranyl chromate or dichromate solutions are of possible interest as homogeneous reactor fuels and because the behavior of chromate under conditions of reactor irradiation is pertinent to the study of the corrosion of stainless steel, a number of samples have been irradiated in the ORNL Graphite Reactor and in the LITR. Samples were placed in quartz ampoules, frozen, pumped to remove the air, and sealed prior to irradiation. The pertinent data and results are given in Table 15.1.

The sample irradiated in the LITR was brown upon removal from the reactor and had some precipitate present, which was removed by centrifugation before the sample was diluted and measured on the spectrophotometer at 3500 Å. Because the sample went into the reactor at room temperature, it is possible that, before the sample warmed up thermally, enough hydrogen peroxide was formed to cause precipitation. Samples of similar appearance occur when hydrogen peroxide is added to 0.05 *M* $UO_2Cr_2O_7$ solutions in the cold. Also, the yield of 1.1 may be high, because the energy input into the solution in the LITR is not too well known.

The rate of reduction seemed to be constant in the Graphite Reactor for 15-min and 1-hr irradiations. The difference in the yields between the 5.04×10^{-2} and the 5.04×10^{-4} *M* $UO_2Cr_2O_7$ samples may be due to several reasons: (1) a concentration effect – the higher concentration was reduced at a faster rate; (2) a pH effect – more acid solutions of chromate reduce at a faster rate below a pH of 3; (3) type of radiation effect – around 30% of the energy is from fission recoils in the more concentrated solution, compared with very little in the dilute solutions. This heavy-particle radiation probably enhances the Cr^{6+} reduction.

15.2 RADIATION STUDIES ON THORIUM NITRATE SOLUTIONS

Additional radiation experiments this past quarter have verified the N_2 and H_2 yields for thorium

TABLE 15.1. REACTOR IRRADIATION OF CHROMATE SOLUTIONS

Solution	pH	Radiation Source and Time	Temperature (°C)	Energy Input		Reduction, Cr^{6+} Disappearance, per 100 ev
				Watts/g/sec	Fission Energy (%)	
5.04×10^{-2} *M* $UO_2Cr_2O_7$	2.20	LITR at one-half power, 20 min	25–150	0.25	≅20	1.1
5.04×10^{-2} *M* $UO_2Cr_2O_7$	2.20	Graphite Reactor, 15 and 60 min	130 ± 5	0.007	≅30	0.7
5.04×10^{-4} *M* $UO_2Cr_2O_7$	2.38*	Graphite Reactor, 10 min	130 ± 5	0.0045	<1	0.3
$5. \times 10^{-4}$ *M* $K_2Cr_2O_7$	2.38*	Graphite Reactor, 10 min	130 ± 5	0.0045	0.0	0.3
10^{-3} *M* K_2CrO_4; 0.02 *M* $CuSO_4$; 0.126 *M* UO_2SO_4	2.8	Graphite Reactor, 10 min	130 ± 5	0.01	≅55	0.5

*Adjusted with H_2SO_4.

nitrate solutions containing uranium[1] and have shown that the yields for pure thorium nitrate solutions may vary considerably for duplicate samples. The values for the uranium-containing samples are probably initial yields, whereas the values for pure thorium nitrate may not be. The H_2 and N_2 yields for 5.8 *m* $Th(NO_3)_4$ solutions reported previously[1,2] should be revised. The number of molecules of hydrogen produced per 100 ev of energy absorbed should be 0.2 instead of 0.04, and the yield for nitrogen should be 0.02 instead of 0.002 to 0.005.

Potassium bromide, 0.02 *m*, was added to several ampoules to minimize the back reaction and thereby give reproducible initial yields of nitrogen and hydrogen. In two instances bromide addition lowered the hydrogen yield instead of enhancing it as was expected. Significant amounts of CO_2 found in these same samples indicated that organic impurities may have entered the mechanism of nitrate reduction in some way and thus cast doubt on the validity of the experiment. A third bromide sample gave the same nitrogen and hydrogen yields as a duplicate sample without bromide.

The nitrite ion is one of the reduction products produced by x or gamma radiation on nitrate solutions. It was thought that if the nitrite ion were involved in the mechanism of N_2 formation then the N_2 yield should be lowered when some material was present during irradiation which would oxidize nitrite to nitrate. Potassium bromate, 0.09 *M*, was added to a sample of 5.8 *M* thorium nitrate containing 1 g of U^{235} per liter to test this hypothesis. Nitrogen and hydrogen yields identical with those from solutions without the bromate were obtained. This suggests that N_2 might be formed by direct dissociation of the nitrate ion to nitrogen and oxygen rather than through the nitrite mechanism. The bromate experiment also indicates that neither bromide ion nor an excess of oxygen will have much effect on the N_2 yield, since a considerable amount of bromide ion and approximately 0.6 atm of O_2 were present at the end of the radiation.

Future studies will be directed toward obtaining initial yield values for pure thorium nitrate solutions, understanding the apparent anomalies in some of the bromide solutions, and determining the mechanism of N_2 formation.

[1] J. W. Boyle and H. A. Mahlman, *HRP Quar. Prog. Rep. July 31, 1954*, ORNL-1772, p 165.

[2] J. W. Boyle, *HRP Quar. Prog. Rep. April 30, 1954*, ORNL-1753, p 147.

16. EFFECTIVE CAPTURE CROSS SECTION OF Np^{239}

J. Halperin
D. E. Ferguson D. R. Hendrix
D. C. Overholt C. M. Stevens[1]
R. W. Stoughton

A preliminary measurement has been made of the effective capture cross section of Np^{239} for thermal reactor neutrons. Two-hundred-gram slugs of U^{238} were irradiated for times varying from 0.5 to 17 days in the high-flux region of the LITR. After adequate cooling, the plutonium that had been formed was chemically separated from the uranium and analyzed mass spectrographically for its Pu^{240} content.

The thermal flux was inferred from the plutonium production by using a calculated value for the effective capture cross section for U^{238} of 3.5 barns. On the basis of this value, effective capture cross sections of 380 ± 40 barns and 80 ± 20 barns were found for Pu^{239} and Np^{239}, respectively.

A detailed account of this work will soon be submitted to *Reactor Science and Technology*.

[1]Argonne National Laboratory.

17. THE SYSTEM UO_3-SO_3-H_2O

G. M. Herbert D. W. Sherwood
C. H. Secoy

Experiments to determine the volume of uranyl sulfate solutions as a function of concentration, temperature, and fractional filling of sealed vessels have been initiated and are continuing. Several mechanical difficulties have developed, necessitating refurbishing the apparatus to shield against heat radiation from the furnace walls and to provide a means of shaking the apparatus to complete the separation of the two liquid phases formed, since droplets of either phase tend to stick to the walls and remain in the region of the other phase. Radiant heating was found to cause marked distillation in the quartz tubes used, and differential thermocouple measurements indicated the temperature differential present between the ends of a 3-in. tube (in a large furnace with rapid air circulation) to be about 0.14°C. Yet, even this small difference caused relatively rapid distillation of water to the top of the tube. Increased shielding between the tubes and the furnace walls overcame the difficulty and allowed the circulating air in the furnace to provide the desired temperature control.

The initial observations that had been made confirm the reasoning which indicated the necessity for measurement of pressure and phase volume as a function of the fractional filling of the container.

Volume-vs-temperature data for 0.255 and 3.03 *m* uranyl sulfate solutions are shown in Figs. 17.1 and 17.2, respectively. It is evident in both figures that the apparent rate of expansion varies markedly with the initial filling fraction. Figure 17.2 shows that, if the container is only about one-quarter filled, loss of material to the vapor phase more than equals the thermal expansion of the remaining liquid and that this phase actually undergoes a loss in net volume with increasing temperature. At about 30 to 35% filling, the two effects (evaporation and expansion) seem to be nearly equal. Only at the highest fractional fillings shown in Fig. 17.1

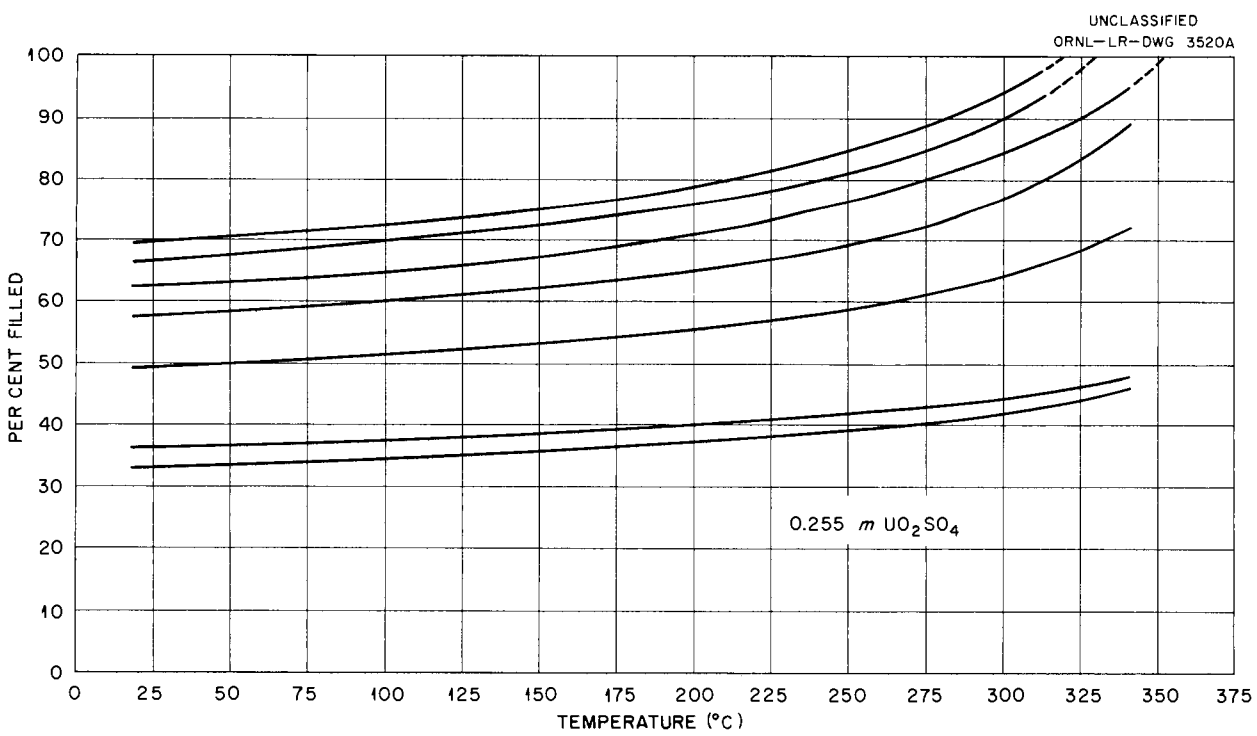

Fig. 17.1. Thermal Expansion of 0.255 *m* UO_2SO_4 Solutions.

is an expansion comparable to the true thermal expansion of the solutions observed.

It may also be noted that the 0.255 *m* solution shows a greater apparent degree of expansion than the more concentrated 3.03 *m* solution when the initial fractional filling is about the same. Apparent expansion coefficients are being calculated as a function of fractional filling and will be reported as the data are completed. The present figures show data which are consistent within themselves but not absolute with regard to the initial fractional filling, since the work has not progressed far enough yet to allow correction for the decreased volumes at the ends of the tubes. Future expansion coefficients will contain this correction.

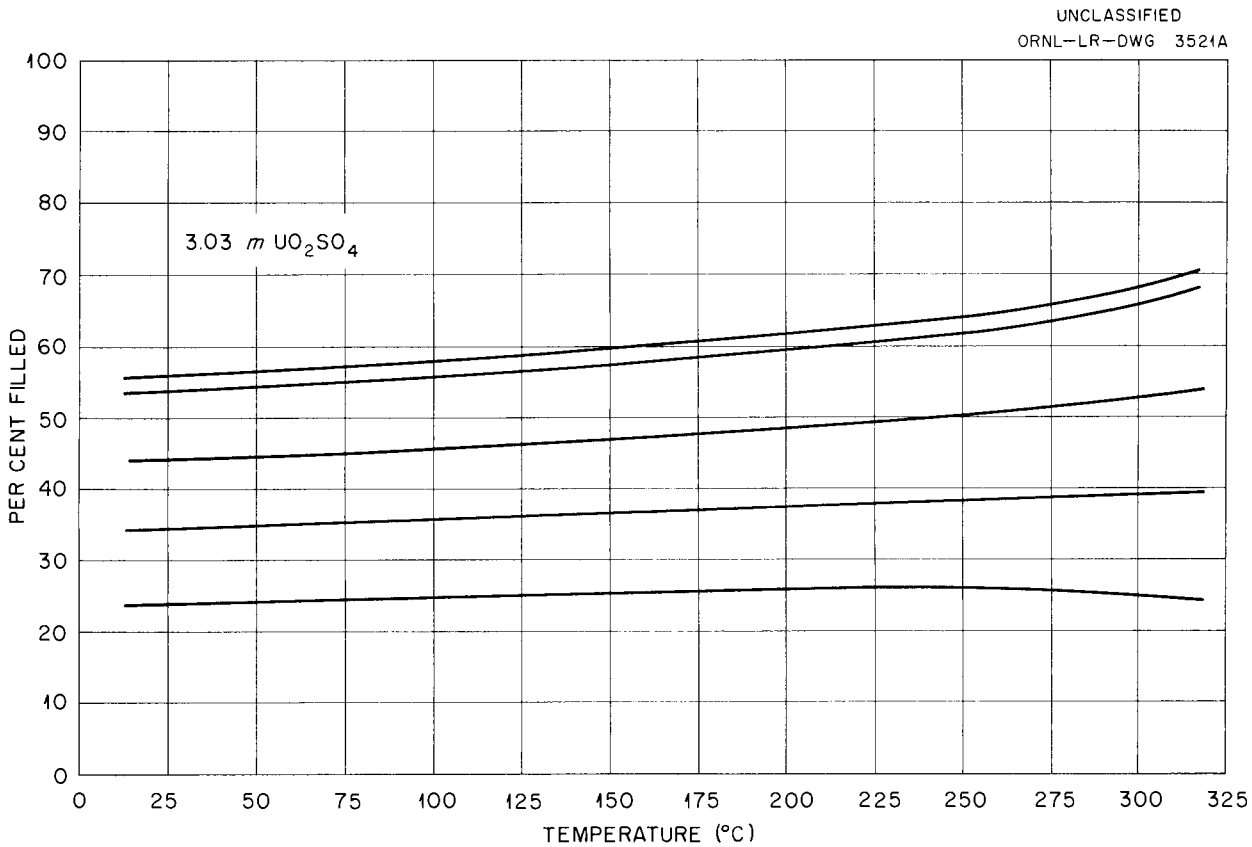

Fig. 17.2. Thermal Expansion of 3.03 *m* UO_2SO_4 Solutions.

18. THE SYSTEM $NiO-UO_3-SO_3-H_2O$

E. V. Jones J. S. Gill
C. H. Secoy

The solubilities of NiO, UO_3, or mixtures of the two in uranyl sulfate solutions of varying concentration have been determined for about 90 different mixtures at 25°C and for several mixtures at 175 and 250°C. Compositions of the wet residues have been determined simultaneously. Equilibration times allowed have been approximately two weeks.

An analysis of the 25°C data shows that equilibrium was not reached. The tie lines are erratic and indicate that slow transformation of the solid oxide(s) to complex salts was in progress. The compositions of the liquid phase, however, are believed to be nearly correct and indicate that the solubility surface is nearly a plane surface.

Data at 175 and 250°C are presented in Tables 18.1 and 18.2, respectively. Extrapolation of tie lines gives clear evidence of the existence of at least three complex salts having the compositions: $NiO{\cdot}UO_3{\cdot}SO_3{\cdot}xH_2O$, $NiO{\cdot}2.5UO_3{\cdot}SO_3{\cdot}6H_2O$, and $NiO{\cdot}4UO_3{\cdot}2SO_3{\cdot}xH_2O$. Since only limited regions have been studied, several additional complex salts may exist. As at 25°C, the solubility surface does not depart markedly from a plane, the solubility of the oxides decreasing with increasing temperature.

Study of the stoichiometric $NiSO_4-UO_2SO_4-H_2O$

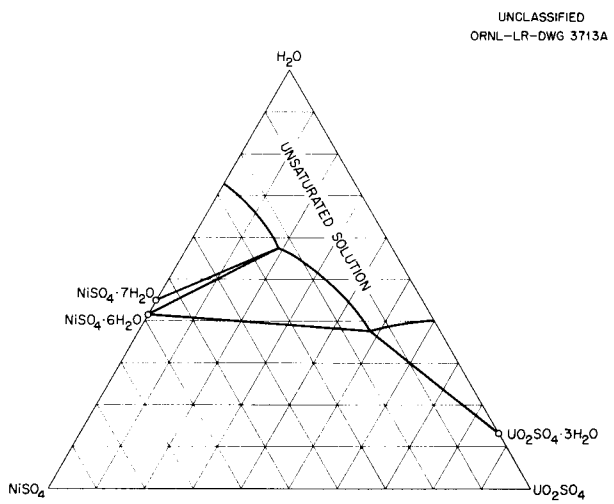

Fig. 18.1. The System $NiSO_4-UO_2SO_4-H_2O$ at 25°C. Compositions plotted in weight per cent.

TABLE 18.1. THE SYSTEM $NiO-UO_3-SO_3-H_2O$ AT 175°C

Experiment No.	Composition of Liquid Phase (%)			Composition of Wet Residues (%)			Solid Phase
	NiO	UO_3	SO_3	NiO	UO_3	SO_3	
C-14	2.63	0.94	3.04				
-11	2.67	9.80	5.11				
-15	0.451	0.090	0.788	13.11	40.01	10.50	Unidentified
-3	1.32	21.13	6.72	5.98	70.41	10.25	
-13	3.55	2.77	4.37	7.64	49.63	8.33	$NiO{\cdot}2.5UO_3{\cdot}SO_3{\cdot}6H_2O$
-12	2.53	7.43	4.42	5.85	38.81	7.17	
-10	2.22	12.60	5.37	6.74	57.80	8.75	
-8	2.04	16.39	5.71	4.20	62.12	8.67	$NiO{\cdot}4UO_3{\cdot}2SO_3{\cdot}xH_2O$
-9	2.22	14.39	5.87	4.33	59.48	9.67	
-7	1.80	17.76	6.16	3.56	59.12	8.00	
-6	1.60	19.78	6.47	2.80	60.80	8.33	
-4	1.54	21.48	6.65	3.31	70.89	10.42	
-2	1.31	22.62	6.96	4.28	70.68	12.08	

system at 25°C has been completed, and the phase diagram is shown in Fig. 18.1. The tentative diagram given in a previous report[1] was in error in several respects. The only solid phases appearing in this system are $UO_2SO_4 \cdot 3H_2O$, $NiSO_4 \cdot 6H_2O$, and $NiSO_4 \cdot 7H_2O$. Some data have been obtained at 100°C but not in sufficient quantity to present the phase diagram.

[1] D. W. Sherwood and C. H. Secoy, *HRP Quar. Prog. Rep. Oct. 31, 1953*, ORNL-1658, p 92–93.

TABLE 18.2. THE SYSTEM $NiO-UO_3-SO_3-H_2O$ AT 250°C

Experiment No.	Composition of Liquid Phase (%)			Composition of Wet Residues (%)			Solid Phase
	NiO	UO_3	SO_3	NiO	UO_3	SO_3	
A-33	0.181	0.672	0.296	12.22	48.18	13.08	$NiO \cdot UO_3 \cdot SO_3 \cdot xH_2O$
-32	0.219	0.631	0.319	11.96	45.42	13.08	
-31	0.216	0.465	0.438	13.24	54.07	14.75	
-30	0.290	1.41	0.671	11.58	46.02	13.25	
-29	0.494	1.91	1.13	9.93	49.27	12.83	Unidentified
-28	0.629	2.94	1.53	13.24	59.24	15.17	
-27	1.09	4.94	2.50	10.69	50.95	12.00	
-26	1.50	5.76	3.25	8.91	61.88	10.33	
-23	1.53	8.47	3.83	8.65	59.72	11.08	
-24	1.73	9.09	4.17	8.40	58.88	9.83	
-22	1.63	9.17	4.20	9.04	59.72	11.17	
-20	1.67	9.60	4.25	8.78	69.93	11.33	
-4	1.52	10.61	4.37	8.02	62.48	10.00	
-2	1.87	12.63	5.24	8.27	69.09	9.75	
-21	1.30	7.65	3.38	7.64	64.53	11.50	$NiO \cdot 2.5UO_3 \cdot SO_3 \cdot 6H_2O$
-18	1.47	9.80	3.89	6.49	62.12	10.92	
-25	1.65	8.60	4.02	7.51	66.69	9.92	
-19	1.74	10.66	4.53	7.25	63.80	10.75	
-3	1.88	11.73	5.07	7.25	69.21	10.67	
-16	1.93	12.65	5.34	6.36	65.13	10.00	
-12	1.40	17.20	5.66	7.00	68.73	11.92	
-15	1.63	15.01	5.68	7.13	71.62	10.42	
-17	2.15	12.97	5.69	6.74	62.60	8.92	
-13	1.68	17.25	6.10	6.49	64.41	9.33	
-11	1.40	19.24	6.15	6.74	64.89	10.75	
-10	1.27	20.25	6.27	7.00	66.69	10.08	
-1	1.40	21.14	6.45	7.00	67.29	9.67	
-7	1.05	23.14	6.69	6.11	68.85	9.83	
-8	1.23	22.49	6.69	4.07	50.11	8.67	

19. THE SYSTEMS $CuO-SO_3-H_2O$ AND $CuO-UO_3-SO_3-H_2O$

F. E. Clark C. H. Secoy

There are approximately 35 individual basic cupric sulfates and hydrated basic cupric sulfates listed by Gmelin.[1] Because these reported compounds were produced by reacting such compounds as NH_4OH, LiOH, NaOH, KOH, $Cu(OH)_2$, MnO, CoO, CuO, etc. with $CuSO_4$ under a wide variety of conditions with respect to temperature, pressure, reactor vessels, and analytical methods, the state of basic cupric sulfate in the system $CuO-SO_3-H_2O$ is still a subject of disagreement in the literature. There is also lack of agreement concerning equilibration times; reported values range from a few days to more than two years at 25°C and from a few hours to two weeks at 200°C. It seems very reasonable to assume that much of this disagreement exists because the manner of preparation of the basic cupric sulfate may have appeared to the chemist to be a relatively simple chemical reaction, while it was really an equilibrium reaction not allowed to go to completion before analysis. A survey of the literature to date concerning the system $CuO-SO_3-H_2O$ indicates some disagreement as to whether true compounds such as $4CuO{\cdot}SO_3{\cdot}xH_2O$ and $3CuO{\cdot}SO_3{\cdot}xH_2O$ are formed or whether the precipitate is a true solid solution.

It was decided to investigate the $CuO-SO_3-H_2O$ system at 25°C, in order to obtain experience relative to the equilibration time and the equipment design and to determine the most accurate, precise, and economic analytical methods that might be applicable to this system and later extrapolated into the study of the four-component system, $CuO-UO_3-SO_3-H_2O$. An initial quantitative investigation has produced the data in Table 19.1.

Conclusions that can be drawn from the above data are in partial agreement with those reported by Young and Stearn[2] to the extent that the copper content of the precipitated basic salt increases directly as the quantity of CuO added to the starting solutions is increased and that, as the quantity of CuO in the salt increases, the H_2O content shows a decrease. Both x-ray diffraction and analytical data tend to indicate incomplete equilibration. Therefore, even though the data are not adequate to settle the long-standing uncertainty with regard to the true composition of the solid phase, the solution phase data are believed to be essentially correct and are presented in their entirety in Table 19.1 to show the uniform CuO-to-SO_3 mole ratio of essentially 1.00 over the entire concentration range. The values for specific gravity are satisfactorily uniform and in agreement with literature values for stoichiometric $CuSO_4$ solutions.

Due to the excessively long equilibration times necessary in this system, no additional work at 25°C is planned. Instead, some preliminary work on the four-component system $CuO-UO_3-SO_3-H_2O$ has been done. This work has revealed that the initial rate of reaction of a solution of uranyl sulfate upon black CuO is rapid and that under the proper conditions a solid gel will result at 25°C. It is also indicated that a basic cupric sulfate appears to precipitate from a solution of $CuSO_4$ upon the addition of UO_3-H_2O.

[1] (Gmelin-Kraut's), *Handbuch der anorganischen Chemie*, Band V, Part I, p 830–839, Carl Winter's Universitatsbuchhandlung, Heidelberg, 1909.

[2] S. W. Young and A. E. Stearn, *J. Am. Chem. Soc.* **38**, 1947-1953 (1916).

TABLE 19.1. THE SYSTEM $CuO-SO_3-H_2O$ AT 25°C

Experiment No.	Solution Phase					Wet Residue		Remarks
	CuO (wt %)	SO_3 (wt %)	Mole Ratio, $CuO:SO_3$	Specific Gravity	pH	CuO (%)	SO_3 (%)	
184	4 (ppm)	0		0.9963	7.3			
175	0.44	0.45	0.9966	1.0060	4.37	30.40	8.43	
139	0.45	0.44	1.0283	1.0059	4.28	20.77	5.75	X-ray pattern – same as for No. 133
138	0.87	0.84	1.0381	1.0134	4.09	15.16	4.68	
137	0.94	0.92	1.0362	1.0140	4.11	12.84	4.01	
136	0.96	0.94	1.0323	1.0164	4.05	9.99	4.03	
135	0.98	0.96	1.0256	1.0173	4.09	9.05	3.45	
174	0.96	0.98	0.9871	1.0152	4.16			
134	0.99	0.98	1.0177	1.0175	4.18			
145	1.53	1.51	1.0186	1.0282	4.02	10.77	3.89	X-ray pattern – same as for No. 133
177	1.54	1.56	0.9931	1.0287	3.91	15.87	5.28	
144	1.92	1.89	1.0194	1.0370	3.95	10.94	4.24	
143	2.01	1.97	1.0284	1.0375	3.92	7.67	3.43	
142	2.02	1.99	1.0182	1.0380	3.95	6.66	3.21	
141	2.03	2.01	1.0161	1.0385	3.95	4.66	3.00	
176	2.03	2.04	1.0012	1.0391	4.10			
140	2.05	2.03	1.0176	1.0380	3.91			
151	2.33	2.33	1.0058	1.0452	3.83	14.48	5.27	X-ray pattern – same as for No. 133
179	2.35	2.36	1.0011	1.0457	3.80	15.34	5.55	
150	2.70	2.65	1.0260	1.0527	3.80	12.38	5.15	
149	2.77	2.76	1.0099	1.0542	3.80	8.65	4.47	
148	2.79	2.77	1.0106	1.0550	3.78	7.84	4.22	
147	2.79	2.80	1.0059	1.0563	3.82	5.83	4.78	
146	2.82	2.80	1.0145	1.0558	3.68			
178	2.81	2.82	1.0009	1.0560	3.96			
181	3.17	3.19	1.0003	1.0646	3.72	19.50	7.07	
157	3.20	3.18	1.0133	1.0636	3.76	19.70	8.19	X-ray pattern of $4CuO \cdot SO_3 \cdot 3H_2O$ plus lesser amount of impurity than for No. 126-1
133	3.37	3.38	1.0036	1.0690	3.95	22.80	8.84	X-ray pattern of $4CuO \cdot SO_3 \cdot 3H_2O$ plus lesser amount of impurity than for No. 126-1
132	3.41	3.41	1.0066	1.0700	3.92	29.99	12.47	
156	3.55	3.52	1.0132	1.0713	3.71	11.78	5.53	Not single phase by x-ray pattern; $4CuO \cdot SO_3 \cdot 3H_2O$ plus major impurity; sample dried out while x ray was run
155	3.60	3.58	1.0120	1.0726	3.70	12.62	6.18	
154	3.62	3.61	1.0094	1.0744	3.78	8.46	5.03	
153	3.63	3.62	1.0088	1.0740	3.72	6.37	4.40	
152	3.65	3.64	1.0088	1.0750	3.55			
180	3.65	3.67	1.0025	1.0743	3.60			
131	3.73	3.75	1.0008	1.0766	3.89	27.44	12.04	

TABLE 19.1. (continued)

Experiment No.	Solution Phase					Wet Residue		Remarks
	CuO (wt %)	SO_3 (wt %)	Mole Ratio, $CuO:SO_3$	Specific Gravity	pH	CuO (%)	SO_3 (%)	
130	3.93	3.95	1.0015	1.0810	3.89	27.85	12.09	X-ray pattern – not single phase; $4CuO \cdot SO_3 \cdot 3H_2O$ plus major impurity (or impurities)
183	4.10	4.13	1.0000	1.0853	3.68	19.61	7.66	
129	4.14	4.14	1.0066	1.0862	3.82	25.62	11.55	
128	4.23	4.25	1.0019	1.0870	3.83	23.88	11.31	
126-L	4.38	4.32	1.0090	1.0902	3.85	18.41	9.21	
126-1	4.39	4.39	1.0059	1.0900	3.90	22.11	9.93	X-ray diffraction pattern of $4CuO \cdot SO_3 \cdot 3H_2O$ plus small amount of impurity; incomplete equilibration
124	4.47	4.46	1.0077	1.0923	4.04	24.08	11.58	
123-L	4.51	4.49	1.0111	1.0922		17.49	8.70	X-ray pattern of $4CuO \cdot SO_3 \cdot 3H_2O$ plus impurity
123	4.52	4.50	1.0095	1.0923	4.28	15.55	15.24	
122	4.50	4.54	0.9991	1.0937	3.97			
127	4.53	4.54	1.0044	1.0961	3.45			
182	4.52	4.56	0.9993	1.0947	3.52			
173	4.72	4.77	0.9959	1.0996	3.82	31.27	11.74	
172	4.99	5.04	0.9968	1.1053	3.75	29.31	13.44	
2-P7	5.99	5.69	1.0588	1.1298		29.04	11.45	
171	6.03	6.07	1.0003	1.1304	3.72	30.06	14.19	
170	8.06	8.07	1.0045	1.1803	3.60	30.15	14.68	
169	8.64	8.65	1.0045	1.1936	3.51	30.14	14.73	
168	9.08	9.10	1.0052	1.2037	3.44	27.09	14.21	
167	9.18	9.18	1.0056	1.2079	3.48	19.39	12.70	
166	9.23	9.21	1.0083	1.2099	3.44	18.74	14.56	
164	9.22	9.24	1.0048	1.2095	2.98			
165	9.26	9.22	1.0112	1.2103	3.47			

20. THE SYSTEM UO_3-CrO_3-H_2O

C. H. Secoy

F. J. Loprest W. L. Marshall

The system UO_3-CrO_3-H_2O has been explored in the past for possible use as a homogeneous reactor fluid.[1,2] In the previous investigations it was shown that soluble mixtures of uranium trioxide, chromium trioxide, and water appeared to be phase-stable at least up to 300°C and, except for a small amount of precipitation and/or decomposition, even above the critical temperature.

Further consideration has been given to this system based on the following possible advantages.

1. The solubility of uranium trioxide in chromic acid solution is high, probably of the order of 500 to 1000 g of uranium per liter at 100°C. The solubility apparently remains high even at temperatures approaching the critical temperature of the system. The Cr:U ratios necessary to produce this high solubility are of the order of 2:1.

2. The above mixtures of UO_3-CrO_3-H_2O apparently are soluble in the supercritical fluid[2] and, for the most part, are stable at least to 400°C, thus offering a fluid which completely fills the container, has a density of 0.6 to 0.8, a pressure of 3000 to 4000 psi, and probably sufficient H_2O or D_2O molecules per uranium atom for neutron moderation.

3. The presence of the large amounts of chromate in the system, as is the case for many other aqueous systems containing small amounts of chromate, appears to confer a high degree of corrosion resistance even upon carbon steel.

4. The oxidizing power of the chromate ion prevents the reduction of U(VI) to U(IV).

Along with these possible advantages are the following known or possible disadvantages.

1. The small quantity of insoluble brick-red–brown precipitate which has been observed[1,2] may indicate that the chromium in the oxidized state is unstable at elevated temperatures and is undergoing partial reduction. However, experiments performed under oxygen pressure indicate that the oxygen might counteract any tendency toward partial reduction. It remains to be discovered what the effect on the oxidation-reduction stability of chromium will be when various ratios of hydrogen to oxygen are maintained in contact with the solution at high pressures and over the temperature range of interest.

2. The neutron-absorption cross section of natural chromium is 2.9 barns, compared with 0.49 barn for sulfur. However, the separated isotope Cr^{52}, occurring in 83.76% abundance, has a cross section of only 0.72 barn, and the Cr^{54} isotope, although only in 2.38% abundance, has a cross section of only 0.006 barn.

3. The radiation stability of chromate under the conditions of possible use (high fission density but in the presence of dissolved oxygen and hydrogen) has not been established. Preliminary irradiation results are reported in Sec. 15.

It may be mentioned that the ThO_2-CrO_3-H_2O system has been considered as a possible breeder solution in view of the previous work[3] at 25°C. Britton's investigation indicates that concentrations as high as 500 g of thorium per liter may be obtained at room temperature. The mole ratio, CrO_3:Th, however, is of the order of 4:1. The thorium system might be considered in conjunction with the uranium system.

Experimental Data. – Solubility data obtained recently by use of the solution sampling assembly previously described[4] are given in Table 20.1 and indicate that, in solution, mole ratios of Cr:U = 1 possibly will be phase-stable at the elevated temperature. At the present time the two-component system, UO_2CrO_4-H_2O, is being studied as a function of temperature.

An exploration has been completed on the behavior of both mild carbon steel (SAE 1010) and type 304 stainless steel in both UO_2SO_4-H_2O and

[1] C. H. Secoy and J. S. Gill, *Chem. Quar. Prog. Rep. March 31, 1950*, ORNL-685, p 34.

[2] W. L. Marshall, *HRP Quar. Prog. Rep. March 31, 1953*, ORNL-1554, p 105.

[3] H. T. S. Britton, *J. Chem. Soc.* 123, 1429 (1923).

[4] W. L. Marshall, *The pH of UO_3-H_2SO_4-H_2O Mixtures at 25°C*, ORNL-1797 (Oct. 18, 1954).

TABLE 20.1. PRELIMINARY PHASE-SOLUBILITY DATA FOR THE SYSTEM UO_3-CrO_3-H_2O

Temperature (°C)	Total Stirring Time (hr)	Liquid Phase (wt %)		Mole Ratio, UO_3:CrO_3	Total Composition of System (wt %)		Comment
		CrO_3	UO_3		CrO_3	UO_3	
150	3.8	4.618	14.32	1.08	4.373	18.76	Saturated UO_3 hydrate
	19	4.638	14.35	1.08	4.373	18.76	Saturated UO_3 hydrate
	1.5	10.30	25.08	0.85	10.06	24.88	Unsaturated but
	2.5	9.89	24.92	0.88	10.06	24.88	phase-stable
	17	12.80	42.59	1.16	?	42.51	Probably unsaturated
225	3	4.677	12.98	0.97			Probably saturated
		10.42	25.11	0.84			Probably unsaturated
290	4	5.24	12.77	0.85	2.402*	78.02*	Dark red-brown solid with some yellow solid
	15.5	9.81	19.34	0.69			Dark red-brown solid; no
	20.5	9.76	18.24	0.65			yellow solid

*Wet residues.

$UO_2Cr_2O_7$-H_2O solutions with and without added oxygen pressure. These experiments were performed in small, 2.5-cc titanium or stainless steel pressure bombs.[5] The metal specimens were cut from sheet material to approximately 2.6-cm^2 total area, polished with very fine emery paper, degreased with acetone, and weighed on an analytical balance. The specimens were placed in the 2.5-cc bombs, and 1.5 cc of UO_2SO_4 or $UO_2Cr_2O_7$ solution was added. For the oxygen runs, an additional 0.1 cc of 30% cp H_2O_2 was added; upon decomposition, H_2O and O_2 were formed. The bombs were sealed, held in a static system for five days at 265°C, then cooled and opened; the specimens were weighed, electrolytically defilmed with 5% H_2SO_4 containing Rhodine inhibitor, and weighed again. Some conclusions from the experiments are given below.

1. Both carbon steel SAE 1010 and type 304 stainless steel showed a remarkable resistance to corrosion in $UO_2Cr_2O_7$-H_2O solution both in the absence and presence of added oxygen (Table 20.2). There was no indication of corrosion of these specimens when they were examined under the microscope. In contrast, both carbon steel and type 304 stainless steel were corroded severely in UO_2SO_4-H_2O solution in the absence of oxygen. Oxygen added initially as H_2O_2 did not protect the carbon steel from attack by uranyl sulfate but, rather, increased the corrosion rate. The added oxygen, however, did protect the type 304 stainless steel. Comparison pictures of stainless steel and carbon-steel corrosion specimens are shown in Figs. 20.1, 20.2, and 20.3.

2. The $UO_2Cr_2O_7$-H_2O solutions after the runs in the absence of oxygen appeared to be unchanged; however, there was a small amount of brick-red precipitate on the surface of the metal. This precipitate also was observed at higher temperatures during shorter lengths of time in sealed silica tubes. Hydrogen peroxide added to the dichromate solution initially precipitated a solid and reduced chromium(VI) to chromium(III). During the experiment the bulk of uranium and chromate redissolved, and the remaining solid had a yellow-tan color. This observation might indicate reversibility of the reduced chromium(III) to chromium(VI) under oxygen pressure.

3. With the exception of the type 304 stainless steel specimen in UO_2SO_4 with added oxygen, the bulk of uranium precipitated from UO_2SO_4 solutions both for type 304 stainless steel in the absence of added oxygen and for carbon steel 1010 both in the absence and presence of added oxygen.

[5] W. L. Marshall, *HRP Quar. Prog. Rep. March 31, 1954*, ORNL-1554, p 106.

TABLE 20.2. COMPARATIVE CORROSION BEHAVIOR OF CARBON STEEL 1010 AND TYPE 304 STAINLESS STEEL TO 0.50 *m* $UO_2Cr_2O_7$ AND 0.28 *m* UO_2SO_4

Experiment No.	Bomb Material	Specimen and Weight (g)	Solution	Specimen Weight After Defilming (g)	Weight Loss (g)	Approximate Penetration (mils)	Solution Final pH
			With No Oxygen Added				
1	Titanium	CS,* 0.3918	$UO_2Cr_2O_7$	0.3901	0.0017	0.031	1.29
2	Type 347 stainless steel	CS,* 0.3755	$UO_2Cr_2O_7$				1.59
3	Titanium	CS,* 0.3600	UO_2SO_4	0.3210	0.0390	0.80	2.71
4	Titanium	SS,** 0.1359	$UO_2Cr_2O_7$	0.1355	0.0004	0.007	1.30
5	Type 347 stainless steel	SS,** 0.1442	$UO_2Cr_2O_7$				1.40
6	Type 347 stainless steel	SS,** 0.1539	UO_2SO_4	0.1403	0.0136	0.22	3.12
			With Oxygen Added (~250 psi)				
7	Titanium	CS,* 0.4264	UO_2SO_4	0.3504	0.0760	1.4	
8	Titanium	CS,* 0.3999	$UO_2Cr_2O_7$	0.3989	0.0010	0.02	
9	Titanium	SS,** 0.1420	UO_2SO_4	0.1414	0.0006	0.01	

*Carbon steel 1010.
**Type 304 stainless steel.

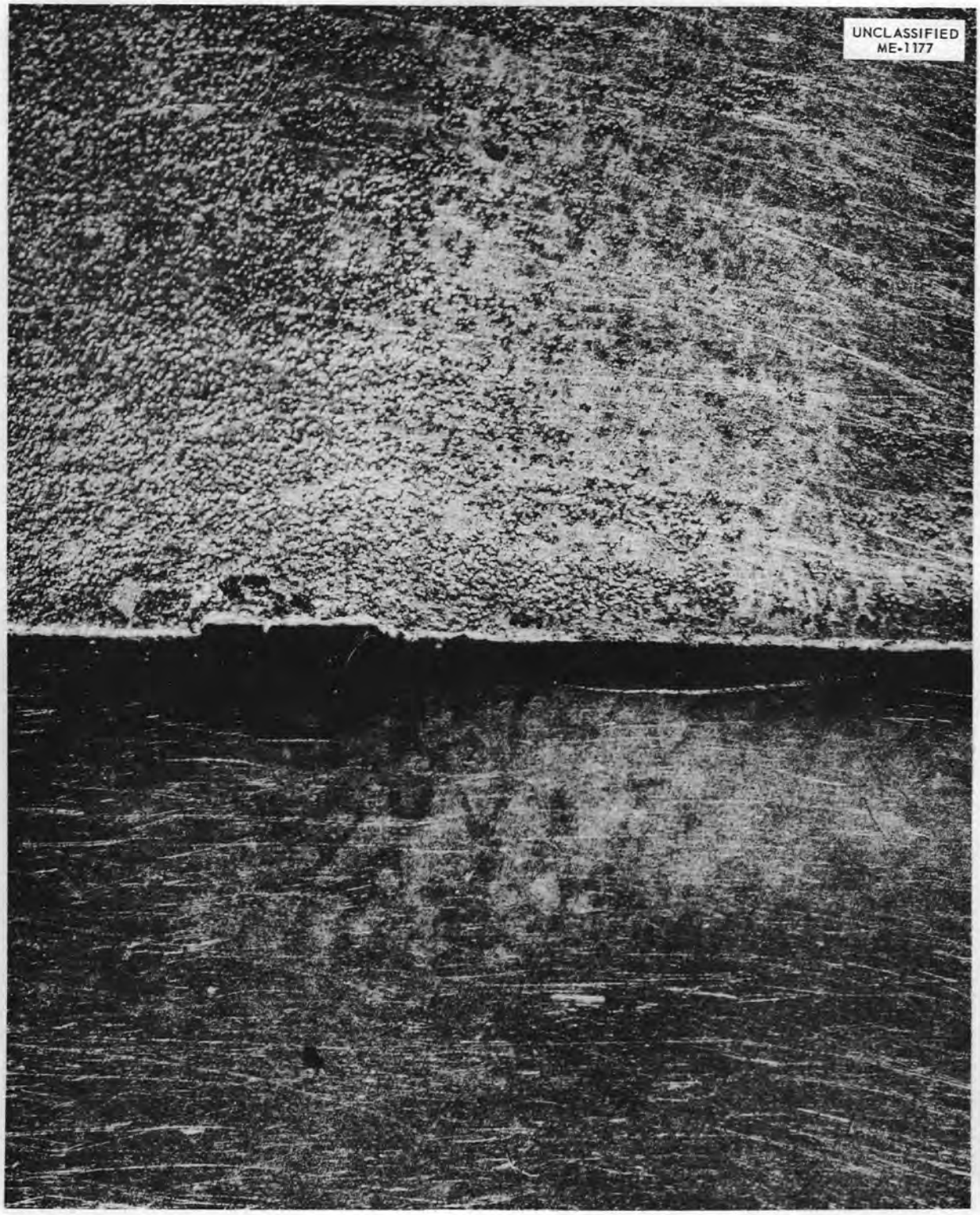

Fig. 20.1. Comparative Metal Surfaces; Type 304 Stainless Steel Specimen in CrO_4 (Experiment No. 4) and SO_4 (Experiment No. 6) Solution; No Oxygen. 50X. Reduced 10.5%.

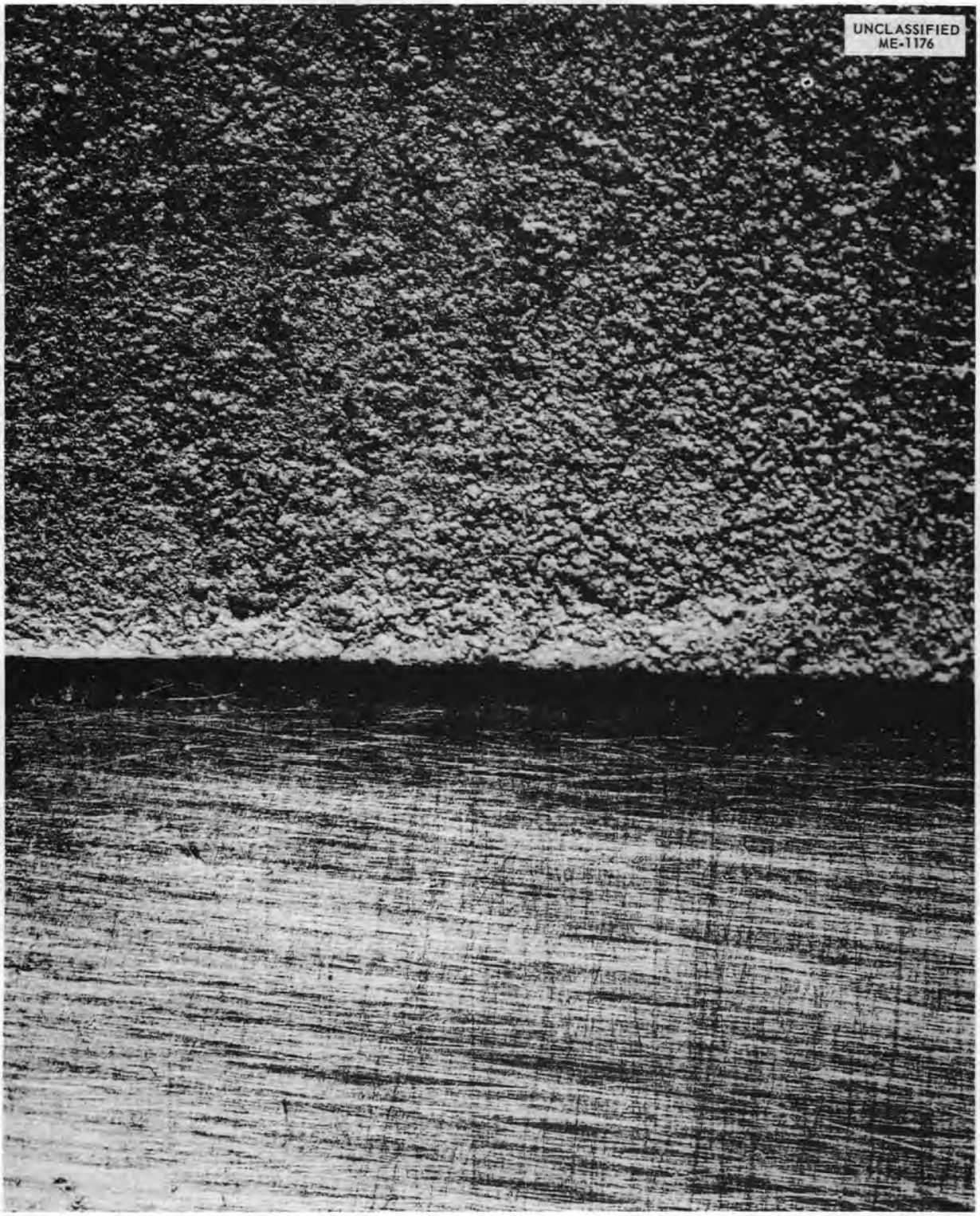

Fig. 20.2. Comparative Metal Surfaces; Carbon Steel SAE 1010 in CrO_4 (Experiment No. 1) and SO_4 (Experiment No. 3) Solution; No Oxygen. 50X. Reduced 10.5%.

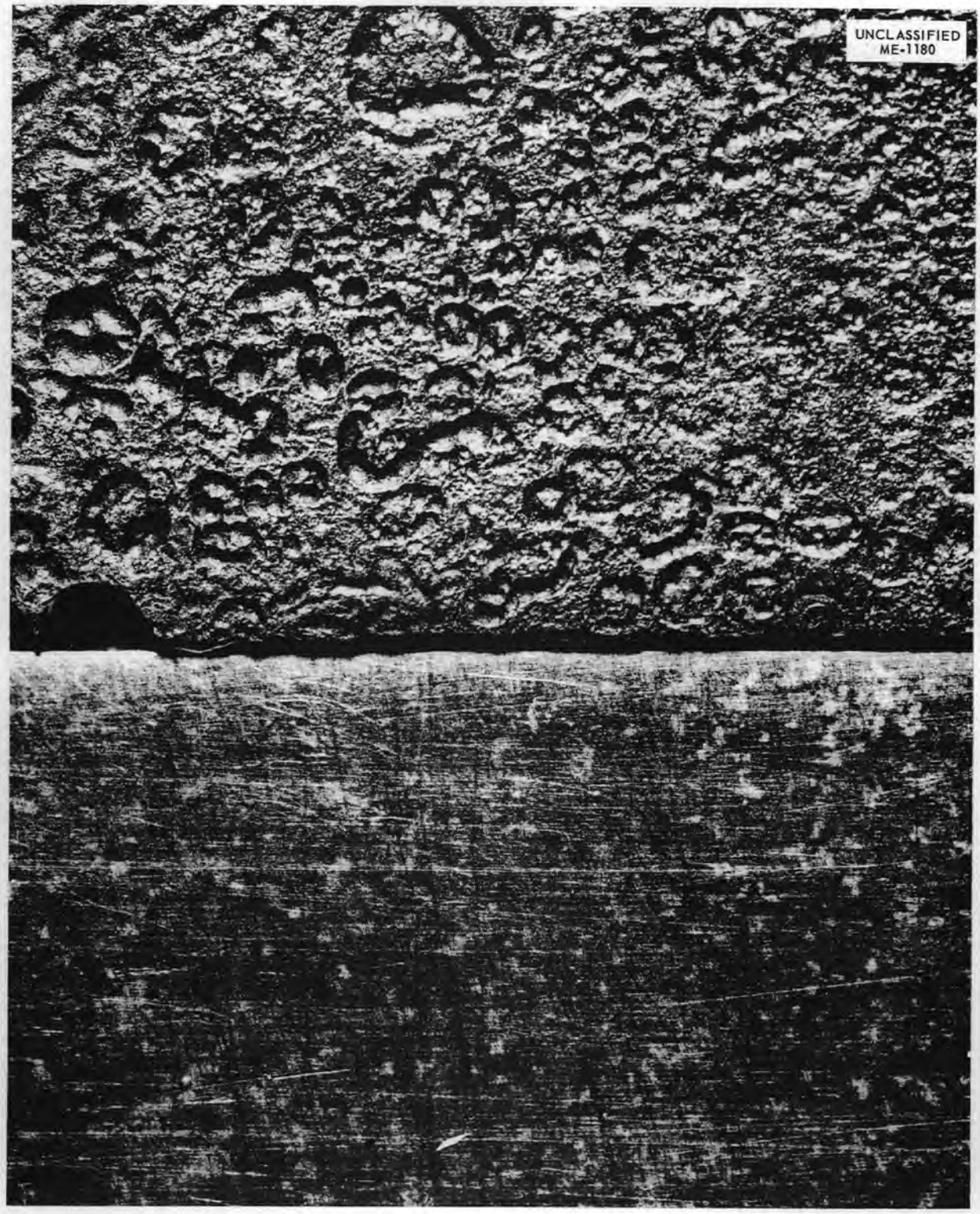

Fig. 20.3. Comparative Metal Surfaces; Carbon Steel SAE 1010 in CrO_4 (Experiment No. 8) and SO_4 (Experiment No. 7) Solution; Oxygen Added. 50X. Reduced 10.5%.

21. CONCENTRATION OF N^{15}

J. S. Drury[1]
G. M. Begun[1] L. L. Brown[1]
A. A. Palko[1]

From a nuclear standpoint the separation of the nitrogen isotopes should be quite worth while. Nitrogen-15 with an abundance of 0.37 at. % has a cross section for the absorption of thermal neutrons of 8×10^{-5} barn, compared with a cross section of 1.78 barns for N^{14}. It has been suggested that nitrate solutions would be useful in homogeneous reactors, especially the breeder type of reactor where a solution of thorium nitrate might be used in the blanket. For this reason, an investigation of possible economic methods of concentrating N^{15} was undertaken with the objective of decreasing the cost of such processes. The early part of this work has been discussed in a previous report,[2] in which numerous literature references are given.

21.1 SEPARATION OF NITROGEN ISOTOPES BY DISTILLATION

L. L. Brown

Distillation will offer an efficient method of isotope concentration if a single-stage separation factor of sufficient magnitude can be obtained. This factor will be large if the vapor pressures of the molecules containing the light and heavy isotopes are sufficiently different. It is difficult to predict these differences theoretically, and the separation factors must be measured experimentally.

A single-stage batch distillation of liquid nitrogen at atmospheric pressure (740 to 745 mm) was performed in this laboratory, and the separation was calculated by means of the Rayleigh equation. Starting with 17,464 g of liquid nitrogen and ending with 53 g, a total separation of 1.017 ± 0.010 (95% confidence interval) was obtained. This gives a calculated α (single-stage separation factor) value of 1.003 ± 0.002 (95% CI). Allowing for an unknown influence of nonequilibrium conditions at some times, pressure fluctuations, oxygen contamination, and the uncertainty of isotopic analysis, the value of α is reasonably close to the 1.004 calculated according to the formula of Kirshenbaum and Urey.[3]

Because of the low separation factor and the expense involved in low-temperature distillations, it was believed that the distillation of liquid nitrogen would not prove to be economically competitive with other nitrogen systems; therefore no more work was done on this system.

The separation factor for the distillation of liquid ammonia given in the literature is even smaller than that for liquid nitrogen and approaches a cross-over point as the pressure becomes higher. It would be interesting to check this point carefully to ascertain whether the equation is accurate in this range. It appears that extremely high pressures would be needed to give appreciable separation in the reverse direction. Because of the low values of separation factor indicated, no experimental work is planned on the distillation of liquid ammonia.

21.2 EXCHANGE IN THE AMMONIA–AMMONIUM CARBONATE SYSTEM

G. M. Begun A. A. Palko

Variations of the ammonia (gas) vs ammonium ion (aqueous) exchange system for nitrogen-isotope concentration have been discussed in a previous report.[2] The following equation illustrates the exchange, with N^{15} becoming concentrated in the aqueous phase as ammonium ion:

$$N^{15}H_3(gas) + N^{14}H_4^{+}(soln) \rightleftarrows N^{14}H_3(gas) + N^{15}H_4^{+}(soln) .$$

It is believed that the best possibility of low-cost production of enriched N^{15} lies in some modification of this basic exchange system.

A proposed ammonia–ammonium carbonate system is shown schematically in Fig. 21.1. It offers the potential advantage of a large reduction of reflux chemical costs as a result of recycling the

[1] Materials Chemistry Division.

[2] A. A. Palko, *Chemical Separation of Isotopes Section Semiann. Prog. Rep. Dec. 31, 1953*, ORNL-1706, p 13.

[3] I. Kirshenbaum and H. C. Urey, *J. Chem. Phys.* 10, 706-17 (1942).

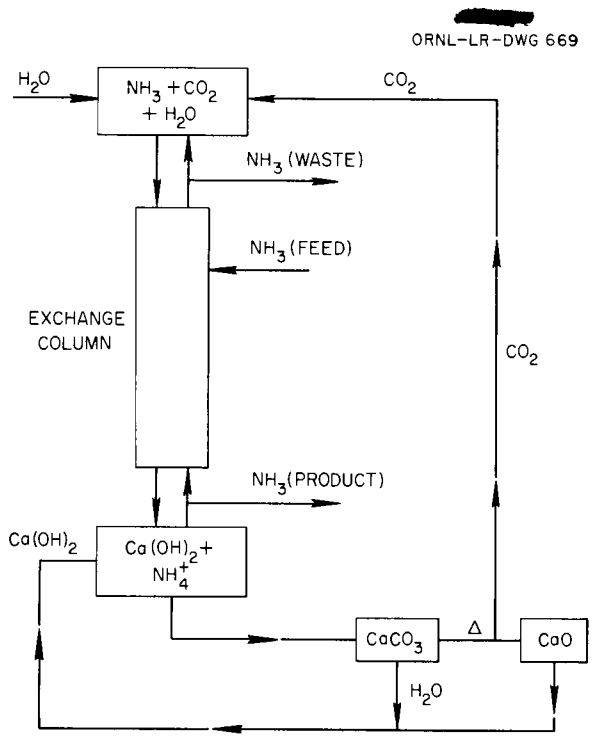

Fig. 21.1. Proposed Ammonia–Ammonium Carbonate Closed System.

chemical products from one end of the system to the other. Preliminary exchange runs on this system, while attempting to use $Ca(OH)_2$ slurry as a refluxing agent, were inconclusive because of the formation of precipitate in the reflux column during the runs. For convenience in operating, NaOH was substituted for $Ca(OH)_2$ as a refluxing agent; then the plugging problem in the reflux column was eliminated. With the use of NaOH a number of exchange runs were carried out in order to evaluate the effective α for the ammonia–ammonium carbonate system.

Since α and N (the number of stages in the exchange column) were both unknown, a number of runs were made to evaluate both unknowns simultaneously by a graphical method. This was done by making a number of runs at the same temperature, pressure, flow rates, and feed concentrations with different, constant product-removal rates. Isotopic samples were assayed and curves for concentration vs time were plotted for each run. From isotopic equilibrium concentrations and the ratio of product removal to interstage flow (D/V), N can be calculated for any assumed α by using the formulas of Shacter and Garrett.[4] These values of N are plotted vs corresponding values of α. Each run gives a different curve. The intersection of these curves gives values of N and α simultaneously. If the runs are perfect and all conditions identical, then the curves should intersect at a single point. However, because of equipment limitations and inaccuracies in analysis, the curves usually intersect in a triangle. The centroid of the triangle may be considered a measure of N and α.

Runs 1 through 7 were made to determine N and α. The data and results are summarized in Tables 21.1 and 21.2 and shown in Fig. 21.2. The flow rates, temperature, pressure, and feed concentrations in the exchange column were kept essentially constant. Product removal was accomplished by bleeding a flow of ammonia gas from the bottom of the exchange column. The rate of removal was kept constant by monitoring the gas flow with a rotameter. Runs were made in which the product withdrawal varied from 0.01 to approximately 23% of the total interstage flow. Table 21.3 is a summary of equilibrium data used to calculate N for various assumed α values. Calculations were made for runs 3, 5, and 7 only, since they were judged to be the best and most comparable runs. These values of N and α are plotted in Fig. 21.3. From the intersection of the curves the value for the effective α is approximately 1.015 and the number of stages in the column under the stated conditions is approximately 23. This compares with a single-stage batch determination of α with the same solutions which gave $\alpha = 1.017$.

During the course of this work there was some concern as to whether the carbamate ion (NH_2COO^-) would exchange rapidly with NH_3 gas. If carbamate ion were to exchange very slowly, then normal-feed-concentration nitrogen would be carried to the product end of the system, where it would be converted to NH_3 gas. This would cause a large reduction in the isotopic separation and possibly destroy the gradient entirely. Run 8 was made to provide data concerning this matter by determining the isotopic gradient within the exchange column. If the total isotopic separation is plotted against the length or height of the column for the usual system at equilibrium, a straight line should be obtained.

[4] J. Shacter and G. A. Garrett, *Analogies Between Gaseous Diffusion and Fractional Distillation*, AECD-1940, p 21 (April 7, 1948).

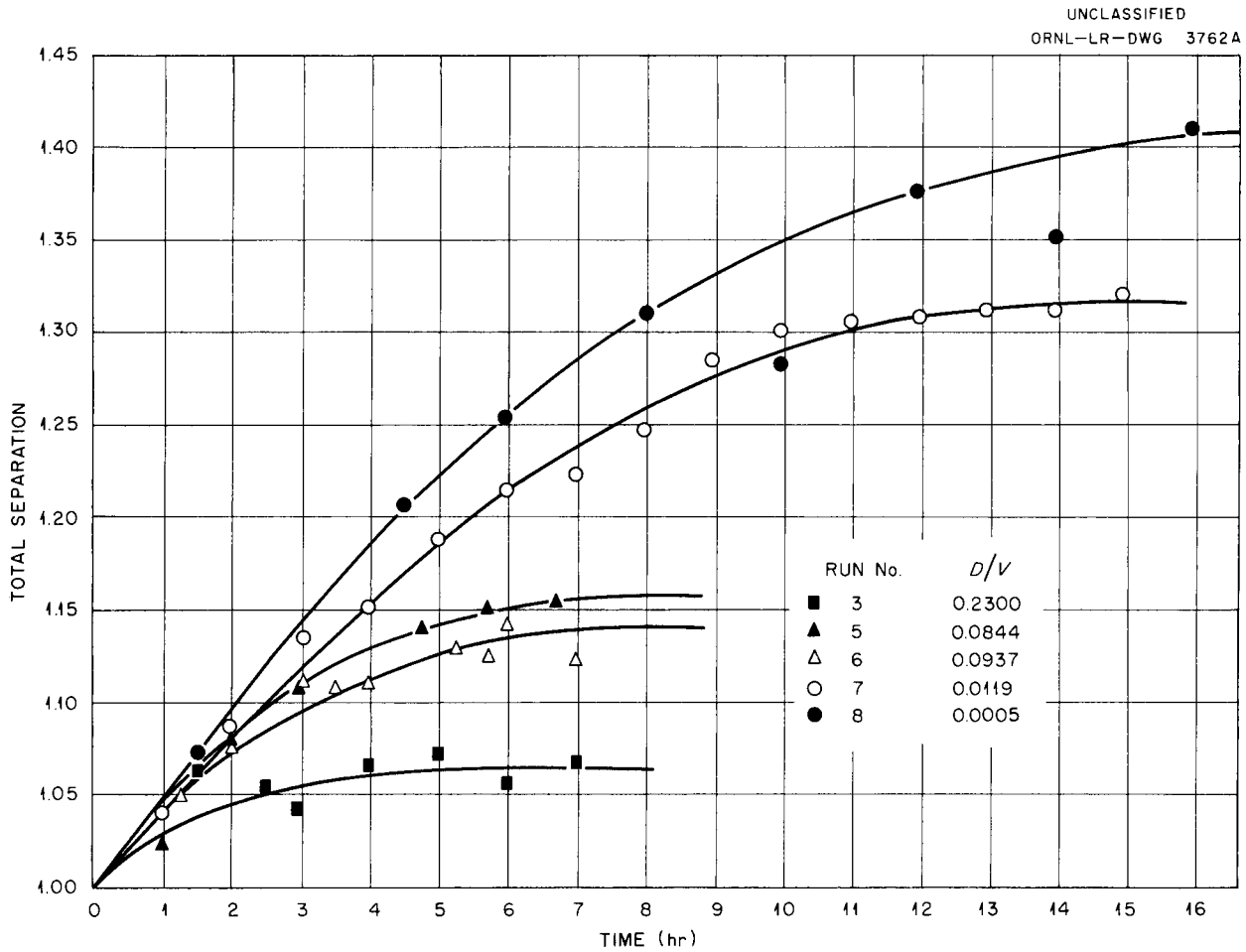

Fig. 21.2. Total Separation vs Time for Various D/V Ratios in the Ammonia–Ammonium Carbonate System.

TABLE 21.1. EXCHANGE RUNS – NH_3 vs NH_4^+ CARBONATE SYSTEM[a]

Total Time (hr)	Exchange Feed		Reflux Feed		Reflux Loss (meq/hr)	Product Removal (meq/hr)	Interstage Flow (meq/hr)	Total Product Removal[c]	Total Separation[d]
	M[b]	cc/hr	M	cc/hr					
5¾	17.5	320	4.0	4200	14.4	5.0	5600	0.346	
7½	17.5	320	4.0	4200	19.3	5.0	5600	0.428	1.60
7	19.0	360	4.0	4600	21.5	1565	6840	23.0	1.045
6¾	19.0	320	4.1	4000	22.9	490.2	6080	8.44	1.156
6½	19.0	322	6.0	3400	19.6	553.5	6118	9.37	1.142
15	19.0	322	6.0	3300	67.7	5.0	6118	1.19	1.314
16	18.0	315	2.6	3680	0.779	2.5	5670	0.0137	1.420

[a]All runs at 30°C and atmospheric pressure.
[b]Total $NH_3 + NH_4^+ + NH_2COO^-$.
[c]Per cent of interstage flow.
[d]From curve extrapolated to equilibrium.

TABLE 21.2. ISOTOPIC ANALYSES FOR RUNS 1 TO 8

Run No.	Time (hr)	Total Separation*
1	0.00	1.000
	3.75	1.206
	4.75	1.232
	5.75	1.269
2	0.00	1.000
	2.00	1.169
	3.25	1.234
	4.50	1.323
	5.50	1.336
	6.50	1.454
	7.50	1.454
3	0.00	1.0000
	1.50	1.0408
	2.50	1.0449
	4.00	1.0444
	5.00	1.0468
	6.00	1.0439
	7.00	1.0463
5	0.00	1.0000
	1.00	1.0218
	2.00	1.0795
	3.00	1.1053
	4.50	1.1337
	5.75	1.1500
	6.75	1.1533
6	0.00	1.0000
	1.25	1.0509
	2.00	1.0826
	3.00	1.1106
	3.50	1.1157
	4.00	1.1184
	4.75	1.1378
	5.25	1.1266
	5.75	1.1229
	6.00	1.1400
	7.00	1.1207
7	0.00	1.0000
	1.00	1.0389
	2.00	1.0863
	3.00	1.1336
	4.00	1.1499
	5.00	1.1870
	6.00	1.2132
	7.00	1.2208
	8.00	1.2438

TABLE 21.2. (continued)

Run No.	Time (hr)	Total Separation*
	9.00	1.2832
	10.00	1.2975
	11.00	1.3029
	12.00	1.3075
	13.00	1.3088
	14.00	1.3106
	15.00	1.3455
8	0.00	1.0000
	1.50	1.0713
	3.00	1.0442
	4.50	1.2068
	6.00	1.2530
	8.00	1.3082
	10.00	1.2811
	12.00	1.3735
	14.00	1.3494
	16.00	1.4094

*(N^{15}/N^{14}) sample/(N^{15}/N^{14}) feed.

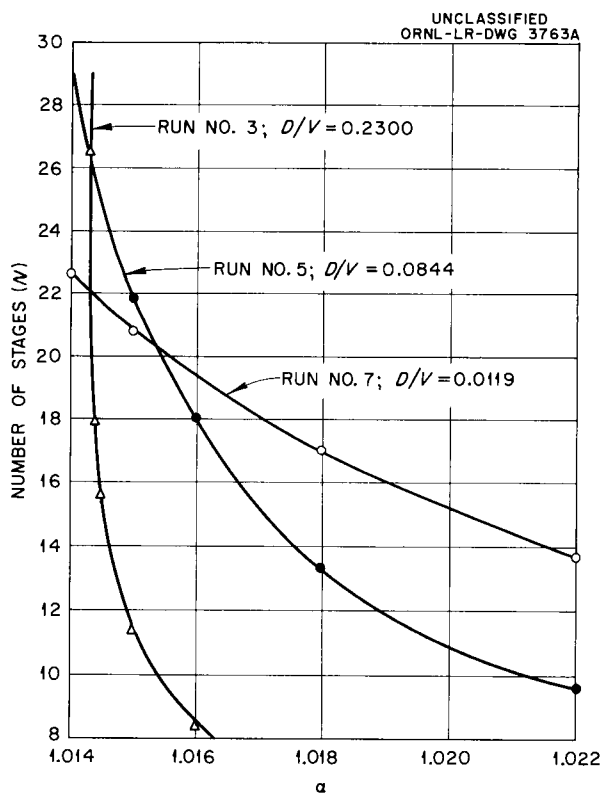

Fig. 21.3. N vs α from Column Runs 3, 5, and 7.

If material of normal isotopic content were being introduced at the product end, then a convex plot would be obtained.

A new exchange column was designed and built for this run so that isotopic samples could be taken throughout the length of the column. A sketch of the column is shown in Fig. 21.4. The ratio of NaOH to HN_4^+ was reduced in order to improve the reflux efficiency. The total product loss in the reflux was 0.014% of the interstage flow. Samples were taken simultaneously at various heights in the exchange column after 14 hr and again after 16 hr. The results of isotopic analyses of these samples are shown in Table 21.4 and plotted in Fig. 21.5. The bend in the lower section of the curves indicates that equilibrium has not quite been attained. The linearity of the upper portion of the lines indicates that carbamate ion is indeed at isotopic equilibrium with the other nitrogen-containing species in the system.

A more detailed description of these studies may be found elsewhere.[5]

TABLE 21.4. ISOTOPIC ANALYSES FROM COLUMN GRADIENT RUN (RUN NO. 8)

Time (hr)	Inches of Column*	Total Separation**
14	0	1.0000
	30	1.0446
	62	1.1432
	94	1.2600
	124	1.3630
16	0	1.0000
	30	1.0527
	62	1.1611
	94	1.2817
	124	1.4194

*From feed point.
**(N^{15}/N^{14}) sample/(N^{15}/N^{14}) feed.

[5] *Chemical Separation of Isotopes Section Semiann. Prog. Rep. June 30, 1954,* ORNL-1815 (to be issued).

TABLE 21.3. VALUES USED IN CALCULATION OF N vs α

Run No.	Mole Fraction, N^{15} (Feed)	Total Separation[(a)]	Mole Fraction, N^{15} (Product)	D/V[(b)]	$\alpha - 1$	Number of Stages[(c)]
3	0.003700	1.062	0.003929	0.230	0.0143	265
					0.0144	17.9
					0.0145	15.5
					0.0150	11.3
					0.0160	8.3
					0.0180	6.1
					0.0220	3.9
5	0.003700	1.156	0.004275	0.844	0.0140	29.2
					0.0150	21.8
					0.0160	18.0
					0.0180	13.3
					0.0220	9.6
7	0.003700	1.314	0.004856	0.0119	0.0140	22.6
					0.0150	20.8
					0.0180	17.0
					0.0220	13.7

(a) (N^{15}/N^{14}) product/(N^{15}/N^{14}) feed.
(b) (Product withdrawal)/(interstage flow).
(c) Calculated from the assumed $\alpha - 1$.

[redacted]

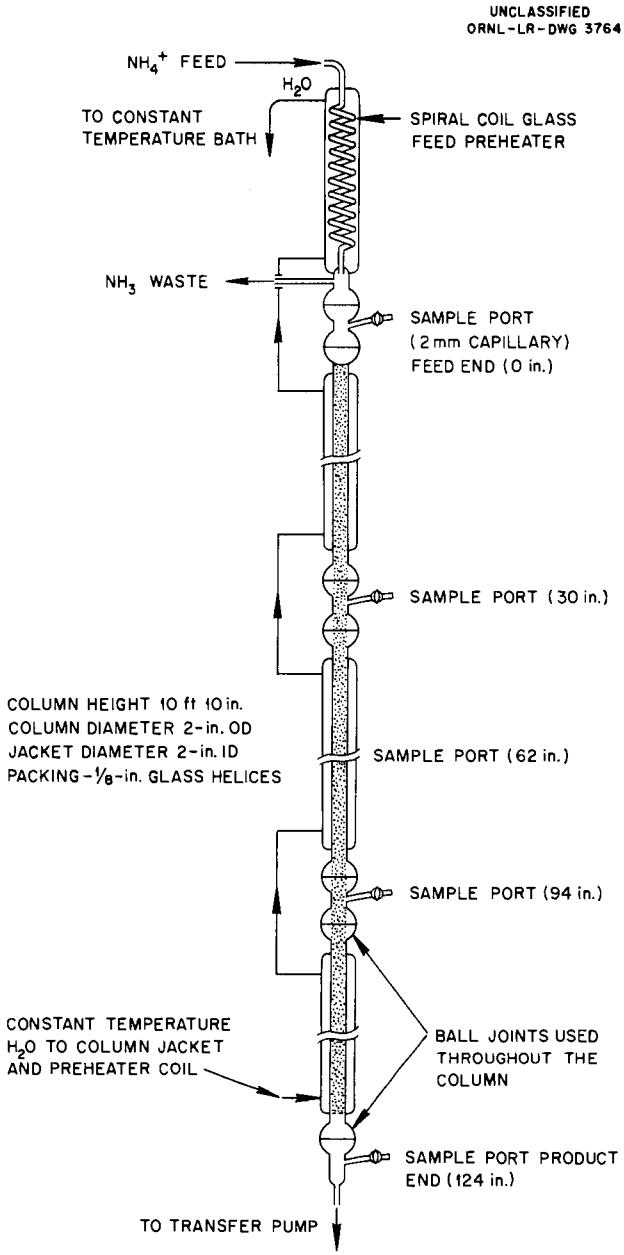

Fig. 21.4. Exchange Column for Isotopic Gradient Study.

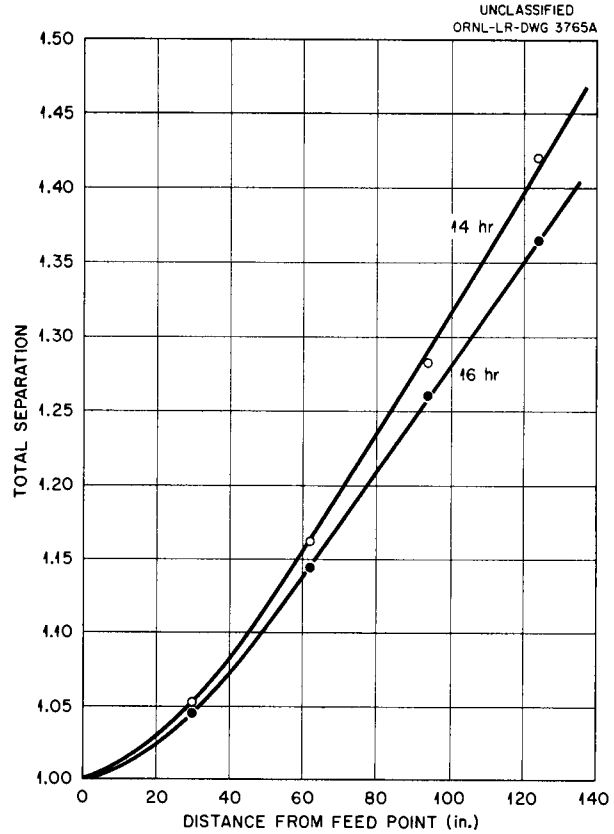

Fig. 21.5. Isotopic Analysis vs Length of Exchange Column.

[redacted]